NAVAL POSTGRADUATE SCHOOL
Monterey, California

DISSERTATION

PERFORMANCE OF SERIALLY CONCATENATED
CONVOLUTIONAL CODES WITH BINARY
MODULATION IN AWGN AND NOISE JAMMING OVER
RAYLEIGH FADING CHANNELS

by

Eng Seng Chia

September 2001

Dissertation Supervisor: Clark Robertson

Approved for public release; distribution is unlimited

Report Documentation Page

Report Date	Report Type	Dates Covered (from... to)
30 Sep 2001	N/A	-

Title and Subtitle	Contract Number
Performance of Serially Concatenated Convolutional Codes with Binary Modulation in AWGN and Noise Jamming over Rayleigh Fading Channels	
	Grant Number
	Program Element Number

Author(s)	**Project Number**
Eng Seng Chia	
	Task Number
	Work Unit Number

Performing Organization Name(s) and Address(es)	**Performing Organization Report Number**
Research Office Naval Postgraduate School Monterey, Ca 93943-5138	

Sponsoring/Monitoring Agency Name(s) and Address(es)	**Sponsor/Monitor's Acronym(s)**
	Sponsor/Monitor's Report Number(s)

Distribution/Availability Statement
Approved for public release, distribution unlimited

Supplementary Notes

Abstract

Subject Terms

Report Classification	Classification of this page
unclassified	unclassified

Classification of Abstract	**Limitation of Abstract**
unclassified	UU

Number of Pages
315

REPORT DOCUMENTATION PAGE			*Form Approved OMB No. 0704-0188*
Public reporting burden for this collection of information is estimated to average 1 hour per response, including the time for reviewing instruction, searching existing data sources, gathering and maintaining the data needed, and completing and reviewing the collection of information. Send comments regarding this burden estimate or any other aspect of this collection of information, including suggestions for reducing this burden, to Washington headquarters Services, Directorate for Information Operations and Reports, 1215 Jefferson Davis Highway, Suite 1204, Arlington, VA 22202-4302, and to the Office of Management and Budget, Paperwork Reduction Project (0704-0188) Washington DC 20503.			
1. AGENCY USE ONLY *(Leave blank)*	**2. REPORT DATE** September 2001	**3. REPORT TYPE AND DATES COVERED** Dissertation	
4. TITLE AND SUBTITLE: Title (Mix case letters) Performance of Serially Concatenated Convolutional Codes with Binary Modulation in AWGN and Noise Jamming over Rayleigh Fading Channels			**5. FUNDING NUMBERS**
6. AUTHOR(S) Eng Seng Chia			
7. PERFORMING ORGANIZATION NAME(S) AND ADDRESS(ES) Naval Postgraduate School Monterey, CA 93943-5000			**8. PERFORMING ORGANIZATION REPORT NUMBER**
9. SPONSORING / MONITORING AGENCY NAME(S) AND ADDRESS(ES) N/A			**10. SPONSORING / MONITORING AGENCY REPORT NUMBER**
11. SUPPLEMENTARY NOTES The views expressed in this thesis are those of the author and do not reflect the official policy or position of the Department of Defense or the U.S. Government.			
12a. DISTRIBUTION / AVAILABILITY STATEMENT Approved for public release; distribution is unlimited			**12b. DISTRIBUTION CODE**

13. ABSTRACT *(maximum 200 words)*

In this dissertation, the bit error rates for serially concatenated convolutional codes (SCCC) for both BPSK and DPSK modulation with different channel conditions and with (and without) spread spectrum are considered. For low signal-to-noise ratios, simulation results are used, while for higher signal-to-noise ratios, an average upper bound is developed to illustrate the achievable performance of SCCC.

The theoretical bounds for SCCC BPSK and SCCC DPSK with AWGN, noise jamming, Rayleigh fading, and spread spectrum are developed, analyzed, and compared with simulation results. The differences in performance between SCCC BPSK and SCCC DPSK are described. Implications for the military communications user and jammer are also discussed.

14. SUBJECT TERMS Serially concatenated convolutional codes, Turbo codes, Noise jamming, Interference, Rayleigh fading			**15. NUMBER OF PAGES**
			16. PRICE CODE
17. SECURITY CLASSIFICATION OF REPORT Unclassified	**18. SECURITY CLASSIFICATION OF THIS PAGE** Unclassified	**19. SECURITY CLASSIFICATION OF ABSTRACT** Unclassified	**20. LIMITATION OF ABSTRACT** UL

THIS PAGE INTENTIONALLY LEFT BLANK

PERFORMANCE OF SERIALLY CONCATENATED CONVOLUTIONAL CODES WITH BINARY MODULATION IN AWGN AND NOISE JAMMING OVER RAYLEIGH FADING CHANNELS

Eng Seng Chia
Major, Republic of Singapore Airforce
B.S., National University of Singapore, 1989
M.S., Naval Postgraduate School, 1998

Submitted in partial fulfillment of the
requirements for the degree of

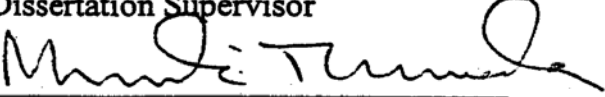## DOCTOR OF PHILOSOPHY IN ELECTRICAL ENGINEERING
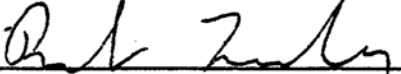
from the

NAVAL POSTGRADUATE SCHOOL
September 2001

Author: _____

Eng Seng Chia

Approved by:

Clark Robertson, Professor
Dept. of Electrical & Computer Engr.
Dissertation Supervisor

Tri T. Ha, Professor
Dept. of Electrical & Computer Engr.
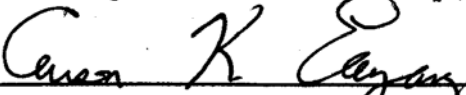
Murali Tummala, Professor
Dept. of Electrical & Computer Engr.

Ramakrishna Janaswamy, Professor
Dept. of Electrical & Computer Engr.

Bert Lundy, Associate Professor
Dept. of Computer Science

Approved by: _____

Jeffrey B. Knorr, Chairman,
Dept. of Electrical & Computer Engr

Approved by: _____

Carson K. Eoyang, Associate Provost for Academic Affairs

iii

THIS PAGE INTENTIONALLY LEFT BLANK

ABSTRACT

In this dissertation, the bit error rates for serially concatenated convolutional codes (SCCC) for both BPSK and DPSK modulation with different channel conditions and with (and without) spread spectrum are considered. For low signal-to-noise ratios, simulation results are used, while for higher signal-to-noise ratios, an average upper bound is developed to illustrate the achievable performance of SCCC.

The theoretical bounds for SCCC BPSK and SCCC DPSK with AWGN, noise jamming, Rayleigh fading, and spread spectrum are developed, analyzed, and compared with simulation results. The differences in performance between SCCC BPSK and SCCC DPSK are described. Implications for the military communications user and jammer are also discussed.

THIS PAGE INTENTIONALLY LEFT BLANK

TABLE OF CONTENTS

THIS PAGE INTENTIONALLY LEFT BLANK

LIST OF FIGURES

THIS PAGE INTENTIONALLY LEFT BLANK

LIST OF TABLES

THIS PAGE INTENTIONALLY LEFT BLANK

ACKNOWLEDGMENTS

First, I would like to thank the Ministry of Defence of Singapore for this opportunity to pursue a Ph.D. degree. Second, I am indebted to my dissertation advisor, Prof. Clark Robertson, for equipping me with the necessary knowledge and tools for research work. He has also been my constant support and guidance. Special thanks to my committee members, Prof. Ha, Prof. Janaswamy, Prof. Tummala and Prof. Lundy, for their teaching and lectures. They are some of the best lecturers that I have come across. The Ph.D. program can at times be tedious and lonely, being away in a foreign country. I would like to thank my Chief Defense Scientist, Prof. Lui Pao Chuen, for being one of the few contacts I have with Singapore, and for providing the necessary support and guidance when needed. I also like to thank the new friends I have made here, the Americans and international students (especially those from Turkey) for their friendship. Last, but not least, I would like to thank the International Program Office; their programs and support have certainly make life more interesting here.

THIS PAGE INTENTIONALLY LEFT BLANK

EXECUTIVE SUMMARY

In this dissertation, the bit error rates of serially concatenated convolutional codes (SCCC) with both BPSK and DPSK modulation, additive white Gaussian noise, noise jamming, Rayleigh fading, and spread spectrum are considered. For low signal-to-noise ratios, simulation results are used, while for higher signal-to-noise ratios, an average upper bound is developed. The results show a considerable improvement in BER over the uncoded case with and without Rayleigh fading is present. For BPSK modulation and Rayleigh fading, channel information offers a one to two dB gain. Without channel information, simulation results show that SCCC BPSK has a coding gain advantage of 5 dB more than SCCC DPSK at large BER.

From the theoretical results, we found that SCCC with spread spectrum, side information, and channel information is the most effective in reducing the effects of jamming and fading. We also find that side information works best for ρ and high overall SNR. When fading is present, barrage jamming is most effective for lower SNRs and SJRs, while smaller ρ are more effective for higher SNRs and SJRs. The theoretical bounds are found not to be accurate for SNR (or SJR) below 2 or 3 dB as expected. The results also show that SCCC DPSK is not as effective in a jamming environment as SCCC BPSK. SCCC DPSK requires at least a SNR of 6 dB to avoid the region of high BER. Frequency-hopped spread spectrum improves the performance of SCCC DPSK in a jamming environment remarkably. DPSK is less affected by Rayleigh fading than BPSK in a jamming environment.

Barrage jamming is the best option for the jammer (with or without fading) unless the overall signal-to- noise ratio is very high. In this case, ρ less than 1.0 may be appropriate. However, very small ρ (< 0.01) are always ineffective. Moreover, such a jammer is easy to detect, and those symbols that are jammed can be erased. For the user, the best defense is to increase SNR and/or improve the factors affecting the performance of the SCCC. Since SCCC suffers longer delays than Turbo codes for the same length interleavers, knowing the minimum number of iterations necessary for the required BER will reduce these delays.

THIS PAGE INTENTIONALLY LEFT BLANK

I. INTRODUCTION

A. ERROR CONTROL CODING

The basic goal in digital communications is to transport bits of information with an acceptable level of reliability. The level of reliability that is tolerable/acceptable varies for different applications. Reliability is measured in terms of the bit error ratio or BER. The BER is the number of bits in error divided by the number of total bits transmitted. A high BER might not even be noticeable when transmitting digital audio; however, a single bit error when transmitting a computer program can render the program inoperable.

A very simple model of a communications system is shown in Figure 1.1. The channel is the physical medium over which the information is transmitted. In the majority of digital communications systems, transmission occurs over either a wired (e.g. telephone lines) or wireless (e.g. cellular telephones) channel.

Data Source	Transmitter	Channel	Receiver	Data Sink
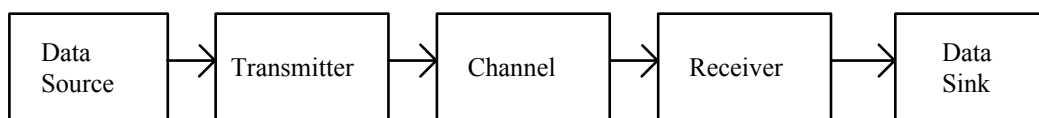
Figure 1.1.   Simplified communications system model.

When the transmitted signal arrives at the receiver after passing through the channel, the received data will have some bits that are in error. This can be due to additive white Gaussian noise (AWGN), jamming (interference), and/or fading. These errors can be minimized through error control coding.

The basic idea behind error control coding is to add redundancy to the transmitted signal. We then exploit this redundancy at the receiver to detect and correct errors. The addition of redundancy to the signal means that more bits are used to convey a message than the number of bits actually needed. Error control codes have a property called Hamming distance. The Hamming distance is defined as the number of bits that differ

between two valid code words and the minimum Hamming distance is the smallest distance obtained when all possible codewords are compared. In general, a larger minimum Hamming distance indicates a code capable of correcting more channel-induced errors. The reason is that more channel bit errors can occur before a received set of bits is mistakenly decoded as another valid code word. The tradeoff for increasing the distance of a code is the transmission of extra bits, and this translates into an increase in bit rate and bandwidth. Another way to reduce channel bit errors is to use higher signal power, i.e., with a higher signal-to-noise ratio, it is easier for the detector/decoder to extract the signal. Thus, error control coding can be considered as a tradeoff between reduced throughput and a reduction in the BER or as a tradeoff between bandwidth and required signal power.

Error correction codes can be broken into two basic types: block codes and convolutional codes. Block codes get their name because the encoder takes in a message block of fixed length, adds redundancy, and produces a code word that is a block of fixed length, albeit longer than the message. Convolutional codes follow a completely different approach to coding. Instead of breaking the message into blocks, the entire message stream is converted into a single code word. Convolutional codes get their name because the encoding process can be viewed as the convolution of the message bit stream with the impulse response of the encoder. The decoding process involves finding the code word sequence that most closely matches the received sequence. However, this process grows exponentially complex with increasing sequence length. The most popular technique for decoding convolutional codes in practice is the Viterbi algorithm. The algorithm works by computing a metric for each path. The metric is related to the difference between the received code sequence and the code sequence for a given path. The decoded sequence is determined from the path with the best metric. Convolutional codes are good at correcting random errors. Convolutional codes can also be a form of block codes when they are terminated after a certain block size is reached.

The use of a simple code is sufficient for many applications; however, many complex modern communications systems employ several different codes in series. A system that uses concatenated coding passes its data through multiple encoders before

transmitting the encoded bit stream. At the receiver end, the signal passes through the corresponding decoders in the reverse order. The motivation for using concatenated coding is that different code classes have different strengths. Thus, performance can be improved by combining different classes of codes to take advantage of these strengths. An example of a common concatenated coding structure is a Reed-Solomon encoder, an interleaver, and a convolutional encoder connected in series. The purpose of the interleaver is to take samples that are contiguously located in time and spread them out to correct for burst errors. This structure is used in many digital communications systems such as digital television, cable modems, and cellular telephones as well as deep-space communications.

B.   THE SHANNON LIMIT

A fundamental concept in coding theory is the Shannon limit. Specifically, let η denote the spectral efficiency of a digital communication system operating over an additive white Gaussian noise channel with power spectral density $N_o/2$ and E_b/N_o as the signal-to-noise ratio, where E_b is the average energy per bit. Then, in principle one can transmit reliably over this channel if [Ref. 1]

$$\frac{E_b}{N_o} \geq \frac{2^{\eta} - 1}{\eta}$$

………(1.1)

The equality represents the absolute Shannon limit. For example, for $\eta = 1$, E_b/N_o must exceed zero dB for reliable communications.

It is known that codes exist that approach this theoretical performance limit. We know that when the codeword length, n, of block codes or the constraint length of convolutional codes is increased, these codes approach the Shannon limit. However, easily decodable codes whose performance approaches the Shannon limit have been a 'Holy Grail' for coding theorists. The complexity of maximum likelihood (ML) decoding algorithms increases as either the block length of a block code or the constraint length of a convolutional code increases, up to a point where decoding becomes

3

physically unrealizable [Ref. 2].   Furthermore, Shannon theory proves that "random" codes are good; their decoding complexity, however, increases exponentially with block length.   On the other hand, the structure imposed on codes in order to decrease their decoding complexity often results in poor performance.   As a result, approaching the channel capacity or, even more modestly, going significantly beyond the channel cutoff rate has been an unreachable dream of coding theorists for many years.

Thus, research in coding theory has seen many proposals aimed at the construction of powerful codes with large equivalent block lengths structured so as to permit breaking the ML decoding into simpler partial decoding steps, thus obtaining a suboptimum yet powerful decoding strategy.   Iterated codes [Ref. 3], product codes and their extension [Ref. 4], concatenation of a convolutional and Reed-Solomon block code [Ref. 5], and large constraint-length convolutional codes with suboptimal decoding strategies, like sequential decoding, are some examples.   Recently, another solution has been found using iterative decoding called "Turbo Codes" [Ref. 6, 7, 8, 9].   Turbo codes have excellent asymptotic performance and coding gain, and decoding complexity is reasonable if iterative decoding is used.   One drawback is the considerable delay in decoding that limits their range of application.   Turbo codes can achieve very low error rates (10^{-6}) while operating at less than one dB above the Shannon limit.   In contrast, most current systems using conventional codes operate three to six dB above this bound. Uncoded systems are typically ten dB above the Shannon limit.

The rationale behind Turbo codes and their decoders is based on a combination of recursive systematic convolutional codes, their parallel concatenation with interleaving, and iterative decoding.   The latter consists of decoding each code bit sequentially and feeding the output of the last decoder back to the first one several times in order to improve the reliability of the decoded symbols.   Implementation requires the decoder to output the probabilities and every bit take on an allowable value (soft decision). This in turn stems from the maximum-a-posteriori (MAP) decoding algorithm introduced in 1974 by Bahl [Ref. 10].   The traditional approach in reducing the bit error probability of a system is to increase the minimum Hamming distance of the code, thus reducing the

word and bit error probabilities. Turbo codes, on the other hand, reduce the multiplicity of codewords with low Hamming weights.

Since the first appearance of Turbo codes in 1993 [Ref. 8, 11], the structural properties of Turbo codes are slowly being put on a firm theoretical footing [Ref. 12, 13, 14], and other forms of concatenations with interleavers have been studied and shown to offer similar, and in some cases even better, performance [Ref. 15, 16, 17]. They form a class of codes that, using iterative decoding, permit us to approach the Shannon capacity with a bit error rate on the order of 10^{-6}. This is still quite far from the unlimited reliability promised by the Shannon capacity theorem, but more than enough for many applications.

Some general characteristics of the ideal application for Turbo codes are when transmitting power is important, soft decision decoding is feasible, and the bits can be encoded in blocks of a few hundred or more. One natural area for Turbo codes is in the wireless networking area. These networks need efficient transmission. The packet sizes are large enough that Turbo codes can work effectively, and wireless network protocols exist that can work effectively with the error rates obtained with Turbo codes. Turbo codes will also be incorporated in the 3G Universal Mobile Transmission System (UMTS). Turbo codes can also be successfully applied to many detection/decoding problems such as channel equalization, coded modulation, multi-user detection, joint source and channel decoding [Ref. 18].

C.   TURBO CODES AND SERIALLY CONCATENATED CONVOLUTIONAL CODES

The serial concatenation of codes had been largely used in past years for forward error control. A classical solution consisting of an outer Reed-Solomon code, an optional interleaver, and an inner binary convolutional code has been analyzed [Ref. 19] and adopted in several applications. Almost always, however, the component codes were decoded separately. In this way, the decoding of the whole concatenated code is highly suboptimal with respect to maximum likelihood (ML) or maximum a posteriori (MAP)

decoding. Also in classical concatenated coding theory, the insertion of an interleaver between the outer and inner encoders was considered only as a way of randomizing the errors produced by the inner encoder and not, as in Turbo codes, to construct a new, more powerful integrated coding scheme.

After Turbo codes were introduced, a new family of serially concatenated convolutional codes (SCCC) was conceived [Ref. 20]. Iterative Soft-in-Soft-Out decoding of simple component codes allows the decoding of a whole SCCC with a limited penalty (less than 1 dB) with respect to ML and MAP decoding [Ref. 21]. Theoretical analysis has shown that SCCC offers some advantages over Turbo codes [Ref. 22]. In general, the Turbo code outperforms the SCCC for high values of BER [Ref. 23]. For very low BER, SCCCs outperforms Turbo codes, especially for a large number of iterations.

A heuristic explanation of the superior behavior of SCCCs with respect to Turbo codes is that Turbo codes are limited by the Hamming weight of error events of the code generated by the information sequences of lowest weight, which is usually two [Ref. 24]. In SCCCs, the input sequence to the inner encoder is not the information sequence, as in Turbo codes, but coded sequences produced by the outer encoder. As a consequence, the lowest weight of these sequences corresponds to the free distance of the outer code, which can be significantly higher than two, thus yielding a higher interleaver gain.

Much research has been carried out on Turbo codes since their discovery. SCCCs, on the other hand, have not received as much attention. Although SCCCs are in many ways similar to Turbo codes, they have their own set of characteristics; for example, SCCCs exhibit no error floor. Although SCCCs suffer longer delays than Turbo codes, their very good performances for small interleavers reduce this latency problem. An evaluation of bit error probability shows an interleaver gain, i.e., the decrease of bit error probability with increasing interleaver length, significantly higher for SCCCs than Turbo codes. Thus, SCCCs are better suited to provide near error-free performance [Ref. 20]. The behavior of SCCCs under Rayleigh fading and jamming has also not been investigated. Therefore, the BER of SCCCs under different channel conditions is examined in this dissertation.

6

D.   INTERFERENCE, FADING, MODULATION AND SPREAD SPECTRUM

The low SNR achieved by turbo codes has drawn much attention despite the delay imposed by the large interleaver. In military communications, low signal power and BER are often more important than moderate delay. Information such as position data, command data, and image data can tolerate delays up to a few seconds or more. Hence Turbo codes and SCCCs are potential candidates for such applications. A reduction in transmitted signal energy means longer battery life and lower probability of detection and interception.

Another problem with communications in the battlefield is interference caused by hostile jammers. Jammers try to disrupt the communication by emitting noise-like interference in the channel. In practice, jammers often adopt partial-band interference or pulsed interference channel to maximize their effect. For example, a frequency-hopped spread-spectrum communication system that is operating in the presence of a partial-band jammer has interference that is on part of the time (when the signal is transmitted in a jammed band) and off part of the time (when the signal is transmitted in a unjammed band). In addition to the interference, there is AWGN that causes additional errors.

Several researchers have analyzed the error probability of some codes in an environment with interference [Ref. 25, 26, 27, 28]. The analyses in these papers have been largely that of determining the bit error probability of convolutional codes, possibly in conjunction with repetition codes and with soft decisions, for which case a union-Chernoff bound has been employed. The effect of background AWGN has largely been ignored. Other papers published [Ref. 29, 30, 31] have shown that thermal noise cannot be neglected in the analyses if accurate results and correct determination of the optimum order of diversity and worst case jamming fraction are to be obtained. We noted in [Ref. 32, 33] that the Chernoff bound approach gave a meaningless result regarding soft decision decoding without side information. Namely, the bound on the probability of error was increasing uniformly with the decrease of the duty cycle of the jammer. In this dissertation, the combined effects of AWGN and interference are considered. It allows us to obtain more accurate results especially for fading channels.

One of the issues involved in the design of a communication system operating in jamming environment, in particular where error correction coding is to be used, is that of side information availability [Ref. 34]. If the decoder has knowledge of which symbols are received when interference is present, then these symbols carry less weight in deciding which codeword is transmitted than those where no interference is present. If the decoder has no such side information, then no such weighting can be made. Moreover, knowledge of the overall signal-to-noise ratio is important to the decoding algorithm of the SCCC. In this dissertation, we present analytical methods for determining the error probability of codes on such channels when side information is available and when side information is not available.

Fading is an important and common channel disturbance in many applications. Turbo and SCCC decoding is based on the concept of maximum likelihood decision on blocks of data. The decision on a bit affects the decoding of subsequent bits. Because the effect of fading can be extended over a period of multiple bits, the impact of fading on performance can become crucial. The interleaver in the SCCC is used to break the correlated channel disturbance into independent corrupted channel symbols that, in turn, can be corrected by the decoder. The larger the interleaver, the wider the correlated symbols can be separated and, consequently, the better the performance. In this dissertation, we consider a general channel model that includes both non-fading and fading channels and derive analytical upper limits of SCCC performance based on the union bound and code weight distributions. Two cases are considered: with and without knowledge of the SNR and fading amplitudes. The fading channel is assumed to be a slowly varying, frequency non-selective and independent Rayleigh fading channel.

Selecting a proper modulation technique for a communication system is a very important factor in optimizing system performance. Ideally, the modulation scheme provides for low BER at low SNR and performs well in fading conditions. Coherent receivers usually give better BER performance [Ref. 35]. However, coherent receivers are usually more complex since a coherent reference is required. In other cases (such as a randomly fading channel), a noncoherent system is more desirable because there may be difficulty in establishing and maintaining a coherent reference. Noncoherent detection

gives the advantage of using less complicated synchronization circuitry that reduces the complexity of the receiver. Signals that can withstand significant degradation before their ability to be detected is affected are clearly more desirable in military and space applications. Thus, two types of modulation techniques are considered here: one that requires the acquisition of a coherent reference at the receiver, i.e., binary phase-shift keying (BPSK) and one that does not require coherent detection, i.e., binary differential phase-shift keying (DPSK).

Spread spectrum techniques were invented to provide secure communications in a military environment. Spread spectrum refers to any modulation technique that produces a spectrum for the transmitted signal much wider than the bandwidth of the information being transmitted [Ref. 36]. There are several reasons for this apparently "wasteful" approach to bandwidth: to provide some degree of resistance to interference and jamming, to lower the probability of intercept, to provide resistance to signal interference from multiple transmission paths, and to provide multiple access. Consequently, no analysis relating to jamming will be complete without including a consideration of spread spectrum systems. In this dissertation, two types of spread spectrum are considered. Direct sequence spread spectrum is incorporated for the SCCC with BPSK modulation (SCCC/BPSK) and frequency-hopped spread spectrum for the SCCC with DPSK modulation (SCCC/DPSK).

E.   OBJECTIVE OF DISSERTATION

The objective of this dissertation is to investigate the behavior of SCCC with BPSK and DPSK modulation and the effects of AWGN, noise jamming, Rayleigh fading and spread spectrum. For low signal-to-noise ratios, simulation results are used, while for higher signal-to-noise ratios, an average upper bound is developed to illustrate the achievable performance of SCCC. The availability of side information (due to noise jamming) and channel information (due to fading) is also considered.

F.   OUTLINE OF DISSERTATION

In this dissertation, the BER of SCCC with AWGN, noise jamming, Rayleigh fading, and spread spectrum are considered. For low signal-to-noise ratios, analytic solutions are difficult to obtain. Thus, simulation results are used to obtain the BER in this case. For higher signal-to-noise ratios, an average upper bound is developed and applied for a variety of channel conditions. The bound serves to illustrate the achievable performance of SCCC. To the knowledge of the author, none of the theoretical bounds and simulations involving interference and Rayleigh fading obtained in this dissertation have been published before.

Chapter I provides an introduction to error control coding including the Shannon limit, the discovery of Turbo codes and SCCC, and the scope of this dissertation. In Chapter II, the SCCC is described, the decoding algorithms are explained, and the theoretical bounds in AWGN and Rayleigh fading are obtained and analyzed. Chapter III describes the simulation model: design considerations as well as transmitter, channel and receiver design. The theoretical BER results, based on this model, are obtained and compared with the simulation results for AWGN with and without Rayleigh fading. The theoretical bounds for SCCC/BPSK with AWGN, pulse-noise jamming (with and without side information), Rayleigh fading (with and without channel information), and with and without direct sequence spread spectrum are obtained in Chapter IV. These bounds are plotted and their behavior investigated. In Chapter V, the simulation results using the model described in Chapter III, for the different channel conditions specified in Chapter IV, are obtained and compared with each other, as well as with their theoretical bounds. These results are also compared with convolutional codes of the same constraint length and uncoded BPSK. Chapter VI and VII are similar to Chapter IV and V, respectively, except that instead of BPSK, pulsed noise jamming and direct sequence spread spectrum, DPSK, partial-band noise jamming and frequency-hopped spread spectrum are considered. The differences in performance between SCCC/BPSK and SCCC/DPSK are discussed in Chapter VIII, together with some implications for military communications. Finally, in Chapter IX, some conclusions and recommendations for future work are made.

II. SERIALLY CONCATENATED CONVOLUTIONAL CODES (SCCC)

A. DESCRIPTION

Forney [Ref. 5], in his goal to find a class of codes whose probability of error decreased exponentially at rates less than capacity, while decoding complexity increased only algebraically, arrived at a solution consisting of a multilevel coding structure called a concatenated code. It consists of the cascade of an inner code and an outer code, which in Forney's approach, would be a relatively short inner code admitting simple maximum likelihood decoding and a long high-rate algebraic non-binary Reed Solomon outer code which could be decoded with a powerful algebraic error correction algorithm, possibly using reliability information from the inner decoder.

Concatenated codes have since evolved as a standard for those applications where very high coding gains are needed, such as deep space applications. Alternative solutions for concatenation have also been studied, such as using trellis-coded schemes for the inner code [Ref. 37] or concatenating two convolutional codes [Ref. 19]. In the latter, the inner Viterbi decoder employs a soft-output decoding algorithm to provide soft-input decisions to the outer Viterbi decoder. An interleaver was also proposed between the two encoders to separate bursts of errors produced by the inner encoder.

A serially concatenated convolutional code (SCCC) is an extension of the concept of conventional concatenated codes. A SCCC consists of an (n_o, k_o) outer encoder and an interleaver (of length N) permuting the outer codewords bits for input into the (n_I, k_I) inner encoder (Figure 2.1). Thus, the SCCC consist of an outer encoder of rate k_o/n_o and an inner encoder of rate k_I/n_I connected by an interleaver of size N. The overall code rate is $R_c=(k_o/n_o).(k_I /n_I)$. Structurally, a SCCC block diagram is equivalent to that of a conventional concatenated code with an interleaver between the inner and outer encoders. The difference is that with SCCC, the interleaver is an integral component of the overall encoder and is not present solely to break up error bursts. The interleaver acts to improve the overall free distance of the SCCC by preventing short merges in the constituent

trellis. These short merges are usually produced by short, low weight input sequences and result in low output parity weight. The interleaver scrambles these 'bad' input sequences for the inner encoder to increase its parity weight.

Source ⟶ [Outer encoder (n_O, k_O)] ⟶ [Interleaver Length = N] ⟶ [Inner encoder (n_I, k_I)] ⟶ to channel
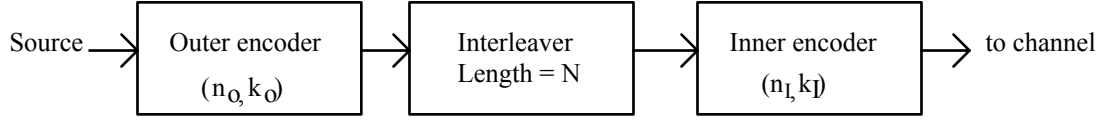
Figure 2.1.   Serially concatenated convolutional code.

Ideally, the code sequences are infinite, and the interleaver is a permutation of the whole integer axis, i.e., infinite. However, in practice, only terminated SCCCs are considered. In this case, an information frame of length k enters the first encoder (assumed to be in the zero state at time zero) and is mapped into $(k.n_o/k_o)$ coded bits. The first encoder is then trellis terminated, i.e., driven back to the zero state in s_o trellis steps, leading to a block of $N = (k + s_o).n_o/k_o$ bits. The minimum number of steps s_o depends on the code and can be shown to be equal to the maximum number of delay cells on an input line of the equivalent feed-forward encoder. The interleaver applies a block permutation of length N. The permutated frame of length N bits at the input of the inner encoder is encoded into a frame of $m = (N.n_I/k_I)$ bits. It is assumed that k_I divides N. The second encoder is also terminated in s_I steps leading to the final block length of $n = (m + s_I.n_I/k_I)$ bits. As a consequence, a terminated SCCC with an interleaver length N is a binary block code (n,k) with

$$k = \frac{N.k_o - s_o.n_o}{n_o}.$$

………..(2.1)

$$n = (N + s_I).\frac{n_I}{k_I}$$

………..(2.2)

Note that even though the interleaver length is N, the latency introduced to the transmission chain is proportional to k, the information frame length.

12

For example, a rate 1/3 SCCC is formed by an outer (3,2) convolutional code of memory two ($s_o = 2$), and an inner (2,1) convolutional code of memory two ($s_I = 2$), joined by an interleaver, $N = 640$. The effective code rate is 64/193.

The component codes are assumed linear so that the SCCC is linear as well. Puncturing of the component codes may be done to achieve desired code rates. In addition, the interleaver is assumed to be uniform, which enables the weight distribution of the SCCC to be computed from the weight distribution of the component codes.

B.   DECODING METHODS

Maximum a posteriori (MAP) decoding and the soft-output Viterbi algorithm (SOVA) are the main algorithms currently used for iterative decoding since they produce soft bit estimates. MAP decoding is a better decoding algorithm for maximum correct symbol detection, but decoding complexity is larger than SOVA because of numerous forward and backward recursions [Ref. 38]. In comparison, the SOVA method is not as complex and can be applied to an SCCC structure with some modifications [Ref. 38, 39, 40, 41].

There is a problem in applying the SOVA for the iterative decoding of a SCCC. This results from the fact that the conventional SOVA produces sub-optimum decision values only for the encoder input bits according to the maximum likelihood sequence estimation rule [Ref. 4]. Therefore, in order to be used for the iterative decoding of SCCC, the SOVA has to be modified to obtain the a-posteriori probability of the encoder output [Ref. 42, 43]. The details of the modifications required are found in [Ref. 39]. It is also shown in the same reference that the SOVA is less than three quarters as complex as (log) MAP decoding for four-state constituent codes and less than half as complex for 16-state constituent codes. The loss in coding gain is about 0.7 dB at 10^{-5} for turbo codes with 16-state encoders and an interleaver size of 4096 when compared with using MAP decoding [Ref. 44]. As a consequence of the foregoing, results are reported assuming the MAP algorithm in this dissertation.

The core of the MAP algorithm is a block called Soft Input Soft Output (SISO). It is a four-port device that accepts as inputs the probability distributions (or the corresponding likelihood ratios) of the information and code symbols labeling the edges of the code trellis, and forms as outputs an update of these probability distributions based upon the code constraints. The SISO is used within the iterative decoding algorithm as shown in Figure 2.2.
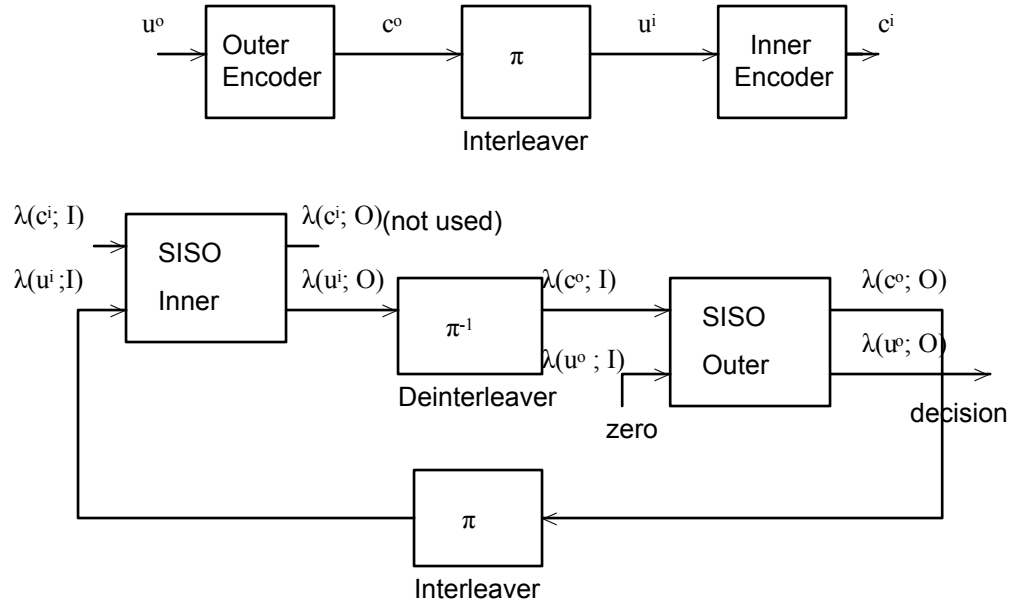
Figure 2.2.   Block diagrams of the encoder and iterative decoder for SCCC.

The symbols $\lambda(.;I)$ and $\lambda(.;O)$ at the input and output ports of the SISO refers to the logarithmic likelihood ratios (LLR), unconstrained when the second argument is I and modified according to the code constraints when it is O. When the first argument is u, this refers to the information symbols of the encoder, whereas c refers to code symbols. When the symbols are binary, only one LLR is needed. Finally, the superscript 'o' refers to the outer encoder and 'i' to the inner encoder. The LLRs are defined as

$$\lambda\left(x;.\right) \underset{=}{\triangle} \log\left[\frac{P(x;.)}{P(x_{ref};.)}\right]$$

……….(2.3)

14

where P(x;.) represents the priori probability distributions. The second argument in the brackets, shown by a dot, may represent I, the input, or O, the output to the SISO. When x is a binary symbol, "0" or "1", x_{ref} is generally assumed to be the "1". In contrast to the iterative algorithm employed for Turbo decoding, in which only the LLRs of information symbols are updated, for SCCCs the LLRs of both information and code symbols must be updated based on the code constraints.

During the first iteration of the SCCC algorithm, the inner SISO is fed with the demodulator soft outputs, consisting of the LLRs of symbols received from the channel, i.e., code symbols from the inner encoder. The second input λ (u^i;I) of the inner SISO is set to zero during the first iteration, since no a priori information is available on the input symbols u^i of the inner encoder.

The LLRs $\lambda(c^i;$ I) are processed by the SISO algorithm, which computes the extrinsic LLRs of the information symbols of the inner encoder $\lambda(u^i;$ O) conditioned on the inner code constraints. The extrinsic LLRs are passed through the inverse interleaver (labeled as π^{-1}), whose outputs correspond to the LLRs of the code symbols of the outer code, i.e.,

$$\pi^{-1}\left[\lambda\left(u^i;O\right)\right]=\lambda\left(c^o;I\right)$$

………(2.4)

These LLRs are then sent to the outer SISO input that corresponds to code symbols. The outer SISO in turn processes the LLRs $\lambda(c^o;$ I) of its unconstrained code symbols, and computes the LLRs of both code and information symbols based on the code constraints. The input $\lambda(u^o;$ I) of the outer SISO is always set to zero, implying equally likely transmitted source information symbols. The output LLRs of information symbols (which yield the a posteriori LLR of the SCCC information symbols) are used in the final iteration to recover the information bits. Prior to the final iteration, the LLRs of outer code symbols, after interleaving, are fed back to the input corresponding to information symbols of the inner code of the inner SISO to start the second iteration. In fact,

$$\pi\left[\lambda\left(c^O;O\right)\right]=\lambda\left(u^i;I\right)$$

<div align="right">……….(2.5)</div>

The SISO has been described in detail in [Ref. 45]. The SISO algorithm represents a slight generalization of the Bahl-Cocke-Jelinek-Raviv (BCJR) algorithm (Ref. 10, 18, 46). Here, the input-output relations are described. They refer to the trellis section of the trellis encoder, assumed to be time invariant as in convolutional codes, shown in Figure 2.3. The symbol e denotes the trellis edges and the information and code symbols associated with the edge e as u(e) and c(e) and the starting and ending states of the edge e as s^S (e) and s^E (e), respectively.
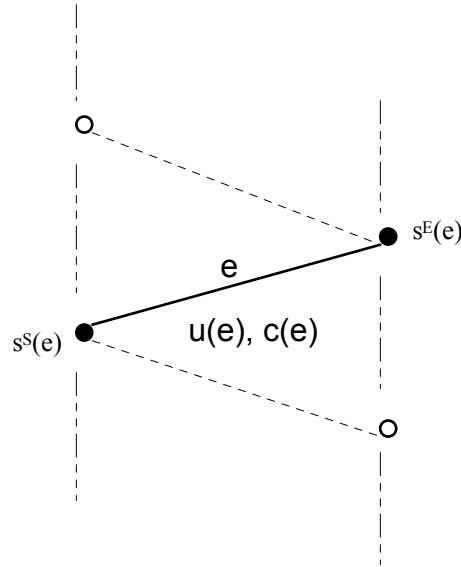
Figure 2.3. Trellis section defining the notations used for the description of the SISO algorithm.

The SISO works at symbol level; i.e., for a (n, k) convolutional code, the SISO operates on information symbols u belonging to an alphabet with size 2^k and on code symbols belonging to an alphabet with size 2^n. Assuming that the information and code symbols are defined over a finite time index set [1, …, K], at time k, k = 1,…K, the output extrinsic LLRs are computed as

$$\lambda_k(c;O) = \max_{e:c(e)=c}^* \left\{ \alpha_{k-1}\left[s^S(e) \right] + \lambda_k[u(e);I] + \beta_k\left[s^E(e) \right] + h_c \right\}$$

..........(2.6)

$$\lambda_k(u;O) = \max_{e:u(e)=c}^* \left\{ \alpha_{k-1}\left[s^S(e) \right] + \lambda_k[c(e);I] + \beta_k\left[s^E(e) \right] + h_u \right\}$$

..........(2.7)

where the symbols in these equations are discussed in the subsequent paragraphs.

The name *extrinsic* given to the LLRs computed according to equations (2.6) and (2.7) derives from the fact that the evaluation of $\lambda_k(c;O)$ and $\lambda_k(u;O)$ does not depend on corresponding simultaneous input $\lambda_k(c;I)$ and $\lambda_k(u;I)$, respectively, so that it can be considered as an update of the input LLR based on information coming from all homologous symbols in the sequence, except the one corresponding to the same symbol interval.

The quantities h_c and h_u in equations (2.6) and (2.7) are normalization constants such that

$$h_c \rightarrow \sum_c \lambda_k[c;O] = 0$$

..........(2.8)

and

$$h_u \rightarrow \sum_c \lambda_k[u;O] = 0$$

..........(2.9)

respectively. This is to prevent excessive growth of the numerical values of the α's and β's.

The quantities $\alpha_k(.)$ and $\beta_k(.)$ in (2.6) and (2.7) are obtained through forward and backward recursions, respectively, as

$$\alpha_k(s) = \max_{e:s^E(e)=s}^{*} \left\{ \alpha_{k-1}\left[s^S(e)\right] + \lambda_k[u(e);I] + \lambda_k[c(e);I] \right\}, \quad k = 1,..,K-1$$

……….(2.10)

$$\beta_k(s) = \max_{e:s^S(e)=s}^{*} \left\{ \beta_{k+1}\left[s^E(e)\right] + \lambda_{k+1}[u(e);I] + \lambda_{k+1}[c(e);I] \right\}, \quad k = 1,..,K-1$$

……….(2.11)

with initial values

$$\alpha_o(s) = \begin{cases} 0, & s = S_o \\ -\infty, & \text{otherwise} \end{cases}$$

……….(2.12)

$$\beta_k(S_i) = \begin{cases} 0, & s = S_K \\ -\infty, & \text{otherwise} \end{cases}$$

……….(2.13)

The operator $\max^{*}$ performs the following operation:

$$\max_{j}^{*}(a_j) \overset{\Delta}{=} \log\left[\sum_{j=1}^{J} e^{a_j} \right]$$

……….(2.14)

This operation, a crucial one in affecting the computational complexity of the SISO, can be performed in practice [Ref. 47 and 48] as

$$\max_{j}^{*}(a_j) = \max_{j}(a_j) + \delta(a_1, a_2, ...a_J)$$

……….(2.15)

where $\delta(a_1, a_2, ... a_J)$ is a correction term that can be computed recursively using a single entry lookup table [Ref. 20 and 21].

The preceding description of the iterative decoder assumed that all operations were performed at symbol level. Quite often, the interleaver operates at the bit level. To perform bit interleaving, the symbol extrinsic LLRs obtained at the output of the first SISO are transformed into extrinsic bit LLRs before they enter the de-interleaver. After de-interleaving, the bit LLRs need to be compacted into symbol LLRs before entering the second SISO block, and so on. These operations are performed with the assumption that the bits forming a symbol are independent.

Assuming an (n, k) code and denoting with $\bar{u} = [u_1, \ldots u_k]$ the information symbol formed by k information bits, the extrinsic LLR λ_i of the ith bit u_i within the symbol $\bar{u}$ is obtained as

$$\lambda_i(u;O) = \max_{u:u_i=0}^{*} \left[\lambda(\bar{u};O) + \lambda(\bar{u};I)\right] - \max_{u:u_i=1}^{*} \left[\lambda(\bar{u};O) + \lambda(\bar{u};I)\right] - \lambda_i(u;I)$$

……….(2.16)

Conversely, the extrinsic LLR of the symbol $\bar{u}$ is obtained from the extrinsic LLRs of its component bits u_i as

$$\lambda(\bar{u}) = \sum_{i=1}^{p} \lambda_i(u_i)$$

……….(2.17)

The previous description makes it clear that the SISO algorithm requires the whole sequence to be received before starting. The reason is due to the backward recursion that starts from the final trellis state. As a consequence, practical application of the SISO algorithm is limited to the case where the duration of the transmission is short (K small). For long transmission, (K long), the received sequence can be segmented into independent consecutive blocks, as in block codes or convolutional codes with trellis termination [Ref. 49]. Furthermore, the SISO algorithm cannot be used for continuous decoding. A more flexible decoding strategy is obtained by modifying the algorithm in such as a way that the SISO module operates on a fixed memory span and outputs the smoothed probability distributions after a given delay. This algorithm is called the

sliding window, soft-input soft-output algorithm (SW-SISO) and is fully described in [Ref. 48]. In the simulation results presented in this dissertation, the SW-SISO algorithm has been applied.

C.   THEORETICAL BOUNDS IN AWGN

1.   BPSK

It is often impractical to generate simulation results for extremely low BER. As a result, bounds are often calculated. Turbo codes and SCCC are linear, so the union bound can be used to obtain an analytic expression for the probability of error. Note that the union bound applies to the optimal decoder, while the MAP iterations of the SCCC decoder are sub-optimal. Consequently, we do not necessarily expect the union bound results to be larger than the simulation results.

Consider the traditional union bound for the maximum likelihood decoding of a (n, k) block code. A linear uniform block (or convolutional code) possesses the uniform error property [Ref. 50], that is, both word and bit error probabilities can be evaluated given the assumption that the all-zero codeword has been transmitted. Without loss of generality, we assume that the all-zeros codeword was sent, and we write the upper bound on the probability of word error as

$$P_w \leq \sum_h \sum_w A_{w,h} P_2(h)$$

……….(2.18)

where $A_{w,h}$ is related to the Input-Output Weight Enumerating Function (IOWEF) defined by

$$A(W,H) = \sum_{w=0}^{k} \sum_{h=0}^{n} A_{w,h} W^w H^h$$

……….(2.19)

and $P_2(h)$ is the probability of incorrectly decoding a binary codeword with weight h. In (2.19), $A_{w,h}$ represents the number of codewords with weight h generated by information weight words of weight w. Hence, the SCCC's error probabilities for maximum likelihood (ML) soft decoding for binary phase-shift keying (BPSK) (or binary pulse

20

amplitude modulation (PAM)) transmission over an additive white Gaussian noise (AWGN) channel with two-sided noise power spectral density $N_o/2$ can be upper bounded as [Ref 20]

$$P_w \leq \sum_{h=h_m}^{N/R_c^i} \sum_{w=w_m^o}^{NR_c^o} A_{w,h}^{C_s} P_2(h)$$

……….(2.20)

and

$$P_b \leq \sum_{h=h_m}^{N/R_c^i} \sum_{w=w_m^o}^{NR_c^o} \frac{w}{NR_c^o} A_{w,h}^{C_s} P_2(h)$$

……….(2.21)

with

$$P_2(h) \leq Q\left(\sqrt{2R_c h E_b / N_o}\right)$$

……….(2.22)

for BPSK signals where

P_w is the word error probability,

P_b is the bit error probability,

E_b/N_o is the effective signal-to-noise ratio,

R_c^i is the code rate of the inner encoder, k_I/n_I,

R_c^o is the code rate of the outer encoder, k_o/n_o,

R_c is the code rate of the overall SCCC encoder given by $R_c^o \cdot R_c^i$,

N is the interleaver length,

h_m is the minimum weight of the codewords of C_s,

w_m^o is the minimum weight of the input sequence generating an error event of the outer code and,

$A_{w,h}^{C_s}$ consists of the weight enumerating coefficients of the concatenated code.

A more compact, but looser, upper bound can be obtained from (2.22) using the inequality

$$Q(x) < \frac{1}{2} e^{-x^2/2}$$

$$\ldots\ldots\ldots(2.23)$$

which yields

$$P_w \leq \sum_{h=h_m}^{N/R_c^i} \sum_{w=w_m^o}^{NR_c^o} \frac{1}{2} A_{w,h}^{C_s} e^{-hR_c E_b/N_o}$$

$$\ldots\ldots\ldots(2.24)$$

$$P_b \leq \sum_{h=h_m}^{N/R_c^i} \sum_{w=w_m^o}^{NR_c^o} \frac{1}{2} \frac{w}{NR_c^o} A_{w,h}^{C_s} e^{-hR_c E_b/N_o}$$

$$\ldots\ldots\ldots(2.25)$$

Note that equations (2.20) to (2.25) stem from the union bound that is based on the fact that the probability of the union of a number of individual events is less than or equal to the sum of probabilities of the individual events. The sums of the individual probabilities of the equations are not probabilities themselves and can assume values greater than one. The bounds are also based on maximum-likelihood decoding, whereas the SCCCs are codes are decoded using a different, suboptimum algorithm. This apparent inconsistency can be resolved through heuristic validation from a large number of simulations, which show the convergence of the simulated performance toward the analytical bounds for large random interleavers [Ref.20].

The coefficients $A_{w,h}^{C_s}$ of the equivalent block code that represents the SCCC can be obtained once the weight structures, $A_{w,l}^{C_o}$ (outer code) and $A_{l,h}^{C_i}$ (inner code), of the constituent codes are known and the interleaver has been defined. Since the coefficients $A_{w,h}^{C_s}$ are interleaver specific, in order to make our results interleaver independent except for interleaver length N, we assume a uniform interleaver. A uniform interleaver is a conceptual interleaver that transforms an input codeword of weight l into one of its distinct $\binom{N}{l}$ permutations with probability $\binom{N}{l}^{-1}$. In this case, the total number of possible codewords at the interleaver output of weight h associated with information

22

weight w is $A_{w,l}^{C_o} . A_{l,h}^{C_i}$, and one of these codewords is generated with probability $\binom{N}{l}^{-1}$.

As a result, for a uniform interleaver

$$A_{w,h}^{C_s} \approx \sum_{l=0}^{N} \frac{A_{w,l}^{C_o} . A_{l,h}^{C_i}}{\binom{N}{l}}$$

$$\ldots\ldots\ldots(2.26)$$

It has been shown that the bounds computed assuming a uniform interleaver are an average of all possible deterministic interleavers of the same length. One interesting result of assuming a uniform interleaver is that the coefficients $A_{w,h}^{C_s}$ are not necessarily integers as they are required to be for actual interleavers.

With block codes as constituent codes, determination of $A_{w,l}^{C_o}$ and $A_{l,h}^{C_i}$ is straightforward. With convolutional codes as constituent codes, determination of $A_{w,l}^{C_o}$ and $A_{l,h}^{C_i}$ is more difficult. By definition, nonzero codewords of the equivalent block code represent concatenations of error events of the constituent convolutional codes when the all-zero codeword is sent. Let $A_{l,h,j}$ be the input-output weight coefficients of a convolutional code given that the code concatenates j error events with a total input weight l and output weight h (Figure 2.4).
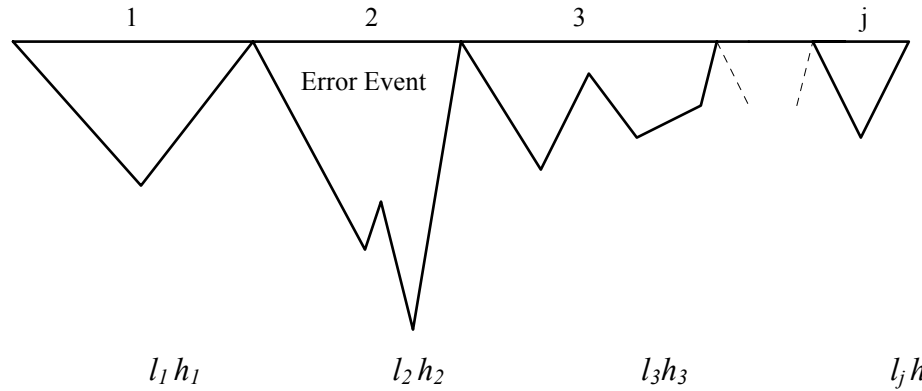
Figure 2.4.   A code sequence in $A_{l,h,j}$

For N much larger than the memory of the convolutional code, the weight coefficients $A_{l,h}^{C}$ of the equivalent block code can be approximated by [Ref. 20]

$$A_{l,h}^{C} \approx \sum_{j=1}^{n_M} \binom{N/p}{j} A_{l,h,j}^{C}$$

……….(2.27)

where n_M is the largest number of error events concatenated in a codeword of weight h and generated by a weight l input sequence, and h and l depend on the encoder.

The ratio N/p derives from the fact that the code rate of the outer encoder is k/p and the code rate of the inner encoder is p/n. (It is assumed here that k_I and n_o of Figure 2.1 are the same, denoted by p). The number of codewords from the outer encoder is N/p where p is the length of the codeword. For the inner encoder, the number of codewords is also p. Thus, N bits correspond to N/p symbols, or equivalently, trellis steps for the inner encoder. Note that N must be a multiple of p. Thus, using the superscripts "o" and "i" to refer to quantities pertaining to the outer and the inner code, respectively, the weight coefficients are:

$$A_{w,l}^{C_o} \approx \sum_{n^o=1}^{n_M^o} \binom{N/p}{n^o} A_{w,l,n^o}^{o}$$

……….(2.28)

$$A_{l,h}^{C_i} \approx \sum_{n^i=1}^{n_M^i} \binom{N/p}{n^i} A_{w,l,n^i}^{i}$$

……….(2.29)

Substituting (2.28) and (2.29) into (2.26), we obtain

$$A_{w,h}^{C_s} \approx \sum_{l=d_f^o}^{N} \sum_{n^o=1}^{n_M^o} \sum_{n^i=1}^{n_M^i} \frac{\binom{N/p}{n^o}\binom{N/p}{n^i}}{\binom{N}{l}} A_{w,l,n^o}^{o} A_{l,h,n^i}^{i}$$

……….(2.30)

where d_f^o is the free distance of the outer code.

24

We need to simplify equation (2.30). To obtain an upper bound, we replace the two binomial coefficients in the numerator with

$$\binom{N}{n} \ \langle \ \frac{N^n}{n!}$$

………..(2.31)

and the binomial coefficient in the denominator with

$$\binom{N}{l} \ \rangle \ \frac{(N-l+1)^l}{l!} \ \rangle \ \frac{N^l}{l^l l!}$$

……….(2.32)

This yields

$$A_{w,h}^{C_s} \approx \sum_{l=d_f^o}^{N} \sum_{n^o=1}^{n_M^o} \sum_{n^i=1}^{n_M^i} N^{n^o+n^i-l} \frac{l^l l!}{p^{n^o+n^i} n^o! n^i!} A_{w,l,n^o}^o A_{l,h,n^i}^i$$

……….(2.33)

Finally, substituting equation (2.33) into (2.24) and (2.25), we get

$$P_w \leq \sum_{h=h_m}^{N/R_c^i} \frac{1}{2} e^{-hR_c E_b/N_o} \sum_{w=w_m^o}^{NR_c^o} \sum_{l=d_f^o}^{N} \sum_{n^o=1}^{n_M^o} \sum_{n^i=1}^{n_M^i} N^{n^o+n^i-l} \frac{l^l l!}{p^{n^o+n^i} n^o! n^i!} A_{w,l,n^o}^o A_{l,h,n^i}^i$$

……….(2.34)

$$P_b \leq \sum_{h=h_m}^{N/R_c^i} \frac{1}{2} e^{-hR_c E_b/N_o} \sum_{w=w_m^o}^{NR_c^o} \sum_{l=d_f^o}^{N} \sum_{n^o=1}^{n_M^o} \sum_{n^i=1}^{n_M^i} N^{n^o+n^i-l-1} \frac{l^l l!}{p^{n^o+n^i-1} n^o! n^i!} \frac{w}{k} A_{w,l,n^o}^o A_{l,h,n^i}^i$$

……….(2.35)

For large N, defined as N >> v, where v is the constraint length of the larger encoder, the coefficient of the dominant term in either (2.34) or (2.35) is the one for which the exponent of N is maximum [Ref.20]. This exponent is defined as

$$\alpha_M = \max_{w,l,h} \{n^o + n^i - l - 1\}$$

……….(2.36)

For recursive convolutional encoders, the minimum weight of input sequences of the inner encoder generating error events is two. As a consequence, an input sequence of

weight l can generate at most $\left\lfloor \dfrac{l}{2} \right\rfloor$ error events, i.e., $n^i = n_M^i = \left\lfloor \dfrac{l}{2} \right\rfloor$. For the outer encoder, the maximum number of concatenated error events is

$$n_M^o \le \left\lfloor \frac{l}{d_f^o} \right\rfloor$$

……….(2.37)

Thus, equation (2.36) becomes

$$\alpha_M \le \max_l \left\{ \left\lfloor \frac{l}{d_f^o} \right\rfloor + \left\lfloor \frac{l}{2} \right\rfloor - l - 1 \right\}$$

$$= \left\{ \left\lfloor \frac{l}{d_f^o} \right\rfloor + \left\lfloor \frac{l+1}{2} \right\rfloor - 1 \right\}$$

……….(2.38)

For $d_f^o \ge 2$, equation (2.38) is maximized when $l = d_f^o$ [Ref. 20]. Thus,

$$\alpha_M = - \left\lfloor \frac{d_f^o + 1}{2} \right\rfloor$$

……….(2.39)

For even d_f^o, the weight h associated with the highest exponent of N is given by [Ref.20]

$$h = \frac{d_f^o d_{f,eff}^i}{2}$$

……….(2.40)

since this is the weight of an inner codeword that concatenates $d_f^o / 2$ error events with weight $d_{f,eff}^i$, where $d_{f,eff}^i$ is the minimum weight of codewords of the inner code generated by weight-2 sequences. Substituting equation (2.40) into (2.36) and (2.37), we get

$$P_w \le \sum_{w=w_m^o}^{NR_c^o} \frac{1}{2} e^{-\frac{d_f^o d_{f,eff}^i}{2} R_c E_b / N_o} N^{-d_f^o/2+1} \frac{d_f^{o\,d_f^o} d_f^o!}{p^{d_f^o/2+1}(d_f^o/2)!} A_{w,d_f^o,1}^o A_{d_f^o,(d_f^o d_{f,eff}^i/2),d_f^o/2}^i$$

……….(2.41)

26

$$P_b \leq \sum_{w=w_m^o}^{NR_c^o} \frac{1}{2} e^{-\frac{d_f^o d_{f,eff}^i}{2} R_c E_b/N_o} N^{-d_f^o/2} \frac{d_f^{o} {}^{d_f^o} d_f^o!}{p^{d_f^o/2}(d_f^o/2)!} \frac{w}{k} A_{w,d_f^o,1}^o A_{d_f^o,(d_f^o d_{f,eff}^i/2),d_f^o/2}^i$$

……….(2.42)

For odd d_f^o the weight h associated with the highest exponent of N is given by [Ref.20]

$$h = \frac{(d_f^o - 3)d_{f,eff}^i}{2} + h_3$$

……….(2.43)

where h_3 is the minimum weight of sequences of the inner code generated by a weight-3 input sequence. In this case we have

$$n_M^i = \frac{d_f^o - 1}{2}$$

……….(2.44)

concatenated error events, of which $n_M^i - 1$ are generated by weight-2 input sequences and one is generated by a weight-3 input sequence. The maximum exponent α_M remains unchanged. Thus, substituting equation (2.43) into (2.36) and (2.37), we get

$$P_w \leq \sum_{w=w_m^o}^{NR_c^o} \frac{1}{2} e^{-\left(\frac{(d_f^o-3)d_{f,eff}^i}{2}+h_3\right)R_c E_b/N_o} N^{-(d_f^o-1)/2} \frac{d_f^{o} {}^{d_f^o} d_f^o!}{p^{(d_f^o+1)/2}((d_f^o-3)/2)!} A_{w,d_f^o,1}^o A_{d_f^o,\frac{(d_f^o-3)d_{f,eff}^i}{2}+h_3,(d_f^o-1)/2}^i$$

……….(2.45)

$$P_b \leq \sum_{w=w_m^o}^{NR_c^o} \frac{1}{2} e^{-\left(\frac{(d_f^o-3)d_{f,eff}^i}{2}+h_3\right)R_c E_b/N_o} N^{-(d_f^o+1)/2} \frac{d_f^{o} {}^{d_f^o} d_f^o!}{p^{(d_f^o-1)/2}((d_f^o-3)/2)!} \frac{w}{k} A_{w,d_f^o,1}^o A_{d_f^o,\frac{(d_f^o-3)d_{f,eff}^i}{2}+h_3,(d_f^o-1)/2}^i$$

……….(2.46)

Recall that the preceding analysis stems from the union bound. The union bound is used extensively as an upper limit to the error probabilities for digital transmission systems. It is common knowledge in the field that union bounds are very close to the true error probability in the case of maximum likelihood decoding for medium to high signal-to-noise ratios. Union bounds become unreliable as the cutoff rate of the channel is approached [Ref.20]

27

Henceforth, equations (2.45) and (2.46) (instead of (2.41) and (2.42)) will be used in this dissertation since the encoder used in the simulations has odd d_f^o. Equations (2.45) and (2.46) can be rewritten in a more generalized way (i.e., in the form of (2.20) and (2.21) and without reference to BPSK) as

$$P_w \le \sum_{w=w_m^o}^{NR_c^o} N^{-(d_f^o-1)/2} \frac{d_f^{o\, d_f^o} d_f^o!}{p^{(d_f^o+1)/2}((d_f^o-3)/2)!} A^o_{w,d_f^o,1} A^i_{d_f^o,h,(d_f^o-1)/2} P_2(h)$$

$$\ldots\ldots\ldots(2.47)$$

$$P_b \le \sum_{w=w_m^o}^{NR_c^o} N^{-(d_f^o+1)/2} \frac{d_f^{o\, d_f^o} d_f^o!}{p^{(d_f^o-1)/2}((d_f^o-3)/2)!} \frac{w}{k} A^o_{w,d_f^o,1} A^i_{d_f^o,h,(d_f^o-1)/2} P_2(h)$$

$$\ldots\ldots\ldots(2.48)$$

For BPSK, $P_2(h)$ is given by (2.22) with h given by (2.43).

2. DPSK

In computing the BER for DPSK, we can apply (2.47) and (2.48) by substituting the equivalent $P_2(h)$ for DPSK [Ref. 51]. For convolutional codes, this is equivalent to binary DPSK with h-order diversity. Thus,

$$P_2(h) = \frac{1}{2^{2h-1}} \exp\left[-\frac{hR_c E_b}{N_o}\right] \sum_{n=0}^{h-1} C_n \left[\frac{hR_c E_b}{N_o}\right]^n$$

$$\ldots\ldots(2.49)$$

where

$$C_n = \frac{1}{n!} \sum_{m=0}^{h-1-n} \binom{2h-1}{m}$$

$$\ldots\ldots(2.50)$$

Substituting (2.49) and (2.50) into (2.47) and (2.48), we obtain

$$P_w \leq \sum_{w=w_m^o}^{NR_c^o} N^{-(d_f^o-1)/2} \frac{d_f^{o d_f^o} d_f^o!}{p^{(d_f^o+1)/2}((d_f^o-3)/2)!} A_{w,d_f^o,1}^o A_{d_f^o,\frac{(d_f^o-3)d_{f,eff}^i}{2}+h_3,(d_f^o-1)/2}^i$$

$$\frac{1}{2^{2\left(\frac{(d_f^o-3)d_{f,eff}^i}{2}+h_3\right)-1}} \exp\left[-\frac{\left(\frac{(d_f^o-3)d_{f,eff}^i}{2}+h_3\right)R_c E_b}{N_o}\right]^{\left(\frac{(d_f^o-3)d_{f,eff}^i}{2}+h_3\right)-1} \sum_{n=0}^{\left(\frac{(d_f^o-3)d_{f,eff}^i}{2}+h_3\right)-1-n} \frac{1}{n!} \sum_{m=0}^{} \left(2\left(\frac{(d_f^o-3)d_{f,eff}^i}{2}+h_3\right)-1\right) \left[\frac{\left(\frac{(d_f^o-3)d_{f,eff}^i}{2}+h_3\right)R_c E_b}{N_o}\right]^n$$

..........(2.51)

$$P_b \leq \sum_{w=w_m^o}^{NR_c^o} N^{-(d_f^o+1)/2} \frac{d_f^{o d_f^o} d_f^o!}{p^{(d_f^o-1)/2}((d_f^o-3)/2)!} \frac{w}{k} A_{w,d_f^o,1}^o A_{d_f^o,\frac{(d_f^o-3)d_{f,eff}^i}{2}+h_3,(d_f^o-1)/2}^i$$

$$\frac{1}{2^{2\left(\frac{(d_f^o-3)d_{f,eff}^i}{2}+h_3\right)-1}} \exp\left[-\frac{\left(\frac{(d_f^o-3)d_{f,eff}^i}{2}+h_3\right)R_c E_b}{N_o}\right]^{\left(\frac{(d_f^o-3)d_{f,eff}^i}{2}+h_3\right)-1} \sum_{n=0}^{\left(\frac{(d_f^o-3)d_{f,eff}^i}{2}+h_3\right)-1-n} \frac{1}{n!} \sum_{m=0}^{} \left(2\left(\frac{(d_f^o-3)d_{f,eff}^i}{2}+h_3\right)-1\right) \left[\frac{\left(\frac{(d_f^o-3)d_{f,eff}^i}{2}+h_3\right)R_c E_b}{N_o}\right]^n$$

..........(2.52)

D.   THEORETICAL BOUNDS IN AWGN AND RAYLEIGH FADING

Since SCCC is based on the concept of maximum likelihood decision on blocks of data, the decision on a bit affects the decoding of subsequent bits. Because the effect of fading can be extended over a period of multiple bits, the impact of fading on SCCC performance is crucial.   A channel interleaver is used to break the correlated channel disturbance into independently corrupted channel symbols that, in turn, can be effectively corrected by forward error correction codes. The interleaver in the SCCC is also used for this purpose. The larger the interleaving size, the wider the correlated symbols can be separated, and consequently, the better the performance. Here, we assume that the fade for each symbol is independent. Others [Ref. 52, 53] have addressed the performance of Turbo codes in the presence of non-fully interleaved flat Rayleigh fading. We also considered the fading to be flat. The term flat fading implies that all frequencies of the transmitted signal are modulated by the same function [Ref. 54]. The fading function is described by a probability density function and a frequency dispersion measure, B, often referred to as the Doppler spread (or bandwidth). If the Doppler spread is small compared to the reciprocal of the symbol rate, the fading process is considered slow. For slow fading processes, the channel gain can be assumed constant over the symbol

duration. Throughout this work, slow fading will be assumed. Receivers may also be able to estimate the channel gains due to fading. Knowledge of the channel gains due to fading will be referred as channel information (CI). Channel information can be gained through the use of an auxiliary channel or from a direct examination of the signal-to-noise ratio.

1.   BPSK

Here we consider coherent BPSK signaling over a flat, frequency non-selective and independent Rayleigh slow fading channel. With appropriate sampling, the discrete representation of this channel is

$$y_k = a_k x_k + n_k$$

……….(2.53)

where k is an integer symbol index, x_k is the BPSK signal amplitude $(\pm\sqrt{E_s})$ and n_k is an independent identically distributed AWGN component with zero mean and two-sided power spectral density $N_o/2$. The channel gain a_k is modeled with a Rayleigh probability density function,

$$p_A(a_k) = 2a_k e^{-a_k^2} \quad \text{for } a_k > 0$$

……….(2.54)

With sufficient channel interleaving (fully interleaved), the a_k's are independent. It is assumed here that the bits are fully interleaved after passing through the interleaver in the SCCC.

For the fully interleaved channel with no channel information, we use the bound developed by Hagenauer [Ref. 55]:

$$P_2(h) \le e^{h(\beta/\gamma)} \left[\frac{\sqrt{1+\left(\frac{2}{\beta}\right)}-1}{\sqrt{1+\left(\frac{2}{\beta}\right)}+1} \right]^h$$

……….(2.55)

where

$$\beta = \sqrt{\gamma^2 + 1} - 1$$

………..(2.56)

and

$$\gamma = \frac{R_c E_b}{N_o}$$

………..(2.57)

For Turbo coded or SCCC systems in fading environments, the channel gain must be provided to the decoder in order to gain the full potential [Ref. 56]. However, in practice, perfect knowledge of the channel gain is difficult to obtain. Several estimation methods for flat fading channels, such as the lowpass filter [Ref. 57] or the pilot symbol assisted modulation technique [Ref. 58], have been proposed. Valenti [Ref. 59] proposed a decision directed channel estimation strategy. Pilot symbols are used to assist channel estimation prior to the first iteration. For subsequent decoder iterations, the channel is re-estimated using both the pilot symbols and the decoded symbols with reliability above a certain threshold. Here, we assume perfect knowledge of the channel gain.

On the fully interleaved channel with channel information, the probability of incorrectly decoding a codeword c_o as codeword c_j which differs from c_o in h bit positions is

$$P(c_o \rightarrow c_j | a) = Q\left(\sqrt{\frac{2R_c E_b}{N_o} \sum_{k=1}^{h} a_{i_k}^2} \right)$$

………..(2.58)

Here, $Q(x)$ is the tail integral of a standard Gaussian density with zero mean and unit variance defined as

$$Q(x) = \int_x^\infty \frac{1}{\sqrt{2\pi}} e^{-\frac{x^2}{2}} \, dz$$

………..(2.59)

To compute the average word error probability, we must average $P(c_o \rightarrow c_j)$ over the channel gains a_k. The result is a multidimensional integral given by

$$P(c_o \rightarrow c_j) = \int_{a_{i_1}} \cdots \int_{a_{i_d}} p_A(a_{i_1}, a_{i_2}, \ldots, a_{i_d}) . P(c_o \rightarrow c_j | a) \, da_{i_1} \ldots da_{i_d}$$

$$\ldots\ldots\ldots(2.60)$$

If the channel gains are independent, the indexes of the differing bit positions are of no importance, only the weight of the incorrect codeword matters. Therefore, we can formulate the probability in terms of only the Hamming distance of the codewords in equations (2.47) and (2.48) as

$$P_2(h) = \int_{a_{i_1}} \cdots \int_{a_{i_d}} p_A(a_{i_1}, a_{i_2}, \ldots, a_{i_d}) . Q\left(\sqrt{\frac{2R_c E_b}{N_o} \sum_{k=1}^{h} a_k^2}\right) da_{i_1} \ldots da_{i_d}$$

$$\ldots\ldots\ldots(2.61)$$

and

$$p_A(a_i, a_i, \ldots, a_i) = \prod_{i=1}^{d} p_A(a_i)$$

$$\ldots\ldots\ldots(2.62)$$

For the average upper bound, we need an exact representation of $P_2(h)$ or a tight upper bound. The exact evaluation of (2.61) is difficult. Some authors have proposed numerical solutions and some upper bounds [Ref. 52, 60, 61]. Exact solutions have been found using diversity techniques and characteristic functions [Ref.51] and integration methods [Ref. 62]. Here, equation (2.58) is represented as

$$P_2(\gamma_b, h) = Q\left(\sqrt{2\gamma_b}\right)$$

$$\ldots\ldots\ldots(2.63)$$

where

$$\gamma_b = \frac{R_c E_b}{N_o} \sum_{k=1}^{h} a_k^2$$

$$= \sum_{k=1}^{h} \gamma_k$$

$$\ldots\ldots\ldots(2.64)$$

and

$$\gamma_k = \frac{R_c E_b a_k^2}{N_o}$$

………..(2.65)

For a Rayleigh fading channel, a_k is modeled as a Rayleigh random variable, and

$$f_{\Gamma_k}(\gamma_k) = \frac{1}{\bar{\gamma}_c} \exp\left(-\frac{\gamma_k}{\bar{\gamma}_c}\right) u(\gamma_k)$$

………..(2.66)

where $\bar{\gamma}_c$ is the average signal-to-noise ratio per channel given by

$$\bar{\gamma}_c = \frac{R_c E_b}{N_o} E(a_k^2)$$
$$= \frac{R_c E_b}{N_o}$$

………..(2.67)

The characteristic function of (2.66) is

$$\varphi_{\gamma_1}(jv) = E\left(e^{jv\gamma_1}\right)$$
$$= \frac{1}{1 - jv\bar{\gamma}_c}$$

………..(2.68)

and $E(a_k^2)$ is one for a central chi-square distribution of degree one.

Since the average SNR per channel is assumed identical for all channels and the fading on the h channels is assumed to be statistically independent, the $\{\gamma_k\}$'s are statistically independent, and the characteristic function of (2.64) is (2.68) raised to the hth power:

$$\varphi_{\gamma_b}(jv) = \frac{1}{\left(1 - jv\bar{\gamma}_c\right)^h}$$

………..(2.69)

This is the characteristic function of a chi-square distributed random variable with $2h$ degrees of freedom. Thus,

33

$$p(\gamma_b) = \frac{1}{(h-1)!\bar{\gamma}_c^h}\gamma_b^{h-1}e^{-\gamma_b/\bar{\gamma}_c}$$

……….(2.70)

We now evaluate the integral

$$P_2(h) = \int_0^\infty P_2(\gamma_b,h)p(\gamma_b)d\gamma_b$$

……….(2.71)

which yields the closed form solution

$$P_2(h) = \left[\frac{1}{2}(1-\mu)\right]^h \sum_{k=0}^{h-1}\binom{h-1+k}{k}\left[\frac{1}{2}(1+\mu)\right]^k$$

……….(2.72)

where

$$\mu = \sqrt{\frac{\bar{\gamma}_c}{1+\bar{\gamma}_c}}$$

……….(2.73)

Equation (2.72) can then be substituted into equations (2.47) and (2.48) to obtain the word and bit probability of error, respectively, for SCCC/BPSK with Rayleigh fading:

$$P_w \le \sum_{w=w_m^o}^{NR_c^o} N^{-(d_f^o-1)/2}\frac{d_f^{o\,d_f^o}d_f^o!}{p^{(d_f^o+1)/2}((d_f^o-3)/2)!}A_{w,d_f^o,1}^o A_{d_f^o,\frac{(d_f^o-3)d_{f,eff}^i}{2}+h_3,(d_f^o-1)/2}^i$$

$$\left[\frac{1}{2}\left(1-\sqrt{\frac{\bar{\gamma}_c}{1+\bar{\gamma}_c}}\right)\right]^{\frac{(d_f^o-3)d_{f,eff}^i}{2}+h_3}\sum_{k=0}^{\frac{(d_f^o-3)d_{f,eff}^i}{2}+h_3-1}\binom{\frac{(d_f^o-3)d_{f,eff}^i}{2}+h_3-1+k}{k}\left[\frac{1}{2}\left(1+\sqrt{\frac{\bar{\gamma}_c}{1+\bar{\gamma}_c}}\right)\right]^k$$

……….(2.74)

$$P_b \le \sum_{w=w_m^o}^{NR_c^o} N^{-(d_f^o+1)/2}\frac{d_f^{o\,d_f^o}d_f^o!}{p^{(d_f^o-1)/2}((d_f^o-3)/2)!}\frac{w}{k}A_{w,d_f^o,1}^o A_{d_f^o,\frac{(d_f^o-3)d_{f,eff}^i}{2}+h_3,(d_f^o-1)/2}^i$$

$$\left[\frac{1}{2}\left(1-\sqrt{\frac{\bar{\gamma}_c}{1+\bar{\gamma}_c}}\right)\right]^{\frac{(d_f^o-3)d_{f,eff}^i}{2}+h_3}\sum_{k=0}^{\frac{(d_f^o-3)d_{f,eff}^i}{2}+h_3-1}\binom{\frac{(d_f^o-3)d_{f,eff}^i}{2}+h_3-1+k}{k}\left[\frac{1}{2}\left(1+\sqrt{\frac{\bar{\gamma}_c}{1+\bar{\gamma}_c}}\right)\right]^k$$

……….(2.75)

where μ is given by (2.73).

2.   DPSK

In order for DPSK to be a viable digital signaling method, the channel variations must be sufficiently slow so that the channel phase shifts do not change considerably over two consecutive signaling intervals. In the BPSK case, it is assumed that noiseless estimates of the channel parameters are available at the receiver. For DPSK, since noncoherent detection is assumed, no channel information is used. For Rayleigh fading without channel information, the same results obtained by different authors, sometimes in different forms, are used to get [Ref. 51, 63, 64]:

$$P_2(h) = \left[\frac{1}{2}(1-\mu) \right]^h \sum_{k=0}^{h-1} \binom{h-1+k}{k} \left[\frac{1}{2}(1+\mu) \right]^k$$

.……….(2.76)

where

$$\mu = \frac{\overline{\gamma}_c}{1+\overline{\gamma}_c}$$

.……….(2.77)

and

$$\overline{\gamma}_c = \frac{R_c E_b}{N_o}$$

.……….(2.78)

Equation (2.76) can then be substituted into equations (2.47) and (2.48) to obtain the word and bit probability of error, respectively, for SCCC/DPSK with Rayleigh fading:

$$P_w \leq \sum_{w=w_m^o}^{NR_c^o} N^{-(d_f^o-1)/2} \frac{d_f^{o\,d_f^o} d_f^o!}{p^{(d_f^o+1)/2} ((d_f^o-3)/2)!} A_{w,d_f^o,1}^o A_{d_f^o, \frac{(d_f^o-3)d_{f,eff}^i}{2}+h_3,(d_f^o-1)/2}^i$$

$$\left[\frac{1}{2} \left(1 - \frac{\overline{\gamma}_c}{1+\overline{\gamma}_c} \right) \right]^{\frac{(d_f^o-3)d_{f,eff}^i}{2}+h_3} \sum_{k=0}^{\frac{(d_f^o-3)d_{f,eff}^i}{2}+h_3-1} \binom{\frac{(d_f^o-3)d_{f,eff}^i}{2}+h_3-1+k}{k} \left[\frac{1}{2} \left(1 + \frac{\overline{\gamma}_c}{1+\overline{\gamma}_c} \right) \right]^k$$

.……….(2.79)

$$P_b \leq \sum_{w=w_m^o}^{NR_c^o} N^{-(d_f^o+1)/2} \frac{d_f^{o\,d_f^o} d_f^o!}{p^{(d_f^o-1)/2}((d_f^o-3)/2)!} \frac{w}{k} A_{w,d_f^o,1}^o A_{d_f^o,\frac{(d_f^o-3)d_{f,eff}^i}{2}+h_3,(d_f^o-1)/2}^i$$

$$\left[\frac{1}{2}\left(1-\frac{\overline{\gamma}_c}{1+\overline{\gamma}_c}\right)\right]^{\frac{(d_f^o-3)d_{f,eff}^i}{2}+h_3} \sum_{k=0}^{\frac{(d_f^o-3)d_{f,eff}^i}{2}+h_3-1} \binom{\frac{(d_f^o-3)d_{f,eff}^i}{2}+h_3-1+k}{k}\left[\frac{1}{2}\left(1+\frac{\overline{\gamma}_c}{1+\overline{\gamma}_c}\right)\right]^k$$

..........(2.80)

E. FACTORS AFFECTING PERFORMANCE

1. Number of iterations

The number of iterations affects the SCCC performance: generally, the greater the number of iterations, the better the performance. However, this performance improvement is limited by the interleaver length and its dispersion and spreading factors (see paragraph 2 below). For a given interleaver length, the performance gain becomes negligible after a certain number of iterations.

2. Interleaver

The interleaver in the SCCC scrambles the bits in each block of data before it enters the second encoder so that the inputs to the individual constituent codes are not correlated. The decoder also assumes that the inputs to the component decoders are not correlated. By de-coupling the inputs to the two encoders, the interleaver provides a good codeword distribution that improves decoder performance.

The performance of the iterative decoder depends on the length, dispersion, and spreading factors of the interleaver. The more random an interleaver is, the higher its dispersion. The spreading factor of an interleaver refers to how far apart two consecutive bits are spread. For a given set of component codes, the SCCC with a longer interleaver has a better performance. Longer interleavers are used for higher data rates where the resulting latency is tolerable. For the same set of component codes and interleaver size, the higher the dispersion and spreading of the interleaver, the better the performance. Research is on-going in the search for the ideal interleaver. Selection based on information bits [Ref. 65, 66], generator matrices [Ref. 67], correlation properties of extrinsic information [Ref. 68], non-uniform interleavers [Ref. 69], interleaver growth

algorithms of polynomial complexity [Ref. 70], the Hungarian method [Ref. 71] and the combination of convolutional code design with interleaver design [Ref. 72] are all under investigation. Definitions of and further discussion on the parameters of interleavers are found in [Ref. 73].

3. Constraint Length

One important measure in designing convolutional codes is the constraint length v, which is related to the number of input bits that affect a single output stream. In general, the constraint length is taken to be the length of the longest input register plus one, $v = m + 1$. Component codes with different constraint lengths produce different results. The higher the constraint length, the better the performance [Ref. 2, 74, 75]. However, computational complexity increases, and the implementation become more expensive, and ultimately, decoding becomes physically unrealizable [Ref. 2]. Battail [Ref. 75] proposes using a decoding algorithm with a complexity that is independent of its constraint length, such as replication decoding.

4. Type of encoding and decoding

Results have shown that continuous encoding always yields the best performance [Ref. 76, 77]. Continuous encoding enjoys a 0.1 dB advantage over block encoding for a 16-state Turbo code. The difference in continuous and block encoding increases as the number of states of the constituent codes increases. Block encoding and decoding with trellis termination is used in this dissertation. This requires the appending of extra bits to the block in order to drive the constituent encoders to the zero state.

5. Puncturing

In general, puncturing degrades performance slightly [Ref. 78], but offers a convenient way to increase the code rate of the SCCC. The same inner decoder can be used as the outer decoder through puncturing and by controlling the metric memory access, soft decisions, and channel state information according to the puncturing rule [Ref. 79]. Other studies show that using a punctured outer encoder instead of a non-recursive encoder can result in better BER performance [Ref. 80].

THIS PAGE INTENTIONALLY LEFT BLANK

III. SIMULATION MODEL

In Chapter II, the SCCC encoder is formed by concatenating the constituent codes in series, with the two encoders separated by an interleaver. As in the original work by Berrou [Ref. 8] for Turbo codes, the constituent codes used here are recursive, systematic convolutional codes; although, the outer encoder for SCCC need not be recursive. The outer encoder takes as input a data sequence, and its output code sequence is interleaved and used as input to the inner encoder. The resulting coded sequence is then modulated and transmitted through a channel with AWGN and narrowband interference such as intentional jamming and/or Rayleigh fading. On the receiver end, the received bits are demodulated and then decoded by the SCCC decoder (Figure 3.1).
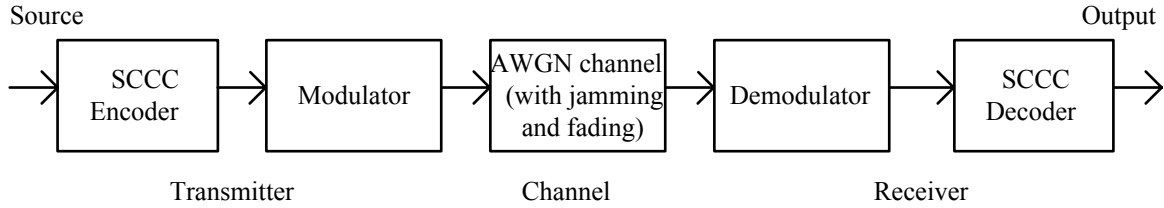
Figure 3.1.   Simulation model.

A.   SCCC TRANSMITTER

The transmitter consists of a SCCC encoder and modulator. The SCCC encoder considered here is a (3,1,N) SCCC using an outer 2-state (3,2) recursive convolutional (RSC) encoder (punctured from a rate ½ encoder) and an inner 2-state (2,1) RSC encoder (Figure 3.2). This gives an overall code rate of 1/3. Two types of modulation will be considered here. The first type is binary phase-shift keying (BPSK) and the second type is binary differential phase-shift keying (DPSK).

Source → Outer encoder (3, 2) → Interleaver Length = 963 → Inner encoder (2, 1) → to modulator
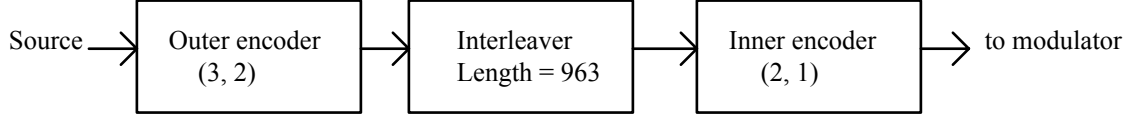
Figure 3.2.   SCCC encoder

1.   Design Rules

To achieve the best results, Benedetto, Divsalar, Montorsi and Pollara [Ref. 20] have formulated several SCCC design rules. The rules are:

a.   Since a recursive systematic convolutional (RSC) inner encoder always yields an interleaver gain, the inner encoder should be a convolutional recursive encoder. Moreover, these RSC encoders exhibited superior performance in regions of low signal-to-noise as compared to the non-recursive ones [Ref. 81].

b.   The effective free distance of the inner code must be maximized.

c.   The interleaver gain is equal to $N^{-(d_f^o/2)}$ for even values of d_f^o and to $N^{-(d_f^o+1/2)}$ for odd values of d_f^o. Thus, to minimize bit error rate, the effective free distance of the outer encoder must be maximized and odd.

d.   It is suggested in [Ref. 20] that a non-recursive convolutional encoder be used as an outer encoder to obtain better performance. Although theoretically this is true, other results indicate that employing a recursive convolutional encoder as an outer encoder results in better BER performance when higher rate outer encoders are obtained via puncturing [Ref. 80]. Moreover, there is commonality when both inner and outer encoders are the same, albeit the outer encoder is punctured to achieve a higher rate. It has also been shown that the same decoder can be used for the punctured code by controlling the metric memory access through the puncturing rule, soft decisions, and channel state information [Ref. 79]. Hence, a recursive outer encoder is used in this dissertation.

Consequently, the best rate ½ recursive convolutional encoder with the best free distance for a given code rate is selected. For ease of implementation, a memory size of two is chosen for each encoder. Encoders with higher memory sizes would improve the BER performance but would also increase the decoding complexity [Ref. 2, 82, 83].

2. Outer Encoder (Rate 2/3 RSC Encoder)

The characteristics of the outer encoder are displayed as follows:

a. the 2-state rate 2/3 encoder is shown in Figure 3.3,

b. the state diagram is shown in Figure 3.4,

c. the trellis diagram is shown in Figure 3.5,

d. the signal flow graph is shown in Figure 3.6,

where the exponent of W represents the Hamming weight of information bits and the exponent of H represents the Hamming weight of the output code sequence for each transition.
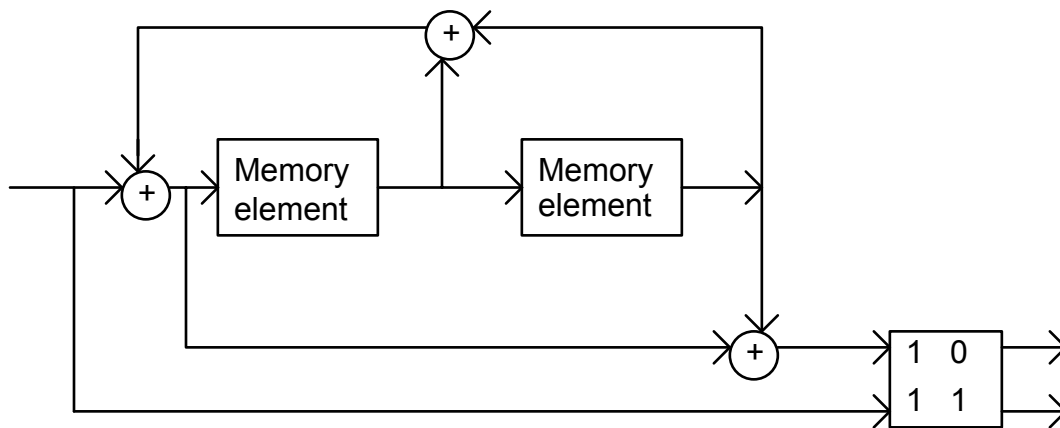
Figure 3.3.   Rate 2/3 encoder (punctured from rate ½ encoder)
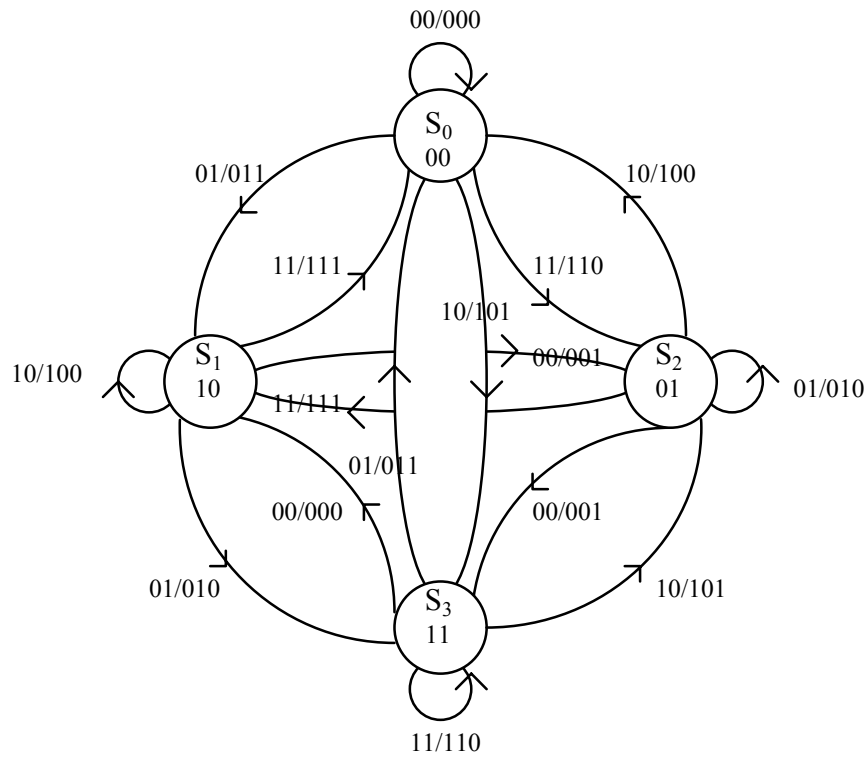
Figure 3.4.   State diagram for rate 2/3 code.
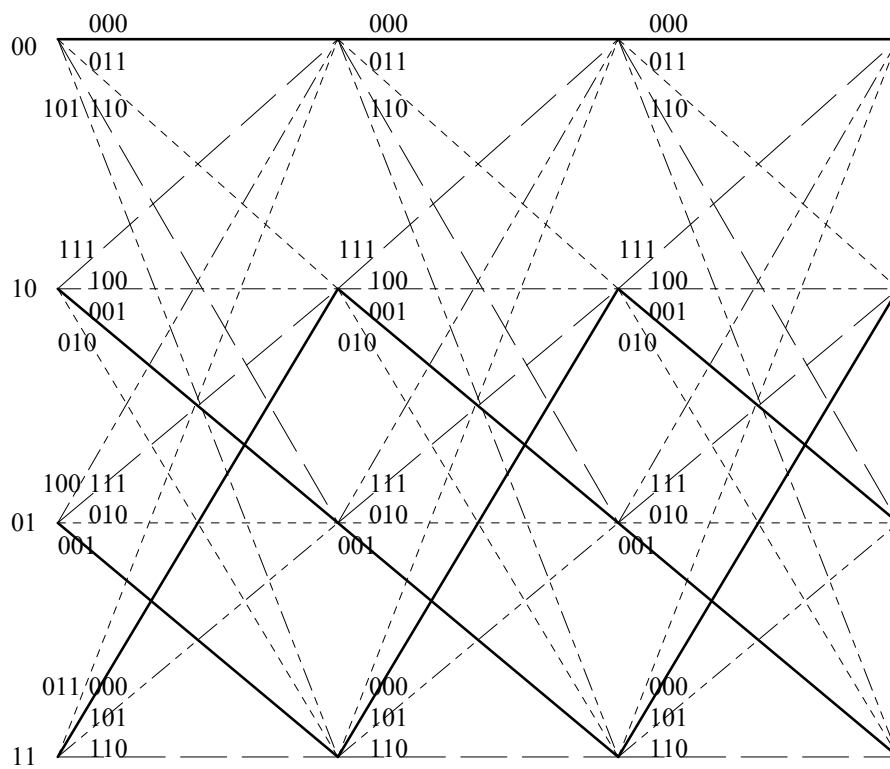
Figure 3.5.   Trellis for Rate 2/3 Code.

42
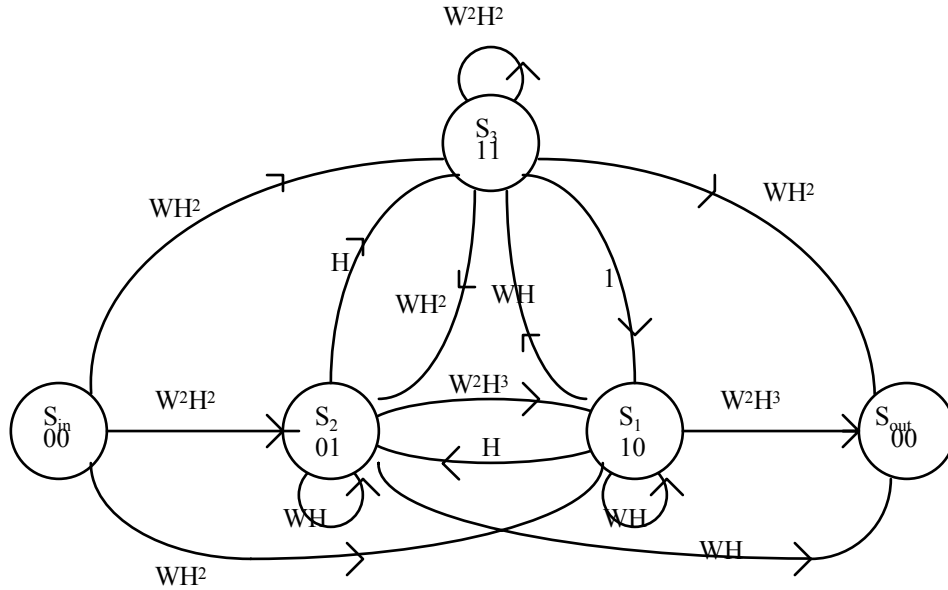
Figure 3.6.   Signal flow graph for rate 2/3 code

The transfer function of a convolutional code may be evaluated by solving equations describing the transitions between the states of the finite state encoder. Following the procedure described by Viterbi [Ref. 84], the state transition behavior within the state diagram may be described by the following matrix equations:

$$\begin{bmatrix} S_1 \\ S_2 \\ S_3 \end{bmatrix} = \begin{bmatrix} WH & W^2H^3 & 1 \\ H & WH & WH^2 \\ WH & H & W^2H^2 \end{bmatrix} \begin{bmatrix} S_1 \\ S_2 \\ S_3 \end{bmatrix} + \begin{bmatrix} WH^2 \\ W^2H^2 \\ WH^2 \end{bmatrix} [S_{in}]$$

..........(3.1)

$$[S_{out}] = [W^2H^3 \quad WH \quad WH^2] \begin{bmatrix} S_1 \\ S_2 \\ S_3 \end{bmatrix}$$

..........(3.2)

These equations can be represented in matrix notation as:

$$X = [A] X + F S_{in}$$

..........(3.3)

$$S_{out} = G X$$

..........(3.4)

43

where **X**, **F**, **[A]**, and **G** can be identified by comparing (3.1) and (3.2) with (3.3) and (3.4). Solving the above two equations, we obtain:

$$T\,(W,\,H) = S_{out}/\,S_{in} = \mathbf{G}\ [\mathbf{I\text{-}A}]^{-1}\,\mathbf{F}$$

………..(3.5)

where **I** is the identity matrix. Substituting the vectors and matrices represented by **G**, **F**, and **[A]** , we get

$$T(W,H) = \frac{S_{out}}{S_{in}} = \begin{bmatrix} W^2H^3 & WH & WH^2 \end{bmatrix}\begin{bmatrix} I - \begin{bmatrix} WH & W^2H^3 & 1 \\ H & WH & WH^2 \\ WH & H & W^{2}2H^2 \end{bmatrix} \end{bmatrix}^{-1}\begin{bmatrix} WH^2 \\ W^2H^2 \\ WH^2 \end{bmatrix}$$

$$= W^3H^3 + (3W^2 + W^4)H^4 + \dots$$

$$= \sum_{h=3}^{\infty}\sum_{w=2}^{\infty} A_{w,h}^{C_o} W^w H^h$$

……….(3.6)

The transfer function yields the coefficients $A_{w,h}^{C_o}$ for the outer encoder.

3.   Inner Encoder (Rate ½ RSC Encoder)

The characteristics of the inner encoder are displayed as follows:

a.   the 2-state rate ½ encoder is shown in Figure 3.7,

b.   the state diagram is shown in Figure 3.8,

c.   the trellis diagram is shown in Figure 3.9,

d.   the signal flow graph is shown in Figure 3.10.
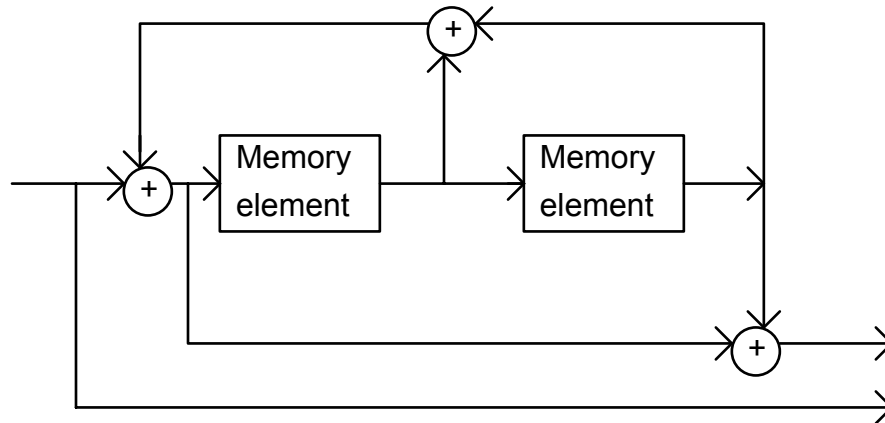
Figure 3.7.   Rate ½ encoder.
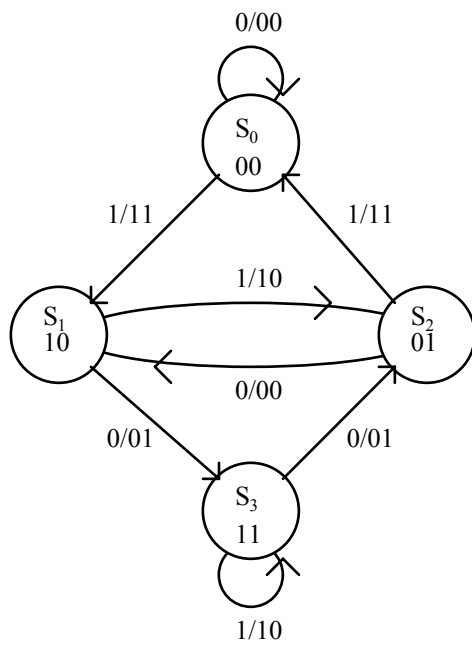
Figure 3.8.   State diagram for rate ½ code.
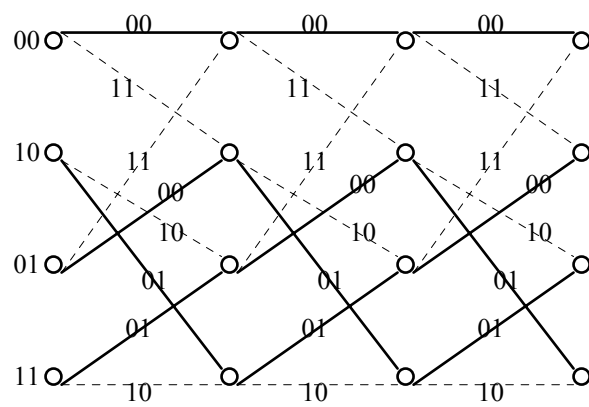
Figure 3.9.   Trellis for rate ½ code.

WH

S_3
11

H   H

S_{in}
00

WH²

S_1
10

WH

1

S_2
01

WH²

S_{out}
00
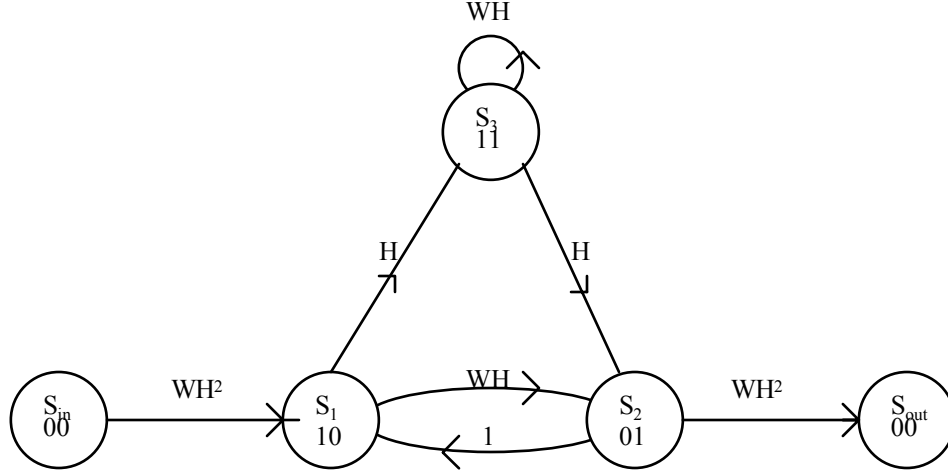
Figure 3.10.   Signal flow graph for rate ½ code.

Using the same procedure described earlier for the outer encoder, the transfer function for the rate 1/2 encoder is obtained from:

$$
\begin{bmatrix} S_1 \\ S_2 \\ S_3 \end{bmatrix} = \begin{bmatrix} 0 & 1 & 0 \\ WH & 0 & H \\ H & 0 & WH \end{bmatrix} \begin{bmatrix} S_1 \\ S_2 \\ S_3 \end{bmatrix} + \begin{bmatrix} WH^2 \\ 0 \\ 0 \end{bmatrix} \begin{bmatrix} S_{in} \end{bmatrix}
$$

……….(3.7)

$$
\begin{bmatrix} S_{out} \end{bmatrix} = \begin{bmatrix} 0 & WH^2 & 0 \end{bmatrix} \begin{bmatrix} S_1 \\ S_2 \\ S_3 \end{bmatrix}
$$

……….(3.8)

where W indicates the number of information bits "1" causing the transition and H indicates the Hamming weight of the transition.

From (3.7) and (3.8), the transfer function of the rate ½ encoder is

$$
T(W,H) = \frac{S_{out}}{S_{in}} = \begin{bmatrix} 0 & WH^2 & 0 \end{bmatrix} \left[I - \begin{bmatrix} 0 & 1 & 0 \\ WH & 0 & H \\ H & 0 & WH \end{bmatrix} \right]^{-1} \begin{bmatrix} WH^2 \\ 0 \\ 0 \end{bmatrix}
$$

$$
= W^3 H^5 + (W^2 + W^4)H^6 + (3W^3 + W^5)H^7 + \dots
$$

$$
= \sum_{h=5}^{\infty} \sum_{w=2}^{\infty} A_{w,h}^{C_i} W^w H^h
$$

……….(3.9)

The transfer function yields the coefficients $A_{w,h}^{C_i}$ for the inner encoder.

46

In summary, the SCCC's overall outer and inner parameters are listed in Table 3.1. Note that the information frame length k is chosen to be 640 to obtain a medium size interleaver. SCCC is not effective for small interleavers, while large interleavers suffer from long delays. From Chapter 2, the interleaver length N works out to be 963.

Code			Outer Code			Inner Code			
	Code	N	Rate	w_m^o	d_f^o	Rate	w_m^i	$df^i_{f,eff}$	h_3
SCCC	Rate		2/3			1/2			
	1/3	963	RSC	2	3	RSC	2	6	5

Table 3.1.   SCCC parameters.

These parameters can be substituted into equations (2.47) and (2.48) to obtain the union bounds on word and bit error rates, respectively.

B.   CHANNEL

The memoryless binary input channel is characterized by the conditional probability density function (pdf) of the observations, given the transmitted bits d = 0,1, that are mapped into the modulator levels x = -1, +1 through the relation

$$x = 2d - 1$$

……….(3.10)

For BPSK with AWGN, the conditional pdf is given by

$$p(y|x) = \frac{1}{\sqrt{\pi N_o}} \exp\left(-\frac{(y - x\sqrt{E_c})^2}{N_o}\right)$$

……….(3.11)

where E_c is the channel bit average signal energy given by $R_c E_b$ and $N_o/2$ is the two-sided AWGN power spectral density.

For both AWGN and noise interference, the conditional pdf is given by

$$p(y|x) = \frac{1}{\sqrt{\pi\left(N_o + N_I/\rho\right)}}\exp\left(-\frac{(y - x\sqrt{E_c})^2}{\left(N_o + N_I/\rho\right)}\right)$$

……….(3.12)

where $N_I/2$ is the two-sided noise interference power spectral density and ρ is the fraction of bits jammed.

With a slow, non-dispersive, independent, and frequency non-selective Rayleigh fading channel,

$$p(y|x,a) = \frac{1}{\sqrt{\pi N_o}}\exp\left(-\frac{(y - xa\sqrt{E_c})^2}{N_o}\right)$$

……….(3.13)

where the fading amplitude *a* is modeled as a Rayleigh probability density function as shown in (2.54).

For AWGN, noise interference, and a Rayleigh fading channel,

$$p(y|x,a) = \frac{1}{\sqrt{\pi\left(N_o + N_I/\rho\right)}}\exp\left(-\frac{(y - xa\sqrt{E_c})^2}{\left(N_o + N_I/\rho\right)}\right)$$

……….(3.14)

The different types of channel are represented as follows:

a.   AWGN in Figure 3.11,

b.   AWGN and noise interference in Figure 3.12,

c.   AWGN and Rayleigh fading in Figure 3.13,

d.   AWGN, noise interference and Rayleigh fading in Figure 3.14.

$x\sqrt{E_c} \longrightarrow \bigoplus \longrightarrow y$

n
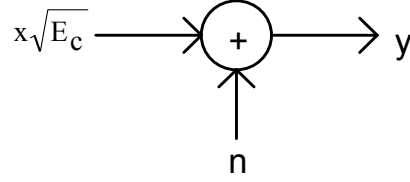
Figure 3.11.   Channel model for AWGN.

$x\sqrt{E_c} \longrightarrow \bigoplus \longrightarrow \bigoplus \longrightarrow y$

$n \qquad n_I$
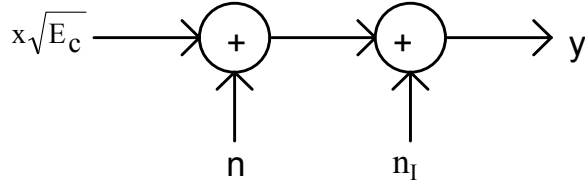
Figure 3.12.   Channel model for AWGN and noise interference.

$x\sqrt{E_c} \longrightarrow \bigotimes \longrightarrow \bigoplus \longrightarrow y$

$a \qquad n$
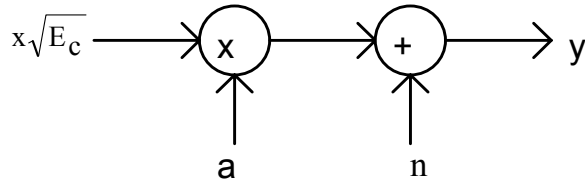
Figure 3.13.   Channel model for AWGN and Rayleigh fading.

$x\sqrt{E_c} \longrightarrow \bigotimes \longrightarrow \bigoplus \longrightarrow \bigoplus \longrightarrow y$

$a \qquad n \qquad n_I$
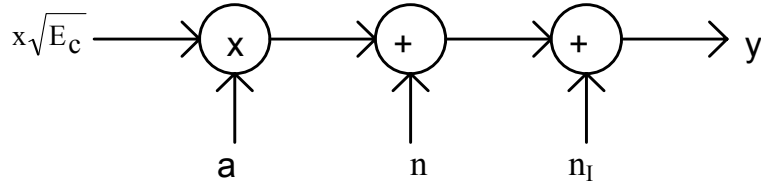
Figure 3.14.   Channel model for AWGN, noise interference and Rayleigh fading.

For pulsed noise jamming, it is assumed that there is a jammer that evenly distributes its power for a fraction ρ of the time. Thus, transmission occurs on a channel that includes wideband noise with power spectral density $N_o/2$ and pulsed noise interference with power spectral density $N_I/2\rho$ that is present a fraction ρ of the time. When the waveform is direct sequence spread spectrum, the wideband noise remains essentially unchanged, while the jammer noise power is spread by the processing gain, or the number of chips per bit, c. Thus, the jammer power spectral density in this case is $N_I/(2\rho c)$. It is assumed that the jammer does not turn on or off in the middle of a bit.

49

For partial-band noise jamming, the SCCC signal is attacked by a bandlimited, noise-like signal that affects only some fraction of the frequency range. Let ρ be the fraction of the bandwidth the jammer affects. The power spectral density (PSD) of the jamming signal when it covers the entire bandwidth is $N_I/2$ over the null-to-null bandwidth of the SCCC signal. Since the overall average power transmitted by the jammer is assumed fixed, i.e., at lower ρ the jamming power spectral density is higher, the jammer's PSD is $N_I/2\rho$. It is assumed that the jammer affects the entire hop if it is jammed. When the waveform is frequency-hopped spread spectrum, the wideband noise remains essentially unchanged, while the jammer noise power is reduced by the processing gain, c. Thus, the jammer power spectral density in this case is $N_I/(2\rho c)$.

C.   SCCC RECEIVER

The receiver consists of the demodulator and the SCCC decoder. The two types of demodulation considered are BPSK and DPSK. The SCCC decoder uses the MAP algorithm that was described in detail in Chapter II. The formulation of the log-likelihood ratios is briefly described here.

When the channel has binary inputs, the log-likelihood functions of the received bits can be represented as single quantities by the log-likelihood ratios (LLR). For the kth bit, the LLR is defined

$$\lambda_k \overset{\Delta}{=} \log \frac{p(y_k|1)}{p(y_k|0)}$$

……….(3.15)

For the AWGN channel, substituting (3.11) into (3.15), we get

$$\lambda_k = 4\frac{E_c}{N_o}\frac{y_k}{\sqrt{E_c}}$$

……….(3.16)

For AWGN with noise interference, substituting (3.12) into (3.15), we get

50

$$\lambda_k = 4 \frac{E_c}{\left(N_o + N_I / \rho\right)} \frac{y_k}{\sqrt{E_c}}$$

……….(3.17)

Knowledge of the signal-to-noise ratio is required for effective SCCC decoding [Ref. 53], and this knowledge allows the receiver to determine the presence of severe channel degradation, such as jamming [Ref. 85, 86]. This side information determines the reliability of the signal received for each code symbol. For decoding in a noise-jamming environment with no side information, which bits are jammed is not known and the total signal-to-noise ratio used by the decoder is an average based on the ratio of the signal power and AWGN plus jamming noise power. For decoding with side information, since which bits are jammed is known, the signal-to-total noise ratio is used by the decoder. It is assumed that this measurement is accurate.

For AWGN and a Rayleigh fading channel with channel information, substituting (3.13) into (3.15), we get

$$\lambda_k(a) = 4a \frac{E_c}{N_o} \frac{y_k}{\sqrt{E_c}}$$

……….(3.18)

For decoding without channel information, λ_k is given in (3.16).

For AWGN, noise interference, and a Rayleigh fading channel with channel information, substituting (3.14) into (3.15), we get

$$\lambda_k(a) = 4a \frac{E_c}{\left(N_o + N_I / \rho\right)} \frac{y_k}{\sqrt{E_c}}$$

……….(3.19)

For decoding without channel information, λ_k is given in (3.17).

These LLRs (equations (3.16) to (3.19)) are computed through the soft demodulator (Figure 3.15). As explained in Chapter II, during the first iteration of the

SCCC algorithm, the inner SISO is fed with the demodulator soft outputs consisting of these LLRs.

$y_k \longrightarrow$ Soft Demodulator $\longrightarrow \lambda_k$
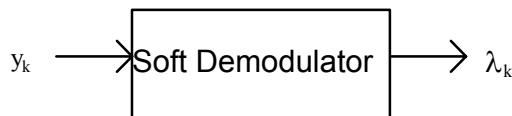
Figure 3.15.   Log-likelihood ratios.

D.   PERFORMANCE IN ADDITIVE WHITE GAUSSIAN NOISE

Using Monte Carlo simulation, we examine the performance of SCCC/BPSK modulation with AWGN.   The results are plotted in Figure 3.16 for from one to ten iterations. As expected, the greater the number of iterations, the better the bit error rate. However, the gain in performance decreases as the number of iterations increases. At the tenth iteration for signal-to-noise ratio (SNR) greater than one dB, all errors were corrected.   By the tenth iteration, the performance gain for additional iterations is insignificant compared to the delay incurred due to additional iterations. Wang [Ref. 83] has also shown that decoding up to ten iterations is adequate. Hence, future simulations will adopt this parameter.

The effect of SNR and the number of iterations on bit error rate is shown in Figure 3.17.   As the SNR increases, the number of iterations required for perfect decoding decreases. At SNR of 3 dB or greater, no more than two iterations are required for perfect decoding.

The analytical bound serves as an upper bound for SNR greater than 2 dB as can be seen in Figure 3.16.   The upper bounds based on the union bound diverge from simulation results at a signal-to-noise ratio close to the channel cut off rate, which in this case is 2.03 dB [Ref. 20].   The derivation of tighter upper bounds capable of extending the validity interval of the union bounds for concatenated codes is an important and still open topic for research.   Tighter bounds could be based on the technique successfully employed in [Ref. 87] for convolutional code or the classic Gallager bound [Ref. 88]. A successful application of the Gallager bound to parallel concatenated codes with

interleavers is described in [Ref. 89], where it is shown that the new bound extends the validity of the union bound for some SNR below the channel cut off rate, typically down to 0.5 dB. However, these attempts are still based on the hypothesis of maximum likelihood decoding. To apply the sub-optimum iterative decoding algorithm to the development of bounds is difficult.

To obtain the convergence of the union bound, one needs to compute a very large number of terms in the summation of equation (2.48). When the interleaver size, N, becomes very large, as is required to approach the channel capacity, only a limited number of terms in the summation can be obtained with reasonable computational complexity. As a consequence, the upper bounds obtained are only valid above the cut-off rate [Ref. 20].

For SCCC/DPSK, the bit error performance as a function of SNR with number of iterations as a parameter is shown in Figure 3.18. For SNR below 5 dB, the decoder is unable to converge resulting in unacceptable BER. However, for SNR greater than 5 dB, the SCCC/DPSK decoder behaves more like a concatenated code. At ten iterations, all errors are corrected for SNR greater than 6 dB. The union bounds are also plotted in Figure 3.18 and show a natural extension of the simulated curves. From Figure 3.19, we clearly see that regardless of the number of iterations, a SNR of less than 6 dB is insufficient for decoding. For SNR greater than 6 dB, only two or fewer iterations are required.

A comparison between SCCC/BPSK and SCCC/DPSK with AWGN (Figure 3.20) shows that at 10^{-2}, SCCC/BPSK has a coding gain of 5 dB more than SCCC/DPSK. The big difference could be due to the fact that DPSK signals suffer more noise than BPSK, and this is detrimental to the iterative algorithm in the decoder. Figure 3.20 also shows that the uncoded BPSK is better than SCCC/BPSK for very small SNR (almost zero). The uncoded DPSK has better performance than SCCC/DPSK for SNR less than 6 dB. However, for SNR greater than 6 dB, SCCC/DPSK performs dramatically better, reaching error free decoding for SNR greater than 6 dB. A comparison of the theoretical results shows that SCCC/BPSK has a coding gain advantage of 2 dB over SCCC/DPSK at 10^{-8}. This shows that SCCC/DPSK is more effective at high SNRs than low SNRs.

E.   PERFORMANCE IN AWGN AND RAYLEIGH FADING

Using Monte Carlo simulation, we simulate the performance for SCCC/BPSK with AWGN, Rayleigh fading, and no channel information. The results are plotted in Figure 3.21 for from one to ten iterations. As expected, the greater the number of iterations, the smaller the bit error ratio. However, the gain in performance decreases as the number of iterations increases. By the fifth iteration, the performance gain is insignificant compared to the delay incurred due to additional iterations. At the tenth iteration, for SNR greater than 4 dB, all errors are corrected. The theoretical result serves as an upper bound for SNR greater than 4.5 dB. Without fading, the union bound diverges from simulated performance at a SNR of about 2 dB. With fading, the divergence is 4.5 dB.

The effect of SNR and the number of iterations on bit error ratio is shown in Figure 3.22. For Rayleigh fading without channel information and for SNR of 4 dB or less, an "error floor" is reached for more than five iterations. For SNR of 4.5 dB, seven iterations are required for perfect decoding.

With channel side information, the performance of a SCCC/BPSK with AWGN and Rayleigh fading is plotted in Figure 3.23 for from one to ten iterations.   As previously for no channel information, by the fifth iteration, the gain in performance is insignificant. At the tenth iteration for SNR greater than 3 dB, as compared to 4 dB for no channel information, all errors are corrected.

The effect of SNR and the number of iterations on BER is shown in Figure 3.24. As the SNR increases, the number of iterations required for correct decoding decreases. For SNR of 3 dB or greater, no more than three iterations are required for perfect decoding. At higher SNR, the number of iterations required approaches one. This is a significant improvement compared to no channel information.

The BER of a SCCC/BPSK with no Rayleigh fading is compared with that obtained for Rayleigh fading without channel side information and Rayleigh fading with channel side information in Figure 3.25. For both simulated and theoretical results, SCCC/BPSK with Rayleigh fading and without channel side information performs the

poorest and the SCCC/BPSK with no fading performs the best. However, all results showed a vast improvement in BER over the uncoded case when Rayleigh fading is present. At a BER of 10^{-2}, the SCCC/BPSK with no Rayleigh fading requires 1.5 dB less than the SCCC/BPSK with Rayleigh fading and channel information and 2.5 dB less than SCCC/BPSK with Rayleigh fading and without channel information. Hall [Ref. 81] shows that fading without channel information can cost about 2 dB over that of AWGN. Based on the results of these simulations, channel information offers about 1 dB gain for the SCCC/BPSK with Rayleigh fading at 10^{-2}. For a rate 1/3 Turbo code with interleaver length of 400 and eight iterations, Frenger [Ref. 90, 91] shows that channel information offers as large as one dB at a BER of 10^{-3}. Hall [Ref. 81] shows that channel information offers 0.8 dB gain for a rate 1/3 Turbo code. From Figure 3.25, we observe that the BER with channel information is one dB better than the SCCC without channel information at 10^{-3}.

Since it is impractical to simulate very low BERs, the theoretical bounds are used. At a BER of 10^{-8}, the SCCC/BPSK with no Rayleigh fading requires 5 dB less than the SCCC/BPSK with Rayleigh fading and channel information and 7 dB less than the SCCC/BPSK with Rayleigh fading and without channel information. Hence, at very low BER, channel information offers about 2 dB gain for SCCC/BPSK with Rayleigh fading at 10^{-8}.

The simulation of a SCCC/DPSK with AWGN and Rayleigh fading with no channel information was carried out and the results plotted in Figure 3.26 for from one to ten iterations. As expected, the greater the number of iterations, the smaller the bit error ratio. However, the gain in performance decreases as the number of iterations increases. By the fourth iteration, the performance gain is insignificant compared to the delay incurred due to additional iterations. At the tenth iteration, for SNRs greater than 8 dB, all errors were corrected. The theoretical curve serves as an upper bound for SNR greater than 9 dB. Without fading, the upper bounds based on the union bound diverge at a SNR of about 6 dB. With fading, the divergence is at 9 dB.

The effect of SNR and the number of iterations on bit error ratio is shown in Figure 3.27. For Rayleigh fading without channel information and for SNR of 7 dB or

less, an "error floor" is reached for more than three iterations. For SNR of 8 dB, seven iterations are required for perfect decoding.

The BER of a SCCC/DPSK with AWGN is compared with SCCC/DPSK with Rayleigh fading and without channel side information in Figure 3.28. For both simulated and theoretical results, the SCCC/DPSK with Rayleigh fading without channel side information performs the poorest and the SCCC/DPSK with no fading performs the best. However, all the results showed a vast improvement in BER over the uncoded case in Rayleigh fading. At a BER of 10^{-2}, the SCCC/DPSK with AWGN requires about 1.5 dB less than SCCC/DPSK with Rayleigh fading and without channel information. From theoretical bounds, at a BER of 10^{-8}, the SCCC/DPSK with AWGN requires 4.5 dB less than SCCC/DPSK with Rayleigh fading and without channel information.

A comparison between SCCC/BPSK and SCCC/DPSK with AWGN and Rayleigh fading is shown in Figure 3.29.   Without channel information, the simulation results shows that SCCC/BPSK has a coding gain advantage of more than 5 dB over the SCCC/DPSK at 10^{-2}. A comparison of the theoretical results shows that SCCC/BPSK with Rayleigh fading and without channel information is slightly worse than SCCC/DPSK with Rayleigh fading and without channel information. This could be due to the imprecise bound developed by Hagenauer in equation (2.55)
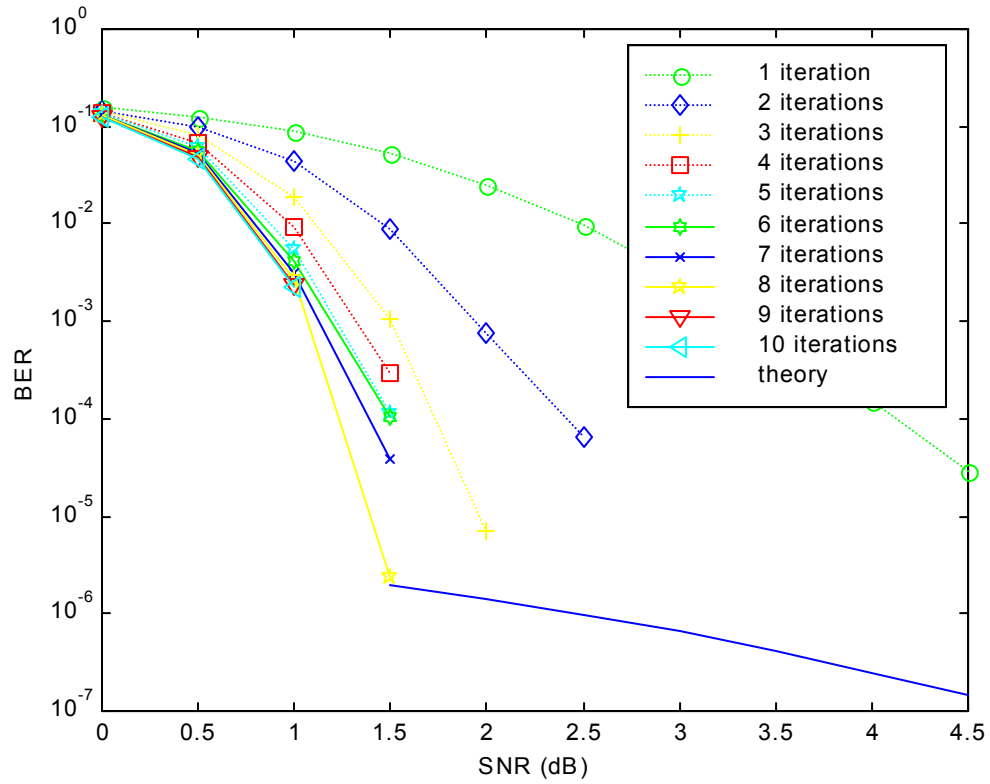
Figure 3.16. Simulated and theoretical SCCC/BPSK with AWGN: effect of SNR on BER for different number of iterations.
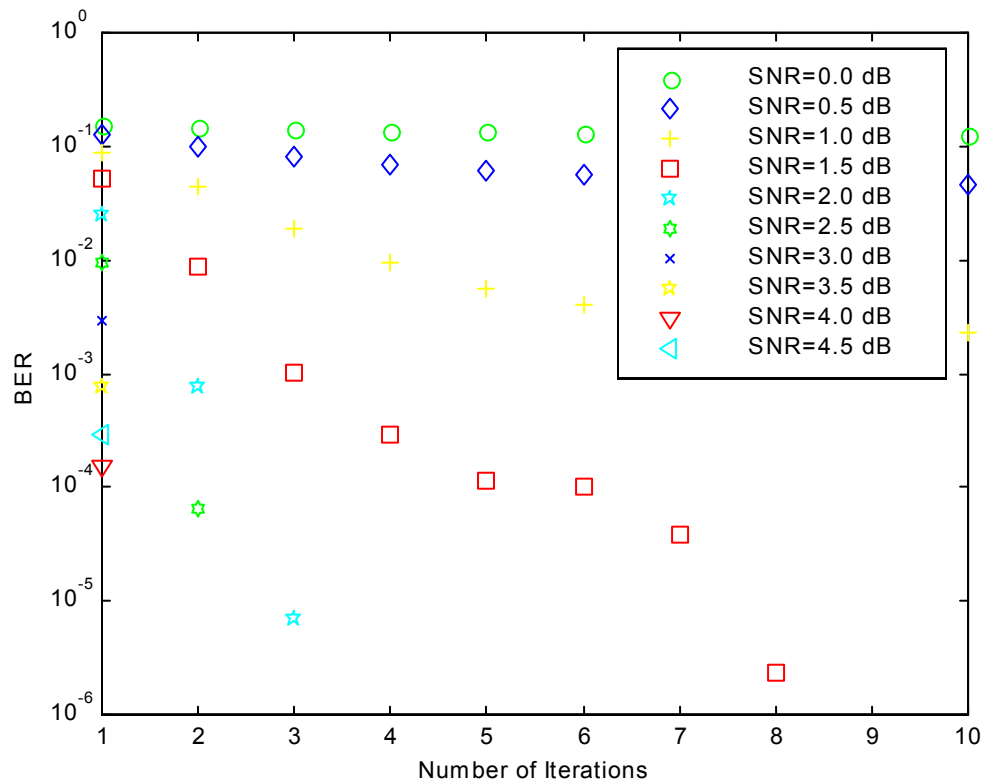
Figure 3.17.   Simulated SCCC/BPSK with AWGN: effect of number of iterations on BER for different values of SNR.
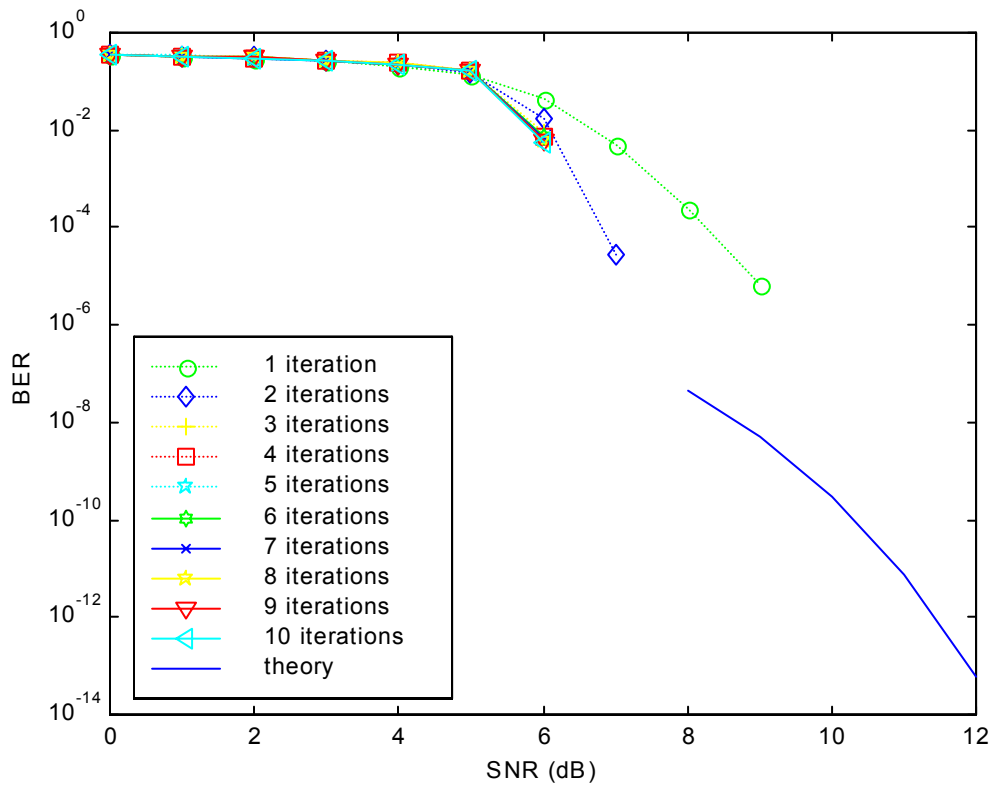
Figure 3.18.   Simulated and theoretical SCCC DPSK with AWGN: effect of SNR on BER for different number of iterations.
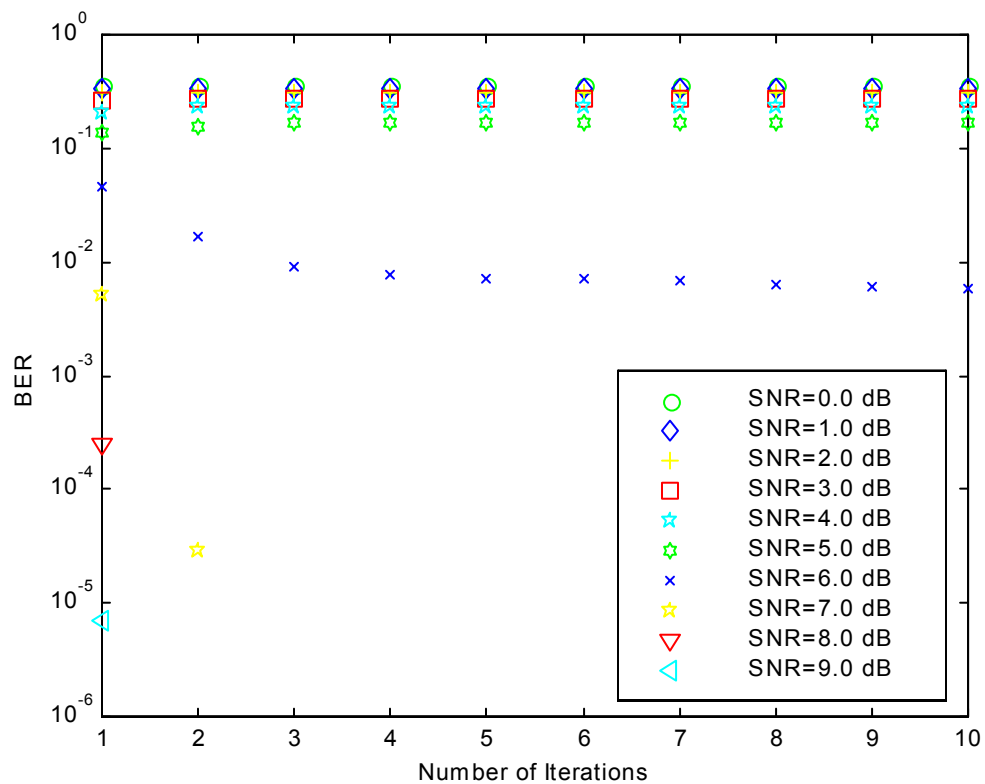
Figure 3.19.   Simulated SCCC DPSK with AWGN: effect of number of iterations on BER for different values of SNR.
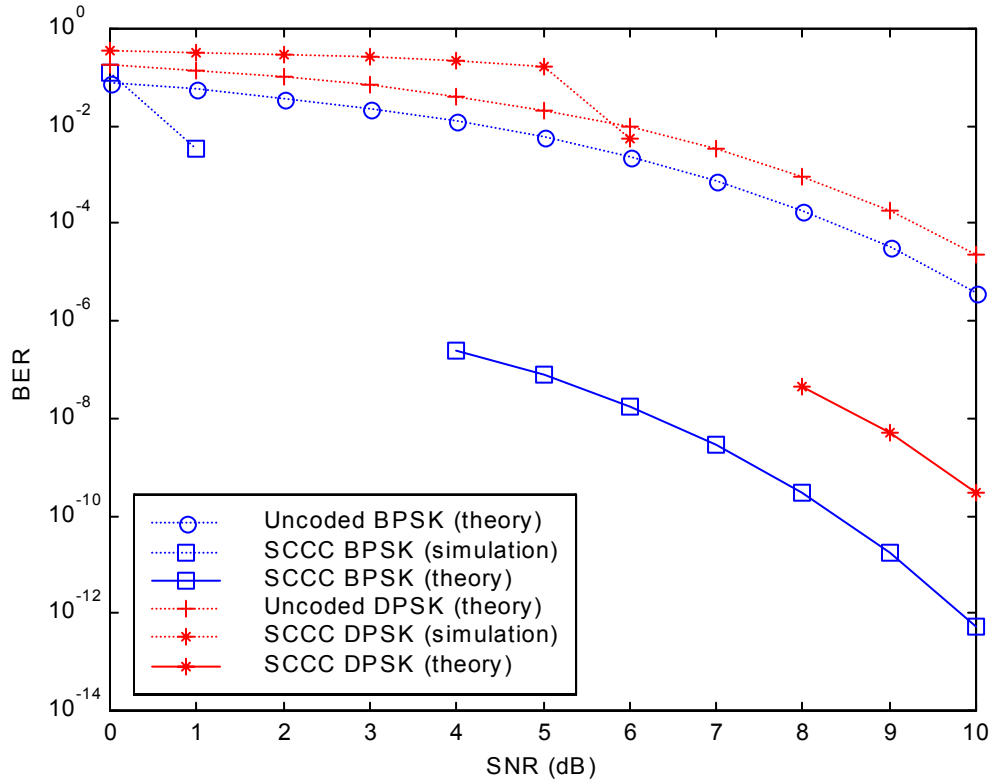
Figure 3.20.   Comparison of simulated and theoretical SCCC/BPSK and SCCC DPSK with AWGN.
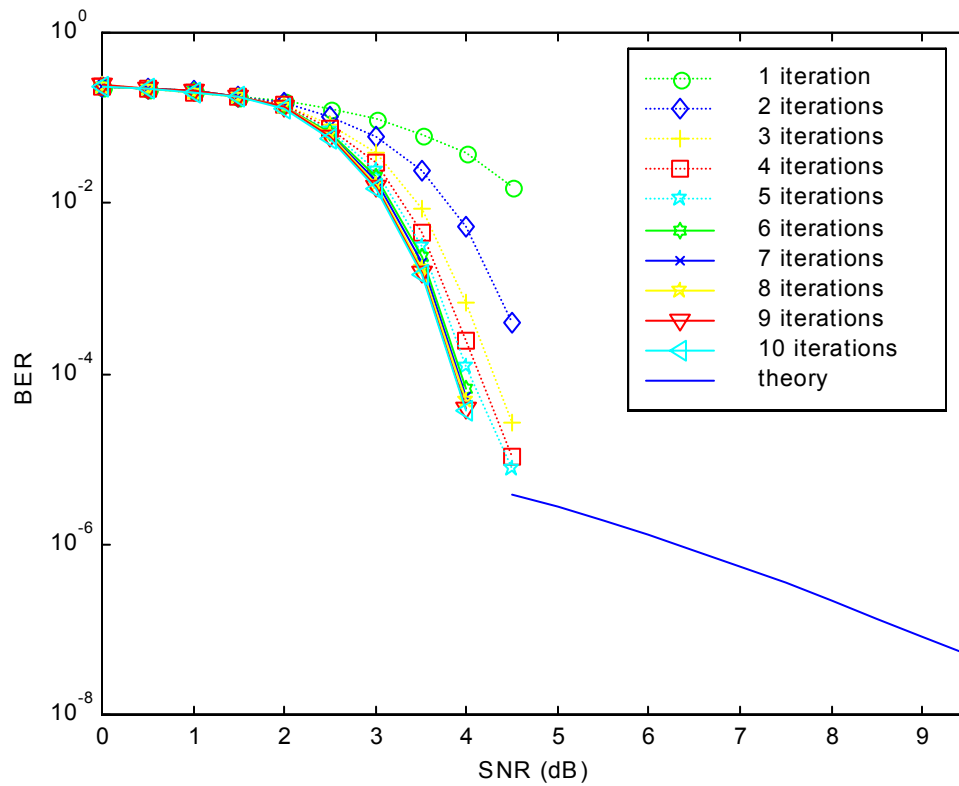
Figure 3.21. Simulated and theoretical SCCC/BPSK with AWGN and Rayleigh fading with no channel information: effect of SNR on BER for different number of iterations.
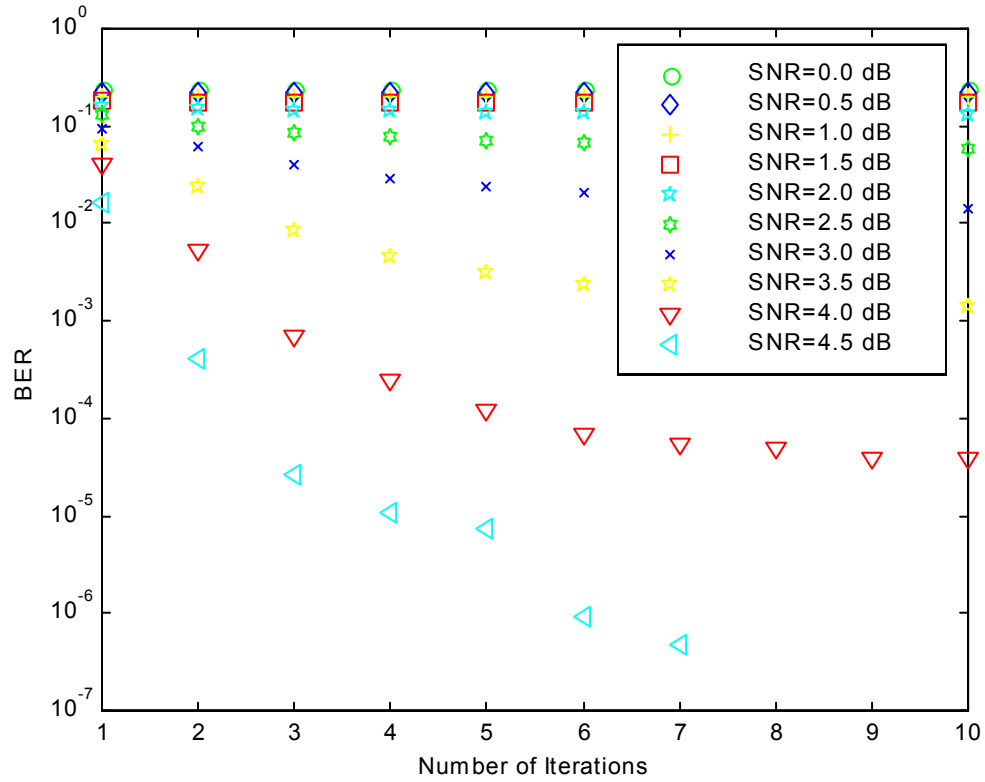
Figure 3.22.   Simulated SCCC/BPSK with AWGN and Rayleigh fading with no channel information: effect of number of iterations on BER for different values of SNR.
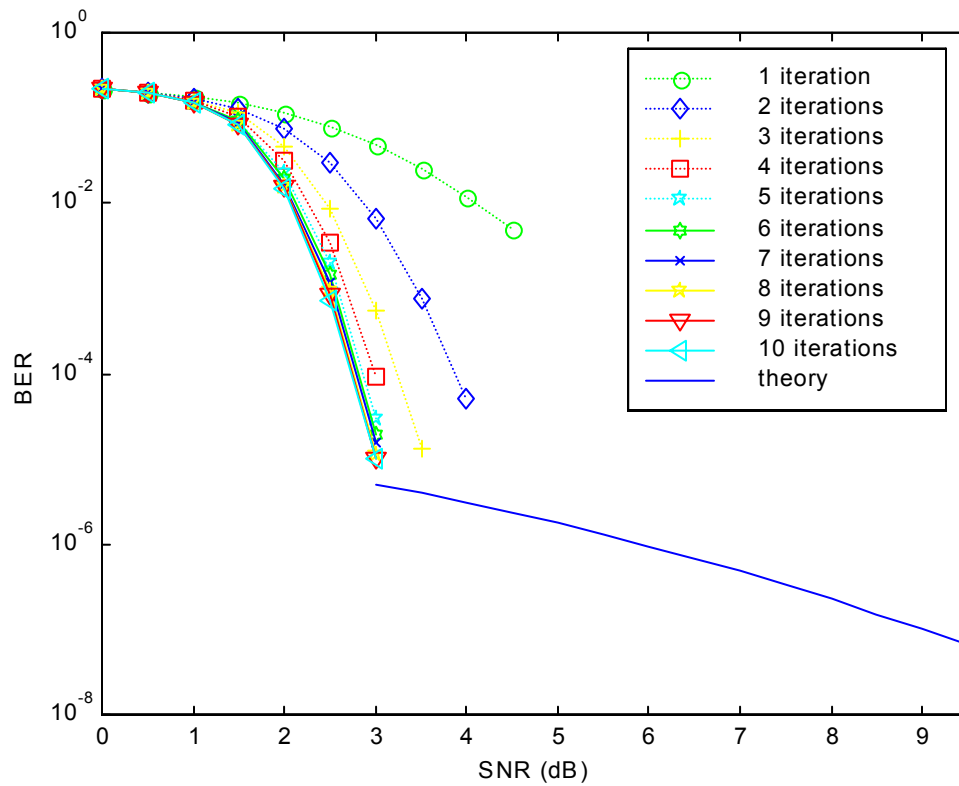
Figure 3.23.   Simulated and theoretical SCCC/BPSK with AWGN and Rayleigh fading with channel information: effect of SNR on BER for different number of iterations.
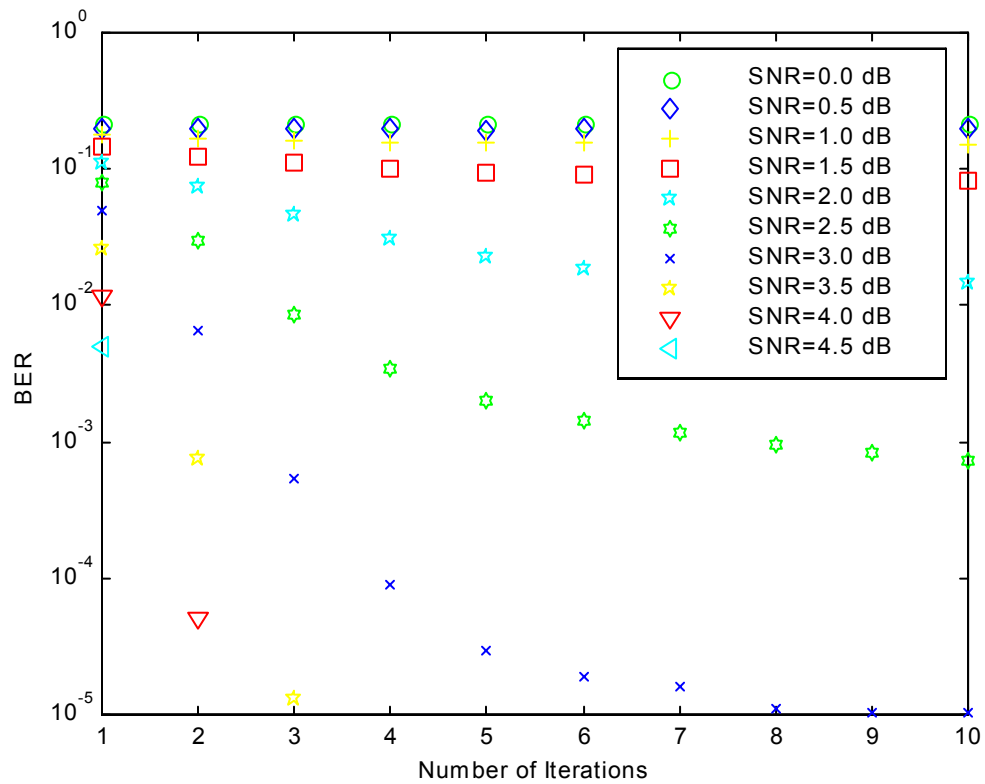
Figure 3.24. Simulated SCCC/BPSK with AWGN and Rayleigh fading with channel information: effect of number of iterations on BER for different values of SNR.
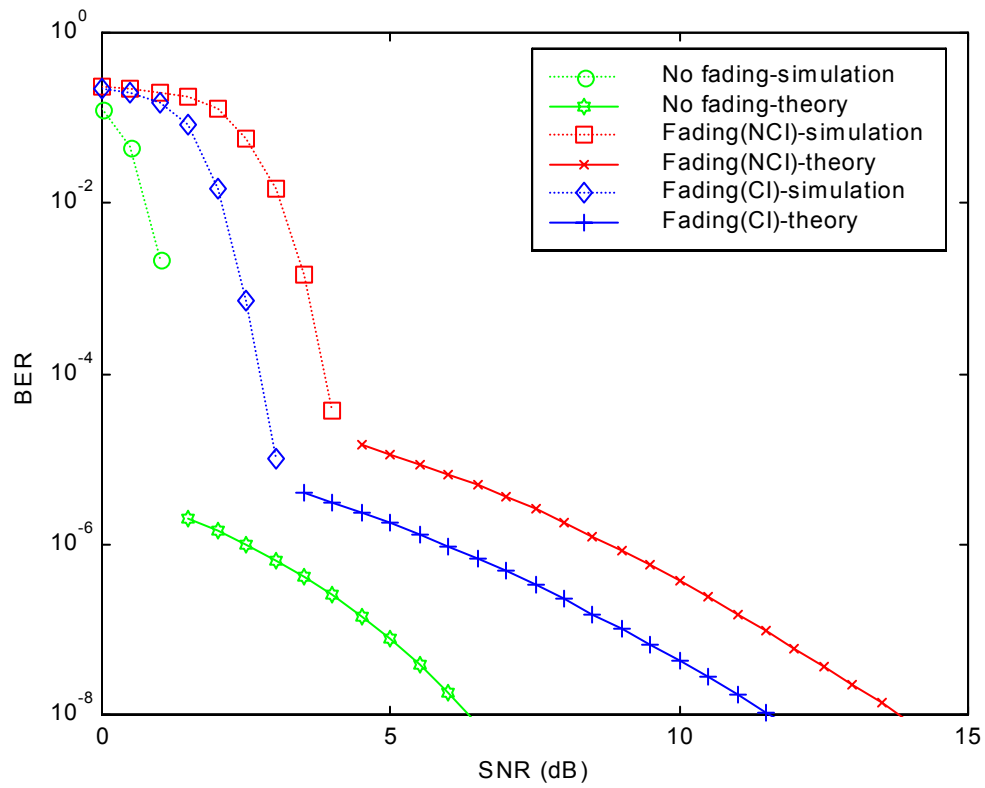
Figure 3.25.   Simulated and theoretical SCCC/BPSK with AWGN: effect of Rayleigh fading (with and without channel information) on BER.
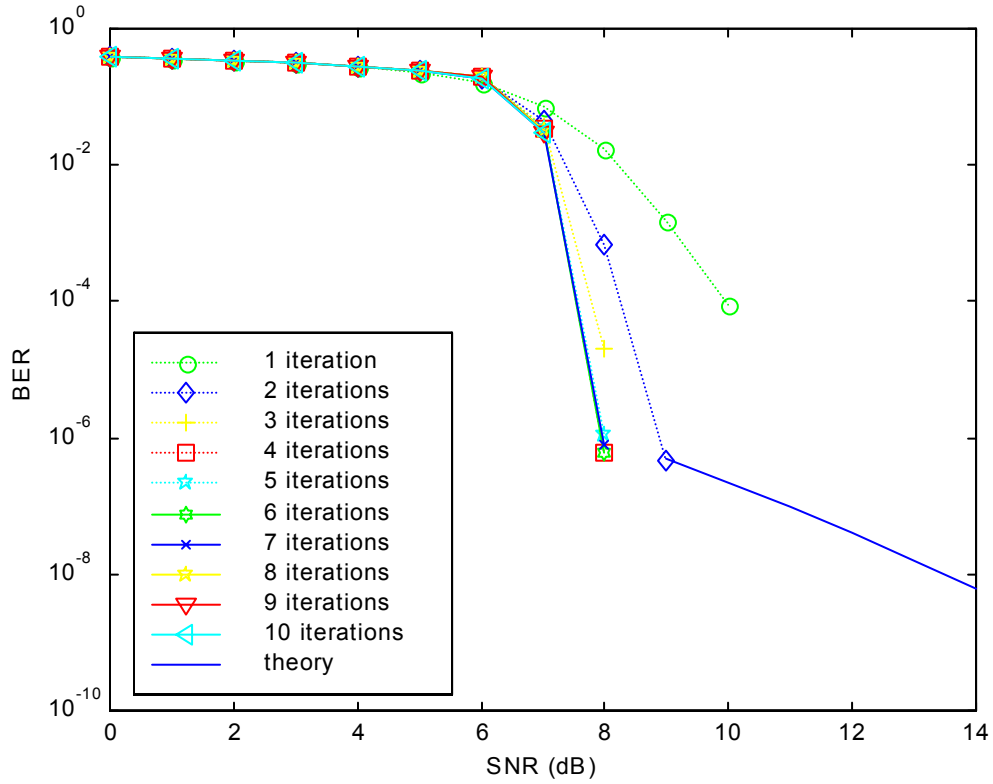
Figure 3.26.   Simulated and theoretical SCCC DPSK with AWGN and Rayleigh fading with no channel information: effect of SNR on BER for different number of iterations.
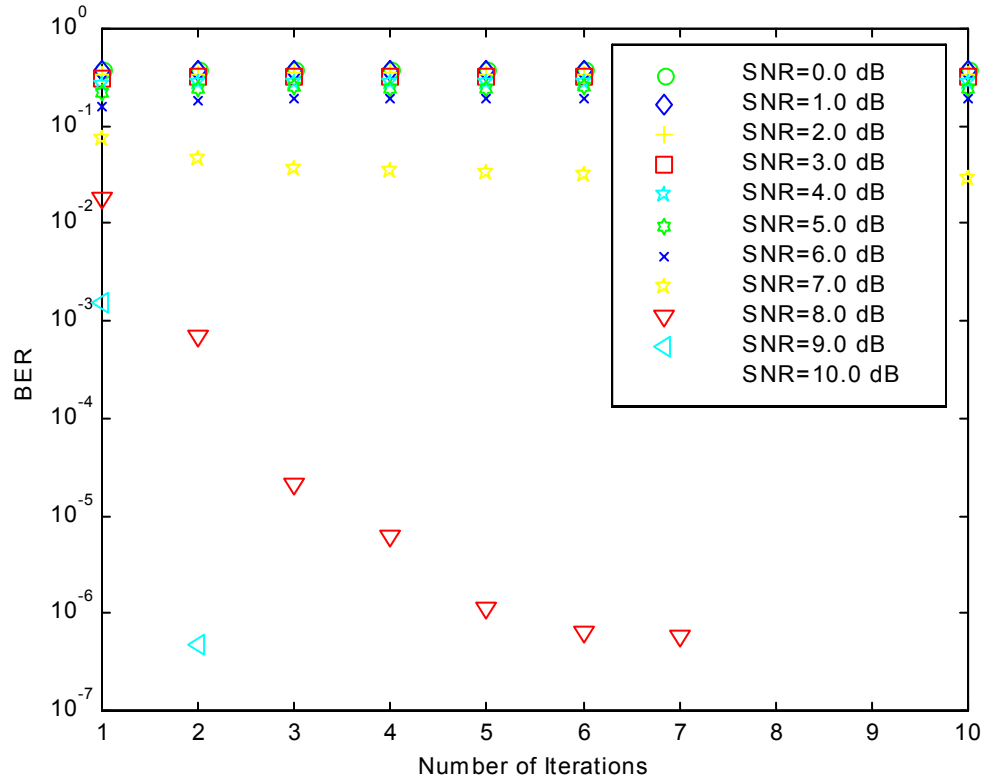
Figure 3.27. Simulated SCCC DPSK with AWGN and Rayleigh fading with no channel information: effect of number of iterations on BER for different values of SNR.
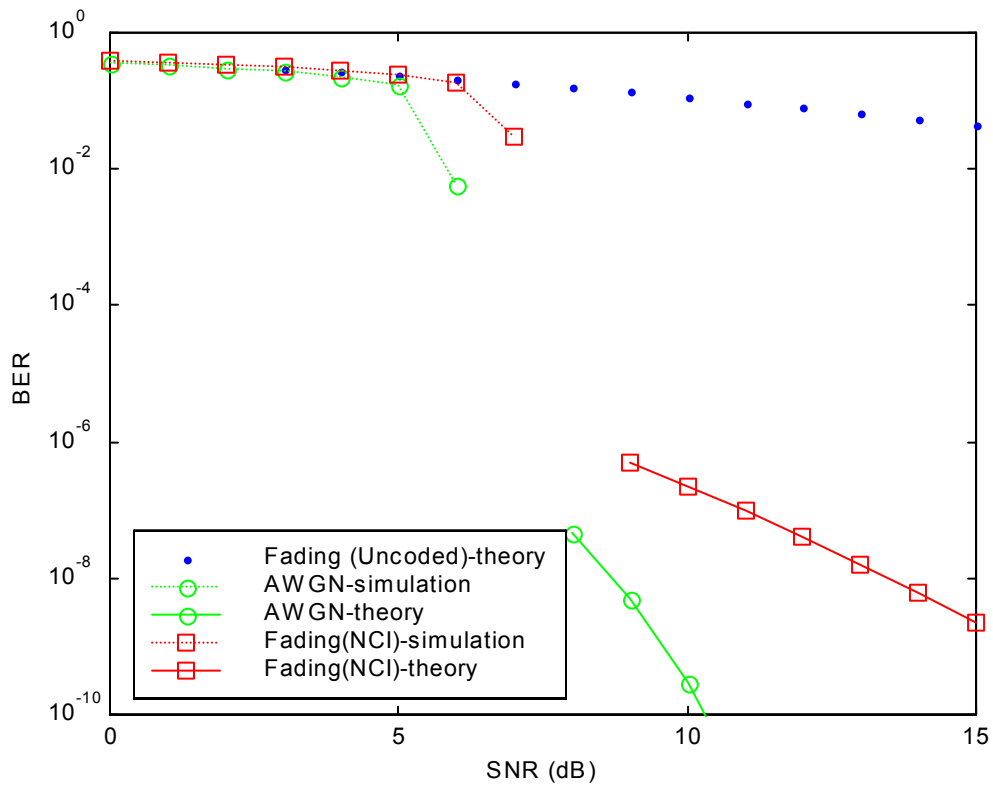
Figure 3.28. Simulated and theoretical SCCC DPSK with AWGN: effect of Rayleigh fading without channel information on BER.
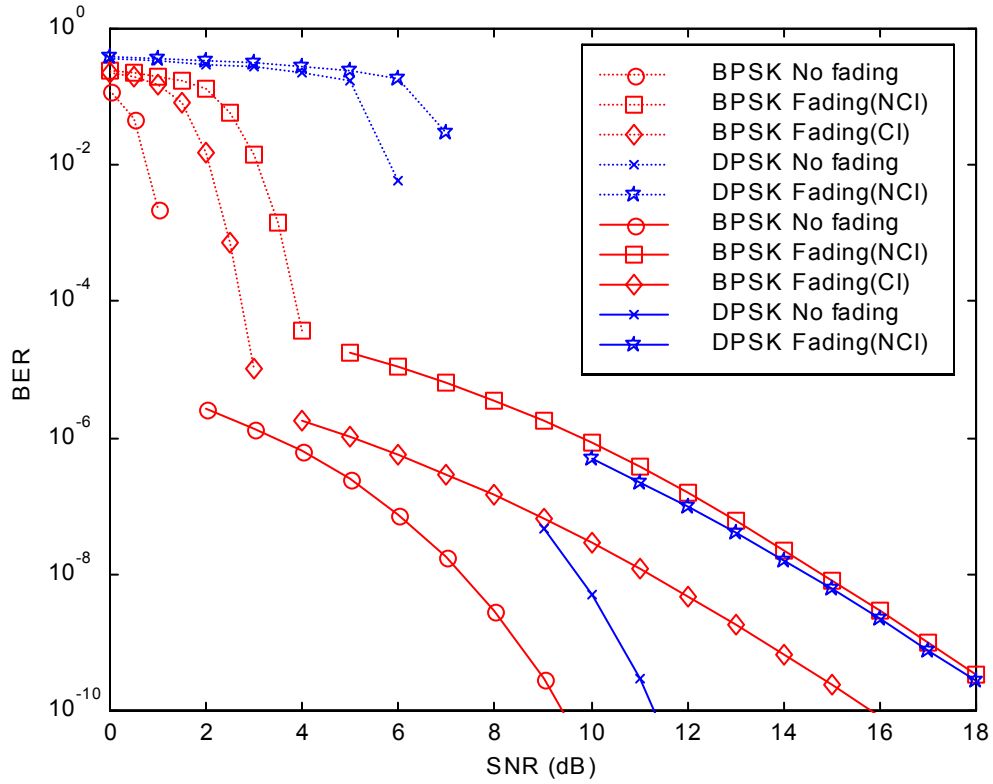
Figure 3.29. Comparison of simulated and theoretical BER of SCCC/BPSK and SCCC DPSK with AWGN and Rayleigh fading. The dotted lines represent simulated results and the full lines represent theoretical results.

IV. THEORETICAL ANALYSIS AND RESULTS OF SCCC WITH COHERENT BPSK IN PULSED NOISE JAMMING, RAYLEIGH FADING AND DIRECT SEQUENCE SPREAD SPECTRUM

The use of coding is extremely important in anti-jam communications systems where coding gains can usually be much greater than in conventional communication systems [Ref. 92]. The evaluation of coded error probabilities for anti-jam communication systems is also more difficult since here the decoding decision metrics are generally no longer maximum likelihood metrics, and there are a variety of detector forms that may be considered. In addition, the receiver may have side information available such as knowledge of when a jammer signal is on or not during the transmission of a coded signal.   Omura and Levitt [Ref. 93] presented a general union-Chernoff bound on the bit error probability for coded communication systems and applied it to examples of anti-jam systems. Hagenauer [Ref. 55] studied Viterbi decoding of BPSK modulation and convolutional codes for fading and burst channels. Vojcic and Pickholtz [Ref. 33] examined into the performance of coded direct sequence spread spectrum in a fading dispersive channel with pulsed noise jamming. Juntti [Ref. 94] examined the performance of a convolutionally coded, hard decision, direct sequence BPSK receiver in pulsed noise interference. Hall and Wilson [Ref. 52] delved into the design issues for Turbo codes using coherent BPSK signaling on the Rayleigh fading channel. Jordan [Ref. 95] studied Turbo code performance in AWGN and partial-band jamming using BPSK and DPSK. Liang and Stark [Ref. 31] explored the performance of Turbo codes with direct sequence spread spectrum in continuous wave jamming and Gaussian noise jamming with perfect side information using adaptive non-linear filtering techniques. Frenger [Ref. 90] recommended a new metric using noisy channel estimates for Turbo decoding on Rayleigh fading channels. Wang [Ref. 53] sought ways to improved faded Turbo code performance using biased channel side information. Kang and Stark [Ref. 96] investigated coherent Turbo code systems in a slow frequency-hopped spread spectrum with partial-band interference and thermal noise present.

In this chapter, serially concatenated convolutional codes (SCCC) with BPSK modulation, AWGN, pulsed noise jamming, slow, independent, frequency non-selective Rayleigh fading and direct sequence spread spectrum (DS) are investigated.   Six scenarios are considered:

a.   Pulsed noise jamming with no side information (NSI).

b.   Pulsed noise jamming with side information (SI).

c.   Pulsed noise jamming with no side information (NSI) and Rayleigh fading with no channel information (NCI) (no amplitude of fade) is available. The pulsed noise interference is assumed to be unaffected by the fading channel.

d.   Pulsed noise jamming with side information and Rayleigh fading with channel information (CI).

e.   Pulsed noise jamming with no side information (NSI) and with direct sequence spread spectrum (DS) incorporated.

f.   Pulsed noise jamming with side information (SI) and with direct sequence spread spectrum (DS) incorporated.

The basic BPSK model is shown in Figure 4.1.
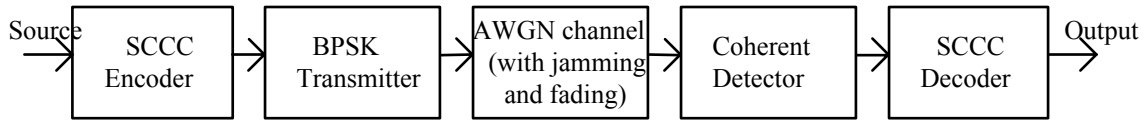
Figure 4.1.   Basic BPSK simulation model.

A.   THEORETICAL BOUNDS

1.   SCCC with Pulsed Noise Jamming and No Side Information

Suppose that the SCCC system is attacked by a band limited noise-like signal that is turned on and off systematically (pulsed). Let ρ be the fraction of time the jammer is turned on and assume that the jammer does not turn on or off during a channel bit interval. It is also assumed that the power spectral density (PSD) of the jamming signal

when on continuously is $N_I/2$ within the null-to-null bandwidth of the SCCC signal. Assume also that the overall average power transmitted by the jammer is the same whether the jammer is pulsed or not, i.e., for smaller ρ the jamming power is higher. Thus, the jammer's PSD is $N_I/2\rho$.

From Chapter II, the word probability of error (2.47) is

$$P_w \leq \sum_{w=w_m^o}^{NR_c^o} N^{-(d_f^o-1)/2} \frac{d_f^o d_f^{d_f^o}!}{p^{(d_f^o+1)/2}((d_f^o-3)/2)!} A_{w,d_f^o,1}^o A_{d_f^o,h,(d_f^o-1)/2}^i P_2(h)$$

……….(4.1)

and the equivalent bit probability of error (2.48) is

$$P_b \leq \sum_{w=w_m^o}^{NR_c^o} N^{-(d_f^o+1)/2} \frac{d_f^o d_f^{d_f^o}!}{p^{(d_f^o-1)/2}((d_f^o-3)/2)!} \frac{w}{k} A_{w,d_f^o,1}^o A_{d_f^o,h,(d_f^o-1)/2}^i P_2(h)$$

……….(4.2)

where

$$P_2(h) = Q(\sqrt{2R_c h E_b/N_o})$$

……….(4.3)

for binary BPSK signals and

$$h = \frac{(d_f^o-3)d_{f,eff}^i}{2} + h_3$$

……….(4.4)

In the case of jamming, given that i bits are jammed and ρ being the percentage of bits jammed [Ref. 97, 98],

$$P_2(h) = \sum_{i=0}^{h} \binom{h}{i} \rho^i (1-\rho)^{h-i} P_h(i)$$

………(4.5)

where $P_h(i)$ is the probability that i of h bits are jammed.

The fundamental approach to calculating pair-wise error probabilities is to compute log likelihood ratios. For the case where the decoder has no side information, this is difficult since the receiver does not know which bits are jammed or the SNR. Thus, for analytical purposes, we will consider the sub-optimal decoder that makes bit

decisions based on the channel outputs. For this sub-optimal decoder, if y_k is the soft demodulator output for the kth bit, then when i bits are jammed,

$$x = \sum_{k=1}^{h} y_k$$

.........(4.6)

Since for coherent detection, y_k is modeled as a Gaussian random variable, then

$$\overline{x} = h\sqrt{E_c}$$

.........(4.7)

where $E_c = R_c E_b$, and

$$\sigma^2(i) = \sum_{k=0}^{h} \sigma_k^2$$
$$= i*(N_o + N_I / \rho) / T_b + (h-i)*N_o / T_b$$

.........(4.8)

For linear (equal gain) combining [Ref. 99],

$$P_h(i) = Q\left(\sqrt{\frac{\overline{x}^2}{\sigma^2(i)}}\right)$$

.........(4.9)

Substituting (4.7) ad (4.8) into (4.9), we get

$$P_h(i) = Q\left(\sqrt{\frac{2R_c hE_b}{\left(N_o + \frac{i}{h}\frac{N_I}{\rho}\right)}}\right)$$

..........(4.10)

Here, we see that the jamming noise PSD is being weighted by the ratio i/h. The same principle will be used for Rayleigh fading with no channel information later.

Substituting (4.10) in (4.5), we obtain $P_2(h)$ with no side information as

$$P_2(h) = \sum_{i=0}^{h} \binom{h}{i} \rho^i (1-\rho)^{h-i} Q\left(\sqrt{\frac{2R_c hE_b}{\left(No + \frac{i}{h}\frac{N_I}{\rho}\right)}}\right)$$

.........(4.11)

Equation (4.11) can be substituted into (4.1) and (4.2) to obtain the word and bit error probabilities, respectively. Thus, for SCCC with AWGN and pulsed noise jamming without side information,

$$P_w \leq \sum_{w=w_m^o}^{NR_c^o} N^{-(d_f^o-1)/2} \frac{d_f^{o\,d_f^o} d_f^o!}{p^{(d_f^o+1)/2}((d_f^o-3)/2)!} A_{w,d_f^o,1}^o A_{d_f^o, \frac{(d_f^o-3)d_{f,eff}^i}{2}+h_3, (d_f^o-1)/2}^i$$

$$\frac{1}{2} \sum_{i=0}^{\frac{(d_f^o-3)d_{f,eff}^i}{2}+h_3} \left(\frac{(d_f^o-3)d_{f,eff}^i}{2}+h_3 \atop i \right) \rho^i (1-\rho)^{\frac{(d_f^o-3)d_{f,eff}^i}{2}+h_3-i} e^{-R_c E_b \left(\frac{\frac{(d_f^o-3)d_{f,eff}^i}{2}+h_3}{N_o + \frac{iN_I}{h\rho}} \right)}$$

……….(4.12)

and

$$P_b \leq \sum_{w=w_m^o}^{NR_c^o} N^{-(d_f^o+1)/2} \frac{d_f^{o\,d_f^o} d_f^o!}{p^{(d_f^o-1)/2}((d_f^o-3)/2)!} \frac{w}{k} A_{w,d_f^o,1}^o A_{d_f^o, \frac{(d_f^o-3)d_{f,eff}^i}{2}+h_3, (d_f^o-1)/2}^i$$

$$\frac{1}{2} \sum_{i=0}^{\frac{(d_f^o-3)d_{f,eff}^i}{2}+h_3} \left(\frac{(d_f^o-3)d_{f,eff}^i}{2}+h_3 \atop i \right) \rho^i (1-\rho)^{\frac{(d_f^o-3)d_{f,eff}^i}{2}+h_3-i} e^{-R_c E_b \left(\frac{\frac{(d_f^o-3)d_{f,eff}^i}{2}+h_3}{N_o + \frac{iN_I}{h\rho}} \right)}$$

……….(4.13)

2. SCCC with Pulsed Noise Jamming and Side Information

When side information is available, i.e., knowledge of which hops are jammed, the LLRs can be calculated in the normal way. From (3.11), the pdf of an unjammed bit is

$$p(y|x) = \frac{1}{\sqrt{\pi N_o}} \exp\left(-\frac{(y-x\sqrt{E_c})^2}{N_o} \right)$$

……….(4.14)

where $E_c = R_c E_b$, and from (3.12), the pdf of a jammed bit is

$$p(y|x_I) = \frac{1}{\sqrt{\pi(N_o + N_I/\rho)}} \exp\left(-\frac{(y-x_I\sqrt{E_c})^2}{N_o + N_I/\rho} \right)$$

……….(4.15)

The log-likelihood ratio (LLR) $\lambda(y)$ is given by

$$\lambda(y) = \log \frac{p(y_1|x=1)p(y_2|x=1)...p(y_h|x=1)}{p(y_1|x=-1)p(y_2|x=-1)...p(y_h|x=-1)}$$

……….(4.16)

With i bits jammed,

$$\lambda(y) = \log \frac{p(y_1|x_I=1)...p(y_i|x_I=1)\,p(y_{i+1}|x=1)...p(y_h|x=1)}{p(y_1|x_I=-1)...p(y_i|x_I=-1)\,p(y_{i+1}|x=-1)...p(y_h|x=1)}$$

……….(4.17)

Since with side information, it is known which bits are jammed and which bits are not jammed, it is possible to separate the LLR into

$$\lambda(y) = \log \frac{p(y_1|x_I=1)...p(y_i|x_I=1)}{p(y_1|x_I=-1)...p(y_i|x_I=-1)} + \log \frac{p(y_{i+1}|x=1)...p(y_h|x=1)}{p(y_{i+1}|x=-1)...p(y_h|x=1)}$$

……….(4.18)

Since the average SNR per channel is assumed identical for channels with the same noise characteristics

$$\lambda(y) = i \log \frac{p(y_1|x_I=1)}{p(y_1|x_I=-1)} + (h-i) \log \frac{p(y_1|x=1)}{p(y_1|x=-1)}$$

……….(4.19)

Substituting equations (4.14) and (4.15) into (4.19), we obtain

$$\lambda(y) = 4\sqrt{E_c}\, y \left[\frac{i}{N_o + N_J/\rho} + \frac{h-i}{N_o} \right]$$

……….(4.20)

From (4.20), we see $\lambda(y)$'s pdf is Gaussian with mean and variance

$$\dddot{\lambda} = \pm\sqrt{2}E_c \left[\frac{i}{N_o + N_J/\rho} + \frac{h-i}{N_o} \right]$$

……….(4.21)

$$\sigma^2 = \left[\frac{i}{N_o + N_J/\rho} + \frac{h-i}{N_o} \right] E_c$$

……….(4.22)

where the '+' sign corresponds to the transmission of a "1" and the '-' sign corresponds to the transmission of a "0". The probability of error is thus given by

$$P_h(i) = Q\left(\sqrt{2R_cE_b\left(\frac{h-i}{N_o} + \frac{i}{N_o + N_I/\rho}\right)}\right)$$

……….(4.23)

Thus, substituting (4.23) into (4.5), we obtain $P_2(h)$ when side information is available as

$$P_2(h) = \sum_{i=0}^{h} \binom{h}{i}\rho^i(1-\rho)^{h-i}Q\left(\sqrt{2R_cE_b\left(\frac{h-i}{N_o} + \frac{i}{N_o + N_I/\rho}\right)}\right)$$

………(4.24)

Equation (4.23) can be substituted into (4.1) and (4.2) to obtain the word and bit error probabilities, respectively. Thus, for SCCC/BPSK with AWGN and pulsed noise jamming with side information,

$$P_w \leq \sum_{w=w_m^o}^{N R_c^o} N^{-(d_f^o-1)/2} \frac{d_f^{o d_f^o} d_f^o!}{p^{(d_f^o+1)/2}((d_f^o-3)/2)!} A^o_{w,d_f^o,1} A^i_{d_f^o,\frac{(d_f^o-3)d_{f,eff}^i}{2}+h_3,(d_f^o-1)/2}$$

$$\cdot \frac{1}{2} \sum_{i=0}^{\frac{(d_f^o-3)d_{f,eff}^i}{2}+h_3} \binom{\frac{(d_f^o-3)d_{f,eff}^i}{2}+h_3}{i} \rho^i(1-\rho)^{\frac{(d_f^o-3)d_{f,eff}^i}{2}+h_3-i} e^{-R_cE_b\left(\frac{\frac{(d_f^o-3)d_{f,eff}^i}{2}+h_3-i}{N_o} + \frac{i}{N_o+N_I/\rho}\right)}$$

……….(4.25)

and

$$P_b \leq \sum_{w=w_m^o}^{N R_c^o} N^{-(d_f^o+1)/2} \frac{d_f^{o d_f^o} d_f^o!}{p^{(d_f^o-1)/2}((d_f^o-3)/2)!} \frac{w}{k} A^o_{w,d_f^o,1} A^i_{d_f^o,\frac{(d_f^o-3)d_{f,eff}^i}{2}+h_3,(d_f^o-1)/2}$$

$$\frac{1}{2} \sum_{i=0}^{\frac{(d_f^o-3)d_{f,eff}^i}{2}+h_3} \binom{\frac{(d_f^o-3)d_{f,eff}^i}{2}+h_3}{i} \rho^i(1-\rho)^{\frac{(d_f^o-3)d_{f,eff}^i}{2}+h_3-i} e^{-R_cE_b\left(\frac{\frac{(d_f^o-3)d_{f,eff}^i}{2}+h_3-i}{N_o} + \frac{i}{N_o+N_I/\rho}\right)}$$

……….(4.26)

3. SCCC with Pulse Noise Jamming and No Side Information and Rayleigh Fading with No Channel Information

For Rayleigh fading, we consider two cases. The first case is SCCC/BPSK with AWGN, jamming without side information and Rayleigh fading without channel information. The second case is SCCC/BPSK with AWGN, jamming with side information, and Rayleigh fading with channel information.

For SCCC with AWGN, jamming without side information, and Rayleigh fading without channel information, $P_h(i)$ in (4.5) can be represented by (2.55)

$$P_h(i) \leq e^{h(\beta/\gamma)} \left[\frac{\sqrt{1+\left(\frac{2}{\beta}\right)} - 1}{\sqrt{1+\left(\frac{2}{\beta}\right)} + 1} \right]^h$$

..........(4.27)

where

$$\beta = \sqrt{\gamma^2 + 1} - 1$$

..........(4.28)

and based on the suboptimal decoder,

$$\gamma = \frac{R_c E_b}{\left(N_o + \dfrac{i}{h}\dfrac{N_I}{\rho}\right)}$$

..........(4.29)

Thus,

$$P_2(h) = \sum_{i=0}^{h} \binom{h}{i} \rho^i (1-\rho)^{h-i} e^{h(\beta/\gamma)} \left[\frac{\sqrt{1+\left(\frac{2}{\beta}\right)} - 1}{\sqrt{1+\left(\frac{2}{\beta}\right)} + 1} \right]^h$$

..........(4.30)

Equation (4.29) can be substituted into (4.1) and (4.2) to obtain the word and bit probability of errors, respectively, for SCCC/BPSK with AWGN, pulsed noise jamming with no side information, and Rayleigh fading with no channel information:

$$P_w \leq \sum_{w=w_m^o}^{NR_c^o} N^{-(d_f^o-1)/2} \frac{d_f^{o\, d_f^o} d_f^o!}{p^{(d_f^o+1)/2}((d_f^o-3)/2)!} A^o_{w,d_f^o,1} A^i_{d_f^o, \frac{(d_f^o-3)d_{f,eff}^i}{2}+h_3,(d_f^o-1)/2}$$

$$\frac{1}{2} \sum_{i=0}^{\frac{(d_f^o-3)d_{f,eff}^i}{2}+h_3} \left(\frac{(d_f^o-3)d_{f,eff}^i}{2} + h_3 \atop i \right) \rho^i (1-\rho)^{\frac{(d_f^o-3)d_{f,eff}^i}{2}+h_3-i} e^{h(\beta/\gamma)} \left[\frac{\sqrt{1+\frac{2}{\beta}}-1}{\sqrt{1+\frac{2}{\beta}}-1} \right]^{\frac{(d_f^o-3)d_{f,eff}^i}{2}+h_3}$$

..........(4.31)

78

and

$$P_b \leq \sum_{w=w_m^o}^{NR_c^o} N^{-(d_f^o-1)/2} \frac{d_f^{o \, d_f^o} d_f^o!}{p^{(d_f^o+1)/2}((d_f^o-3)/2)!} \frac{w}{k} A_{w,d_f^o,1}^o A_{d_f^o,\frac{(d_f^o-3)d_{f,eff}^i}{2}+h_3,(d_f^o-1)/2}^i$$

$$\frac{1}{2} \sum_{i=0}^{\frac{(d_f^o-3)d_{f,eff}^i}{2}+h_3} \left(\frac{\frac{(d_f^o-3)d_{f,eff}^i}{2}+h_3}{i} \right) \rho^i \left(1-\rho\right)^{\frac{(d_f^o-3)d_{f,eff}^i}{2}+h_3-i} e^{h(\beta/\gamma)} \left[\frac{\sqrt{1+\frac{2}{\beta}}-1}{\sqrt{1+\frac{2}{\beta}}-1} \right]^{\frac{(d_f^o-3)d_{f,eff}^i}{2}+h_3}$$

..........(4.32)

4. SCCC with Pulsed Noise Jamming and Side Information and Rayleigh Fading with Channel Information

For Rayleigh fading with channel information, the signal level is affected as in (2.58). However, with jamming, the noise statistics will be different for each bit, depending on whether the bit is jammed or not. In the case of jamming, given that i bits are jammed and ρ being the percentage of bits jammed, $P_2(h)$ is given in (4.5). In this case $P_h(i)$ for Rayleigh fading is given by

$$P_h(i,\gamma_b) = Q\left(\sqrt{2\gamma_b}\right)$$

.........(4.33)

where

$$\gamma_b = \frac{R_c E_b}{N_o + N_I/\rho} \sum_{j=1}^{i} a_j^2 \quad + \quad \frac{R_c E_b}{N_o} \sum_{k=1}^{h-i} a_k^2$$

$$= \sum_{j=1}^{i} \gamma_j + \sum_{k=1}^{h-i} \gamma_k$$

..........(4.34)

with

$$\gamma_j = \frac{R_c E_b a_j^2}{N_o + N_I/\rho}$$

.........(4.35)

and

$$\gamma_k = \frac{R_c E_b a_k^2}{N_o}$$

..........(4.36)

79

Since the average SNR per channel is assumed identical for channels with the same noise characteristics and the fading on the h channels is mutually statistically independent, the $\{\gamma_j\}$ and $\{\gamma_k\}$ are statistically independent. Hence, the characteristic function for γ_b is simply the product of the characteristic functions of the two, raised to the ith power for $\{\gamma_j\}$ and $(h\text{-}i)^{th}$ power for $\{\gamma_k\}$ respectively, i.e.,

$$\varphi_{\gamma_b}(j\nu) = \frac{1}{\left(1 - j\nu\overline{\gamma}_{jc}\right)^i} \cdot \frac{1}{\left(1 - j\nu\overline{\gamma}_c\right)^{h-i}}$$

……….(4.37)

with

$$\overline{\gamma}_{jc} = \frac{R_c E_b}{N_o + N_I / \rho}$$

……….(4.38)

and

$$\overline{\gamma}_c = \frac{R_c E_b}{N_o} E(a_k^2)$$

$$= \frac{R_c E_b}{N_o}$$

……….(4.39)

No simple analytic solutions exist for the inverse Fourier transform of (4.37) except when $i = 0$ or $i = h$, and (4.37) has to be determined numerically. By averaging the inverse Fourier transform of the pdf given in (4.37) with (4.33), we obtain:

$$P_h(i) = \int_0^\infty P_h(i, \gamma_b) p(\gamma_b) d\gamma_b$$

……….(4.40)

When perfect side information is available, i.e., we know which hops are jammed and which are not, we can disregard the jammed hops so that for $i < h$, the decision statistics consist of the summation of the signals of only the unjammed hops. This yields a more conservative solution without resorting to numerical methods.

Hence, the receiver with perfect side information has an equivalent diversity of $(h-i)$ when $i < h$, and $P_h(i)$ is the same probability of bit error as (2.73) but with $(h-i)$ instead of h. Therefore, for $i < h$ we have

$$P_h(i) = \left[\frac{1}{2}(1-\mu)\right]^{h-i} \sum_{k=0}^{h-i-1}\binom{h-i-1+k}{k}\left[\frac{1}{2}(1+\mu)\right]^k$$

.........(4.41)

For $i = h$, all hops of a bit are used to compute the decision statistics, and $P_h(h)$ is the same as the probability of bit error as (2.73)

$$P_h(i) = \left[\frac{1}{2}(1-\mu_j)\right]^{i} \sum_{k=0}^{i-1}\binom{i-1+k}{k}\left[\frac{1}{2}(1+\mu_j)\right]^k$$

..........(4.42)

but with

$$\mu_j = \sqrt{\frac{\bar{\gamma}_{jc}}{1+\bar{\gamma}_{jc}}}$$

..........(4.43)

Hence, $P_2(h)$ is given by

$$P_2(h) = \left\{\sum_{i=0}^{h-1}\binom{h-1}{i}\rho^i(1-\rho)^{h-i-1}\left[\frac{1}{2}(1-\mu)\right]^{h-i}\sum_{k=0}^{h-i-1}\binom{h-i-1+k}{k}\left[\frac{1}{2}(1+\mu)\right]^k\right\} + \rho^h\left[\frac{1}{2}(1-\mu_J)\right]^{h}\sum_{k=0}^{h-1}\binom{h-1+k}{k}\left[\frac{1}{2}(1+\mu_J)\right]^k$$

..........(4.44)

Thus, equation (4.44) can be substituted into (4.1) and (4.2) to obtain the word and bit probability of errors, respectively, for SCCC/BPSK with AWGN, pulsed noise jamming with side information, and Rayleigh fading with channel information:

$$P_w \leq \sum_{w=w_m^o}^{N R_c^o} N^{-(d_f^o - 1)/2} \frac{d_f^o{}^{d_f^o} d_f^o!}{p^{(d_f^o + 1)/2}((d_f^o - 3)/2)!} A_{w,d_f^o,1}^o A_{d_f^o,\frac{(d_f^o - 3)d_{f,eff}^i}{2}+h_3,(d_f^o - 1)/2}^i$$

$$\left\{\left[\sum_{i=0}^{\frac{(d_f^o-3)d_{f,eff}^i}{2}+h_3-1}\binom{\frac{(d_f^o-3)d_{f,eff}^i}{2}+h_3-1}{i}\rho^i(1-\rho)^{\frac{(d_f^o-3)d_{f,eff}^i}{2}+h_3-i-1}\left[\frac{1}{2}(1-\mu)\right]^{\frac{(d_f^o-3)d_{f,eff}^i}{2}+h_3-i}\sum_{k=0}^{\frac{(d_f^o-3)d_{f,eff}^i}{2}+h_3-i-1}\binom{\frac{(d_f^o-3)d_{f,eff}^i}{2}+h_3-i-1+k}{k}\left[\frac{1}{2}(1+\mu)\right]^k\right] \right.$$

$$\left. + \rho^h\left[\frac{1}{2}(1-\mu_J)\right]^{\frac{(d_f^o-3)d_{f,eff}^i}{2}+h_3}\sum_{k=0}^{\frac{(d_f^o-3)d_{f,eff}^i}{2}+h_3-1}\binom{\frac{(d_f^o-3)d_{f,eff}^i}{2}+h_3-1+k}{k}\left[\frac{1}{2}(1+\mu_J)\right]^k\right\}$$

..........(4.45)

and

$$P_b \leq \sum_{w=w_m^o}^{NR_c^o} N^{-(d_f^o-1)/2} \frac{d_f^{o d_f^o} d_f^o!}{p^{(d_f^o+1)/2}((d_f^o-3)/2)!} \frac{w}{k} A_{w,d_f^o,1}^o A_{d_f^o,\frac{(d_f^o-3)d_{f,eff}^i}{2}+h_3,(d_f^o-1)/2}^i$$

$$\left\{ \begin{array}{l} \left[\sum_{i=0}^{\frac{(d_f^o-3)d_{f,eff}^i}{2}+h_3-1} \binom{\frac{(d_f^o-3)d_{f,eff}^i}{2}+h_3-1}{i} \rho^i(1-\rho)^{\frac{(d_f^o-3)d_{f,eff}^i}{2}+h_3-i-1}\left[\frac{1}{2}(1-\mu)\right]^{\frac{(d_f^o-3)d_{f,eff}^i}{2}+h_3-i} \sum_{k=0}^{\frac{(d_f^o-3)d_{f,eff}^i}{2}+h_3-i-1} \binom{\frac{(d_f^o-3)d_{f,eff}^i}{2}+h_3-i-1+k}{k}\left[\frac{1}{2}(1+\mu)\right]^k \right] \\[2em] + \rho^h \left[\frac{1}{2}(1-\mu_J)\right]^{\frac{(d_f^o-3)d_{f,eff}^i}{2}+h_3} \sum_{k=0}^{\frac{(d_f^o-3)d_{f,eff}^i}{2}+h_3-1} \binom{\frac{(d_f^o-3)d_{f,eff}^i}{2}+h_3-1+k}{k}\left[\frac{1}{2}(1+\mu_J)\right]^k \end{array} \right\}$$

………(4.46)

5. SCCC with Pulsed Noise Jamming and No Side Information and with Direct Sequence Spread Spectrum

The simulation model for SCCC/BPSK and direct sequence spread spectrum is shown in Figure 4.2.
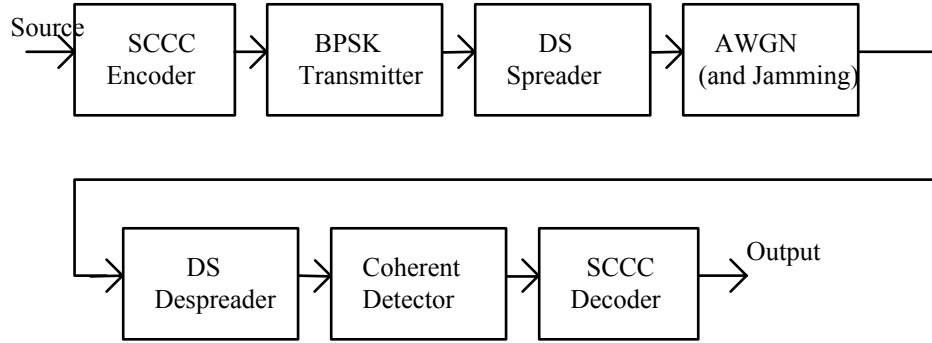
Figure 4.2.   SCCC/BPSK simulation model with DS.

The effect of direct sequence spread spectrum is to decrease the narrowband noise PSD by the number of chips per bit, c. Thus, N_I in (4.12) and (4.13) is reduced to N_I/c. Hence, we obtain for SCCC/BPSK with AWGN, pulsed noise jamming without side information, and direct sequence spread spectrum:

$$P_w \leq \sum_{w=w_m^o}^{NR_c^o} N^{-(d_f^o-1)/2} \frac{d_f^{o d_f^o} d_f^o!}{p^{(d_f^o+1)/2}((d_f^o-3)/2)!} A_{w,d_f^o,1}^o A_{d_f^o,\frac{(d_f^o-3)d_{f,eff}^i}{2}+h_3,(d_f^o-1)/2}^i$$

$$\frac{1}{2} \sum_{i=0}^{\frac{(d_f^o-3)d_{f,eff}^i}{2}+h_3} \binom{\frac{(d_f^o-3)d_{f,eff}^i}{2}+h_3}{i} \rho^i (1-\rho)^{\frac{(d_f^o-3)d_{f,eff}^i}{2}+h_3-i} e^{-R_c E_b \left(\frac{\frac{(d_f^o-3)d_{f,eff}^i}{2}+h_3}{N_o + \frac{i}{h}\frac{N_I}{\rho c}} \right)}$$

………(4.47)

82

$$P_b \leq \sum_{w=w_m^o}^{NR_c^o} N^{-(d_f^o+1)/2} \frac{d_f^{o\,d_f^o} d_f^o!}{p^{(d_f^o-1)/2}((d_f^o-3)/2)!} \frac{w}{k} A^o_{w,d_f^o,1} A^i_{d_f^o,\frac{(d_f^o-3)d_{f,eff}^i}{2}+h_3,(d_f^o-1)/2}$$

$$\frac{1}{2} \sum_{i=0}^{\frac{(d_f^o-3)d_{f,eff}^i}{2}+h_3} \binom{\frac{(d_f^o-3)d_{f,eff}^i}{2}+h_3}{i} \rho^i (1-\rho)^{\frac{(d_f^o-3)d_{f,eff}^i}{2}+h_3-i} e^{-R_c E_b \left(\frac{\frac{(d_f^o-3)d_{f,eff}^i}{2}+h_3}{N_o+\frac{i}{h}\frac{N_I}{\rho c}} \right)}$$

……….(4.48)

6. SCCC with Pulsed Noise Jamming and Side Information and with Direct Sequence Spread Spectrum

For SCCC/BPSK with AWGN, pulsed noise jamming with side information, and direct sequence spread spectrum,

$$P_w \leq \sum_{w=w_m^o}^{NR_c^o} N^{-(d_f^o-1)/2} \frac{d_f^{o\,d_f^o} d_f^o!}{p^{(d_f^o+1)/2}((d_f^o-3)/2)!} A^o_{w,d_f^o,1} A^i_{d_f^o,\frac{(d_f^o-3)d_{f,eff}^i}{2}+h_3,(d_f^o-1)/2}$$

$$\frac{1}{2} \sum_{i=0}^{\frac{(d_f^o-3)d_{f,eff}^i}{2}+h_3} \binom{\frac{(d_f^o-3)d_{f,eff}^i}{2}+h_3}{i} \rho^i (1-\rho)^{\frac{(d_f^o-3)d_{f,eff}^i}{2}+h_3-i} e^{-R_c E_b \left(\frac{\frac{(d_f^o-3)d_{f,eff}^i}{2}+h_3-i}{N_o}+\frac{i}{N_o+N_1/\rho c} \right)}$$

……….(4.49)

$$P_b \leq \sum_{w=w_m^o}^{NR_c^o} N^{-(d_f^o+1)/2} \frac{d_f^{o\,d_f^o} d_f^o!}{p^{(d_f^o-1)/2}((d_f^o-3)/2)!} \frac{w}{k} A^o_{w,d_f^o,1} A^i_{d_f^o,\frac{(d_f^o-3)d_{f,eff}^i}{2}+h_3,(d_f^o-1)/2}$$

$$\frac{1}{2} \sum_{i=0}^{\frac{(d_f^o-3)d_{f,eff}^i}{2}+h_3} \binom{\frac{(d_f^o-3)d_{f,eff}^i}{2}+h_3}{i} \rho^i (1-\rho)^{\frac{(d_f^o-3)d_{f,eff}^i}{2}+h_3-i} e^{-R_c E_b \left(\frac{\frac{(d_f^o-3)d_{f,eff}^i}{2}+h_3-i}{N_o}+\frac{i}{N_o+N_1/\rho c} \right)}$$

……….(4.50)

B. THEORETICAL RESULTS

1. SCCC with Pulsed Noise Jamming and No Side Information

To study the effect of AWGN or SNR in a jamming environment, the theoretical results are plotted for three SNR values: 2 dB (low SNR), 10 dB (medium SNR), and 20 dB (high SNR where AWGN can be considered negligible). To analyze the effect of percentage of signal jammed (ρ), values of 0.001, 0.01, 0.1 and 1.0 are used. The

theoretical results are found to be flat for $\rho = 0.001$ and $\rho = 0.01$ with a bit error ratio (BER) of around 10^{-6} and 10^{-5}, respectively, for different values of SNRs and SJRs (Figures 4.3, 4.4 and 4.5 with 'NSI' labels). Increasing SNR has little effect on the BER. Since ρ is very small, the number of bits that is affected is small. The SCCC is able to correct most erroneous data. The low BER is due to the interleaver gain. For $\rho = 0.1$ and $\rho = 1.0$, the typical 'waterfall' shape is obtained only for high SNR ≥ 10 dB (Figure 4.4). As SNR is increased, the improvement in BER is best for $\rho = 1.0$ (compare Figures 4.4 and 4.5) and for high signal-to-jamming noise ratio (SJR). This is because, although all the bits are jammed, the amount of jamming is small for high SJR. The SCCC decoder is effective for low power levels of barrage jamming. For low SJR (< 0 dB), the theoretical worst case ρ is 1.0 for SNR < 10 dB. For low SJR, with all the bits jammed, the high jamming power creates too many errors for the SCCC decoder to correct, resulting in high BER (this will be discussed further when the theoretical results are compared with the simulation results in Chapter V). For SNR > 14 dB, $\rho = 0.1$ is worst-case, followed by 0.01 and 0.001, respectively, for increasing SJR (Figure 4.5). As SJR increases, the SCCC decoder is more effective, especially for $\rho = 1.0$, since the jamming level has decreased. Jamming with smaller ρ is more effective for high SJR since the power is more concentrated and makes it more difficult for the SCCC decoder to correct. For low SNR, the worst case ρ is 0.1 for SJR ≥ 4dB. For medium SNR, the worst case ρ is 0.1 for SJR ≥ -1 dB. For large SNR, the worst-case ρ is 0.1 for -2 dB $\leq$ SJR ≤ 4 dB. For large SNR and for SJR > 4 dB, the worst-case ρ is 0.01 initially and then 0.001 for higher SJR.

2.   SCCC with Pulsed Noise Jamming and Side Information

Analogous to the case with NSI, the theoretical results were plotted and found to be flat for $\rho = 0.001$ and 0.01 (Figures 4.3, 4.4 and 4.5 with 'SI' labels). As SNR increases, the BER improves, although, the results remain flat. With SI, similar results are also obtained for $\rho = 0.1$. However, unlike the case with NSI, the improvement in BER is greater as SNR increases. For $\rho = 1.0$, the BER continues to improve as SJR increases. For high SNR, the improvement in BER is best for $\rho = 1.0$ (Figure 4.5), although, it is still worst case for SJR < 8 dB. This is because, although all the bits are jammed, the amount of jamming is small for high SJR, and the SCCC decoder is

84

effective for low levels of barrage jamming. However, overall performance is much better for small ρ. For low SJR (< 0 dB), the theoretical worst-case ρ is 1.0. For low SJR, with all the bits jammed, the jamming is too high for the SCCC decoder to correct all errors, resulting in higher BER. As SJR increases, the SCCC decoder is more effective since the power of the jamming decreases. This effect can be seen in Figure 4.4 where the worst case ρ is 0.1 for SJR > 9 dB.

In all cases except $\rho = 1.0$, SCCC/BPSK performs better with SI than without (Figures 4.3, 4.4, and 4.5). For low SNR, the difference in BER between SCCC with SI and SCCC without SI is small for $\rho = 0.001$ and large for $\rho = 0.1$. As SNR increases, the difference in BER between SCCC with SI and SCCC without SI gets larger for small ρ and smaller for large ρ. For $\rho = 1.0$, SI is of no value since all the bits are jammed.

3. SCCC with Pulsed Noise Jamming and No Side Information and Rayleigh Fading with No Channel Information.

The theoretical results were plotted and found to be flat for $\rho = 0.001$ and $\rho = 0.01$ at bit error ratio (BER) of around 10^{-4} for low SNR (Figure 4.6 with 'fading' labels). For higher SNRs, the BER reduces to about 10^{-5} and 10^{-6} for $\rho = 0.01$ and $\rho = 0.001$, respectively (Figures 4.7 and 4.8). When ρ is very small, the number of bits affected is small. The SCCC is able to correct most of these erroneous data, independent of SJR. The low BER is due to the interleaver gain. From Figure 4.6, we see that for high SJRs, the results converge. This means that there is no noticeable difference in BER for different values of ρ. For low SNR, the best case ρ is 0.001 and the worst-case ρ is 1.0 (Figure 4.6) for $-10 \leq$ SJR ≤ 10 dB. For low SNR (< 6 dB), the theoretical worst case ρ is 1.0. For these SNRs, with all the bits jammed, it is possible that the jamming is too high for the SCCC decoder to correct, resulting in higher BER. As SNR increases, the SCCC decoder is more effective since the jamming has decreased. For SNR = 10 dB, $\rho = 0.1$ is worst case for SJR > 4.5 dB (Figure 4.7). As SNR increases to 20 dB, the crossover point for worst-case ρ occurs earlier, i.e., at a SJR of 3 dB (Figure 4.8). Jamming for small ρ is more effective for high SJR since the power is more concentrated and makes it more difficult for the SCCC decoder to correct.

Comparing the BER for SCCC/BPSK with jamming with and without fading, we see that the BER is worse off with fading for all SNRs (Figures 4.6, 4.7 and 4.8), with the fading results being more linear. For higher SNRs, the worst-case crossover point for $\rho = 1.0$ and $\rho = 0.1$ occurs at lower SJRs for the case without fading (Figures 4.7 and 4.8). Fading introduces more noise and uncertainty to the decoder. Thus, it takes greater SJR for $\rho = 0.1$ to become the worst case.

4.   **SCCC with Pulsed Noise Jamming and Side Information and Rayleigh Fading with Channel Information**

The theoretical results are plotted and found to be flat for $\rho = 0.001, 0.01$, and 0.1 for $-10 \leq SJR \leq 10$ dB and for low, medium and high SNRs (Figures 4.9, 4.10, and 4.11 with 'SI and CI' labels). Only for very high SNRs and SJRs do these results start to slope down (Figure 4.12). The worst-case is $\rho = 1.0$ for SNR ≤ 20 dB. For SNR $= 40$ dB and SJR > 19 dB, the worst-case ρ is 0.1 (Figure 4.12). Thus, only at very high SNR and SJR is barrage jamming less effective.

In all cases, SCCC/BPSK with side information and channel information performs better than without (Figures 4.9, 4.10, and 4.11). For smaller ρ, the differences in BER are larger for larger SNR. For $\rho = 1.0$, although SI is of no value since all the bits are jammed, channel information is useful when fading occurs. Thus, SCCC with barrage jamming and Rayleigh fading with channel information performs better than without channel information.

5.   **SCCC with Pulsed Noise Jamming and No Side Information and with Direct Sequence Spread Spectrum (DS)**

With direct sequence spread spectrum, the disparity in BER for different ρ is small for low SNR (Figure 4.15 with 'DS' labels). For higher SNRs and SJRs, $\rho = 0.001$ quickly becomes the worst case (Figures 4.14 and 4.15). This is because for high ρ, due to the processing gain of the DS, the jamming is reduced to a level low enough for the SCCC decoder to correct the errors. For low ρ, the level of jamming is not low enough for the SCCC decoder to be as effective, resulting in more errors. In Figure 4.13, we see that $\rho = 0.001$ is the best case for SJR < 0 dB. For higher SJRs, the BERs for different ρ

are almost the same since their jamming powers are reduced to almost the same levels by DS. For higher SNRs, $\rho = 0.001$ is worst-case at lower SJR, i.e., for SNR = 10 dB and SNR = 20 dB, $\rho = 0.001$ is worst-case for SJR < –4 dB (Figures 4.14 and 4.15).

As expected, SCCC with DS and NSI achieved better results than SCCC with no DS and NSI in all cases (Figures 4.13, 4.14, and 4.15). The use of direct sequence spread spectrum reduces the jamming noise level, thus achieving better results. The gain in performance is largest for $\rho = 1.0$ and smallest for $\rho = 0.001$. This difference in performance is also greater for larger SNRs.

A comparison of a SCCC with no DS and SI with a SCCC with DS and NSI reveals the latter to be more effective for large ρ and less effective for small ρ. From Figure 4.16, we observe that for low SNR and small ρ (≤ 0.01), SI is more important than DS, especially for SJR < 0 dB. It could be that for small ρ, the number of jammed bits is small and, consequently, DS does not play a significant role in reducing the BER. Thus, although with DS the jamming level is lower, without SI the SCCC decoder is not as effective. However, for large ρ, although the number of bits jammed is larger, DS is able to reduce the jamming power significantly so as to reduce the BER. Similar results were obtained for higher SNRs (Figures 4.17 and 4.18). However, we observe that for high SNRs and SJRs, the BER is better for small ρ with DS and NSI than without DS and with SI. This is because the jamming power has become so low that SI is not as useful and the decoder is able to correct many of the errors. In all the cases mentioned, $\rho = 1.0$ with DS and NSI is better than without DS and with SI as expected.

6.   **SCCC with Pulsed Noise Jamming and Side Information and with Direct Sequence Spread Spectrum**

The theoretical results are plotted and found to be flat for $\rho = 0.001$ and 0.01 for –$10 \leq$ SJR ≤ 10 dB and low, medium, and high SNRs (Figures 4.19, 4.20, and 4.21 with 'SI' labels). For low SNR and low SJR (i.e., high jamming), $\rho = 1.0$ is the worst case since all bits are jammed and the jamming power is high enough to disrupt the decoding algorithm (Figure 4.19). For low SNR and high SJR, the differences in BER between

different values of ρ are negligible, since DS reduces the jamming powers to similar levels.

For higher SNR and ρ = 1.0, DS is able to reduce the jamming noise level enough for decoding to be more effective. Thus, ρ = 0.1 is worst case for lower SJRs, and ρ = 0.01 is the worst case for higher SJRs (Figures 4.20 and 4.21). In Figure 4.21, we see that for high SJR, ρ = 0.001 will be the worst-case.

In all cases except ρ = 1.0, DS SCCC performs better with SI than with NSI (Figures 4.19. 4.20, and 4.21). For ρ = 1.0, SI is of no value since all the bits are jammed. Thus, both graphs (SI and NSI) are the same. Note that SI is more effective for small values of ρ and higher SNRs.

As expected, SCCC with SI and DS achieved better results than SCCC with SI and no DS in all cases (Figures 4.22, 4.23, and 4.24). The DS is able to reduce the jamming noise level, thus achieving better BER. The gain in performance is largest for ρ = 1.0.

When compared with SCCC with no DS and NSI, SCCC with DS and SI is superior: with DS the jamming power is reduced, and with SI the decoder is able to correct better. Thus, SCCC with DS and SI outperforms SCCC with no DS and NSI (Figure 4.25, 4.26, and 4.27). The gain in performance is better for small ρ and high SNRs.

C.   SUMMARY OF RESULTS

From the theoretical results, the following conclusions can be made:

1.   SCCC with direct sequence spread spectrum, side information, and channel information is the most effective in reducing the effects of jamming and fading.

2.   Side information works best for high values of ρ when SNR is low and low values of ρ when SNR is high.

3.   When fading is present, barrage jamming is most effective for lower SNRs and SJRs while smaller values of ρ are more effective for higher SNRs and SJRs.

4.   Direct sequence spread spectrum works best for high values of ρ, i.e., barrage jamming, and low overall SNR.
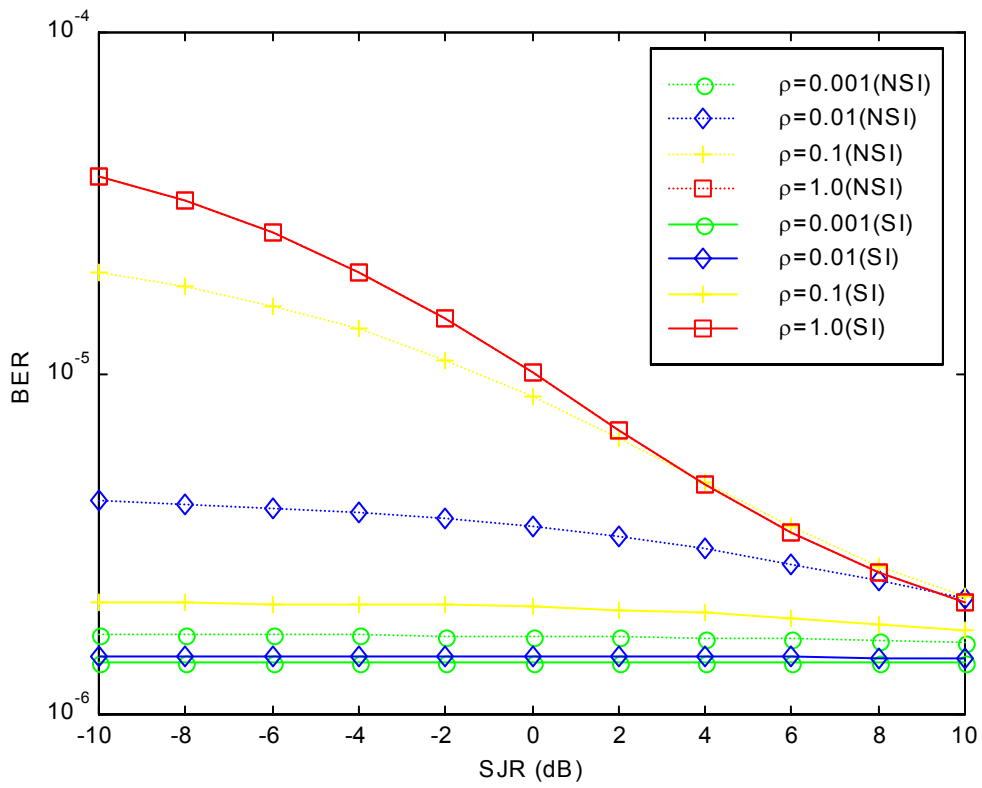
Figure 4.3.   Theoretical SCCC/BPSK with AWGN and pulsed noise jamming: effect of side information on BER for ρ = 0.001, 0.01, 0.1 and 1.0, SNR = 2 dB and SJR = -10 to 10 dB.

Figure 4.4.   Theoretical SCCC/BPSK with AWGN and pulsed noise jamming: effect of side information on BER for ρ = 0.001, 0.01, 0.1 and 1.0, SNR = 10 dB and SJR = -10 to 10 dB.

Figure 4.5.   Theoretical SCCC/BPSK with AWGN and pulsed noise jamming: effect of side information on BER for ρ = 0.001, 0.01, 0.1 and 1.0, SNR = 20 dB and SJR = -10 to 10 dB.

Figure 4.6.   Theoretical SCCC/BPSK with AWGN and pulsed noise jamming with no side information: effect of Rayleigh fading with no channel information on BER for ρ = 0.001, 0.01, 0.1 and 1.0, SNR = 2 dB and SJR = 0 to 10 dB.

Figure 4.7.   Theoretical SCCC/BPSK with AWGN and pulsed noise jamming with no side information: effect of Rayleigh fading with no channel information on BER for ρ = 0.001, 0.01, 0.1 and 1.0, SNR = 10 dB and SJR = 0 to 10 dB.

Figure 4.8.   Theoretical SCCC/BPSK with AWGN and pulsed noise jamming with no side information: effect of Rayleigh fading with no channel information on BER for ρ = 0.001, 0.01, 0.1 and 1.0, SNR = 20 dB and SJR = 0 to 10 dB.

Figure 4.9.   Theoretical SCCC/BPSK with AWGN, pulsed noise jamming and Rayleigh fading: effect of side information and channel information on BER for $\rho = 0.001$, 0.01, 0.1 and 1.0, SNR = 2 dB and SJR = 0 to 10 dB.
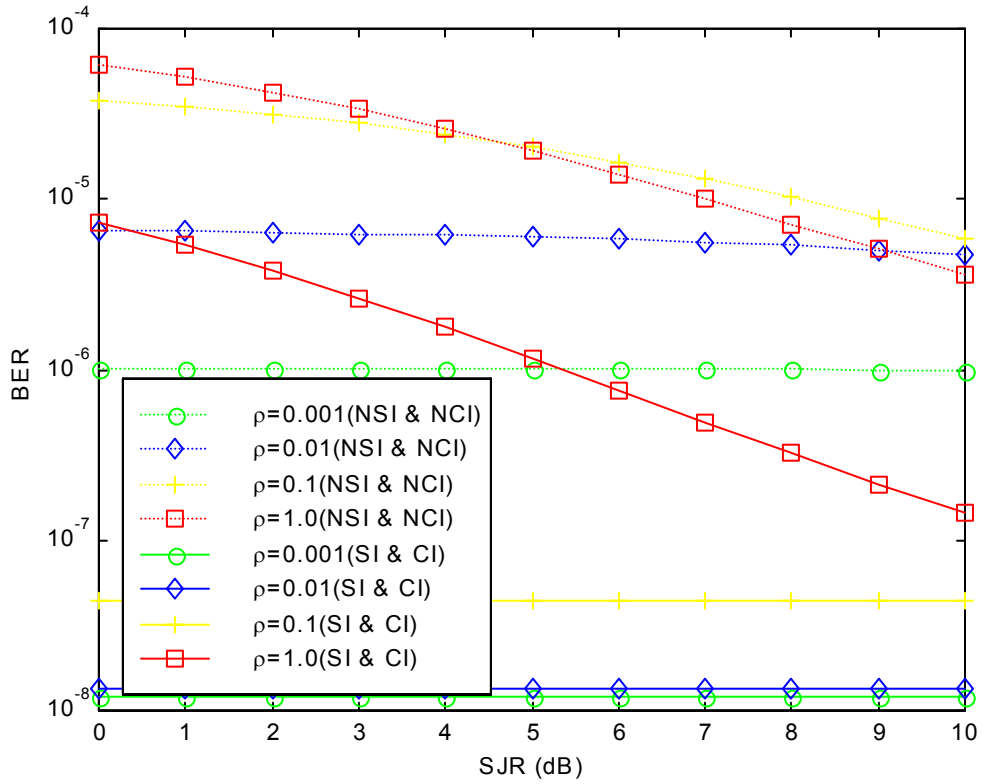
Figure 4.10.   Theoretical SCCC/BPSK with AWGN, pulsed noise jamming and Rayleigh fading: effect of side information and channel information on BER for ρ = 0.001, 0.01, 0.1 and 1.0, SNR = 10 dB and SJR = 0 to 10 dB.
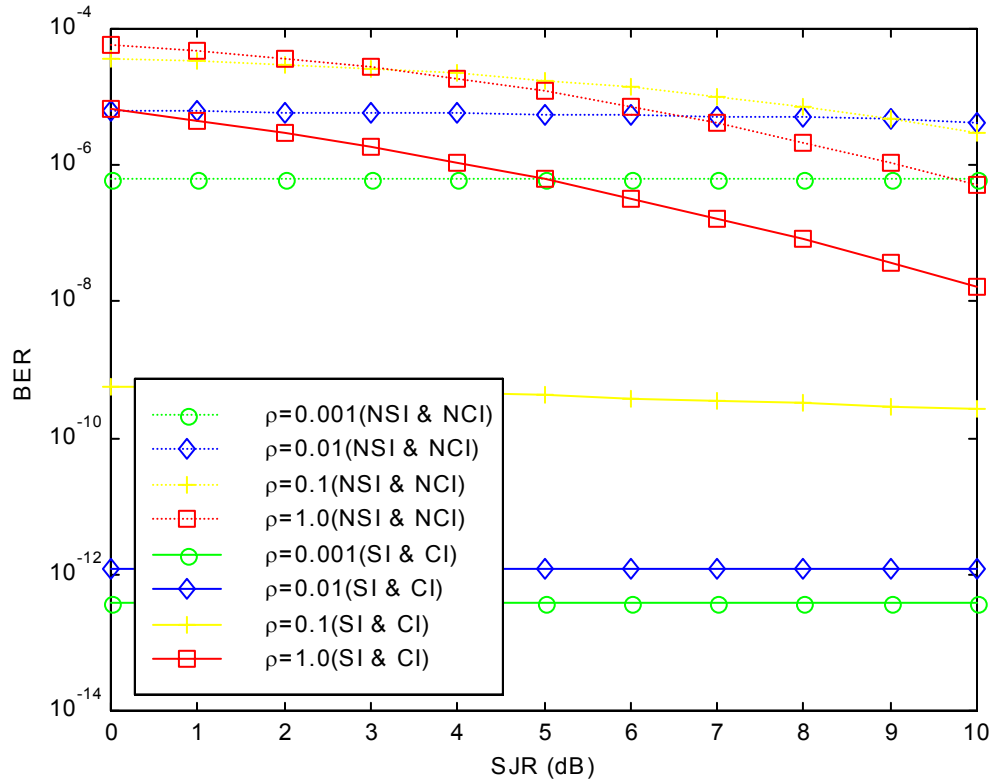
Figure 4.11.   Theoretical SCCC/BPSK with AWGN, pulsed noise jamming and Rayleigh fading: effect of side information and channel information on BER for ρ = 0.001, 0.01, 0.1 and 1.0, SNR = 20 dB and SJR = 0 to 10 dB.
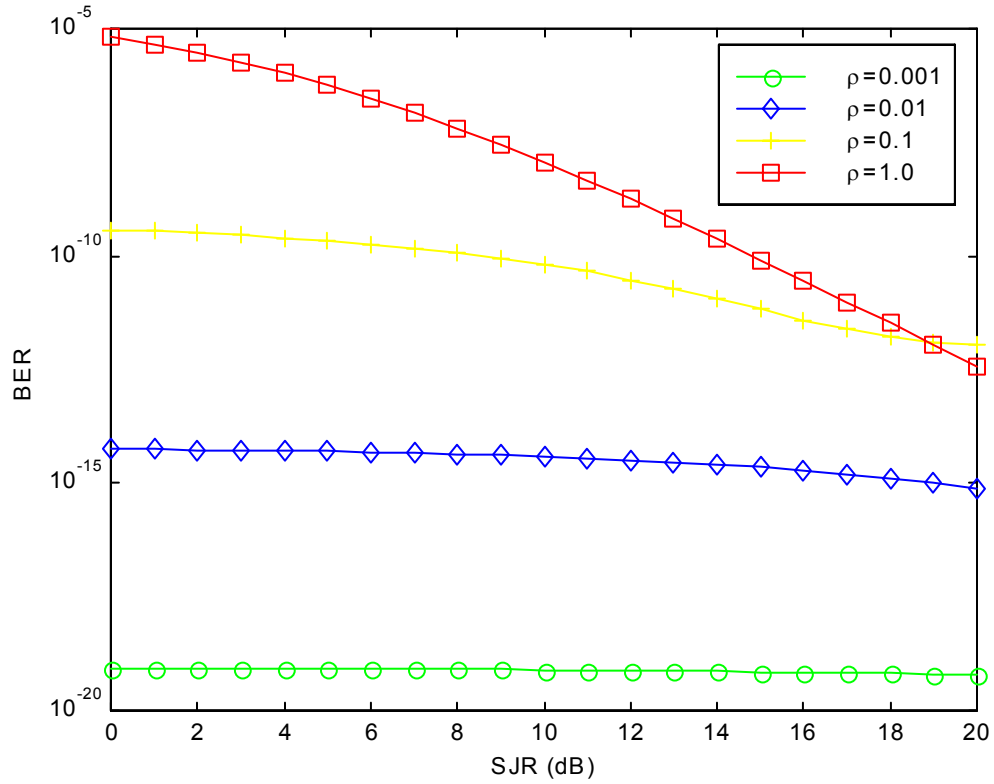
Figure 4.12.   Theoretical SCCC/BPSK with AWGN, pulsed noise jamming with side information and Rayleigh fading with channel information: effect of SJR on BER for ρ = 0.001, 0.01, 0.1 and 1.0, SNR = 40 dB and SJR = 0 to 20 dB.
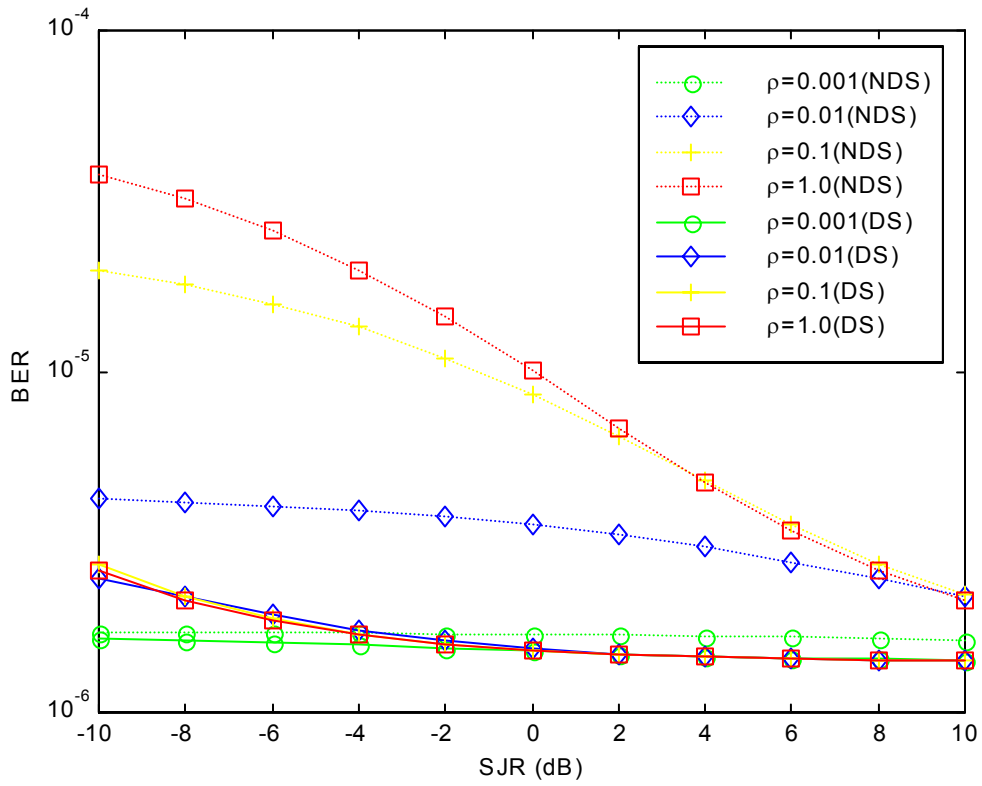
Figure 4.13.   Theoretical SCCC/BPSK with AWGN and pulsed noise jamming with no side information: effect of direct sequence spread spectrum on BER for ρ = 0.001, 0.01, 0.1 and 1.0, SNR = 2 dB and SJR = -10 to 10 dB.
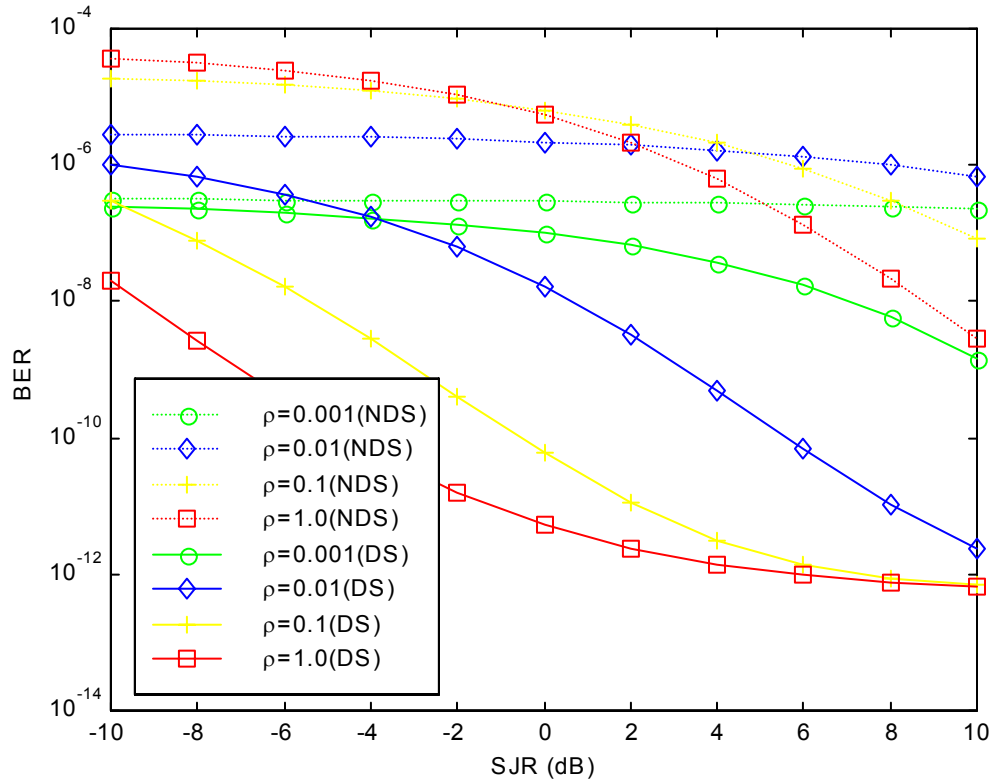
Figure 4.14.   Theoretical SCCC/BPSK with AWGN and pulsed noise jamming with no side information: effect of direct sequence spread spectrum on BER for ρ = 0.001, 0.01, 0.1 and 1.0, SNR = 10 dB and SJR = -10 to 10 dB.
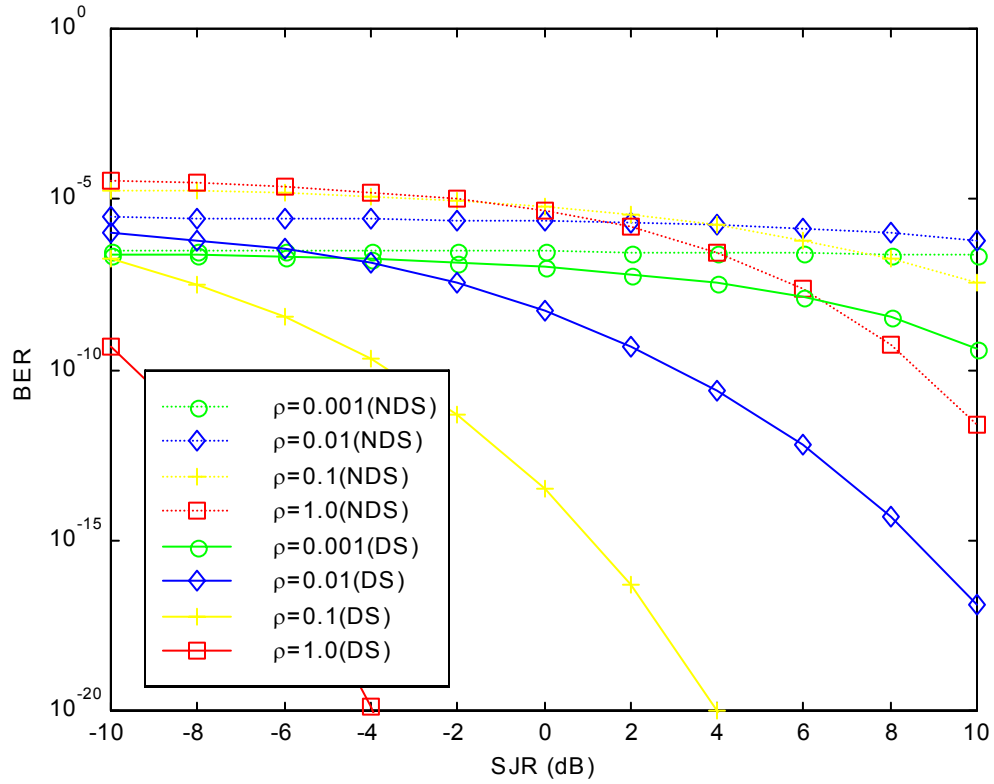
Figure 4.15.   Theoretical SCCC/BPSK with AWGN and pulsed noise jamming with no side information: effect of direct sequence spread spectrum on BER for ρ = 0.001, 0.01, 0.1 and 1.0, SNR = 2 dB and SJR = -10 to 10 dB.
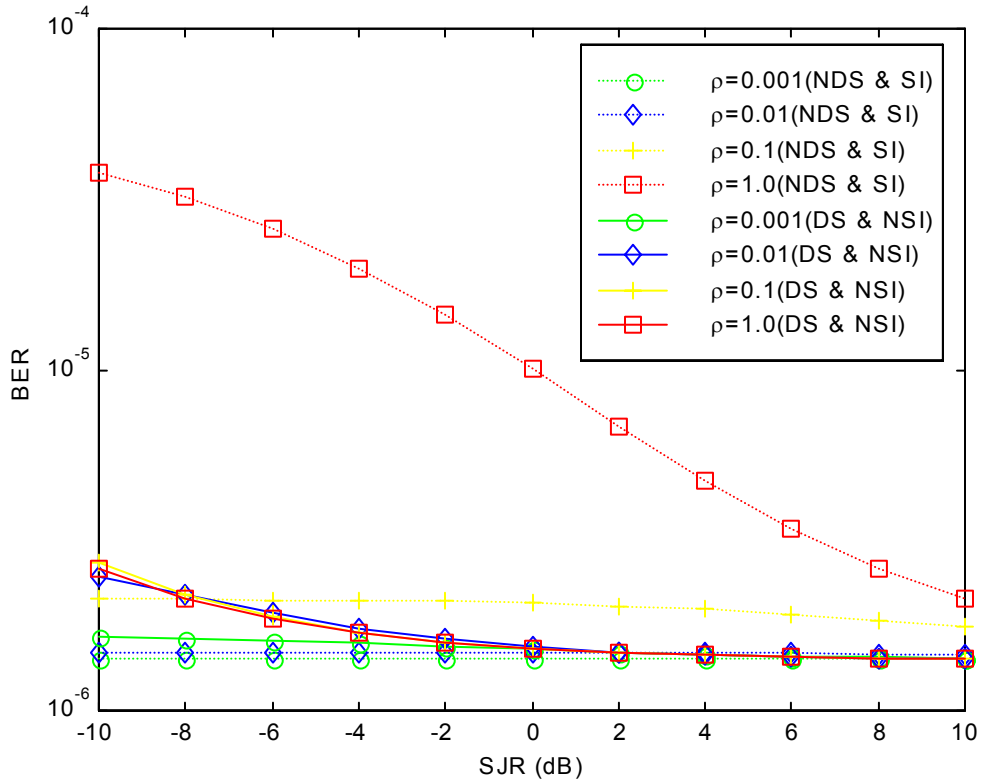
Figure 4.16. Theoretical SCCC/BPSK with AWGN and pulsed noise jamming: Comparison of SCCC with direct sequence spread spectrum and no side information with SCCC with no direct sequence spread spectrum and with side information for $\rho = 0.001$, 0.01, 0.1 and 1.0, SNR = 2 dB and SJR = -10 to 10 dB.
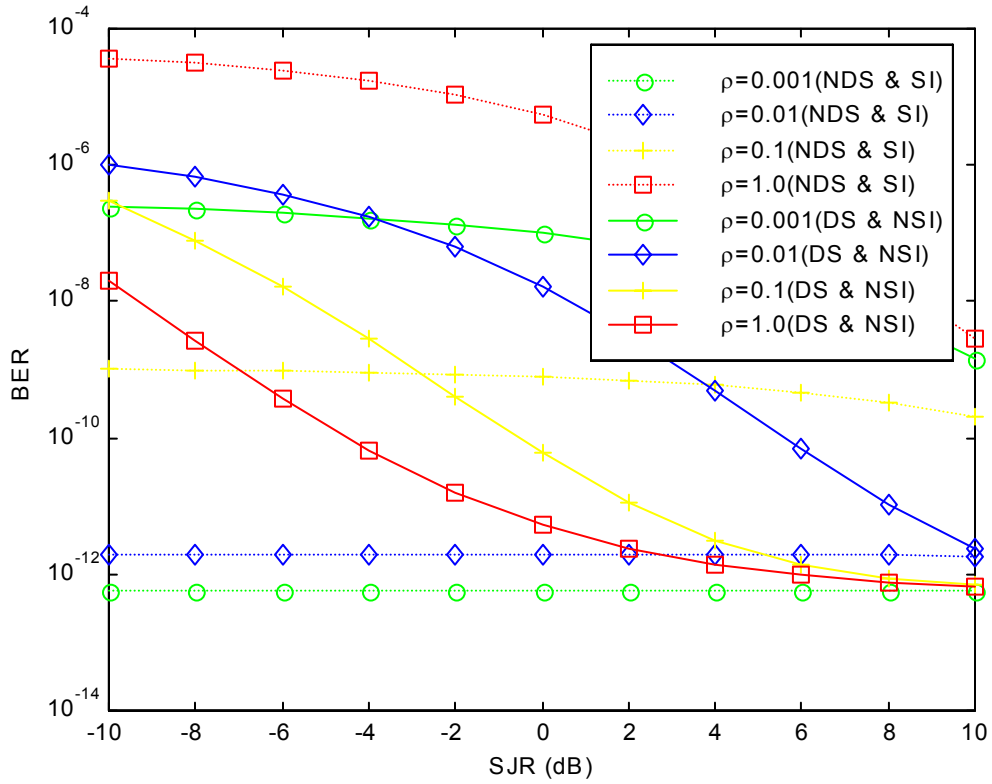
Figure 4.17. Theoretical SCCC/BPSK with AWGN and pulsed noise jamming: Comparison of SCCC with direct sequence spread spectrum and no side information with SCCC with no direct sequence spread spectrum and with side information for ρ = 0.001, 0.01, 0.1 and 1.0, SNR = 10 dB and SJR = -10 to 10 dB.
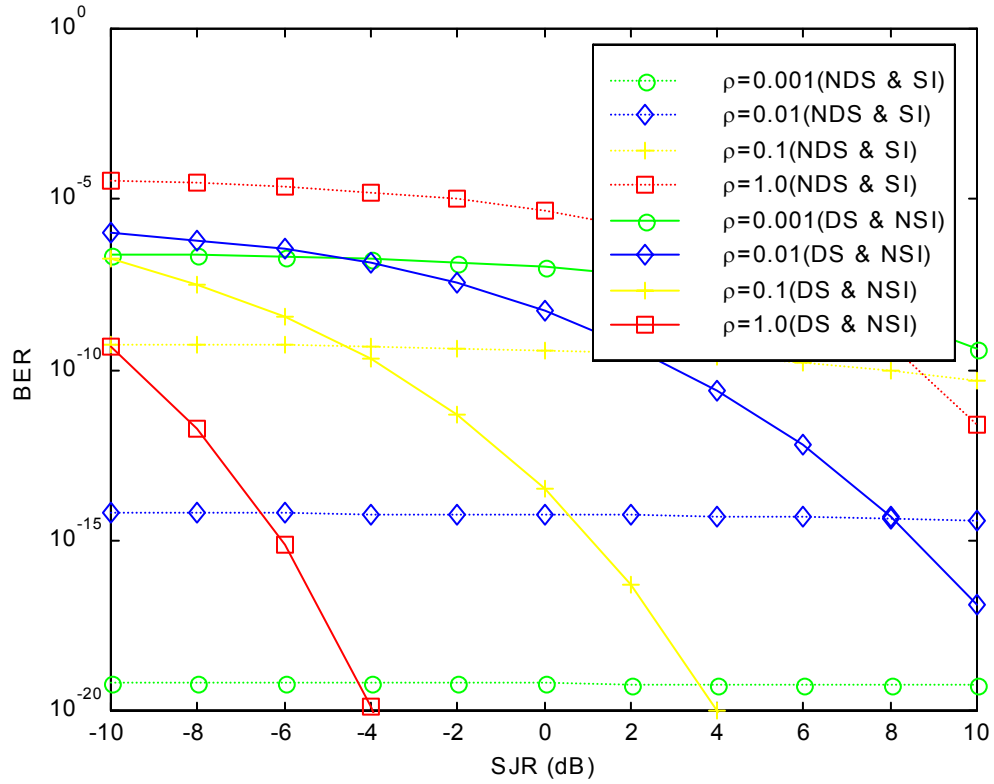
Figure 4.18. Theoretical SCCC/BPSK with AWGN and pulsed noise jamming: Comparison of SCCC with direct sequence spread spectrum and no side information with SCCC with no direct sequence spread spectrum and with side information for ρ = 0.001, 0.01, 0.1 and 1.0, SNR = 20 dB and SJR = -10 to 10 dB.

Figure 4.19.   Theoretical SCCC/BPSK with AWGN, pulsed noise jamming and direct sequence spread spectrum: effect of side information on BER for ρ = 0.001, 0.01, 0.1 and 1.0, SNR = 2 dB and SJR = -10 to 10 dB.
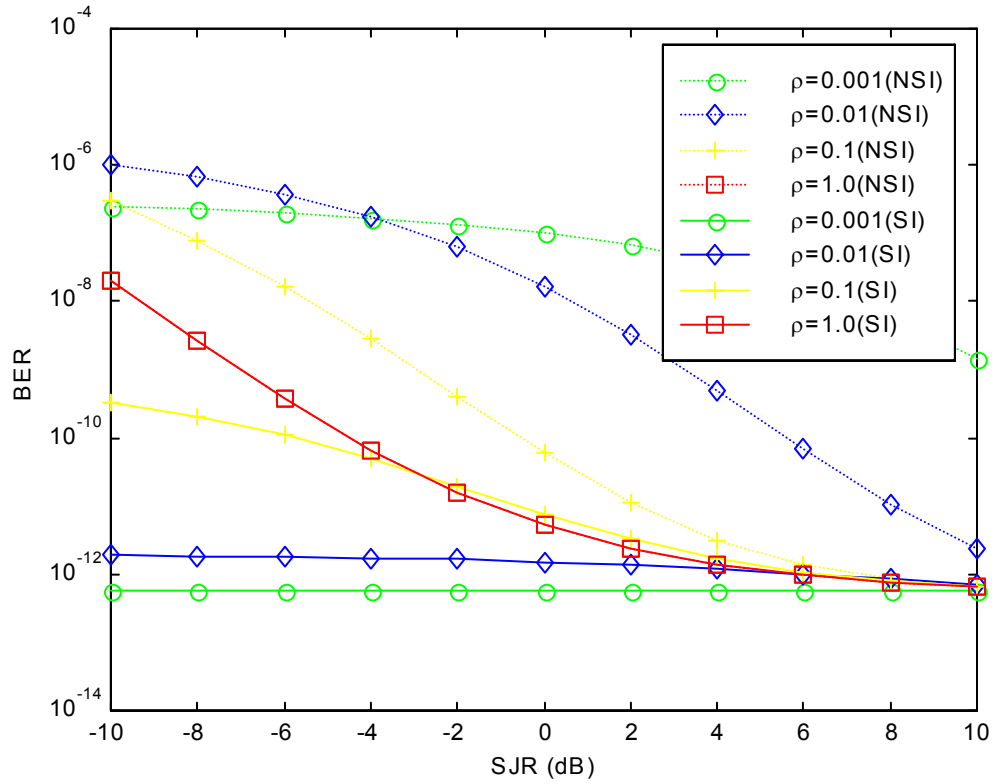
Figure 4.20.   Theoretical SCCC/BPSK with AWGN, pulsed noise jamming and direct sequence spread spectrum: effect of side information on BER for ρ = 0.001, 0.01, 0.1 and 1.0, SNR = 10 dB and SJR = -10 to 10 dB.
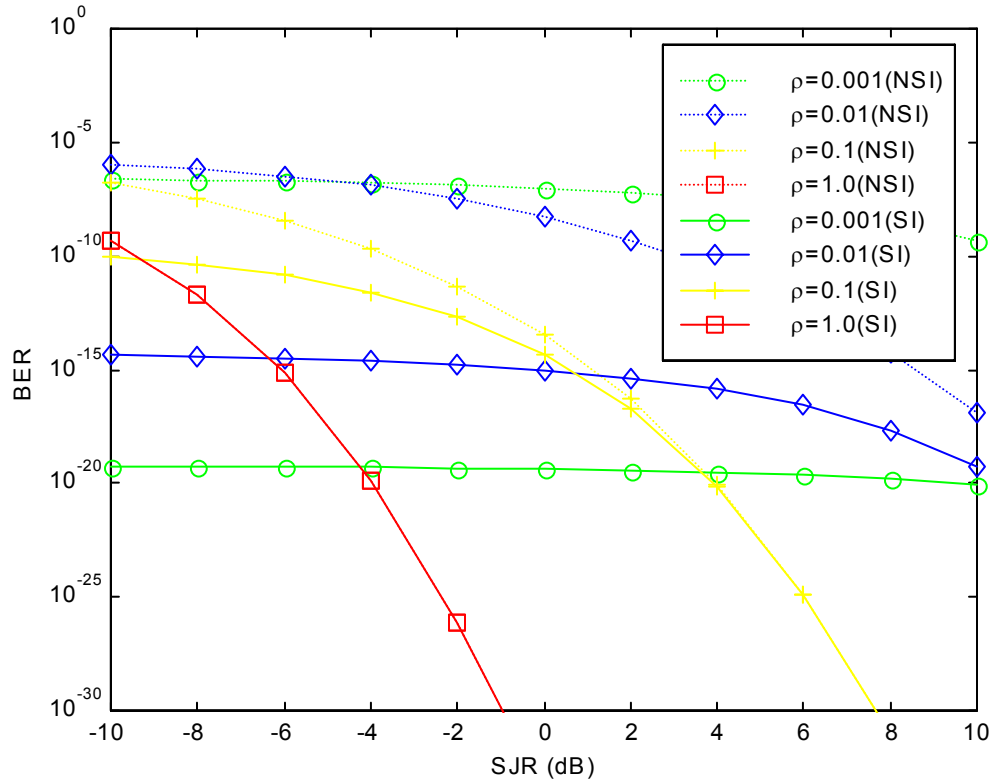
Figure 4.21. Theoretical SCCC/BPSK with AWGN, pulsed noise jamming and direct sequence spread spectrum: effect of side information on BER for ρ = 0.001, 0.01, 0.1 and 1.0, SNR = 20 dB and SJR = -10 to 10 dB.
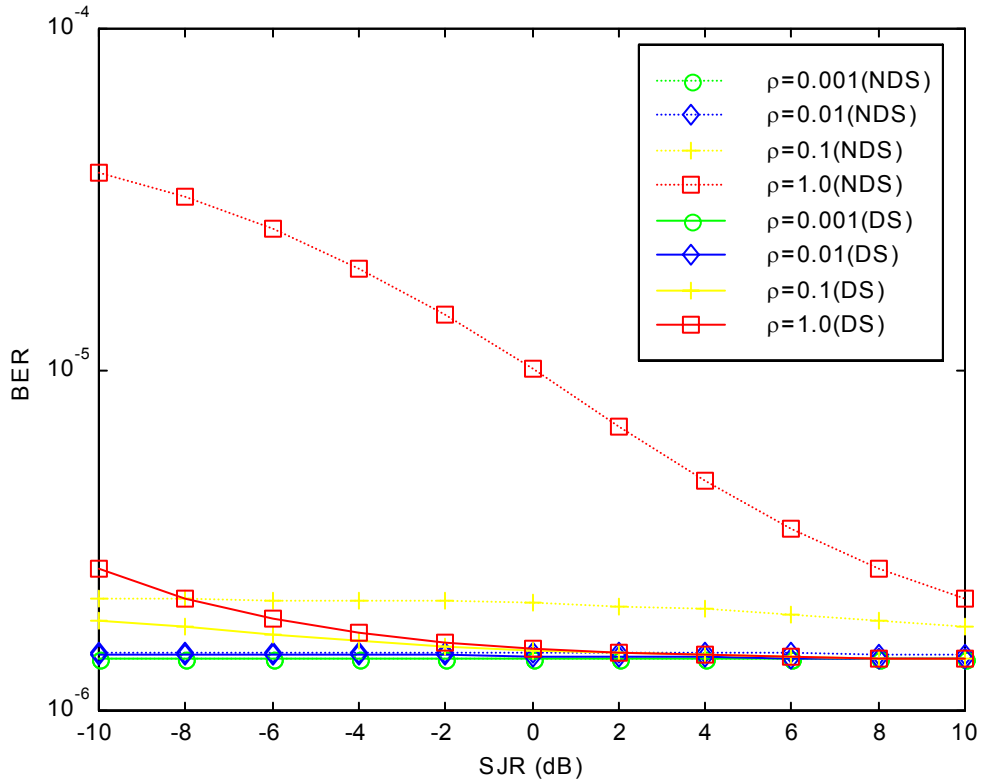
Figure 4.22.　　Theoretical SCCC/BPSK with AWGN and pulsed noise jamming with side information: effect of direct sequence spread spectrum on BER for ρ = 0.001, 0.01, 0.1 and 1.0, SNR = 2 dB and SJR = -10 to 10 dB.
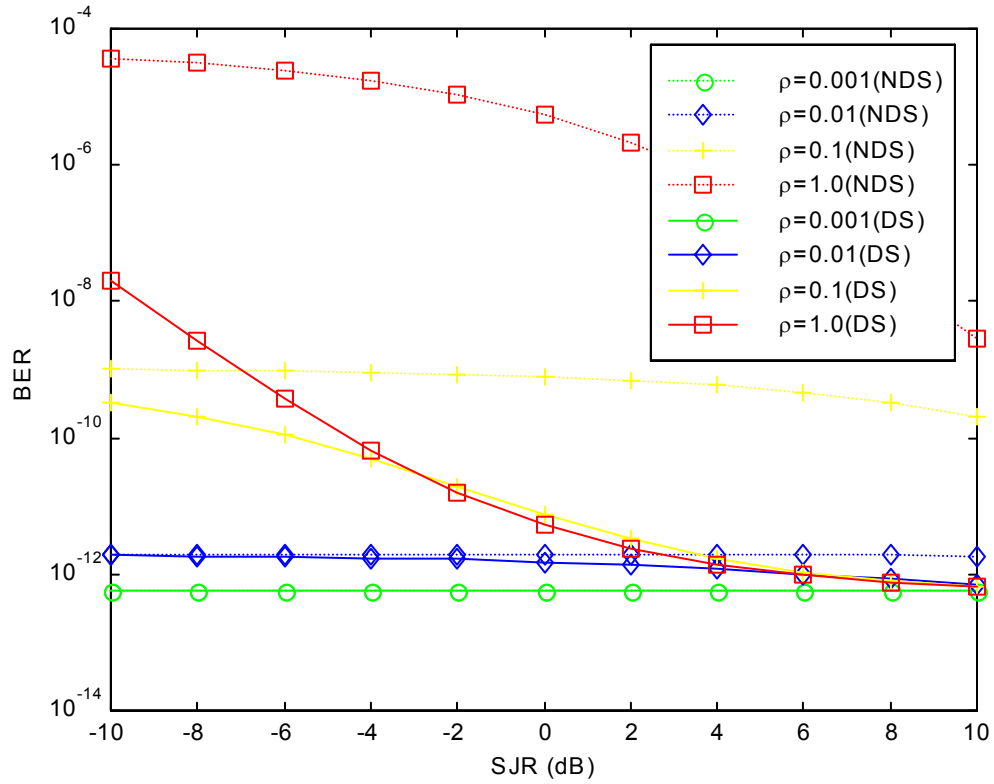
Figure 4.23.   Theoretical SCCC/BPSK with AWGN and pulsed noise jamming with side information: effect of direct sequence spread spectrum on BER for ρ = 0.001, 0.01, 0.1 and 1.0, SNR = 10 dB and SJR = -10 to 10 dB.
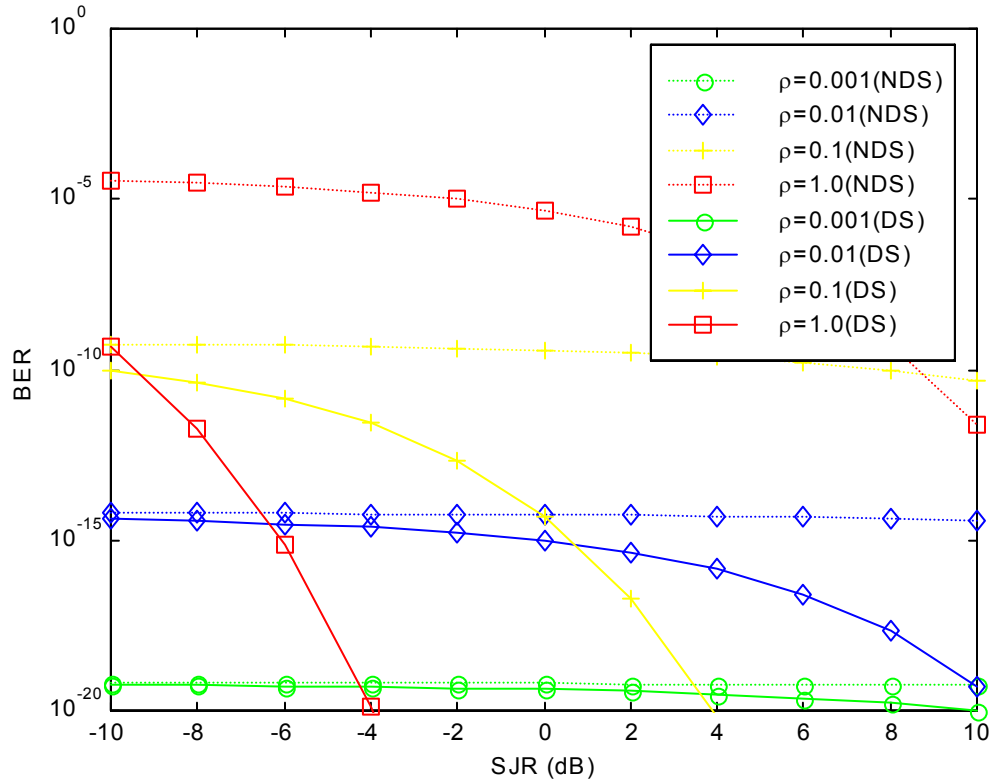
Figure 4.24. Theoretical SCCC/BPSK with AWGN and pulsed noise jamming with side information: effect of direct sequence spread spectrum on BER for ρ = 0.001, 0.01, 0.1 and 1.0, SNR = 20 dB and SJR = -10 to 10 dB.
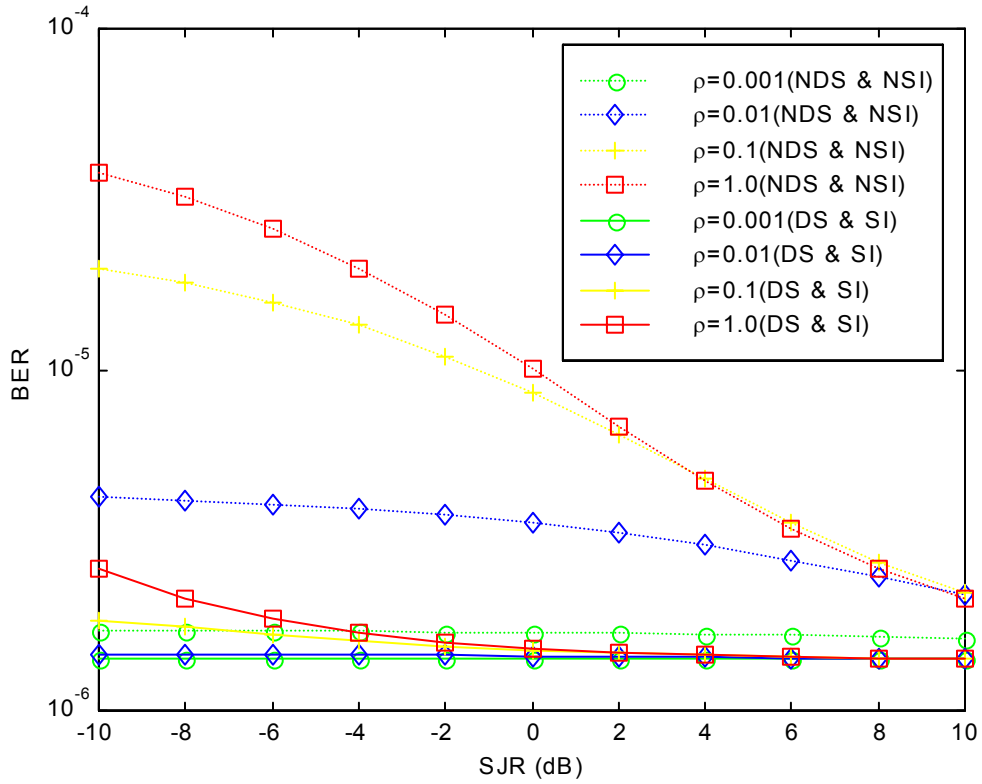
Figure 4.25. Theoretical SCCC/BPSK with AWGN and pulsed noise jamming: Comparison of SCCC with direct sequence spread spectrum and side information with SCCC with no direct sequence spread spectrum and with no side information for ρ = 0.001, 0.01, 0.1 and 1.0, SNR = 2 dB and SJR = -10 to 10 dB.
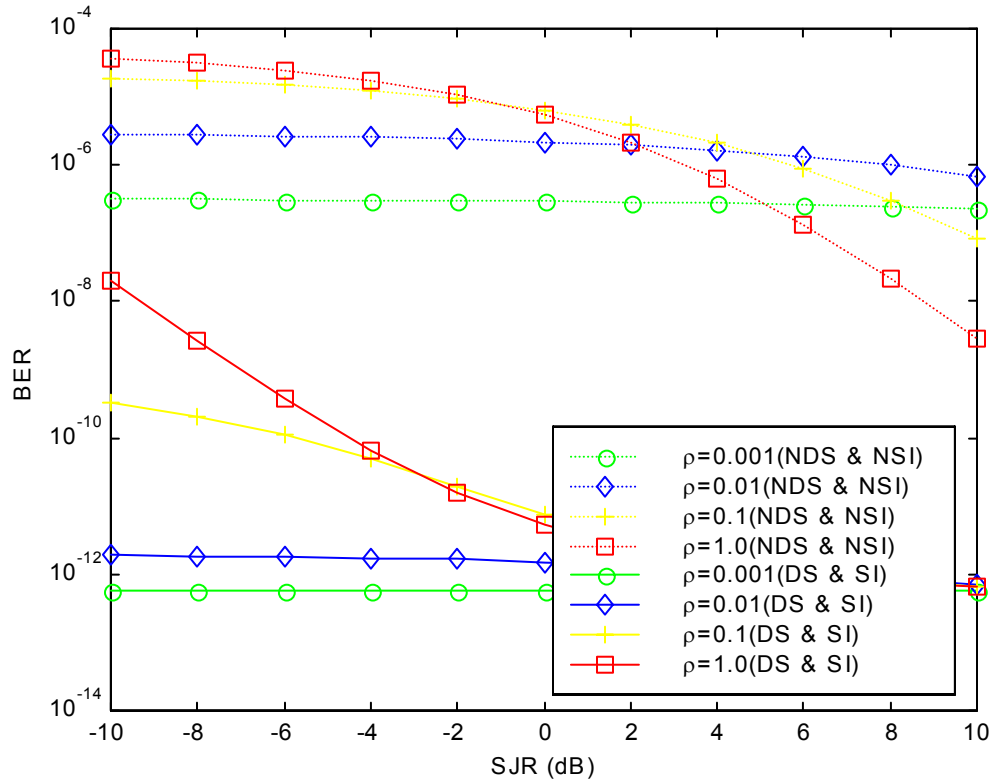
Figure 4.26. Theoretical SCCC/BPSK with AWGN and pulsed noise jamming: Comparison of SCCC with direct sequence spread spectrum and side information with SCCC with no direct sequence spread spectrum and with no side information for ρ = 0.001, 0.01, 0.1 and 1.0, SNR = 10 dB and SJR = -10 to 10 dB.
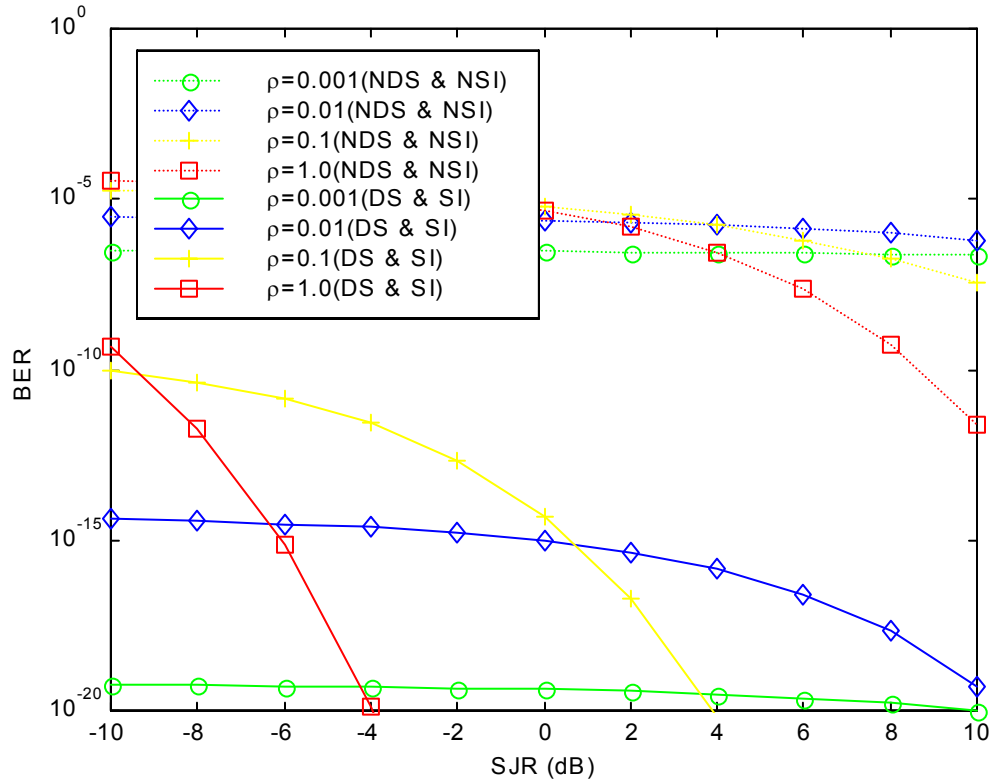
Figure 4.27. Theoretical SCCC/BPSK with AWGN and pulsed noise jamming: Comparison of SCCC with direct sequence spread spectrum and side information with SCCC with no direct sequence spread spectrum and with no side information for ρ = 0.001, 0.01, 0.1 and 1.0, SNR = 20 dB and SJR = -10 to 10 dB.

V. SIMULATION RESULTS OF SCCC WITH COHERENT BPSK IN PULSED NOISE JAMMING, RAYLEIGH FADING AND DIRECT SEQUENCE SPREAD SPECTRUM

A. SIMULATION PARAMETERS

In this chapter, pulsed noise jamming (both with and without side information) was simulated for various conditions: AWGN, Rayleigh fading (with and without channel information) and direct sequence spread spectrum with a processing gain of 64. The pulsed noise interference is assumed to be unaffected by the fading channel.

The Monte Carlo simulations were carried out with the following parameter values: a) ten iterations of the decoding algorithm, b) signal-to-noise ratio (SNR) from 0 to 20 dB in increments of 2 dB (in some cases increments of 0.2 dB were used), c) signal-to-jammer ratio (SJR) from −10 to 10 dB in increments of 2 dB, d) percentage of signal jammed (ρ) of 0.1%, 1%, 10%, and 100%. In addition, based on the bit error ratio (BER), the worst case ρ (ρ_{wc}) for each SJR was also determined,

The following types of graphs were plotted: a) BER vs. SJR for each value of SNR and with ρ as a parameter, b) BER vs. SJR for each value of SNR and for $\rho = 0.1$ to 1.0, c) theoretical bounds on BER vs. SNR.

The following comparisons will be made: a) SCCC/BPSK with pulsed noise jamming and no side information compared to SCCC/BPSK with side information, b) SCCC/BPSK with pulsed noise jamming both with and without Rayleigh fading, and c) SCCC/BPSK with pulsed noise jamming both with and without direct sequence spread spectrum. Theoretical bounds will be compared with the simulation results where possible.

B.   SCCC   WITH   PULSED   NOISE   JAMMING   AND   NO   SIDE INFORMATION

For the simulations in this section, the decoder has no side information (NSI), i.e., no information on which bits are jammed or knowledge of the SNR transmitted.

1.   Observations

The general performance of the SCCC with NSI is shown in Figure 5.1 for values of SJR from zero to ten dB and for SNR from zero to twenty dB. In the figure, in order to show the graphs for the different values of ρ, the SJR is offset by ρ in dB. Thus, for ρ = 0.001, 0.01, 0.1, 1.0, there are offsets of -30, -20, -10, 0 dB, respectively. In general, for a given SJR, BER improves as SNR increases. For zero SNR, BER is almost independent of SJR. As SNR increases, the effect of both ρ and SJR become more pronounced. It is obvious that BER worsens as ρ increases. It will be shown later that the value of ρ_{wc} is dependent on SJR.

For ρ = 0.001, the effect of SJR is, over the range of SJR considered, negligible regardless of SNR; i.e., it does not matter what the value of SJR is. Since ρ is very small, the number of bits affected is small. The SCCC is able to correct most of the erroneous data bits. For SNR above 1.6 dB, all errors are corrected. This is about half a dB above the SNR where all erroneous data bits are correctly decoded for SCCC with AWGN only. In other words, this fraction of pulsed noise jamming only degrades overall performance by about 0.5 dB.

For ρ = 0.01, the BER decreases as SNR increases. For SNR > 4 dB, all errors are corrected. The effect for SJR < 0 dB on BER is also minimal. In this case, pulsed noise jamming degrades the overall performance by about 3 dB when compared with SCCC with AWGN only. For ρ = 0.1, the BER is almost independent of SNR for SJR < 0 dB. When SNR > 4 dB and SJR > 8 dB, all the errors are corrected.

The worst case ρ is 1.0 for SNR < 4 dB.   For SNR $\leq$ 1.6 dB, the effect of SJR on BER is minimal. As SNR increases, the BER graphs take the usual 'waterfall' shapes for increasing SJR.

For low SNR ($<$ 4 dB) and as ρ increases, BER worsens for small SJR (Figure 5.2 with 'simulation' labels). This is expected since more bits are affected. However, higher jamming power occurs for smaller ρ. This affects the ability to correct errors. For SNR greater than 4 dB, worst case ρ (ρ_{wc}) depends on SJR. For low SJR ($<$ 4 dB), ρ_{wc} is 1.0. As SJR increases, ρ_{wc} becomes smaller: when 4 dB$<$ SJR $<$ 7 dB, ρ_{wc} = 0.1; when SJR $>$ 7 dB, ρ_{wc} = 0.01. Similar trends were also observed elsewhere [Ref. 95] for Turbo codes at higher SNR.

When SNR is increased to 6 dB, the SCCC is able to correct all errors that are introduced when ρ = 0.01 for the range of SJR examined. Thus, when ρ = 0.01, the jammer does not contribute to the BER. For low SJR ($<$ 1 dB), ρ_{wc} = 1.0. As SJR increases, ρ_{wc} decreases to 0.4 and then 0.1 (Figure 5.3).

When SNR increases to 8 dB, ρ_{wc} = 1.0 for low SJR ($<$ 0 dB), ρ_{wc} = 0.5 for 0 $<$ SJR $<$ 3 dB and ρ_{wc} = 0.4 for SJR $>$ 3 dB (Figure 5.4). For higher SNR ($>$ 8 dB), ρ_{wc} is between 0.3 and 0.6, but the improvement in BER is insignificant as SNR increases. For larger SJR, only the smaller range of ρ leads to uncorrected errors.

For sufficiently high SNR ($\geq$ 10 dB), all errors are corrected except for SJR $<$ 4 dB (Figure 5.1). If SNR is large enough, the BER approaches asymptotically that obtained with no jamming as expected. For ρ = 0.1, all errors are corrected for SJR $>$ 0 dB, while for ρ = 1.0, SJR $>$ 2 dB is required to correct all errors. Increasing SNR more than 10 dB has little effect on the BER.

2.   Comparison with Theoretical Values

For extremely low BERs, bounds are often calculated as it is often impractical to generate simulation results. For zero SNR, the simulation results showed BER at around 0.1 independent of SJR and ρ while theoretical results showed BER to be 10^{-5} independent of SJR and ρ. Thus, the bounds are not valid for SNR = 0 dB. From Figure 5.2, for SNR = 4 dB and SJR $>$ 8 dB, ρ_{wc} is 0.01 for both theory and simulation. The theoretical bounds appear to be an extension of the simulation results. Note that for these cases, AWGN is not ignored. Thus, for low SNR ($<$ 4 dB), the theoretical bounds correctly predicted ρ_{wc}.

117

More often than not, the amount of jamming noise is much greater than AWGN so that AWGN can be ignored. In Figure 5.5, the theoretical bounds for $\rho = 0.1$ to 1.0 and SNR = 20 dB are compared with simulation results. The bounds are known to diverge from simulation results for SJRs (or SNRs) below 2 or 3 dB [Ref. 100], i.e., they are no longer accurate. Thus, we cannot concretely determine the precision of the bounds. Note, however that the general shape of the bounds conforms to what is expected. For high SJRs, when every bit is jammed ($\rho = 1.0$) the jamming power is so low that the SCCC is able to correct more errors. Thus, BER with $\rho = 1.0$ is best for high SJR. For low SJRs, $\rho = 1.0$ is predicted to perform the worst. With high jamming power, i.e., low SJR, the SCCC decoder is unable to correct the data bits properly since all bits are jammed at a high noise power. Thus, the simulation results show $\rho = 1.0$ to be the worst case. If the theoretical bounds are extended for SJR < 6 dB, they intersect simulation results where $\rho = 1.0$ becomes the worst case. Thus, both simulation and theory results agree.

C.   SCCC WITH PULSED NOISE JAMMING AND SIDE INFORMATION

In these simulations, the decoder is assumed to have knowledge of the jammed bits and their overall signal-to-total noise ratios (SI). This SI is used in the decoding algorithm.

1.   Observations

The general performance of the SCCC with SI is shown in Figure 5.6 for values of SJR greater than zero and for SNR from 0 to 20 dB in increments of 2 dB. In the figure, in order to show the graphs for the different values of ρ, the SJR is offset by ρ in dB. Thus, for $\rho = 0.001, 0.01, 0.1, 1.0$, there will be offsets of $-30, -20, -10, 0$ dB, respectively. In general, the BER improves as SNR increases. For zero SNR, the BER is almost independent of SJR and ρ. As SNR increases, the effect of both ρ and SJR become more pronounced. It is apparent that BER decreases as ρ increases. In general, $\rho_{wc} = 1.0$. It will be shown later that the value of ρ_{wc} is also dependent on SJR.

For $\rho = 0.001$, the effect of SJR on BER is negligible. Since ρ is very small, the number of bits that is affected is small and the SCCC is able to correct most of the erroneous data. For SNR above 1.6 dB, all errors with $\rho = 0.001$ are corrected. This is about half a dB above the SNR where all data bits are correctly decoded with only AWGN. This is the same result obtained in the NSI case. Thus, SI does not improve the BER when ρ is very small. For $\rho = 0.01$, the BER performance improves as SNR increases. For SNR > 4 dB, all errors are corrected. The effect of SJR < 0 dB on BER is also minimal. In this case, pulsed noise jamming degrades the overall performance by about 3 dB compared with SCCC with AWGN only. Thus, SI does not improve the BER when ρ is small. For $\rho = 0.1$, the BER is independent of the SNR for SJR < 0 dB. When SNR ≥ 4 dB and SJR ≥ 8 dB, all the errors are corrected.

The worst case ρ is 1.0 for SNR < 2 dB. For low SNR (< 1.5 dB), the effect of SJR on BER is marginal. As SNR increases, the BER graphs take the usual 'waterfall' shapes for increasing SJR.

At low SNR (< 4 dB) and as ρ increases, BER worsens for small SJR (Figure 5.7). This is expected since more bits are affected. However, higher jamming power occurs for smaller ρ. This affects the ability to correct errors. For SNR greater than 4 dB, worst case ρ (ρ_{wc}) depends on SJR. For low SJR (< 4 dB), ρ_{wc} is 1.0. As SJR increases, ρ_{wc} becomes smaller: when 4 dB$<$ SJR < 6 dB, $\rho_{wc} = 0.1$; when SJR > 6 dB, $\rho_{wc} = 0.01$.

When SNR is increased to 6 dB, the SCCC is able to correct all errors when $\rho = 0.01$ for the range of SJR examined. Thus, when $\rho = 0.01$ the jammer does not contribute to the BER. For SJR < 2 dB, $\rho_{wc} = 1.0$. As SJR increases, ρ_{wc} decreases to 0.4 and then 0.2 (Figure 5.8).

When SNR is increased to 8 dB, $\rho_{wc} = 1.0$ for SJR < 2 dB and $\rho_{wc} = 0.4$ for higher SJR (Figure 5.9). For higher SNR (> 8 dB), ρ_{wc} is between 0.3 and 0.6, but the improvement in BER is insignificant as SNR increases. For larger SJR, only a small range of ρ leads to uncorrected errors.

For sufficiently high SNR, all errors are corrected except with SJR < 2 dB, i.e., if the SNR is large enough, the BER approaches asymptotically to that obtained with no jamming as expected. For $\rho = 0.1$, all errors are corrected for SJR > 0 dB while for $\rho = 1.0$, SJR > 2 dB is required. Increasing SNR has little effect on the BER for SNR > 10 dB (Figure 5.6).

2. Comparison with Theoretical Values

For SNR = 0 dB, the simulation results predict a BER of about 0.1 independent of SJR and ρ while theoretical results predicted a BER of about 10^{-5} independent of SJR and ρ. Thus, the theoretical bounds are not accurate for SNR = 0 dB. From Figure 5.7, we observe that for low SJR, the simulation results show $\rho_{wc} = 1.0$. As SJR increases, ρ_{wc} becomes smaller: when 4 dB< SJR < 6 dB, $\rho_{wc} = 0.1$; when SJR > 6 dB, $\rho_{wc} = 0.01$. Thus, for 4 dB $\leq$ SJR $\leq$ 10 dB, the smaller values of ρ makes it more difficult to correct the errors due to the higher jamming noise power. However, when SJR > 12 dB, it is possible that the smaller noise power causes the jammer to be less effective for $\rho < 0.1$, especially since the decoder has SI. For $\rho = 1$, SI is not useful. Thus, $\rho = 1.0$ becomes the worst case as shown by the theoretical results, although the BERs for the different values of ρ are small.

For SNR > 4 dB, the theoretical results show the worst case for ρ to be 1.0, which agrees with the simulation (Figure 5.10). Figure 5.10 is a plot of the BER of the SCCC with SI and negligible AWGN. The general shape of the bound conforms to what is expected. For low SJRs the jamming noise power is sufficiently high so that the code performs most poorly when $\rho = 1.0$. This worst-case result was also obtained by Jordan for Turbo codes [Ref. 95]. As SJR increases, the SCCC is more effective for large ρ since the effective signal-to-noise ratio for each bit is lowered. Thus, performance is best for $\rho = 1.0$ with high SJRs (> 9 dB). Kang and Stark [Ref. 96] reported similar results for Turbo codes. Note that this is in contrast to the case of no side information (Figure 5.7) where $\rho = 1.0$ is the worst case for high SJR.

3.   Comparison with SCCC with Pulsed Noise Jamming and No Side Information

The performance of the SCCC with SI is better than with NSI when SJR is greater than 0 dB. For SJR < 0 dB, there is practically no difference in performance. SCCC with SI is more effective for larger ρ than for smaller ρ (Figure 5.11). For large ρ, there are more errors to correct and SI enables the SCCC to better correct these errors. For small ρ (≤ 0.01), the differences between SI and NSI are minimal. This is expected since the number of jammed bits is small and, consequently, the contribution made by SI is small.

The SCCC with SI is also more effective for low SNR than for high SNR. For example, for SNR = 8 dB, the BER differences between the two are much less than for 4 dB as can be seen comparing Figures 5.11 and 5.12. The need for SI is less for high SNR since the high SNR enables more errors to be corrected.

D.   SCCC WITH PULSED NOISE JAMMING AND NO SIDE INFORMATION AND RAYLEIGH FADING WITH NO CHANNEL INFORMATION

In this section, both pulsed noise jamming and Rayleigh fading are simulated. The decoder has neither side information (NSI) on the jammed bits nor fade amplitudes or channel information (NCI) of the Rayleigh fading.

1.   Observations

The general performance of the SCCC with pulsed noise jamming and NSI and Rayleigh fading with NCI is shown in Figure 5.13 for values of SJR from zero to ten dB and for SNR from zero to twenty dB. In the figure, in order to show the graphs for the different values of ρ, the SJR is offset by ρ in dB. Thus, for $\rho = 0.001, 0.01, 0.1, 1.0$, there are offsets of –30, -20, -10, 0 dB, respectively. In general, for a given SJR, BER improves as SNR increases. For SNR of ≤ 2 dB, BER is almost independent of SJR. As SNR increases, the effect of ρ becomes more pronounced. It is obvious that BER worsens as ρ increases. It will be shown later that the value of ρ_{wc} is dependent on SJR.

From Figure 5.13, we observe that for $\rho = 0.001$, the effect of SJR is, over the range of SJR considered, negligible regardless of SNR; i.e., it does not matter what the value of SJR is. Since ρ is very small, the number of bits affected is small. The SCCC is able to correct most of the erroneous data bits when SNR is large enough. For SNR above 5.6 dB, all errors are corrected. This is about 1.5 dB above the SNR where all erroneous data bits are correctly decoded for SCCC/BPSK with fading only, i.e., no pulsed noise jamming, and 4 dB above the case with pulsed noise jamming and no side information and no fading. In other words, Rayleigh fading degrades overall performance by about 4 dB in pulsed noise jamming environment. Pulsed noise jamming degrades overall performance by 1.5 dB on a fading channel, compared to half a dB for a non-fading channel. For $\rho = 0.01$, the BER decreases as SNR increases. For SNR of greater than 6 dB, all errors are corrected (Figure 5.13). In this case, Rayleigh fading degrades the overall performance by about 5 dB in a pulsed noise jamming environment. Pulsed noise jamming, on the other hand, degrades overall performance by 2 dB on a fading channel. For $\rho = 0.1$, for SNR $\geq$ 8 dB and SJR $\geq$ 8 dB, all the errors are corrected.

2. Comparison with Theoretical Values

The simulation and theoretical bounds for SNRs of 8 dB and 20 dB, respectively are shown in Figures 5.14 and 5.15. We observe that the simulation results can generally be extended by the theoretical bounds, especially for high SNRs.

3. Comparison with SCCC with Pulsed Noise Jamming and No Side Information and No Rayleigh Fading

With Rayleigh fading, the BER plots are similar to those without fading except that they are more linear in shape, and for a given SNR and SJR, probability of bit error is worse.

At SNR = 0 dB, their performances are comparable. However, as SNR increases, the BER plots for fading are worse as expected. For SNR = 4 dB and $\rho = 0.001$, all errors are corrected with no fading, while the BER is flat (about 10^{-5}) for the fading case (Figure 5.16). For $\rho = 0.01$, the two plots are almost parallel. For a given SJR, the probability of bit error is one order of magnitude less for the fading case. For $\rho = 0.1$ and 1.0, their performances are close for SJR < 0 dB. However, as SJR increases, their BERs diverge.

The BER plots for the fading case are still quite flat, while the BER plots for the non-fading case have assumed "waterfall" shapes.

For SNR = 8 dB, all errors are corrected for ρ = 0.01 (Figure 5.17). The difference in performance between the non-fading case and the fading case is between 3 to 10 dB for ρ = 0.1 and less than 4 dB for ρ = 1.0. Note that in both fading and non-fading cases, ρ_{wc} = 0.1 for SJR > 2 dB and SJR > 6 dB, respectively. This means that the decoder is having more difficulty in correcting the jammed bits due to the higher power in each jammed bit. When SNR is increased further to 20 dB, the difference in performance narrows to less than 4 dB for ρ = 0.1 and less than 2 dB for ρ = 1.0 (Figure 5.18). For this SNR, worst-case ρ is 1.0.

E.   SCCC WITH PULSED NOISE JAMMING AND SIDE INFORMATION AND RAYLEIGH FADING WITH CHANNEL INFORMATION

In these simulations, the decoder is assumed to have side information (SI) when pulsed noise jamming occurs and channel or amplitude information (CI) for Rayleigh fading.

1.   Observations

The general performance of the SCCC with SI is shown in Figure 5.19 for values of SJR greater than zero and for SNR from 0 to 20 dB in increments of 2 dB. In the figure, in order to show the graphs for the different values of ρ, the SJR is offset by ρ in dB. Thus, for ρ = 0.001, 0.01, 0.1, 1.0, there will be offsets of –30, -20, -10, 0 dB, respectively. In general, the BER improves as SNR increases. For zero SNR, the BER is almost independent of SJR and ρ. As SNR increases, the effect of ρ becomes more pronounced. It is apparent that BER decreases as ρ increases. In general, the ρ_{wc} = 1.0. It will be shown later that the value of ρ_{wc} is also dependent on SJR.

From Figure 5.19, we observe that for ρ = 0.001, the effect of SJR on BER is negligible. Since ρ is very small, the number of bits that is affected is small and the SCCC is able to correct most of the erroneous data. For SNR above 3.8 dB, all errors with ρ = 0.001 are corrected. This is almost one dB above the SNR where all data bits

are correctly decoded with only AWGN and Rayleigh fading and half a dB above the case with pulsed noise jamming and SI. In other words, fading with CI causes the overall performance to degrade by half dB when pulsed noise jamming is present and pulsed noise jamming with SI causes the overall performance to degrade by one dB for a Rayleigh fading channel with CI. With side and channel information, there is an improvement of 1.8 dB when compared with the case without either. With $\rho = 0.01$, BER performance improves as SNR increases. For SNR > 6 dB, all errors are corrected for $\rho = 0.01$ (Figure 5.19). For $\rho = 0.1$, the graphs start to branch out for SNR > 4 dB. For SNR > 10 dB and SJR > 6 dB, all the errors are corrected. For SNR > 10 dB and $\rho = 1.0$, all errors are corrected for SJR > 6 dB (Figure 5.19). Further increases in SNR only improve the BER marginally.

2. Comparison with Theoretical Values

The simulation and theoretical bounds for SNRs of 8 dB and 20 dB, respectively, are shown in Figures 5.20 and 5.21. We can observe that the simulation results can generally be extended by the theoretical bounds, especially for high SNRs. In these figures, for both theoretical and simulated results, $\rho_{wc} = 1.0$ for SJR < 12 dB.

3. Comparison with SCCC with Pulsed Noise Jamming and Side Information and No Rayleigh Fading

With Rayleigh fading, the BERs plots are similar to those without fading except that they are more linear, and for a given SNR and SJR, BER is worse.

For SNR = 0 dB, their performances are comparable. However, as SNR increases, the BER graphs for fading are worse than those without fading. For SNR = 4 dB and for $\rho = 0.001$, all errors are corrected with or without fading (Figure 5.22). For $\rho = 0.01$, the gap between fading and non-fading cases closes as SJR increases. For both $\rho = 0.1$ and 1.0, their BER is close for SJR < 0 dB. However, for SJR > 0, their performances diverge: the BER graphs for the fading case do not improve as rapidly.

When SNR is increased to 20 dB, the difference in performance narrows to less than 4 dB for $\rho = 0.1$ and less than 2 dB for $\rho = 1.0$ (Figure 5.23). We also observe that for high SNR is $\rho_{wc} = 1.0$.

4. Comparison with Pulsed Noise Jamming and No Side Information and Rayleigh Fading with No Channel Information

As expected, SCCC/BPSK in a pulsed noise jamming and fading environment with side and channel information performs better than without. For lower SNRs (4 dB or less), the difference in BER is large (Figure 5.24). For higher SNRs, e.g. at 8 dB, difference in performance narrows down to less than 1 dB (Figure 5.25). Thus, SI and CI are more useful at lower SNRs. For $\rho = 1.0$, since SI does not contribute any information, the difference in performance is due solely to CI.

F. SCCC WITH PULSED NOISE JAMMING AND NO SIDE INFORMATION AND WITH DIRECT SEQUENCE SPREAD SPECTRUM

In these simulations, the decoder has no side information (NSI) about the jammed bits, but the pulsed noise jamming noise power is reduced by direct sequence spread spectrum (DS) with a processing gain (PG) of 64.

1. Observations

The general performance of the SCCC with NSI and without DS is shown in Figure 5.26 for values of SJR from zero to ten dB and for SNR from zero to twenty dB. In the figure, in order to show the graphs for the different values of ρ, the SJR is offset by ρ in dB. Thus, for $\rho = 0.001, 0.01, 0.1, 1.0$, there are offsets of $-30, -20, -10, 0$ dB, respectively. The effect of DS is tremendous. As shown in Figure 5.26, for SNR > 4 dB, all the data bits are decoded correctly. We will therefore concentrate our simulations for SNR < 4 dB. Notice that for a given SNR, BER increases as SJR increases. This is in contrary to what is expected and will be explained shortly.

For $\rho = 0.001$, the effect of SJR is, over the range of SJR considered, negligible regardless of SNR; i.e., it does not matter what the value of SJR is (Figure 5.26). Since ρ is very small, the number of bits affected is small. The SCCC is able to correct most of the erroneous data bits. For SNR above 1.6 dB, all errors are corrected. This is about half a dB above the SNR where all erroneous data bits are correctly decoded for AWGN only. In other words, this level of pulsed noise jamming only degrades overall performance by

about 0.5 dB. This is the same result obtained earlier for SCCC with no side information and no DS. Since the number of bits jammed is small, the reduced jamming power due to DS does not make much difference to the SCCC.

One requirement of the decoder, for use with the maximum a posteriori (MAP) algorithm [Ref. 10] to estimate a posteriori probabilities, is knowledge of the SNR for a Gaussian noise channel. In essence, this is needed to supply the proper combination of prior bit statistics. These statistics are obtained from raw channel measurements, which are Gaussian random variables, and a posteriori data from previous iterations. Although the MAP algorithm requires an SNR parameter to produce the correct MAP estimates, it is not widely known how sensitive decoder error is to mismatch of this parameter [Ref. 101]. This mismatch is seen in the performance for SNR between 0 and 4 dB for SCCC with DS with NSI. This mismatch does not occur when there is no DS or when there is SI. A graph (Figure 5.27) is plotted which shows the performance for SNR = 2 dB and ρ = 0.1 for different values of the processing gain (PG) due to DS. In this graph, when the processing gain is greater than four, the BER worsens when SJR increases. There are two possible reasons for this. First, there is an SNR estimation mismatch. In these simulations, there is NSI, thus the overall SNR used in the decoder is based on the estimated (average) noise power (AWGN and jamming noise). Various papers have shown that an SNR mismatch can result in inferior BER performance in Turbo codes. Dunham and Tzou [Ref. 102] have shown that for convolutional codes with Viterbi decoders in Gaussian noise, performance is more sensitive for a large mismatch. Summers and Wilson [Ref. 101] found that for Turbo codes with AWGN, the mismatch is more tolerable for overestimation than underestimation. They posited that the required accuracy is perhaps –3 dB to +6 dB. Worm, Hoeher and Wehn [Ref. 103] carried out simulations on Turbo codes with AWGN and flat fading channels. They also found that the mismatch is more tolerable for overestimation than underestimation. Wang [Ref. 53] found that slight underestimation gives better performance for Turbo codes with AWGN and flat Rayleigh fading. Jordan and Nichols [Ref. 104] carried out the sensitivity analysis using different interleaver sizes. They found that the decoder is more sensitive to estimation errors when it is operating close to the SNR threshold. Note that none has

included interference in their simulations. With pulsed noise jamming and DS, this threshold was found to be between SNR 0 to 4 dB for the range of SJR considered. In the previous simulations with SI (and later with DS and SI), this anomaly did not occur. Second, there may be a quantization problem. With AWGN, it has been shown [Ref. 105] that the 3-bit quantization suffers less than 0.25 dB loss compared to the infinite case. However, in the presence of pulsed noise jamming, as was shown in [Ref. 106, 107 and 108], this is not the case unless side information is given. With the jamming noise power reduced by direct sequence spread spectrum, the total signal-to-noise ratio (for SNR between 0 to 4 dB) differs by a little, and it is possible that the three bit quantization is insufficient. Thus, the SCCC decoding algorithm is unable to converge, resulting in erroneous outputs.

For SNR < 2 dB and as ρ increases, BER worsens (Figure 5.26). The worst case ρ is 1.0 and is almost independent of SJR. The BER performance with $\rho = 1.0$ and SJR corrected by an offset factor is shown in Figure 5.28 This offset factor takes into account the total noise, i.e., AWGN and pulsed noise jamming noise. An offset factor greater than 0 dB corresponds to an estimate larger than the actual signal-to-total noise ratio used in the simulation. The SNR mismatch here is not critical since the BER is high. It is difficult to assess the impact of an SNR mismatch when ρ is less than one. For example, for $\rho = 0.1$, one does not know what proportion of the BER is due to the SNR mismatch and what proportion is due to the decoding algorithm since only 10% of the bits are jammed. An underestimation of the SJR up to 2 dB results in improvement in BER (Figure 5.29). However, further underestimation causes the BER to deteriorate. Dunham and Tzou [Ref. 102] also reported that a slight underestimation for convolutional codes with Viterbi decoding gave the best performance and further underestimation is detrimental to the BER. Wang [Ref. 53] found that underestimation of 3 to 4.5 dB will improve the performance of Turbo codes with AWGN. Summers and Wilson [Ref. 101] found that 1 dB or 2 dB underestimation is tolerable, but degradation becomes large for a greater mismatch. Similar results can also be obtained for smaller values of ρ. An underestimation of the SJR up to 2 dB results in improvement in BER

for $\rho = 1.0$ (Figure 5.30). An overestimation of SJR is detrimental to the BER performance.

For SNR > 4 dB, all errors are corrected (Figure 5.26). At higher SNR, the SCCC decoding algorithm is able to overcome the estimation mismatch and quantization/convergence problems.

2. Comparison with Theoretical Values

At zero SNR, the simulation results show BER to be flat at 10^{-1} independent of SJR and ρ, while theoretical bounds show BER to be 10^{-5} independent of SJR and ρ. Thus, the theoretical bounds are not accurate for SNR = 0 dB. For SNR = 4 dB and SJR < -8 dB, the simulation results give $\rho_{wc} = 0.01$, which agrees with theory (Figure 5.31).

3. Comparison with SCCC with Pulsed Noise Jamming and No Side Information and with No Direct Sequence Spread Spectrum

The SCCC with DS generally performs better, especially for low SJRs, i.e., for high jamming noise power since DS is able to spread the noise. For SNR > 4 dB, the SCCC with DS is able to correct all errors even for high jamming power (SJR > –6 dB). Their BERs are compared in Figure 5.32. For SNR = 4 dB and $\rho = 0.01$, the SCCC with DS has a difference in performance of 18 dB at 10^{-4} over SCCC without DS.

G. SCCC WITH PULSED NOISE JAMMING AND SIDE INFORMATION AND WITH DIRECT SEQUENCE SPREAD SPECTRUM

In these simulations, the decoder is assumed to have SI and DS in incorporated in the SCCC.

1. Observations

For low SNR, unlike the case with no DS, the effect of ρ does not become more pronounced (Figure 5.33). The BER plots tend to bunch closely together, improving as SNR is increased. However, the worst case ρ is not always 1.0 for these low SNRs, but varies between 1.0 and 0.01 inclusive, but their BER differences are marginal. The resultant jamming powers for various values of ρ are small since DS reduces them. Thus, the BERs for different values of ρ are close. For SNR = 1 dB and SJR < 0 dB, the graphs

diverge for low SJR (SJR < –4 dB), tapering and bunching up for higher SJR (Figure 5.33). They also tend to slope downwards for low SJR and become flatter for high SJR. For high SNR, the DS is able to reduce the jamming noise significantly such that the BERs for higher SJRs do not improve significantly. For SNR $\geq$ 1.8 dB, all errors are corrected for SJR > –4 dB.

For ρ = 0.001, the effect of SJR on BER is negligible. Since ρ is very small, the number of bits that is affected is small, and the SCCC is able to correct most of the erroneous data. For SNR above 1.6 dB, all errors with ρ = 0.001 are corrected (Figure 5.34). This is about half a dB above the SNR where all data bits are correctly decoded with AWGN. This is the same result obtained earlier for the SCCCs with no side information (with and without DS) and for SCCC with side information. Thus, DS and SI does not improve the BER when ρ is very small.

For SNR < 2 dB and as ρ increases, BER worsens. This is expected since more bits are affected. However, higher jamming power occurs for smaller ρ. This affects the ability to correct errors. For low SJR (< -8 dB), ρ_{wc} is 1.0 (Figure 5.35). As SJR increases, ρ_{wc} becomes smaller. For SJR > –4 dB, all errors are corrected.

2. Comparison with Theoretical Values

At zero SNR, the simulation results showed BER at around 0.1 independent of SJR and ρ while theoretical results showed BER to be 10^{-5} independent of SJR. Thus, theoretical results are not accurate for SNR = 0 dB. For SNR 1.8 dB, the theoretical values can serve as an extension of the simulation results (Figure 5.36). Both theoretical and simulation results show ρ = 1.0 to be the worst case, followed by ρ = 0.1 and then ρ = 0.01.

3. Comparison with SCCC with Pulsed Noise Jamming and No Side Information and with Direct Sequence Spread Spectrum

The performance of the SCCC with SI is better than without SI in all cases, especially for SJR > 0 dB. For SNR > 2 dB and SJR > 0 dB, all errors are corrected for SCCC with SI. For SNR = 2 dB and SJR < 0 dB, SCCC with SI performs better than with NSI for ρ = 1.0 and 0.1 (Figure 5.37). For ρ = 0.01, the performance is slightly

better with SI. Note that for $\rho = 1.0$, there is a difference in performance. With SI, it is not just the knowledge of whether a bit is jammed, but also the signal-to-noise plus jamming ratio which is important to the SCCC decoding algorithm. The algorithm is more effective when this information is correctly provided.

The SCCC with SI is more effective for large ρ than for small ρ when SJR < 0 dB (Figure 5.37). For large ρ, there are more errors to correct and SI enables the SCCC to better correct these errors. For $\rho < 0.01$, the BER differences between SI and NSI are minimal. It is possible that with small ρ, the number of bits jammed is too small to make SI effective.

4. Comparison with SCCC with Pulsed Noise Jamming and Side Information and with No Direct Sequence Spread Spectrum

The performance of the SCCC with SI and DS is definitely better than the SCCC with SI and NDS. The improvement in BER performance is significant. The difference in performance at 10^{-3} for SNR = 2 dB is about 18 dB for $\rho = 1.0$, 0.1 and 0.01 (Figure 5.38).

H. CONCLUSIONS

SCCC/BPSK has proven its ability to make a good error correction code in AWGN. The simulation results showed that SCCC is also effective in a pulsed noise jamming environment. SCCC with DS and SI is even more effective. The theoretical bounds were found not to be accurate for SNR (or SJR) below 2 or 3 dB [Ref. 20]. Rayleigh fading is most detrimental to SCCC/BPSK with pulsed noise jamming at small ρ and low SNR. SI is more effective for large ρ and low SNR. With DS, SI is important to the decoding algorithm to ensure that there are no anomalous results.
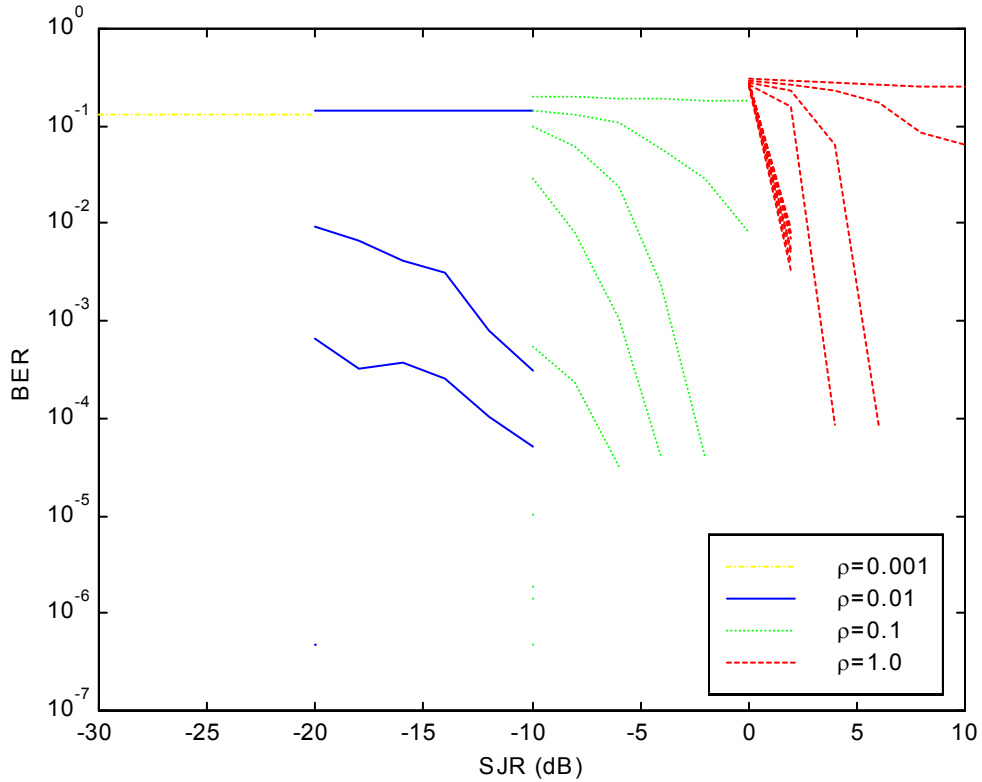
Figure 5.1.   Simulated SCCC/BPSK with AWGN and pulsed noise jamming with no side information: effect of SJR on BER for ρ = 0.001, 0.01, 0.1 and 1.0, SNR = 0 to 20 dB and SJR = 0 to 10 dB. Note that in order to show the graphs for the different values of ρ, the SJR is offset by ρ in dB. Thus, for ρ = 0.001, 0.01, 0.1 and 1.0, there are offsets of – 30, -20, -10, 0 dB, respectively. The graphs start at 0 dB at the top with increments of 2 dB for each subsequent graph downwards. Note that when there is no graph for a particular SNR, it means that all errors were corrected for that SNR for the range of SJR considered.
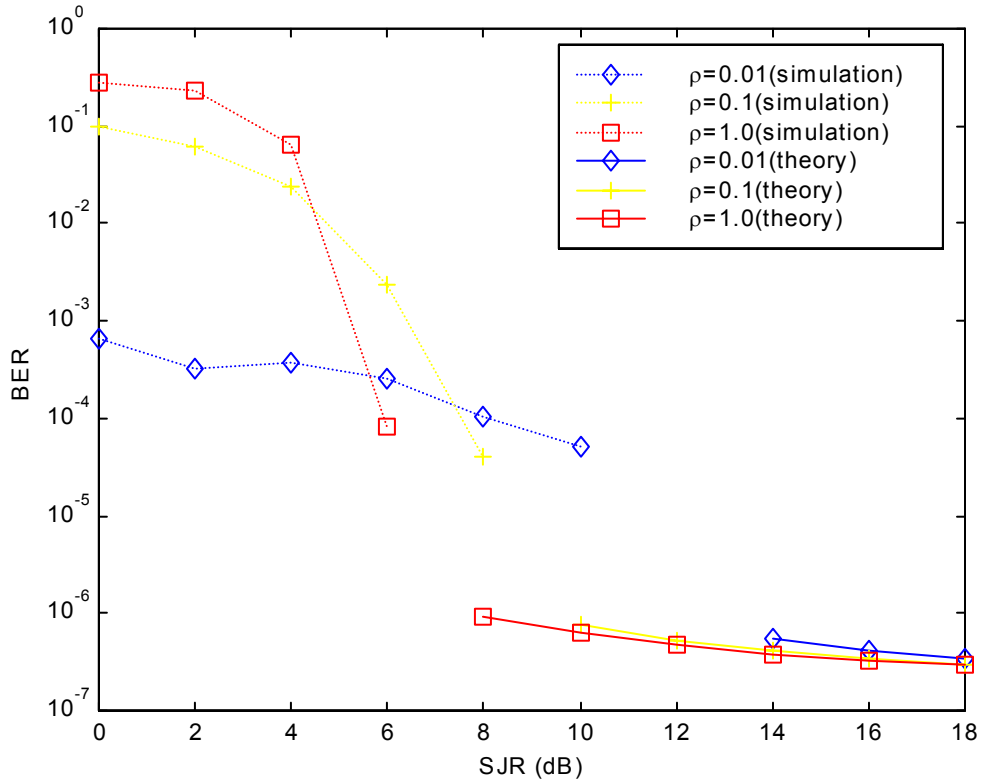
Figure 5.2.   Simulated and theoretical SCCC/BPSK with AWGN and pulsed noise jamming with no side information: effect of ρ on BER for ρ = 0.01, 0.1 and 1.0, SNR = 4 dB and SJR = 0 to 18 dB.
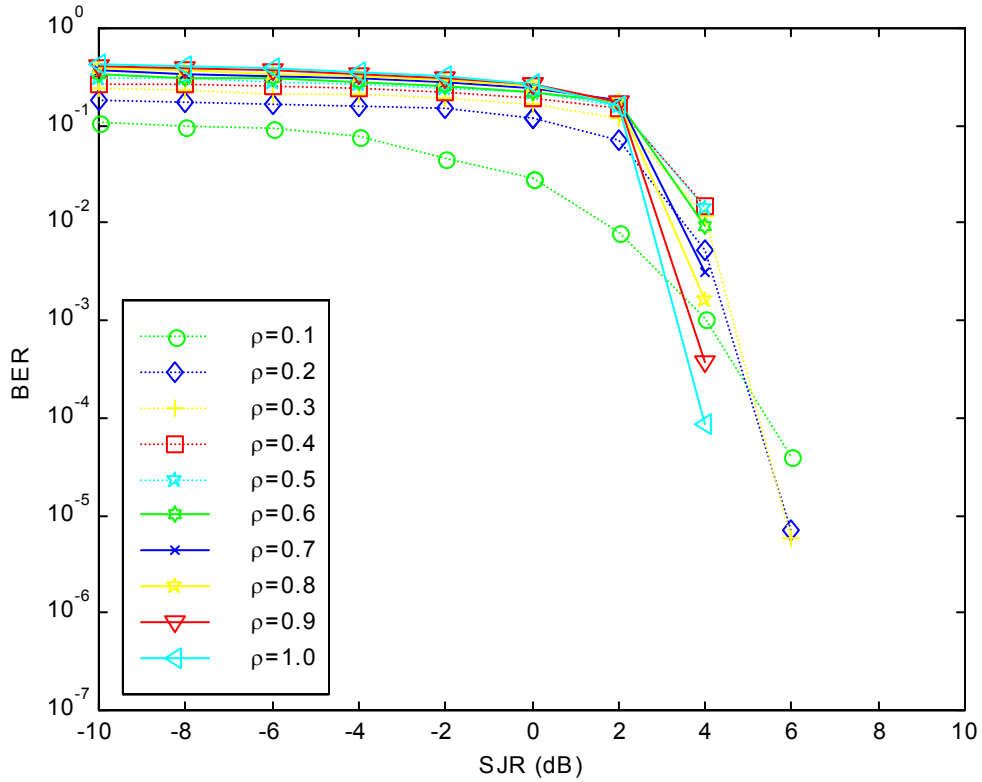
Figure 5.3.   Simulated SCCC/BPSK with AWGN and pulsed noise jamming with no side information: effect of ρ on BER for ρ = 0.1 to 1.0, SNR = 6 dB and SJR = -10 to 10 dB.
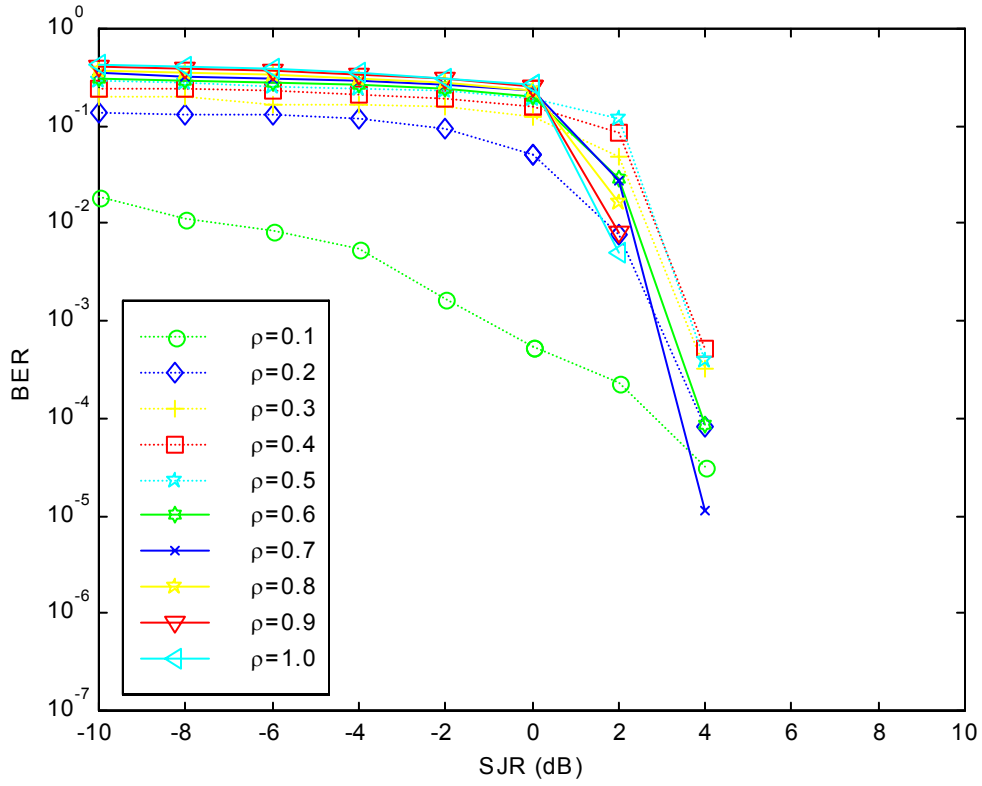
Figure 5.4.   Simulated SCCC/BPSK with AWGN and pulsed noise jamming with no side information: effect of ρ on BER for ρ = 0.1 to 1.0, SNR = 8 dB and SJR = -10 to 10 dB.
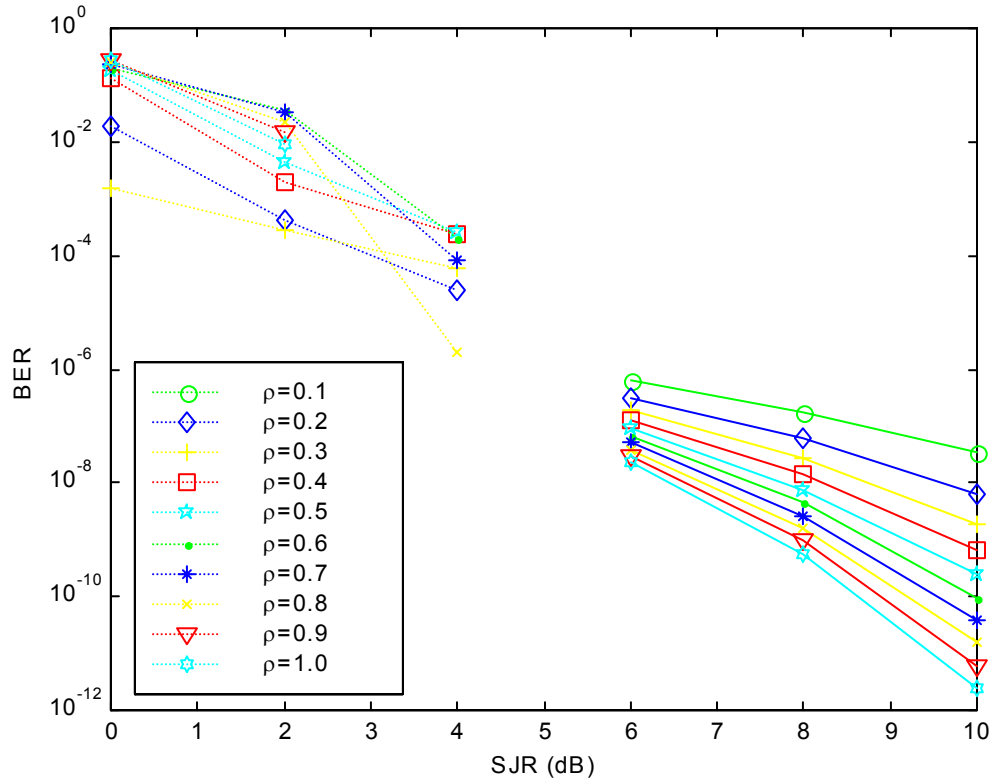
Figure 5.5.   Simulated and theoretical SCCC/BPSK with AWGN and pulsed noise jamming with no side information: effect of ρ on BER for ρ = 0.1 to 1.0, SNR = 20 dB and SJR = 0 to 10 dB.
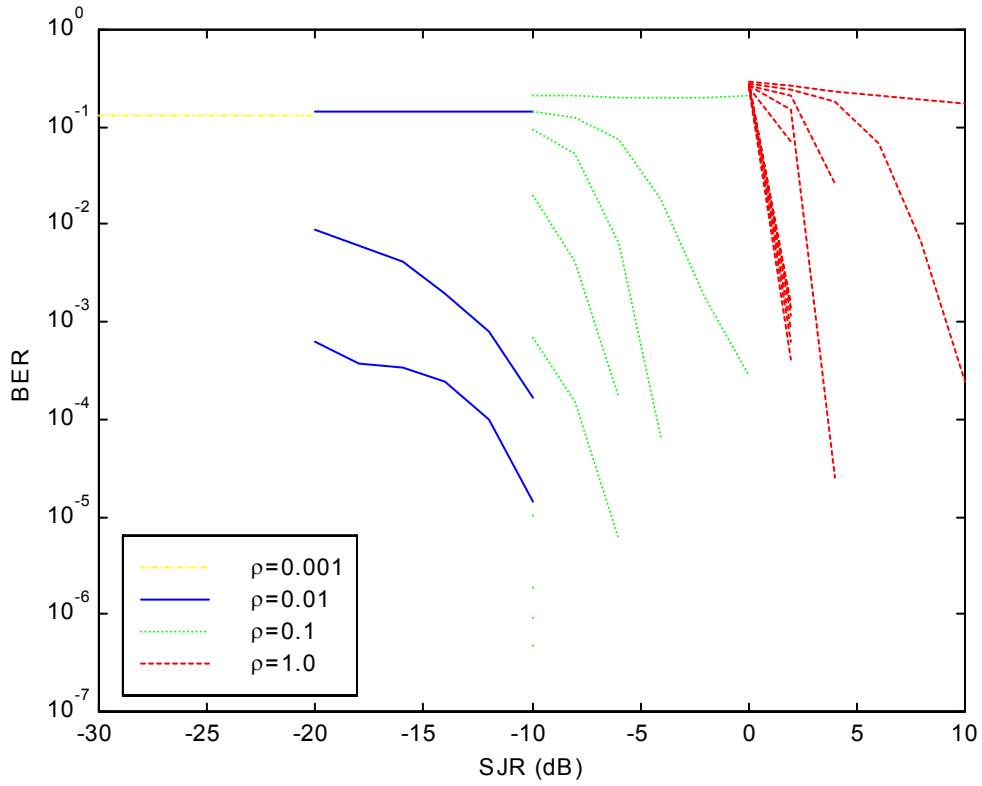
Figure 5.6. Simulated SCCC/BPSK with AWGN and pulsed noise jamming with side information: effect of SJR on BER for ρ = 0.001, 0.01, 0.1 and 1.0, SNR = 0 to 20 dB and SJR = 0 to 10 dB. Note that in order to show the graphs for the different values of ρ, the SJR is offset by ρ in dB. Thus, for ρ = 0.001, 0.01, 0.1, 1.0, there are offsets of –30, -20, -10, 0 dB, respectively. The graphs start at 0 dB at the top with increments of 2 dB for each subsequent graph downwards. Note that when there is no graph for a particular SNR, it means that all errors were corrected for that SNR for the range of SJR considered.
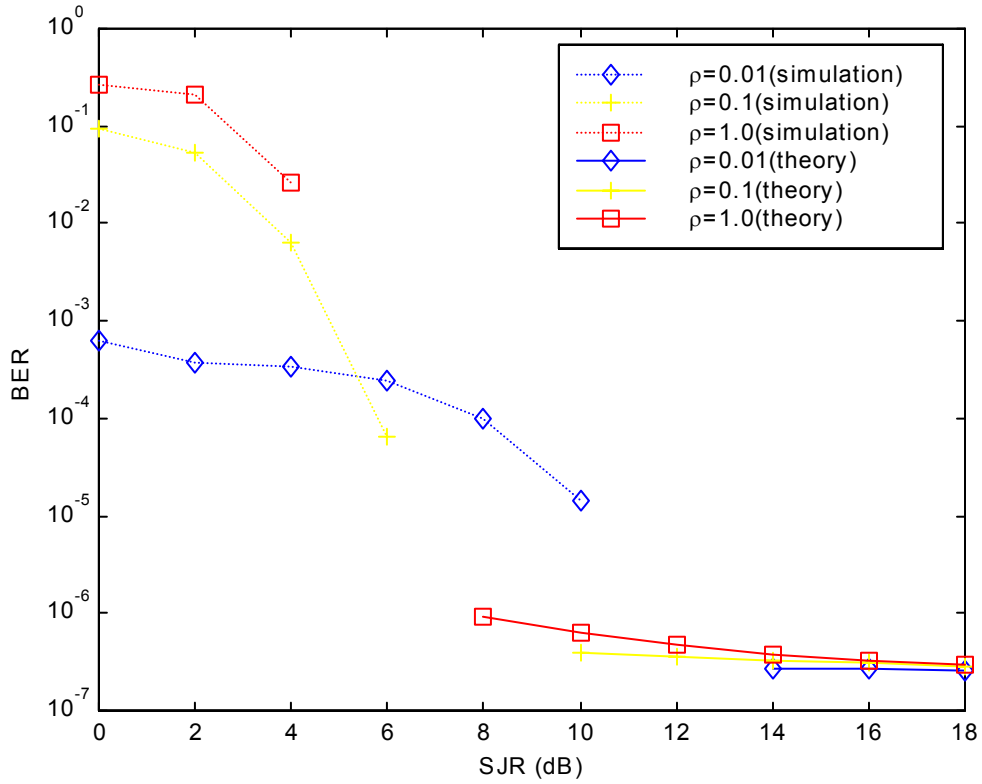
Figure 5.7. Simulated and theoretical SCCC/BPSK with AWGN and pulsed noise jamming with side information: effect of ρ on BER for ρ = 0.01, 0.1 and 1.0, SNR = 4 dB and SJR = 0 to 18 dB.
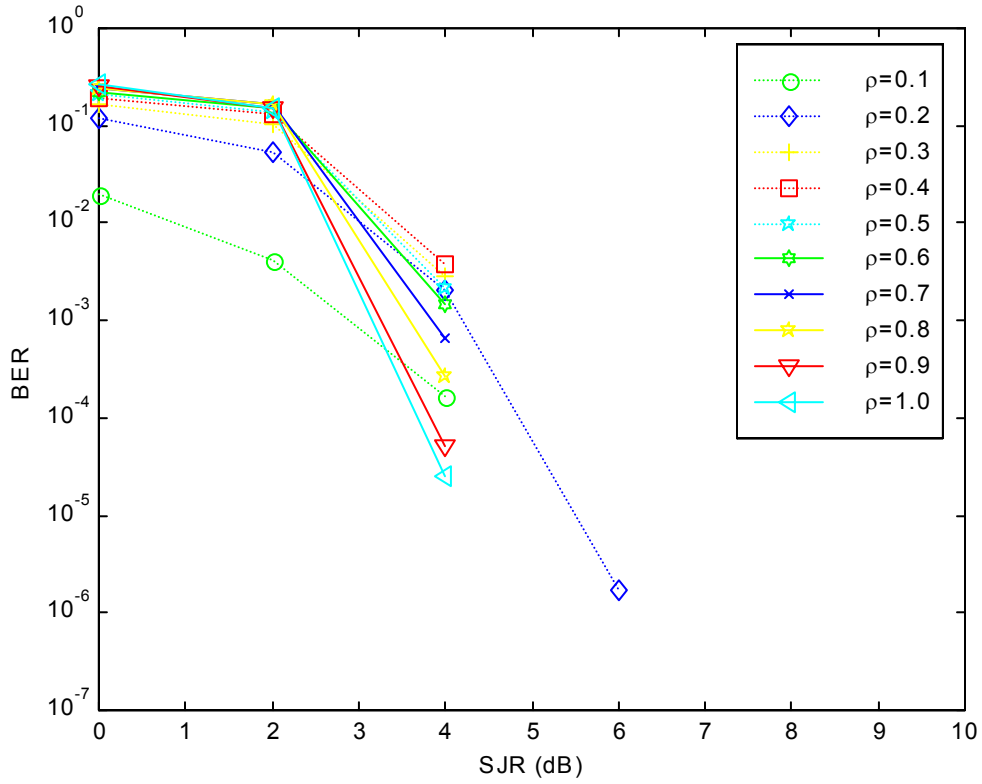
Figure 5.8.   Simulated SCCC/BPSK with AWGN and pulsed noise jamming with side information: effect of ρ on BER for ρ = 0.1 to 1.0, SNR = 6 dB and SJR =-10 to 10 dB.
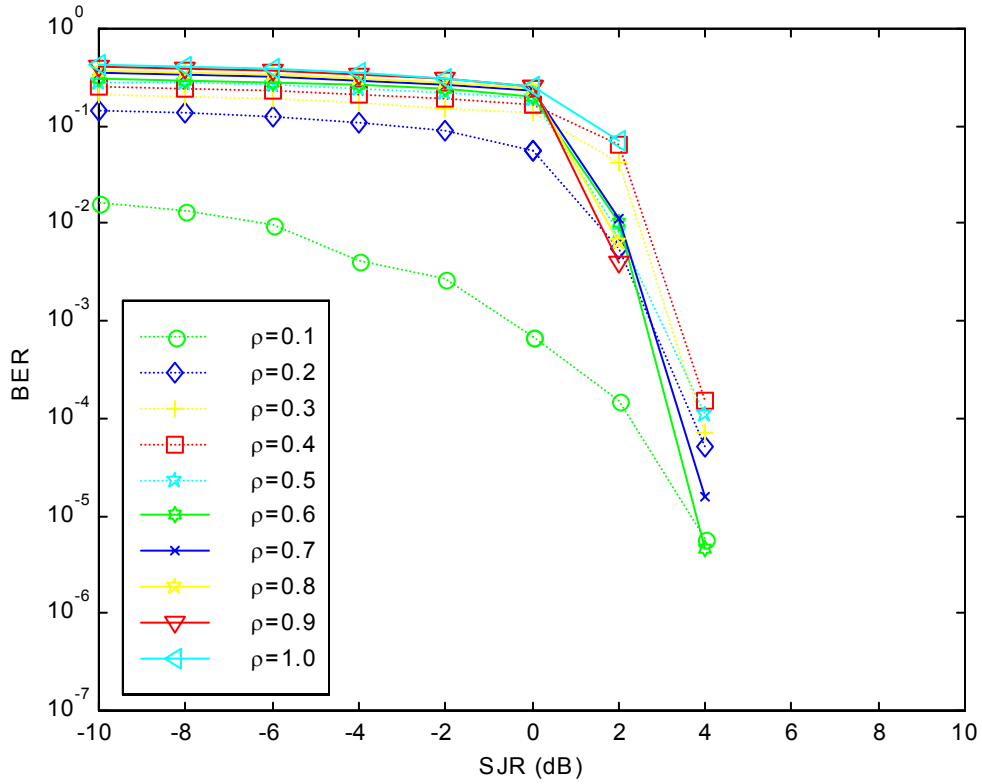
Figure 5.9. Simulated SCCC/BPSK with AWGN and pulsed noise jamming with side information: effect of ρ on BER for ρ = 0.1 to 1.0, SNR = 8 dB and SJR =-10 to 10 dB.
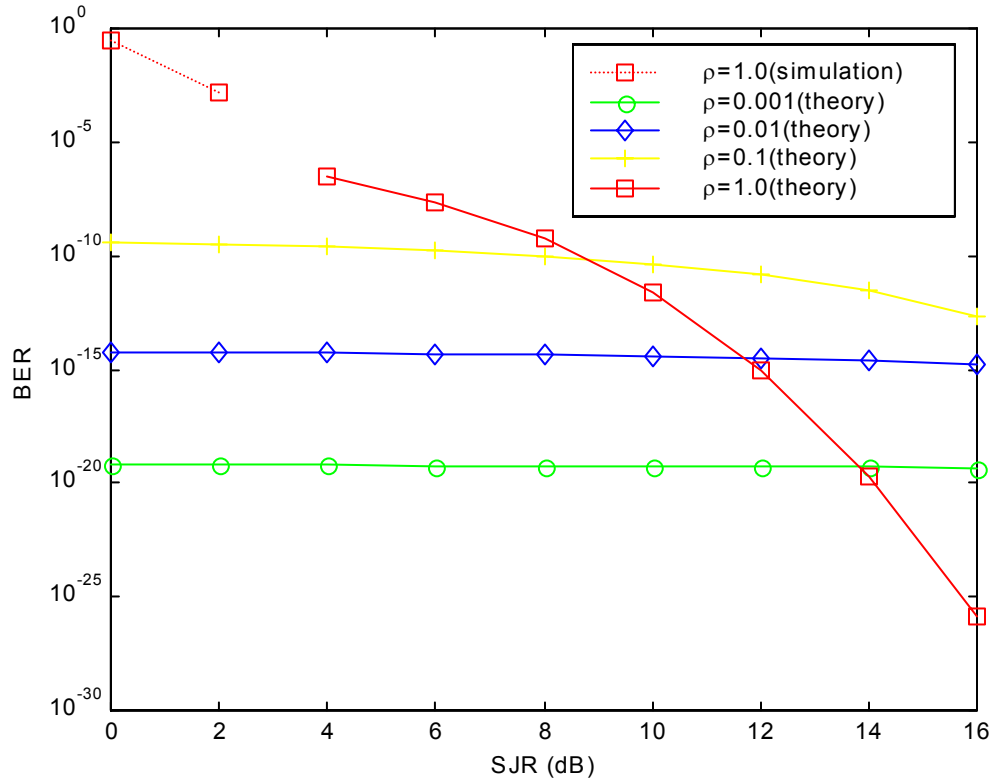
Figure 5.10.   Simulated and theoretical SCCC/BPSK with AWGN and pulsed noise jamming with side information: effect of ρ on BER for ρ = 0.01, 0.1 and 1.0, SNR = 20 dB and SJR = 0 to 10 dB. Note that all errors were corrected for ρ = 0.001, 0.01 and 0.1 for the range of SJR considered.
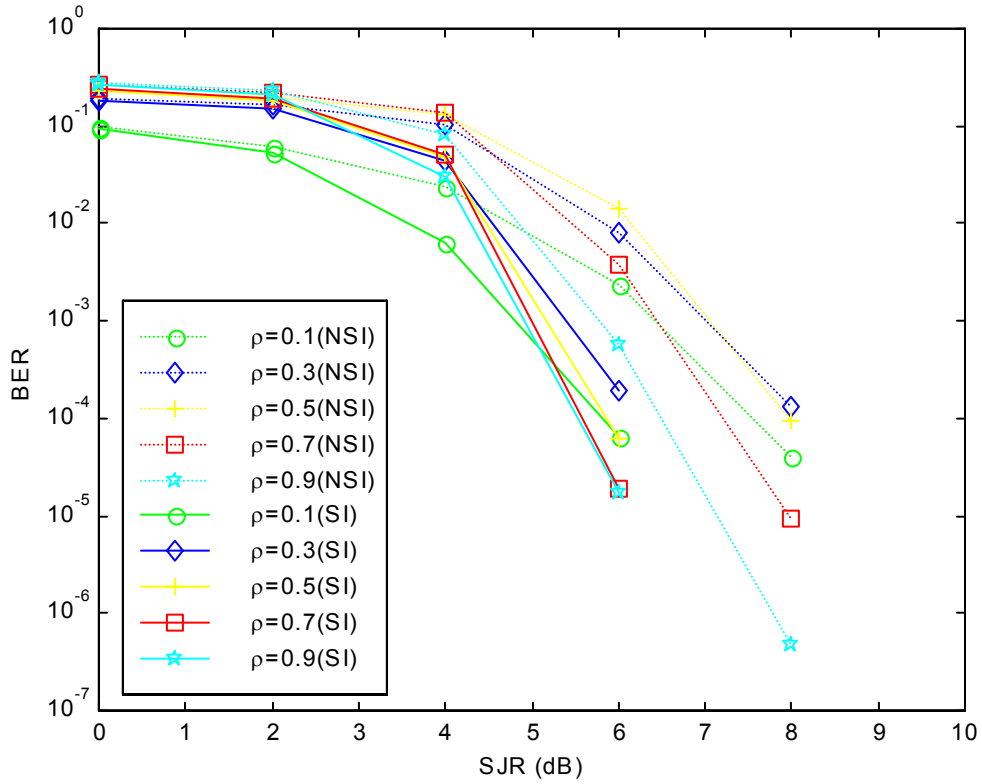
Figure 5.11.　Simulated SCCC/BPSK with pulsed noise jamming: effect of side information on BER for ρ between 0.1 and 1.0, SNR = 4 dB and SJR = 0 to 10 dB.
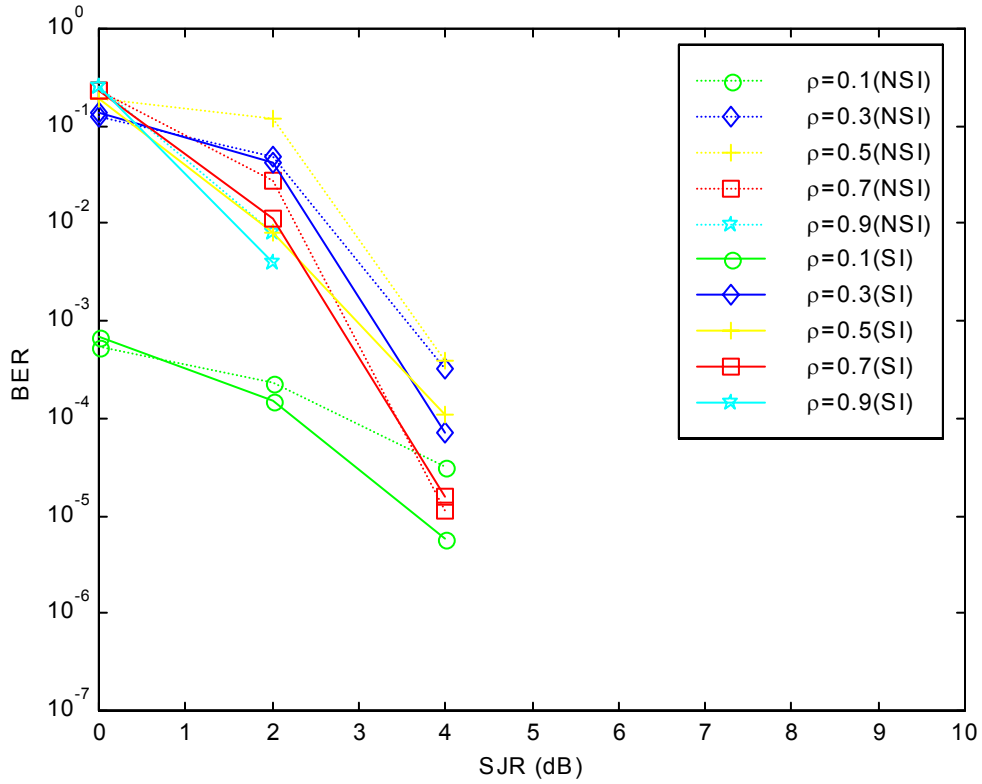
Figure 5.12. Simulated SCCC/BPSK with pulsed noise jamming: effect of side information on BER for ρ between 0.1 and 1.0, SNR = 8 dB and SJR = 0 to 10 dB.
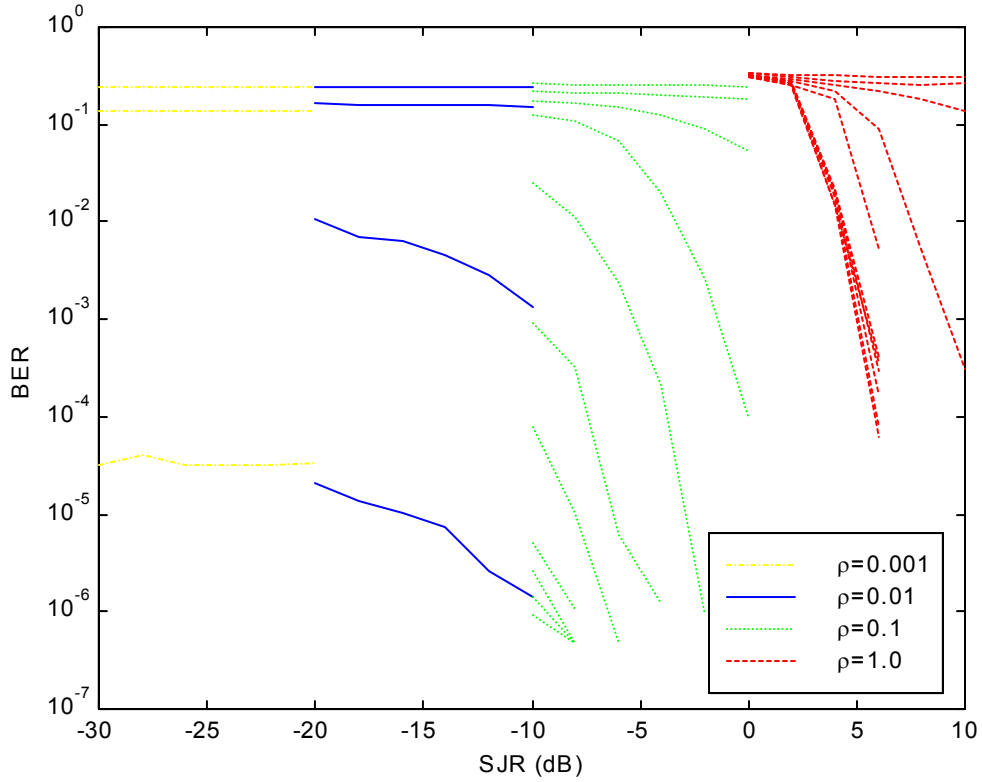
Figure 5.13.   Simulated SCCC/BPSK with AWGN and pulsed noise jamming with no side information and Rayleigh fading with no channel information: effect of SJR on BER for ρ = 0.001, 0.01, 0.1 and 1.0, SNR = 0 to 20 dB and SJR = 0 to 10 dB. Note that in order to show the graphs for the different values of ρ, the SJR is offset by ρ in dB. Thus, for ρ = 0.001, 0.01, 0.1, 1.0, there are offsets of –30, -20, -10, 0 dB, respectively. The graphs start at 0 dB at the top with increments of 2 dB for each subsequent graph downwards. Note that when there is no graph for a particular SNR, it means that all errors were corrected for that SNR for the range of SJR considered.

Figure 5.14.   Simulated and theoretical SCCC/BPSK with AWGN and pulsed noise jamming with no side information and Rayleigh fading with no channel information: effect of ρ on BER for ρ = 0.1 and 1.0, SNR = 8 dB and SJR = 0 to 18 dB. Note that for ρ = 0.001 and 0.01, all errors were corrected for the range of SJR considered.
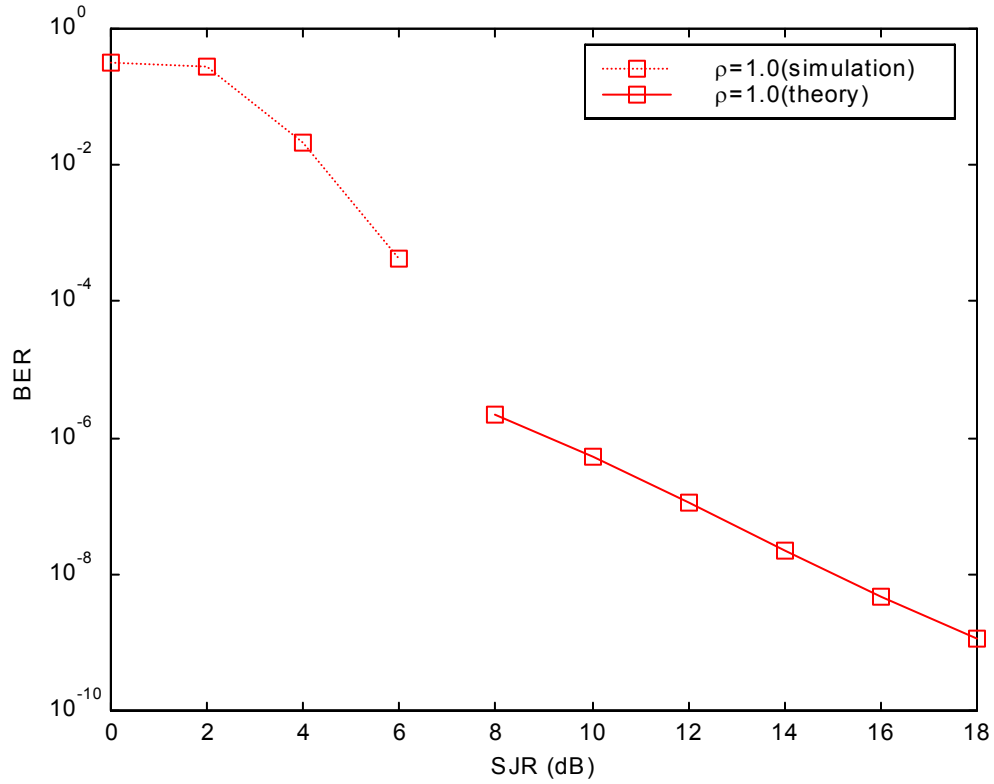
Figure 5.15.   Simulated and theoretical SCCC/BPSK with AWGN and pulsed noise jamming with no side information and Rayleigh fading with no channel information: effect of SJR on BER for ρ = 1.0, SNR = 20 dB and SJR = 0 to 18 dB. Note that for ρ = 0.001, 0.01 and 0.1, all errors were corrected for the range of SJR considered.

Figure 5.16. Simulated SCCC/BPSK with AWGN and pulsed noise jamming with no side information: effect of Rayleigh fading with no channel information on BER for ρ = 0.01, 0.1 and 1.0, SNR = 4 dB and SJR = -10 to 10 dB. Note that for the case without fading with ρ = 0.001, all errors were corrected for the range of SJR considered.
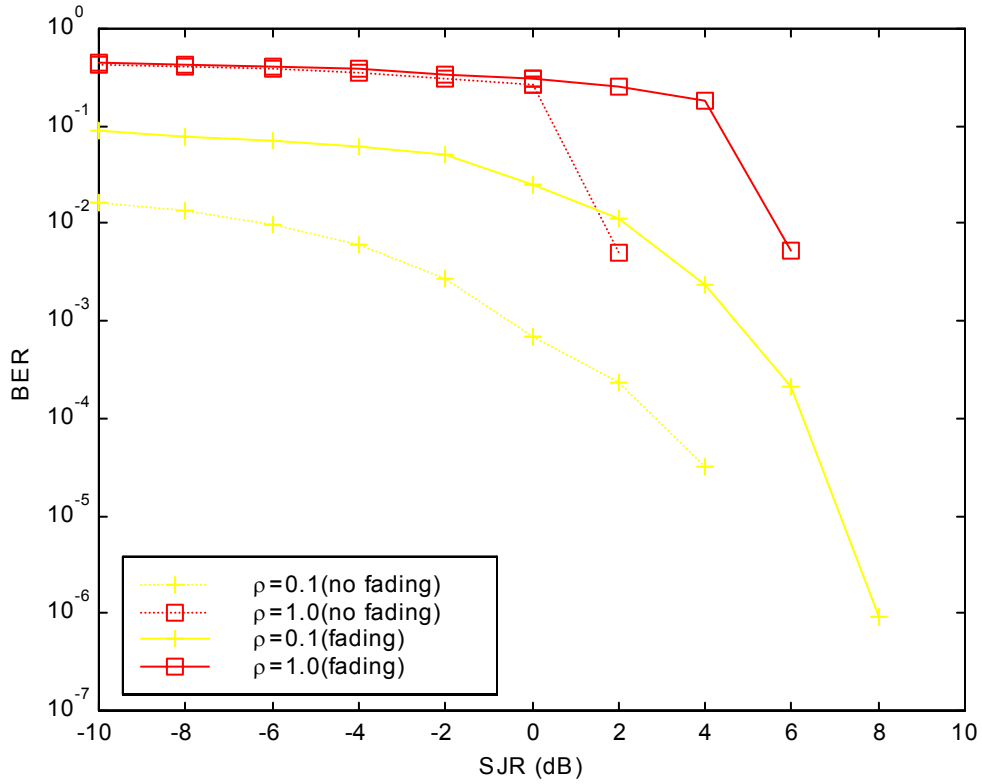
Figure 5.17.   Simulated SCCC/BPSK with AWGN and pulsed noise jamming with no side information: effect of Rayleigh fading with no channel information on BER for ρ = 0.1 and 1.0, SNR = 8 dB and SJR = -10 to 10 dB. Note that for ρ = 0.001 and 0.01, all errors have been corrected for the range of SJR considered.
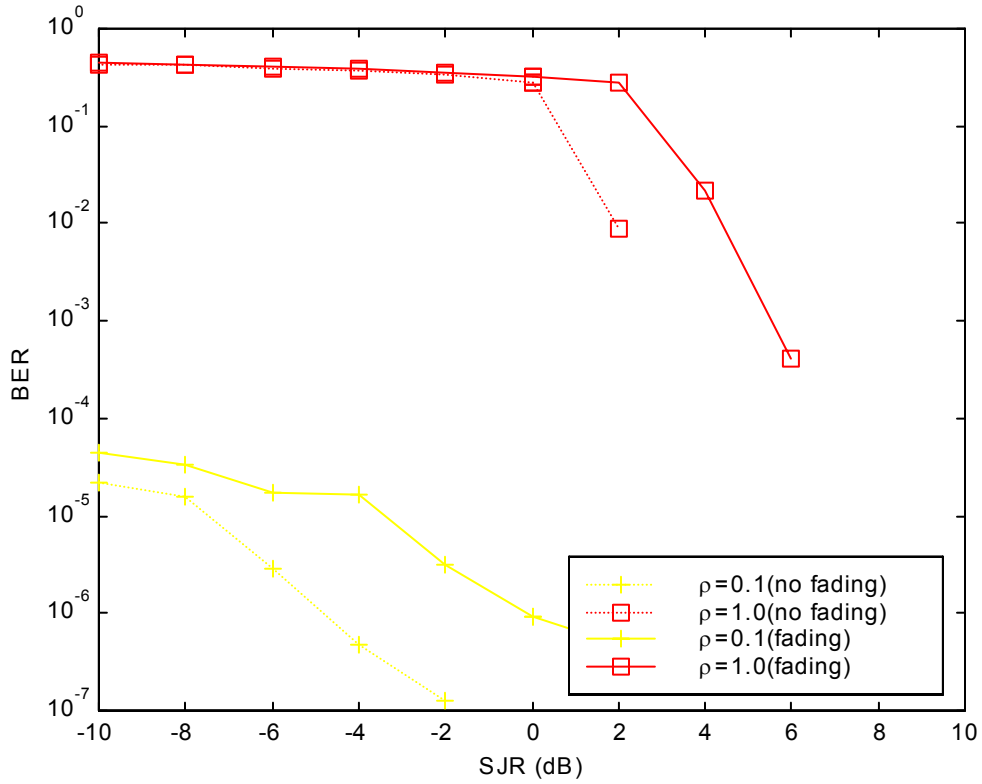
Figure 5.18.   Simulated SCCC/BPSK with AWGN and pulsed noise jamming with no side information: effect of Rayleigh fading with no channel information on BER for ρ = 0.1 and 1.0, SNR = 20 dB and SJR = -10 to 10 dB. Note that for ρ = 0.001 and 0.01, all errors were corrected for the range of SJR considered.
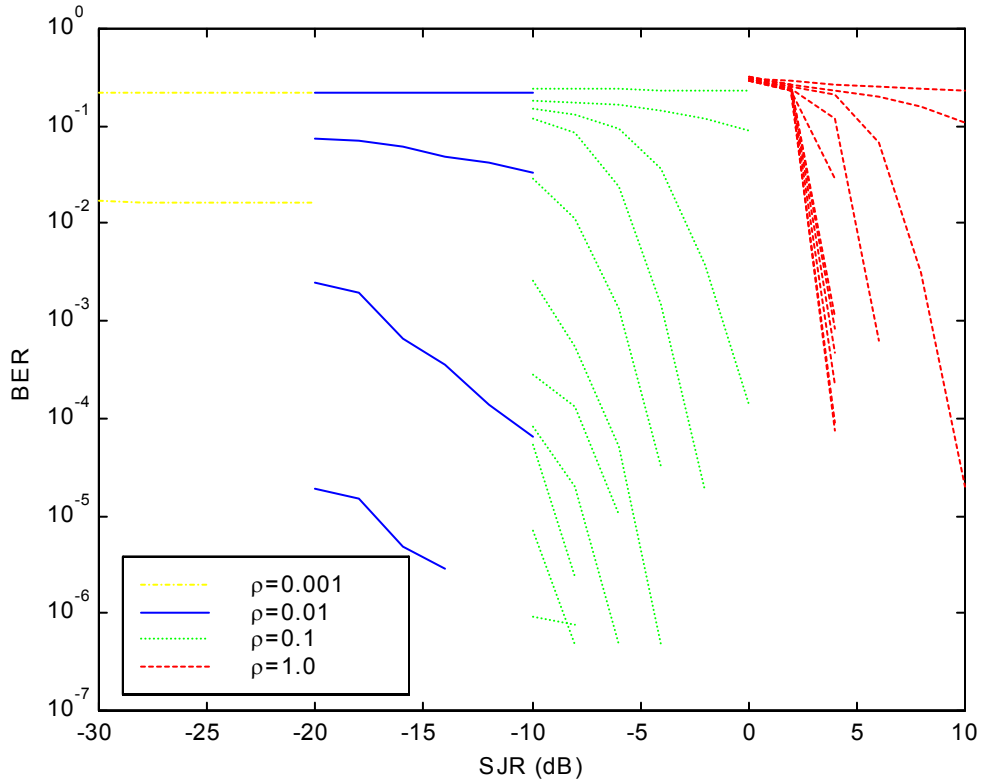
Figure 5.19.   Simulated SCCC/BPSK with AWGN and pulsed noise jamming with side information and Rayleigh fading with channel information: effect of SJR on BER for ρ = 0.001, 0.01, 0.1 and 1.0, SNR = 0 to 20 dB and SJR = 0 to 10 dB. Note that in order to show the graphs for the different values of ρ, the SJR is offset by ρ in dB. Thus, for ρ = 0.001, 0.01, 0.1, 1.0, there are offsets of −30, -20, -10, 0 dB, respectively. The graphs start at 0 dB at the top with increments of 2 dB for each subsequent graph downwards. Note that when there is no graph for a particular SNR, it means that all errors were corrected for that SNR for the range of SJR considered.

Figure 5.20. Simulated and theoretical SCCC/BPSK with AWGN and pulsed noise jamming with side information and Rayleigh fading with channel information: effect of ρ on BER for $\rho = 0.1$ and 1.0, SNR = 8 dB and SJR = 0 to 18 dB. Note that for $\rho = 0.001$ and 0.01, all errors were corrected for the range of SJR considered.
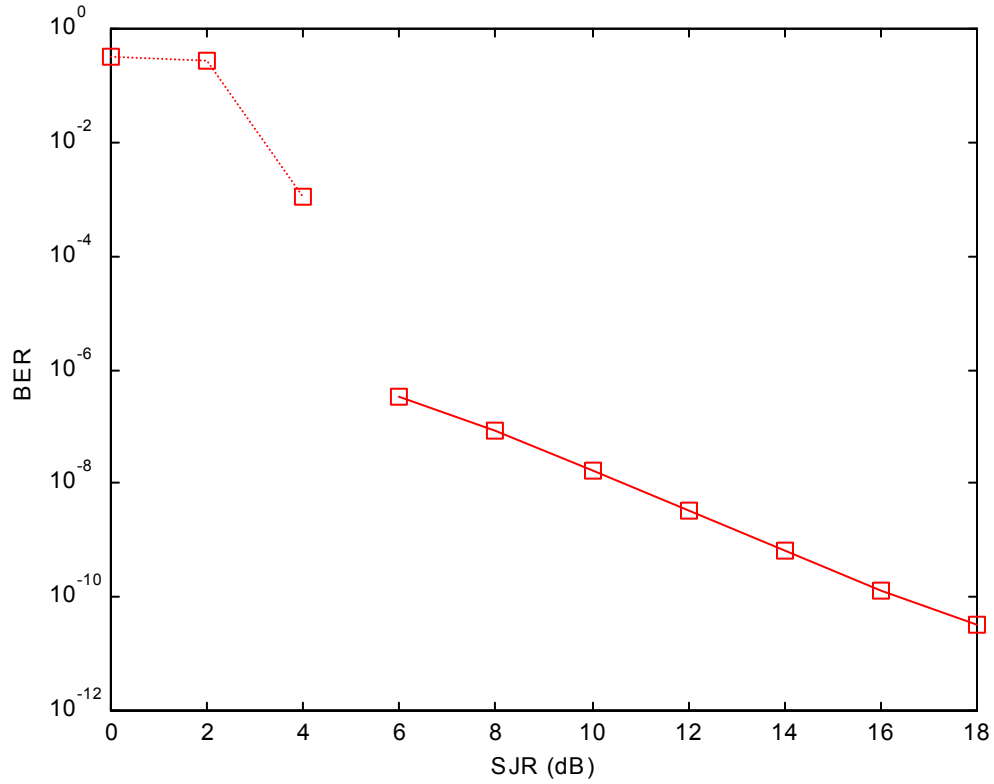
Figure 5.21. Simulated and theoretical SCCC/BPSK with AWGN and pulsed noise jamming with side information and Rayleigh fading with channel information: effect of SJR on BER for $\rho = 1.0$, SNR = 20 dB and SJR = 0 to 18 dB. Note that for $\rho = 0.001$, 0.01 and 0.1, all errors were corrected for the range of SJR considered.
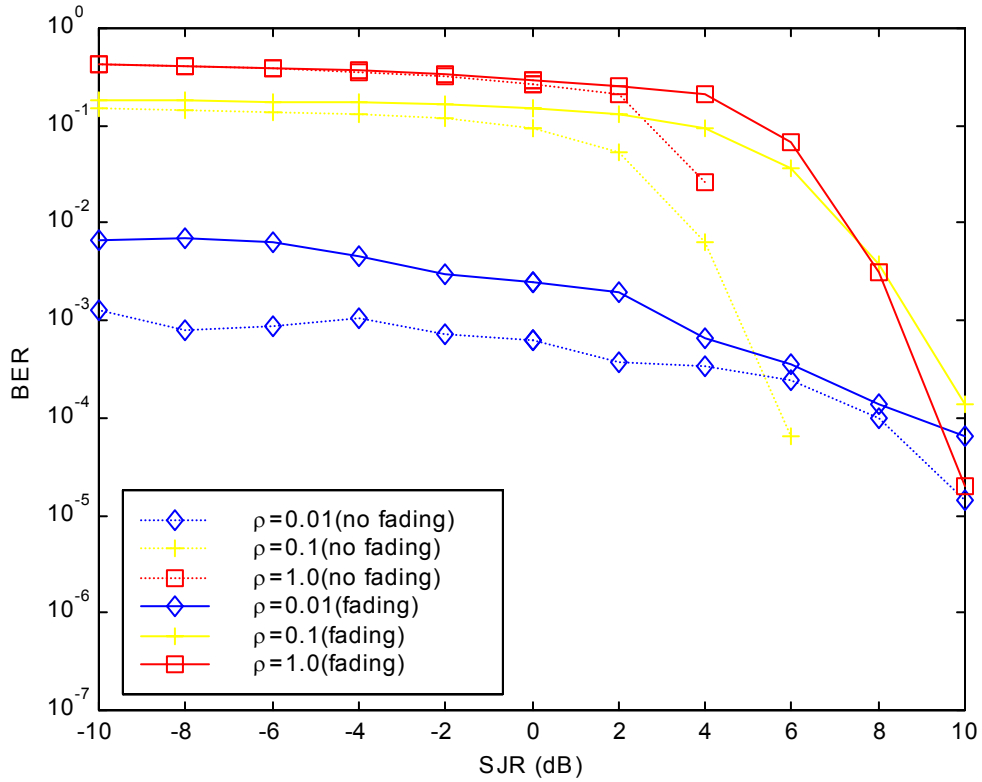
Figure 5.22.   Simulated SCCC/BPSK with AWGN and pulsed noise jamming with side information: effect of Rayleigh fading with channel information on BER for ρ = 0.01, 0.1 and 1.0, SNR = 4 dB and SJR = -10 to 10 dB. Note that for ρ = 0.001, all errors were corrected for the range of SJR considered.
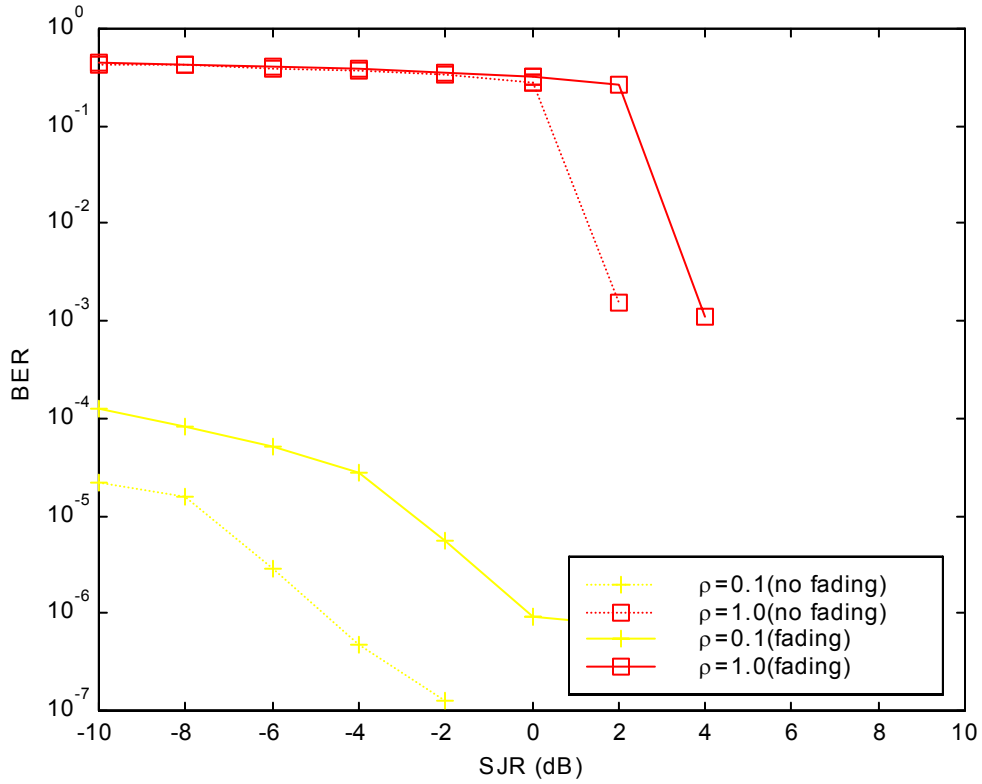
Figure 5.23.   Simulated SCCC/BPSK with AWGN and pulsed noise jamming with side information: effect of Rayleigh fading with channel information on BER for ρ = 0.1 and 1.0, SNR = 20 dB and SJR = -10 to 10 dB. Note that for ρ = 0.001 and 0.01, all errors were corrected for the range of SJR considered.
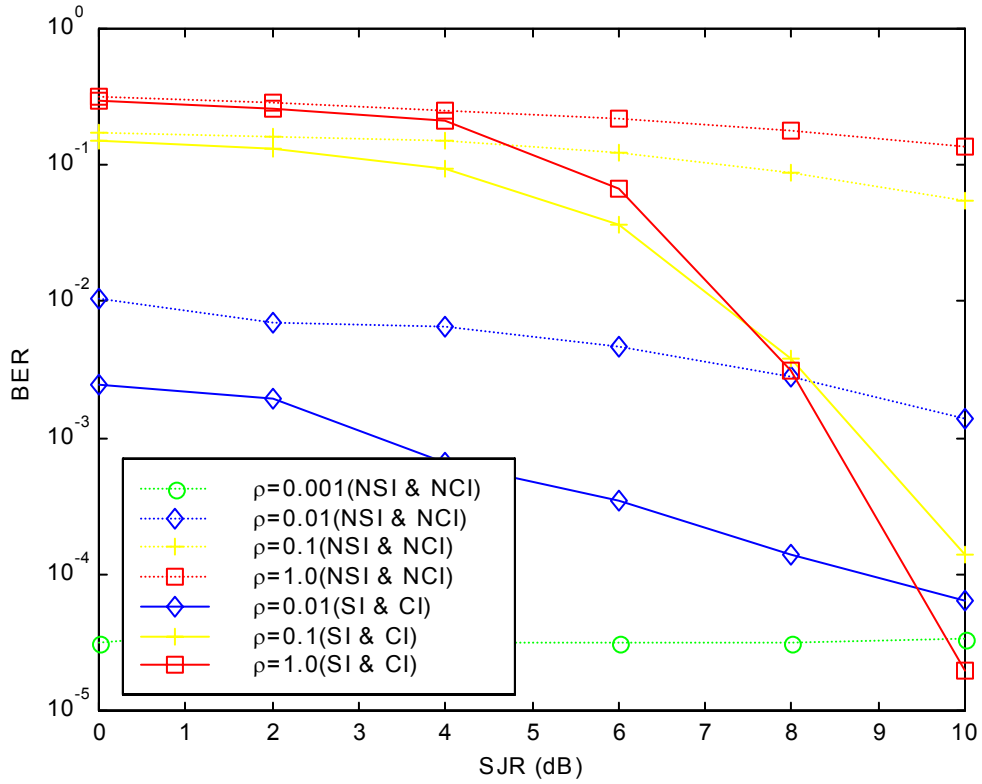
Figure 5.24. Simulated SCCC/BPSK with AWGN and pulsed noise jamming with Rayleigh fading: effect of side and channel information on BER for ρ = 0.01, 0.1 and 1.0, SNR = 4 dB and SJR = 0 to 10 dB. Note that for the case ρ = 0.001 with side and channel information all errors were corrected for the range of SJR considered.
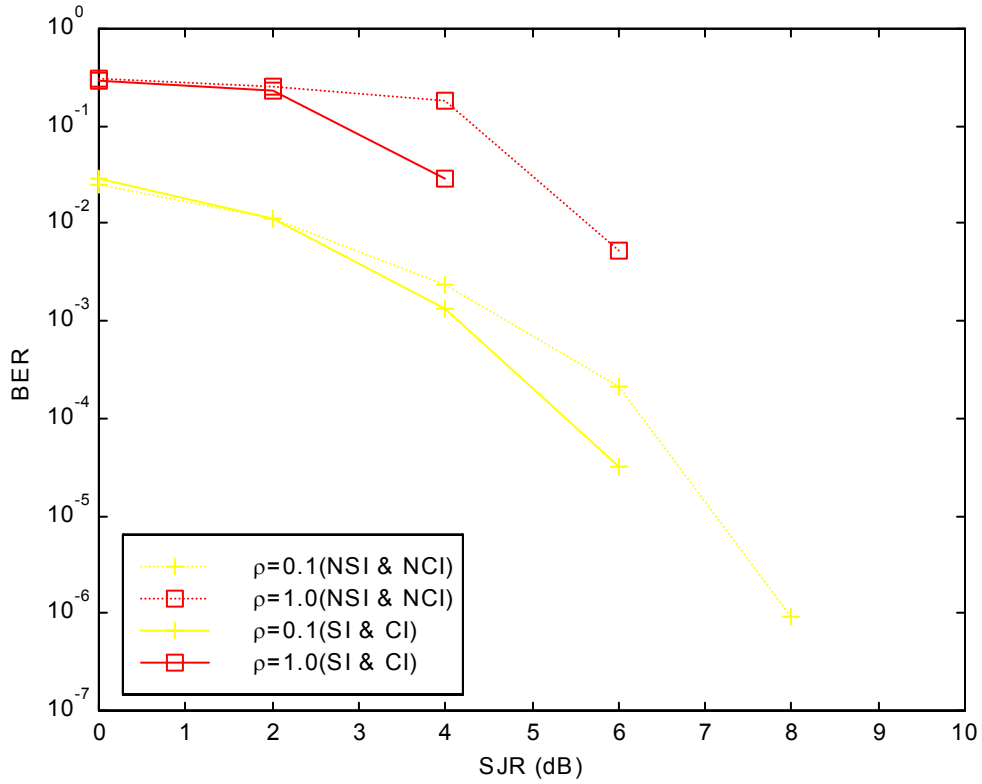
Figure 5.25.   Simulated SCCC/BPSK with AWGN and pulsed noise jamming with
Rayleigh fading: effect of side and channel information on BER for ρ = 0.1 and 1.0, SNR
= 8 dB and SJR = 0 to 10 dB. Note that for the case ρ = 0.001 and 0.01 all errors were
corrected for the range of SJR considered.
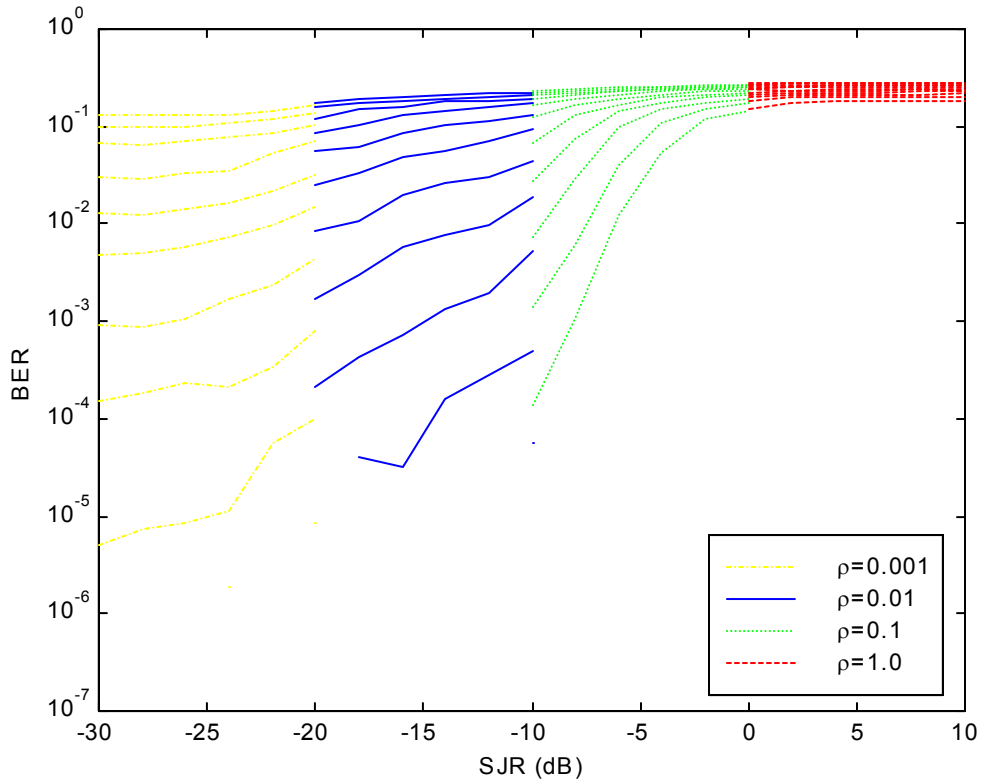
Figure 5.26.   Simulated SCCC/BPSK with AWGN and pulsed noise jamming with no side information and direct sequence spread spectrum: effect of SJR on BER for ρ = 0.001, 0.01, 0.1 and 1.0, SNR = 0 to 2 dB and SJR = 0 to 10 dB. Note that in order to show the graphs for the different values of ρ, the SJR is offset by ρ in dB. Thus, for ρ = 0.001, 0.01, 0.1, 1.0, there are offsets of –30, -20, -10, 0 dB, respectively. The graphs start at 0 dB at the top with increments of 0.2 dB for each subsequent graph downwards. Note that when there is no graph for a particular SNR, it means that all errors were corrected for that SNR for the range of SJR considered.
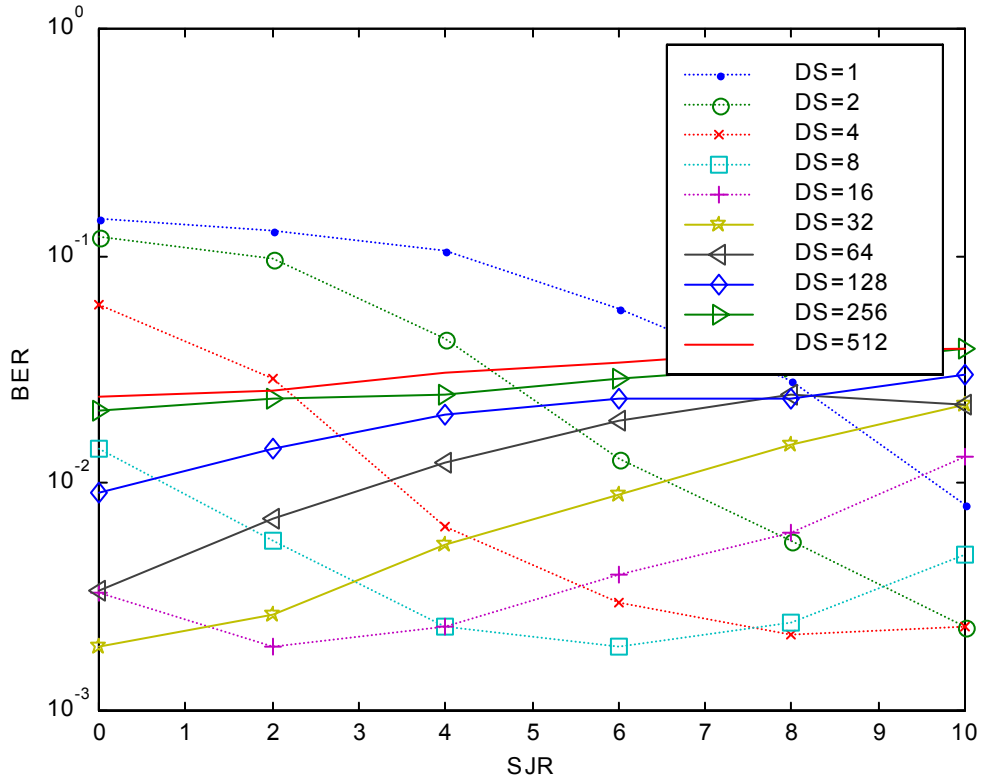
Figure 5.27.   Simulated SCCC/BPSK with AWGN and pulsed noise jamming with no side information: effect of processing gain of direct sequence spread spectrum on BER for $\rho = 0.1$, SNR = 2 dB and SJR = 0 to 10 dB.
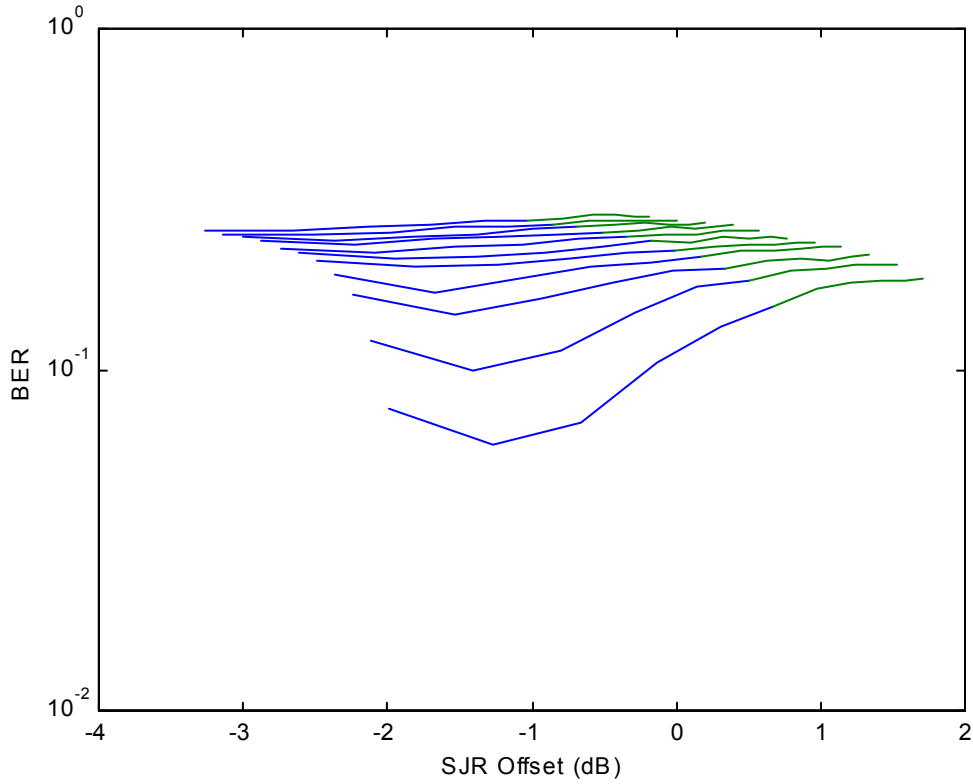
Figure 5.28.   Simulated SCCC/BPSK with AWGN and pulsed noise jamming with no side information and direct sequence spread spectrum: effect of SNR mismatch on BER for $\rho = 1.0$ = 0 to 2 dB. The graphs start at 0 dB at the top with increments of 0.2 dB for each subsequent graph downwards. Note that when there is no graph for a particular SNR, it means that all errors were corrected for that SNR for the range of SJR considered.
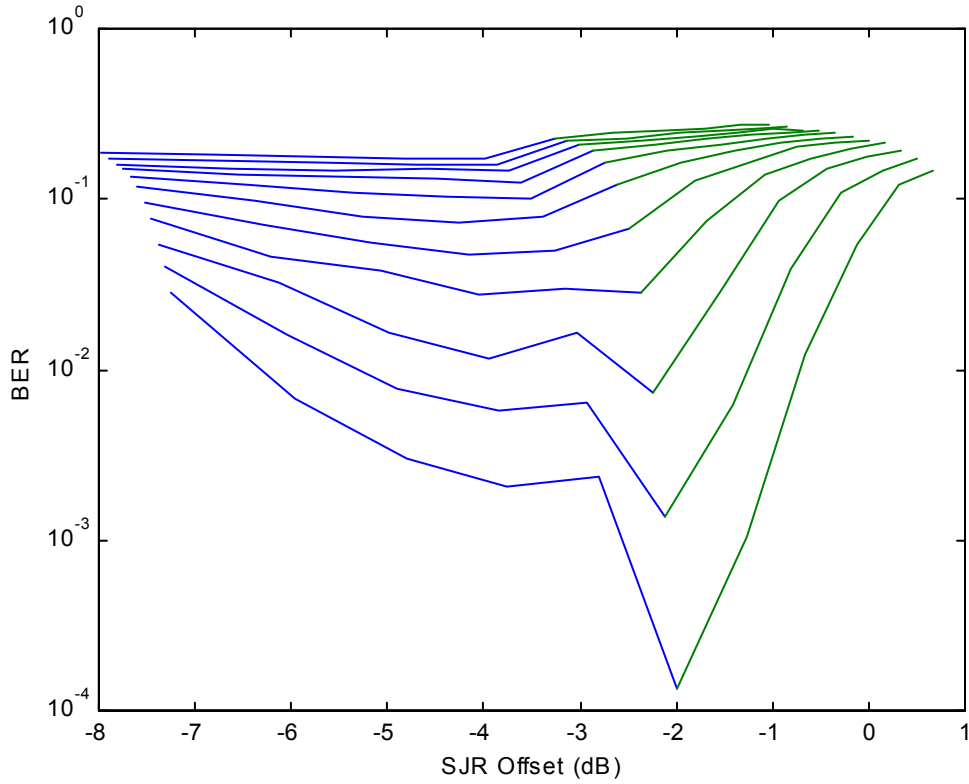
Figure 5.29.   Simulated SCCC/BPSK with AWGN and pulsed noise jamming with no side information and direct sequence spread spectrum: effect of SNR mismatch on BER for ρ = 0.1 = 0 to 2 dB. The graphs start at 0 dB at the top with increments of 0.2 dB for each subsequent graph downwards. Note that when there is no graph for a particular SNR, it means that all errors were corrected for that SNR for the range of SJR considered.
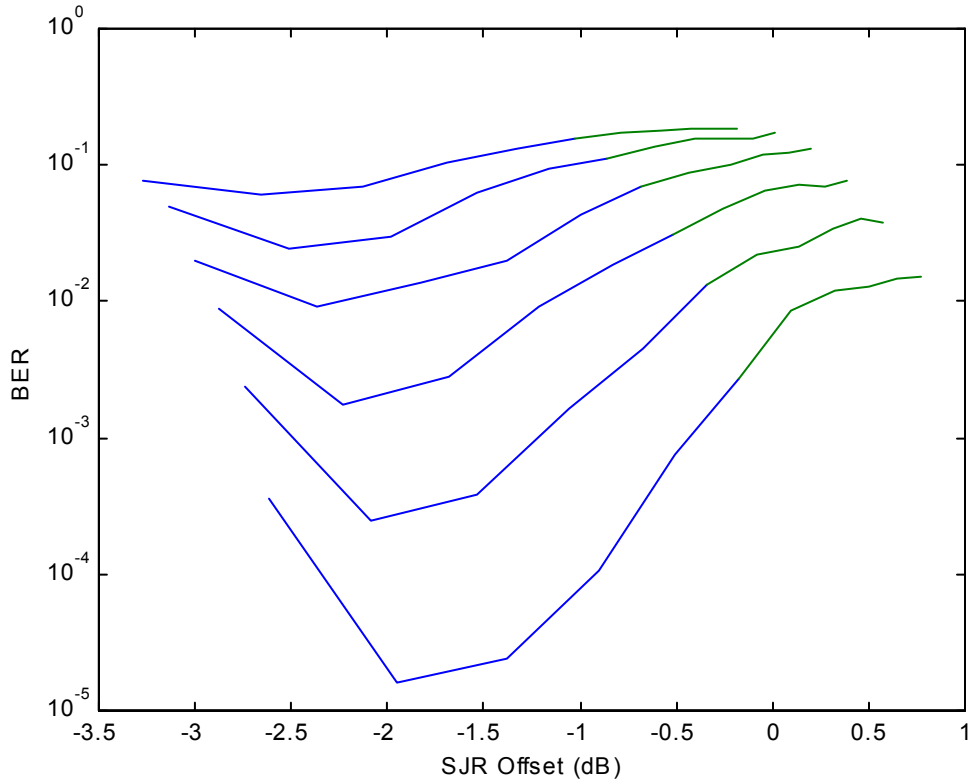
Figure 5.30.   Simulated SCCC/BPSK with AWGN and pulsed noise jamming with no side information and direct sequence spread spectrum: effect of SNR mismatch on BER for $\rho = 1.0$ = 2 to 4 dB. The graphs start at SNR 2 dB at the top with increments of 0.2 dB for each subsequent graph downwards. Note that when there is no graph for a particular SNR, it means that all errors were corrected for that SNR for the range of SJR considered.
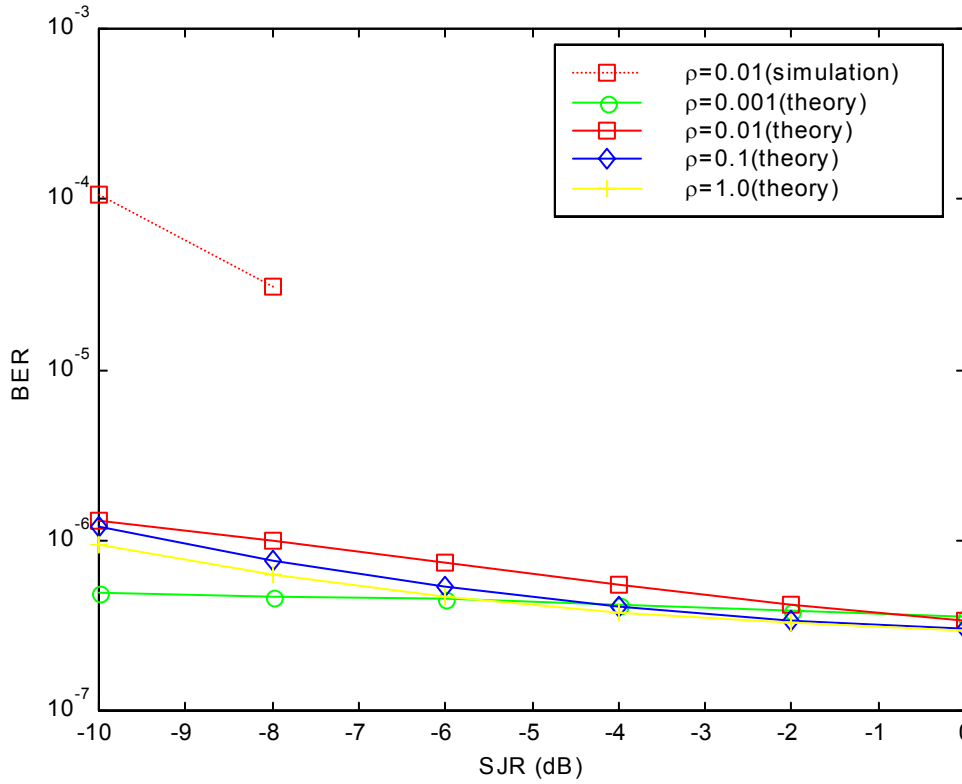
Figure 5.31. Simulated and theoretical SCCC/BPSK with AWGN and pulsed noise jamming with no side information and direct sequence spread spectrum: effect of ρ on BER for ρ = 0.001, 0.01, 0.1 and 1.0, SNR = 4 dB and SJR = -10 to 0 dB. Note that for ρ = 0.001, 0.01 and 0.1 all errors were corrected for the range of SJR considered.
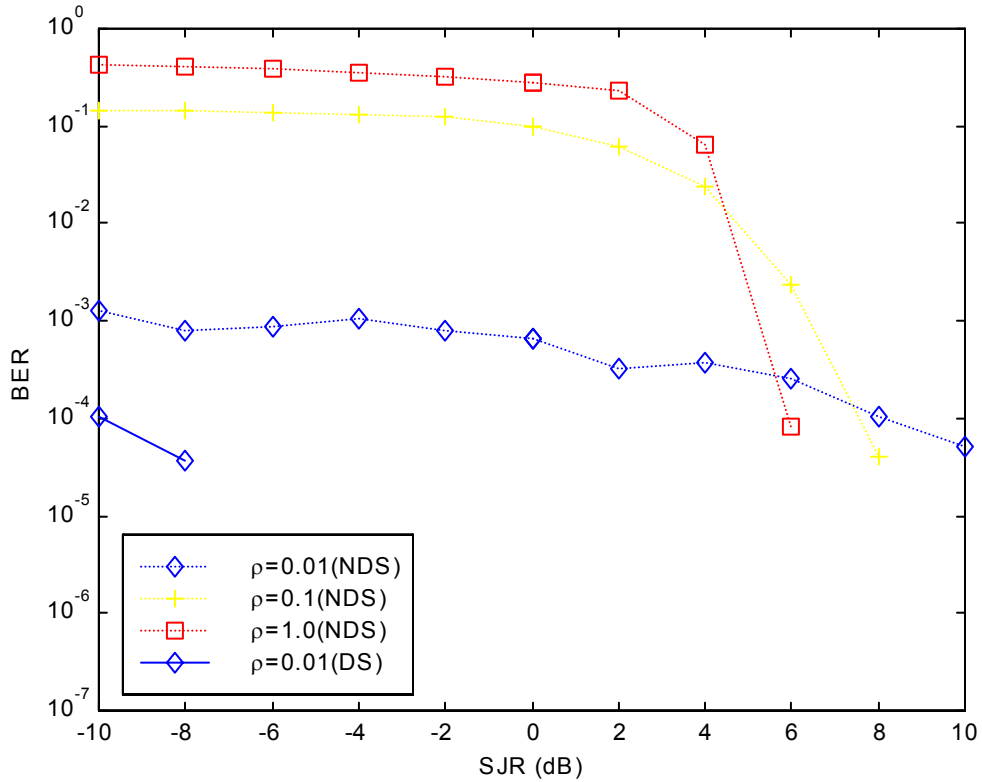
Figure 5.32.   Simulated SCCC/BPSK with AWGN and pulsed noise jamming with no side information: effect of direct sequence spread spectrum on BER for ρ = 0.01, 0.1 and 1.0, SNR = 4 dB and SJR =-10 to 10 dB. Note that for ρ = 0.001, all errors were corrected for both SCCC with direct sequence spread spectrum (DS) and without (NDS). For the SCCC with DS, for ρ = 0.1 and 1.0, all errors were corrected for the range of SJR considered.
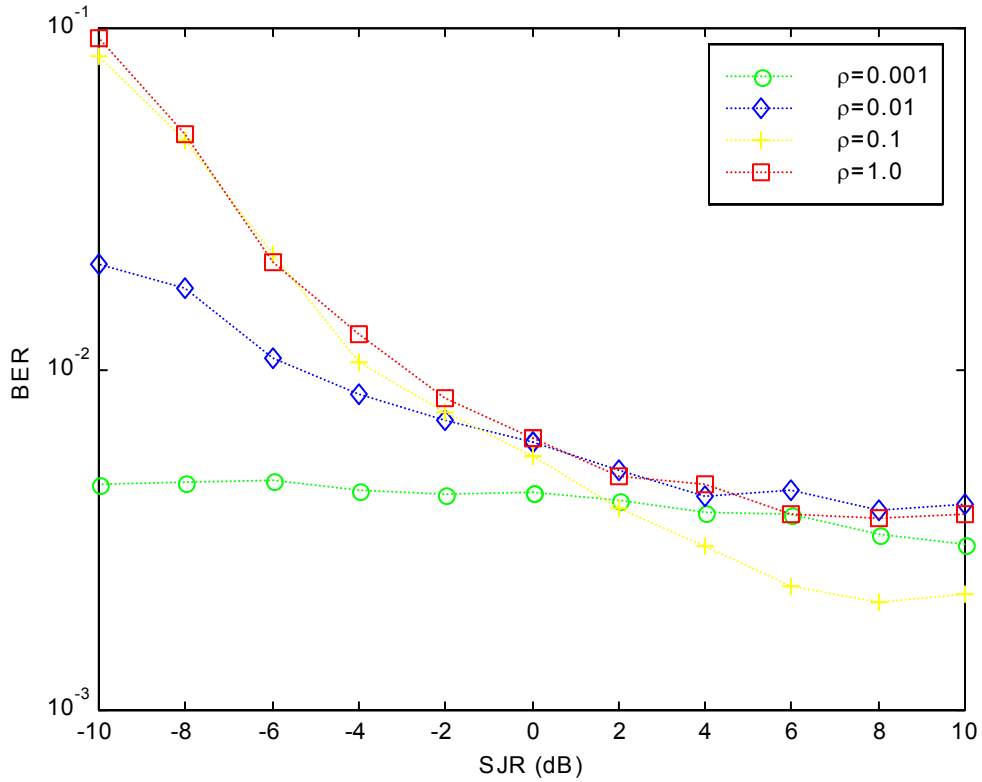
Figure 5.33.   Simulated SCCC/BPSK with AWGN and pulsed noise jamming with side information and direct sequence spread spectrum: effect of ρ on BER for ρ = 0.001, 0.01, 0.1 and 1.0, SNR = 1 dB and SJR =-10 to 10 dB.
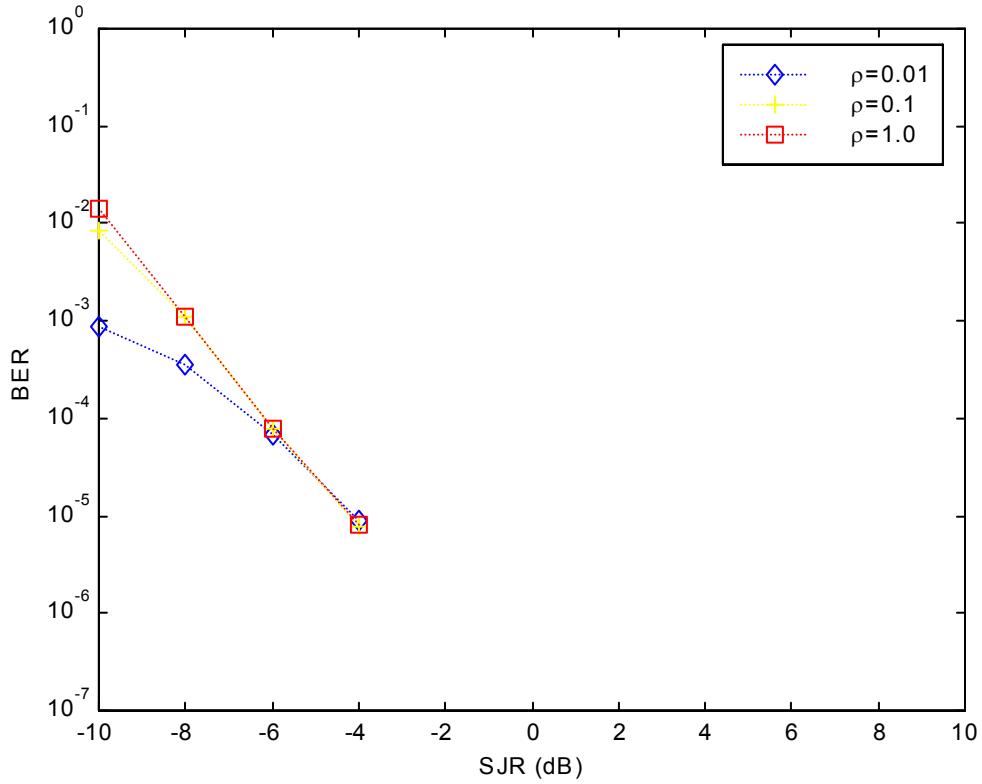
Figure 5.34.　　Simulated SCCC/BPSK with AWGN and pulsed noise jamming with side information and direct sequence spread spectrum: effect of ρ on BER for ρ = 0.01, 0.1 and 1.0, SNR = 1.6 dB and SJR =-10 to 10 dB.　Note that for ρ = 0.001, all errors were corrected for the range of SJR considered.
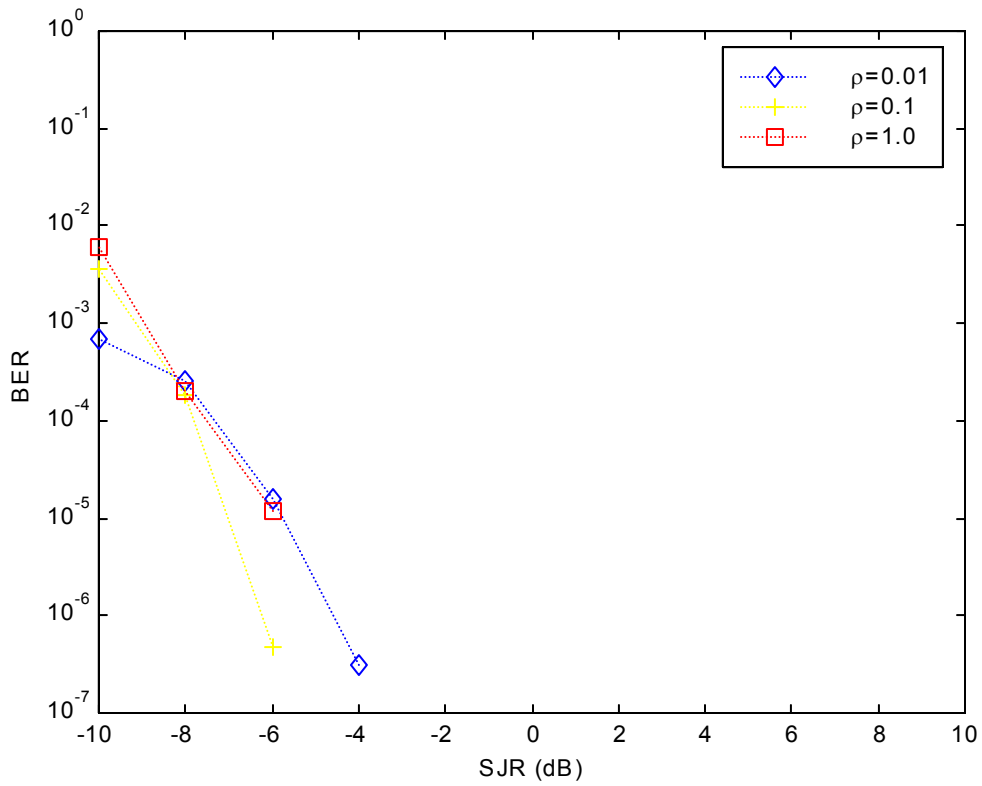
Figure 5.35.   Simulated SCCC/BPSK with AWGN and pulsed noise jamming with side information and direct sequence spread spectrum: effect of ρ on BER for ρ = 0.01, 0.1 and 1.0, SNR = 2 dB and SJR =-10 to 10 dB. Note that for ρ = 0.001, all errors were corrected for the range of SJR considered.
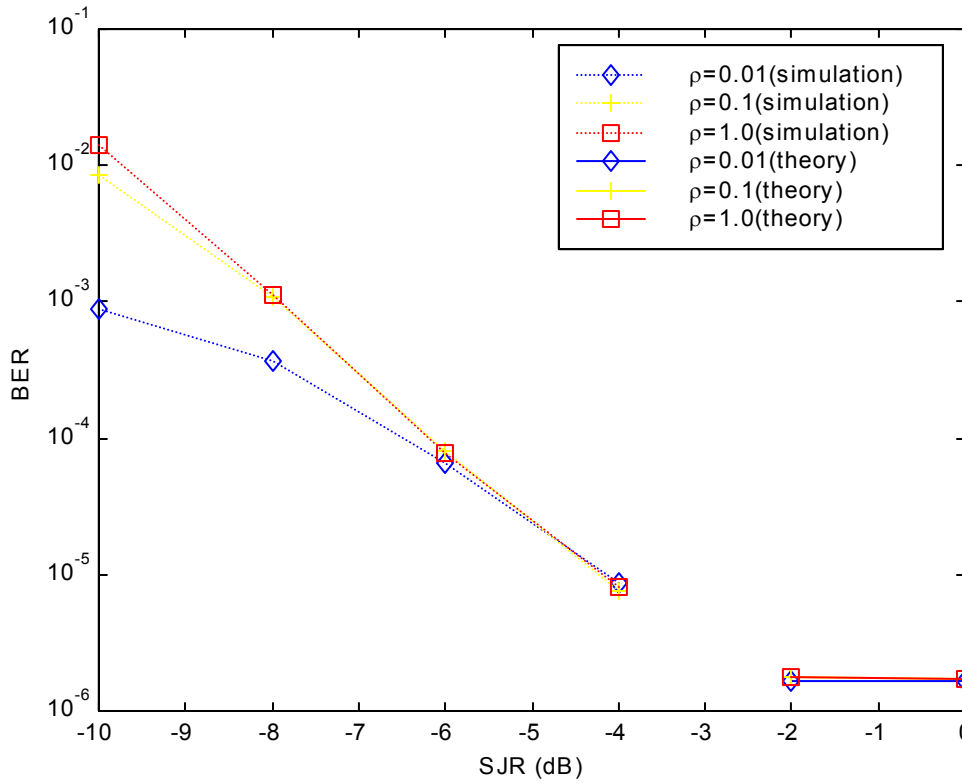
Figure 5.36.   Simulated and theoretical SCCC/BPSK with AWGN and pulsed noise jamming with side information and direct sequence spread spectrum: effect of ρ on BER for ρ = 0.01, 0.1 and 1.0, SNR = 1.8 dB and SJR =-10 to 0 dB. Note that for ρ = 0.001, all errors were corrected for the range of SJR considered.
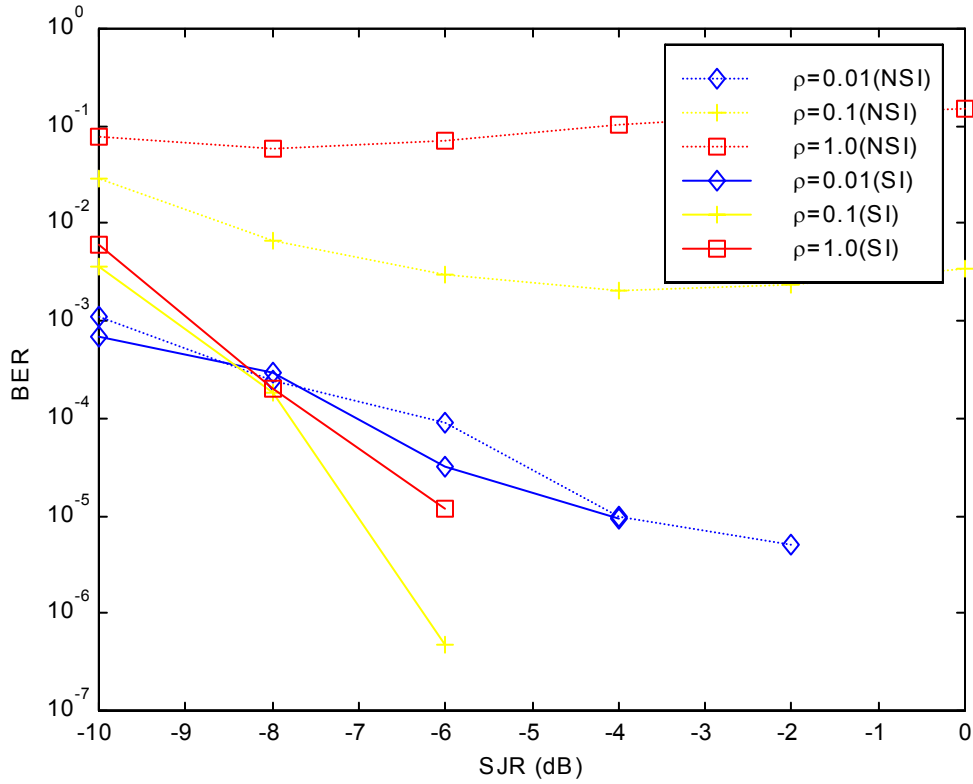
Figure 5.37.   Simulated SCCC/BPSK with AWGN and pulsed noise jamming with direct sequence spread spectrum: effect of side information on BER for ρ = 0.01, 0.1 and 1.0, SNR = 2 dB and SJR =-10 to 0 dB. Note that for ρ = 0.001, all errors were corrected for the range of SJR considered.
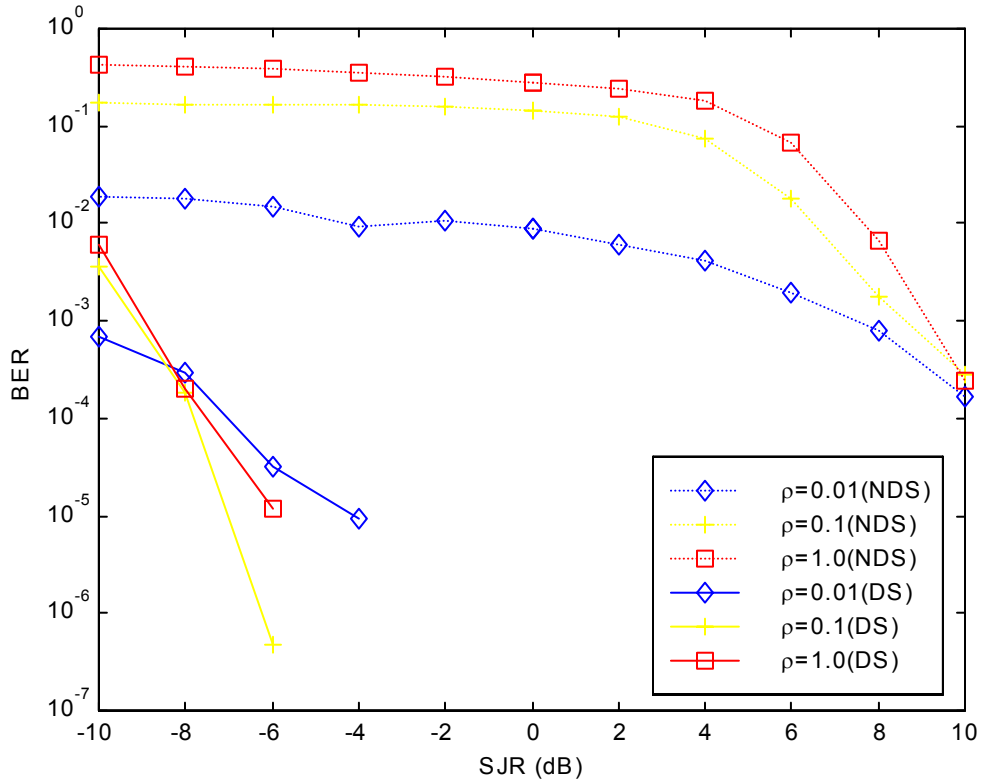
Figure 5.38. Simulated SCCC/BPSK with pulsed noise jamming with side information: effect of direct sequence spread spectrum on BER for ρ = 0.01, 0.1 and 1.0, SNR = 2 dB and SJR =-10 to 10 dB. Note that for ρ = 0.001, all errors were corrected for the range of SJR considered.

VI. THEORETICAL ANALYSIS AND RESULTS OF SCCC WITH NONCOHERENT DPSK IN PULSED/ PARTIAL-BAND NOISE JAMMING, RAYLEIGH FADING AND SLOW FREQUENCY-HOPPED SPREAD SPECTRUM

Research in partial-band noise jamming of noncoherent DPSK began in the 1970s. Anti-jam capabilities of binary and 4-ary slow FH/DPSK systems were analyzed by Houston [Ref. 109]. Cooper and Nettleton [Ref. 110] proposed a Hadamard-coded fast FH/DPSK system to provide a mobile radio service; both linear and nonlinear receivers were considered [Ref. 111]. Hard-decision decoded FH/DPSK performance in partial-band noise jamming can be found in [Ref. 112]. Lee and Miller [Ref. 113] derived the uncoded bit error rate for a fast FH/DPSK system, also in partial-band interference. Simon [Ref. 106] generalized Houston's analysis to FH/DPSK in partial-band multi-tone jamming and in partial-band noise jamming. Each of these investigations has considered only either the uncoded or hard-decision decoded system behavior, and many of them have assumed zero thermal noise in their analysis. Simulation results for soft-decision performance of coded FH/DPSK in the presence of partial-band noise jamming and Rayleigh fading was reported by Yost [Ref. 114]. However, Yost concentrated his efforts on comparison of various demodulator structures rather than metric design and did not give any analytical results. Su [Ref. 108] analyzed the effects of side information on a variety of soft decision metrics for slow FH/DPSK receiver in the presence of partial-band noise jamming. Jordan [Ref. 95] investigated the effects of partial-band noise jamming for DPSK in Turbo codes using both hard and soft decision variables. Kang and Stark [Ref. 96, 115] studied the effects of partial-band interference and Rayleigh fading for Turbo codes using BFSK. No research which includes SCCC, partial-band noise jamming and AWGN, Rayleigh fading and frequency-hopped spread spectrum has been carried out before.

It is the purpose of this chapter to analyze the effects of pulse/ partial-band noise jamming for serially concatenated convolutional codes (SCCC) with noncoherent binary

differential phase shift keying (DPSK) and taking into consideration thermal noise (AWGN) and slow, independent, frequency non-selective Rayleigh fading and slow frequency-hopped spread spectrum (FH). Five scenarios are considered:

a. Pulsed noise jamming with no side information (NSI).

b. Pulsed noise jamming with side information (SI).

c. Pulsed noise jamming with no side information (NSI) and Rayleigh fading with no channel information (NCI) (no amplitude of fade) is available. The pulsed interference is assumed to be unaffected by the fading channel.

d. Partial-band noise jamming with no side information (NSI) and with slow frequency-hopped spread spectrum (FH) incorporated.

e. Partial-band noise jamming with side information (SI) and slow frequency-hopped spread spectrum (FH) incorporated.

The basic DPSK model is shown in Figure 6.1. Note that the interleaver here is used to break up burst errors.
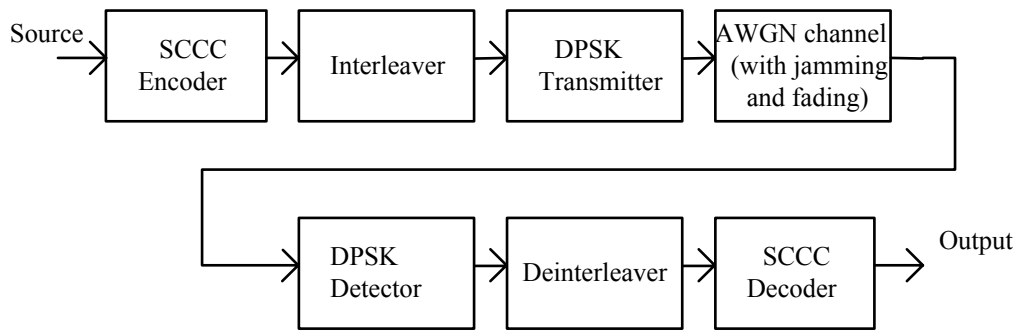
Figure 6.1.   Basic DPSK simulation model.

A.   THEORETICAL BOUNDS

1.   SCCC with Pulsed Noise Jamming and No Side Information

Suppose the SCCC system is attacked by a band-limited, noise-like signal that is turned on and off systematically (pulsed). Let ρ be the fraction of time the jammer is

turned on and assume that the jammer does not turn on or off during a channel bit interval. It is also assumed that the power spectral density (PSD) of the jamming signal when on continuously is $N_I/2$ within the null-to-null bandwidth of the SCCC signal. Assume also that the overall average power transmitted by the jammer is the same whether the jammer is pulsed or not, i.e., for smaller ρ the jamming PSD is higher. Thus, the jammer's PSD is $N_I/2\rho$. With DPSK, we assume that two consecutive bits are either jammed or unjammed, i.e., we neglect the case where one bit is jammed and the other bit is unjammed. This is valid if the jammed bit sequence is long.

From Chapter II, the word probability of error (2.47) is bounded by

$$P_w \le \sum_{w=w_m^o}^{N R_c^o} N^{-(d_f^o-1)/2} \frac{d_f^{o\,d_f^o} d_f^o!}{p^{(d_f^o+1)/2}((d_f^o-3)/2)!} A_{w,d_f^o,1}^o A_{d_f^o,h,(d_f^o-1)/2}^i P_2(h)$$

………(6.1)

and the equivalent bit probability of error (2.48) is bounded by

$$P_b \le \sum_{w=w_m^o}^{N R_c^o} N^{-(d_f^o+1)/2} \frac{d_f^{o\,d_f^o} d_f^o!}{p^{(d_f^o-1)/2}((d_f^o-3)/2)!} \frac{w}{k} A_{w,d_f^o,1}^o A_{d_f^o,h,(d_f^o-1)/2}^i P_2(h)$$

………(6.2)

In the case of pulsed noise jamming, given that i bits are jammed with ρ being the percentage of bits jammed [Ref. 116],

$$P_2(h) = \sum_{i=0}^{h} \binom{h}{i} \rho^i (1-\rho)^{h-i} P_h(i)$$

………(6.3)

where $P_h(i)$ is the probability of selecting a code word a Hamming distance h from the correct code word given that i of h bits are jammed. For a system employing convolutional coding and soft decision Viterbi decoding, P_h is equivalent to a system with h order diversity [Ref. 51]. For a square-law combining detector, the bit error probability for DPSK is equivalent to that of noncoherent binary frequency-shift keying (NCBFSK) with twice the SNR [Ref. 51]. A model of a NCBFSK system is shown in Figure 6.2.

171
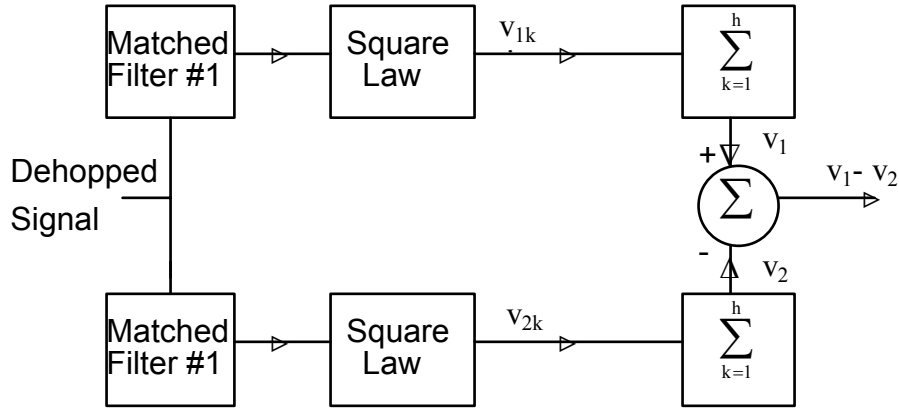
Figure 6.2.   Model equivalent of linear combining SCCC BFSK receiver employing soft decision MAP decoding.

For a BFSK system, $P_h(i)$ is given by [Ref. 117, 118, 119]

$$P_h(i) = \int_0^\infty f_{V_1}(v_1|i)\left[1 - \int_0^{v_1} f_{V_2}(v_2|i)dv_2\right]dv_1$$

………(6.4)

where V_1 and V_2 represents the decision variables for the branch containing the signal and the branch without the signal, respectively. V_{1k} and V_{2k} are random variables that model the output of the two branches of the BFSK detector.   The probability density functions (pdfs) for the decision variables V_{1k} and V_{2k} are

$$f_{V_{1k}}(v_{1k}) = \frac{1}{2\sigma_k^2}\exp\left[-\frac{(v_{1k} + 2A_c^2)}{2\sigma_k^2}\right]I_0\left(\frac{A_c\sqrt{2v_{1k}}}{\sigma_k^2}\right)$$

………(6.5)

$$f_{V_{2k}}(v_{2k}) = \frac{1}{2\sigma_k^2}\exp\left(-\frac{v_{2k}}{2\sigma_k^2}\right)$$

………(6.6)

If we indicate the jammed bits and bits which are not jammed by the superscripts (1) and (2), respectively, the pdfs for the decision variables V_1 and V_2 are [Ref. 111, 112, 120]

172

$$f_{V_{1|i}}(v_1|i) = \left[f_{V_{1k}}^{(1)}(v_{1k})\right]^{\otimes i} \otimes \left[f_{1k}^{(2)}(v_{1k})\right]^{\otimes(h-i)}$$

$$\ldots\ldots\ldots(6.7)$$

$$f_{V_{2|i}}(v_2|i) = \left[f_{V_{2k}}^{(1)}(v_{2k})\right]^{\otimes i} \otimes \left[f_{2k}^{(2)}(v_{2k})\right]^{\otimes(h-i)}$$

$$\ldots\ldots\ldots(6.8)$$

where $\otimes$ indicates convolution. We designate the noise power σ_k^2 for jammed bits as σ_1^2 and for non-jammed bits as σ_2^2 where

$$\sigma_1^2 = \frac{N_o + \dfrac{N_I}{\rho}}{2R_cT_b}$$

$$\ldots\ldots\ldots(6.9)$$

$$\sigma_2^2 = \frac{N_o}{2R_cT_b}$$

$$\ldots\ldots\ldots(6.10)$$

and R_c is the code rate, T_b is the duration of a bit and the factor of two is due to DPSK detection. Substituting the pdfs of V_{1k} and V_{2k} into (6.7) and (6.8) and taking the Laplace transforms, we obtain

$$F_{V_{1|i}}(s) = \left[\frac{1}{2\sigma_1^2 s+1}\exp\left(\frac{-A_c^2}{\sigma_1^2}\frac{s}{s+\dfrac{1}{2\sigma_1^2}}\right)\right]^i \left[\frac{1}{2\sigma_2^2 s+1}\exp\left(\frac{-A_c^2}{\sigma_2^2}\frac{s}{s+\dfrac{1}{2\sigma_2^2}}\right)\right]^{h-i}$$

$$\ldots\ldots\ldots(6.11)$$

$$F_{V_{2|i}}(s) = \left[\frac{1}{2\sigma_1^2 s+1}\right]^i \left[\frac{1}{2\sigma_2^2 s+1}\right]^{h-i}$$

$$\ldots\ldots\ldots(6.12)$$

No simple analytic solutions exist for the inverse Laplace transforms of the above expressions; therefore, the inverse Laplace transforms are determined numerically. Computation of the probability of bit error involves the numerical evaluation of (6.4) for each of the possible combinations of jammed and unjammed bits, followed by, after using the results of (6.4) in (6.3), an evaluation of (6.2). In addition, except for the special cases of either all bits are jammed or all bits are free of interference, the

conditional probability density of V_1 (6.7) must be evaluated numerically. The most efficient way to evaluate (6.7) is to Laplace transform it into (6.11) and then invert (6.11) numerically [Ref. 121]. The integral of the pdf of V_2 (6.8) contained in the bracketed term of (6.4) is calculated by taking the inverse Laplace transforms of (6.12) multiplied by 1/s. Equation (6.4) is then calculated using a Simpson's rule numerical integration [Ref. 122].

2. SCCC with Pulsed Noise Jamming and Side Information

When perfect side information is available, i.e., we know which bits are jammed and which are not, we can disregard the jammed bits so that for $i < h$, the decision statistics consist of the summation of the signals of only the unjammed bits. Hence, the receiver with perfect side information has an equivalent diversity of $(h-i)$ when $i < h$, and $P_h(i)$ has the same probability of bit error for DPSK with $(h-i)$ fold diversity. The probability of error for binary DPSK with h-fold diversity is given in [Ref. 51]. Therefore, for $i < h$, we have

$$P_h(i) = \frac{1}{2^{2(h-i)-1}} \exp\left[-\frac{(h-i)R_c E_b}{N_o}\right] \sum_{n=0}^{h-i-1} C_n \left[\frac{(h-i)R_c E_b}{N_o}\right]^n$$

.........(6.13)

where

$$C_n = \frac{1}{n!} \sum_{m=0}^{h-i-1-n} \binom{2(h-i)-1}{m}$$

.........(6.14)

For $i = h$, all bits are used to compute the decision statistics, and $P_h(i = h)$ is the same as the probability of bit error of DPSK with h-fold diversity:

$$P_h(i = h) = \frac{1}{2^{2h-1}} \exp\left[-\frac{hR_c E_b}{N_o + N_I/\rho}\right] \sum_{n=0}^{h-1} C_{nh} \left[\frac{hR_c E_b}{N_o + N_I/\rho}\right]^n$$

.........(6.15)

where

$$C_{nh} = \frac{1}{n!} \sum_{m=0}^{h-1-n} \binom{2h-1}{m}$$

.........(6.16)

Therefore, $P_2(h)$ is given by

$$P_2(h) = \left\{ \sum_{i=0}^{h-1} \binom{h}{i} \rho^i (1-\rho)^{h-i} \frac{1}{2^{2(h-i)}} \exp\left[-\frac{(h-i)R_c E_b}{N_o} \right] \sum_{n=0}^{h-i-1} C_n \left[\frac{(h-i)R_c E_b}{N_o} \right]^n \right\} +$$

$$\frac{\rho^h}{2^{2h-1}} \exp\left[-\frac{hR_c E_b}{N_o + N_I/\rho} \right] \sum_{n=0}^{h-1} C_{nh} \left[\frac{hR_c E_b}{N_o + N_I/\rho} \right]^n$$

………(6.17)

where C_n and C_{nh} are given by (6.14) and (6.16), respectively. Substituting (6.17) into (6.1) and (6.2) with h from (2.43), we obtain

$$P_w \le \sum_{w=w_m^o}^{NR_c^o} N^{-(d_f^o-1)/2} \frac{d_f^o d_f^o d_f^o!}{p^{(d_f^o+1)/2}((d_f^o-3)/2)!} A_{w,d_f^o,1}^o A_{d_f^o, \frac{(d_f^o-3)d_{f,eff}^i}{2}+h_3,(d_f^o-1)/2}^i$$

$$\left\{ \left[\sum_{i=0}^{\frac{(d_f^o-3)d_{f,eff}^i}{2}+h_3-1} \left(\frac{(d_f^o-3)d_{f,eff}^i}{2}+h_3 \right) \rho^i (1-\rho)^{\frac{(d_f^o-3)d_{f,eff}^i}{2}+h_3-i} \frac{1}{2^{2\left(\frac{(d_f^o-3)d_{f,eff}^i}{2}+h_3-i\right)-1}} \right. \right.$$

$$\left. \exp\left[-\frac{\left(\frac{(d_f^o-3)d_{f,eff}^i}{2}+h_3-i \right)R_c E_b}{N_o} \right] \sum_{n=0}^{\frac{(d_f^o-3)d_{f,eff}^i}{2}+h_3-i-1} C_n \left[\frac{\left(\frac{(d_f^o-3)d_{f,eff}^i}{2}+h_3-i \right)R_c E_b}{N_o} \right]^n \right]$$

$$\frac{\rho^{\frac{(d_f^o-3)d_{f,eff}^i}{2}+h_3}}{2^{2\left(\frac{(d_f^o-3)d_{f,eff}^i}{2}+h_3\right)-1}} \exp\left[-\frac{\left(\frac{(d_f^o-3)d_{f,eff}^i}{2}+h_3 \right)R_c E_b}{N_o + N_I/\rho} \right] \sum_{n=0}^{\frac{(d_f^o-3)d_{f,eff}^i}{2}+h_3-1} C_{nh} \left[\frac{\left(\frac{(d_f^o-3)d_{f,eff}^i}{2}+h_3 \right)R_c E_b}{N_o + N_I/\rho} \right]^n \right\}$$

……….(6.18)

175

and the equivalent bit probability of error (2.48) is

$$
P_b \leq \sum_{w=w_m^o}^{NR_c^o} N^{-(d_f^o+1)/2} \frac{d_f^o d_f^{d_f^o}!}{p^{(d_f^o-1)/2}((d_f^o-3)/2)!} w A_{w,d_f^o,1}^o A_{d_f^o,\frac{(d_f^o-3)d_{f,eff}^i}{2}+h_3,(d_f^o-1)/2}^i
$$

$$
\left\{ \left[\sum_{i=0}^{\frac{(d_f^o-3)d_{f,eff}^i}{2}+h_3-1} \binom{\frac{(d_f^o-3)d_{f,eff}^i}{2}+h_3}{i} \rho^i (1-\rho)^{\frac{(d_f^o-3)d_{f,eff}^i}{2}+h_3-i} \frac{1}{2^{2(\frac{(d_f^o-3)d_{f,eff}^i}{2}+h_3-i)-1}} \right. \right.
$$

$$
\exp\left[-\frac{\left(\frac{(d_f^o-3)d_{f,eff}^i}{2}+h_3-i\right)R_c E_b}{N_o} \right]^{\frac{(d_f^o-3)d_{f,eff}^i}{2}+h_3-i-1} \sum_{n=0} C_n \left[\frac{\left(\frac{(d_f^o-3)d_{f,eff}^i}{2}+h_3-i\right)R_c E_b}{N_o} \right]^n \right]
$$

$$
\left. \frac{\rho^{\frac{(d_f^o-3)d_{f,eff}^i}{2}+h_3}}{2^{2\left(\frac{(d_f^o-3)d_{f,eff}^i}{2}+h_3\right)-1}} \exp\left[-\frac{\left(\frac{(d_f^o-3)d_{f,eff}^i}{2}+h_3\right)R_c E_b}{N_o+N_I/\rho} \right]^{\frac{(d_f^o-3)d_{f,eff}^i}{2}+h_3-1} \sum_{n=0} C_{nh} \left[\frac{\left(\frac{(d_f^o-3)d_{f,eff}^i}{2}+h_3\right)R_c E_b}{N_o+N_I/\rho} \right]^n \right] \right\}
$$

………(6.19)

3. SCCC with Pulsed Noise Jamming and No Side Information and Rayleigh Fading with No Channel Information

In this section, we derive the bit error probability versus the bit energy-to-interference power spectral density ratio (SJR) given the Rayleigh statistics of the fading channel. For this analysis, we refer to the same model equivalent of the system shown in Figure 2. The probability density functions of the random variables V_{1k} were derived analytically for the general Rician fading case for NCBFSK [Ref. 120, 123]. We will adapt it for Rayleigh fading by letting the direct signal power $\alpha^2 = 0$ and doubling the SNR for DPSK.

First, we assume without loss of generality that the signal is present in the branch 1 of the demodulator. The probability density function of the quadratic detector output of branch 1 conditioned on a_k is [Ref. 120]

$$
f_{V_{1k}}(v_{1k}|a_k) = \frac{1}{2\sigma_k^2} \exp\left[-\frac{v_{1k}+2a_k^2}{2\sigma_k^2} \right] I_o\left(\frac{a_k\sqrt{2v_{1k}}}{\sigma_k^2} \right) u(v_{1k})
$$

………(6.20)

176

where u($\bullet$) is the unit step function, a_k is the Rayleigh random variable representing the fading of bit k with a signal amplitude of $\sqrt{2}a_k$. The probability density function of the random variable a_k is

$$f_{A_k}(a_k) = \frac{a_k}{\sigma^2} \exp\left(-\frac{a_k^2}{2\sigma^2}\right) u(a_k)$$

………(6.21)

where $2\sigma^2$ is the average power of the diffuse power component of the signal which is assumed constant from bit to bit in this dissertation. The probability density function of the random variable V_{1k} is

$$f_{V_{1k}}(v_{1k}) = \int_0^\infty f_{V_{k1}}(v_{1k}|a_k) f_{A_k}(a_k) da_k$$

………(6.22)

for which the solution is

$$f_{V_{1k}}(v_{1k}) = \frac{1}{2(\sigma_k^2 + 2\sigma^2)} \exp\left(-\frac{1}{2}\frac{v_{1k}}{(\sigma_k^2 + 2\sigma^2)}\right) u(v_{1k})$$

………(6.23)

To find the probability density function of the random variable V_{2k} that corresponds to the output of branch 2 of the demodulator that contains no signal component, from (6.23), replace V_{1k} with V_{2k} and let $2\sigma^2 = 0$ to yield

$$f_{V_{2k}}(v_{2k}) = \frac{1}{2\sigma_k^2} \exp\left(-\frac{1}{2}\frac{v_{2k}}{\sigma_k^2}\right)$$

………(6.24)

If we indicate the jammed bits and bits which are not jammed by the superscripts (1) and (2), respectively, the pdfs for the decision variables V_1 and V_2 are

$$f_{V_{1|i}}(v_1|i) = \left[f_{V_{1k}}^{(1)}(v_{1k})\right]^{\otimes i} \otimes \left[f_{1k}^{(2)}(v_{1k})\right]^{\otimes(h-i)}$$

………(6.25)

$$f_{V_{2|i}}(v_2|i) = \left[f_{V_{2k}}^{(1)}(v_{2k})\right]^{\otimes i} \otimes \left[f_{2k}^{(2)}(v_{2k})\right]^{\otimes(h-i)}$$

………(6.26)

where $\otimes$ indicates convolution. We designate the noise power σ_k^2 for jammed bits as σ_1^2 and for non-jammed bits as σ_2^2 where

$$\sigma_1^2 = \frac{N_o + \dfrac{N_I}{\rho}}{2R_c T_b}$$

………(6.27)

$$\sigma_2^2 = \frac{N_o}{2R_c T_b}$$

………(6.28)

where R_c is the code rate, T_b is the duration of a bit, and the factor of two is due to DPSK detection. Substituting for the pdfs of V_{1k} and V_{2k} into (6.25) and (6.26), respectively, and taking the Laplace transforms, we obtain

$$F_{V_{1|i}}(s) = \left[\frac{1}{2(\sigma_1^2 + 2\sigma^2)}\frac{1}{s+1}\right]^i \left[\frac{1}{2(\sigma_1^2 + 2\sigma^2)}\frac{1}{s+1}\right]^{h-i}$$

………(6.29)

$$F_{V_{2|i}}(s) = \left[\frac{1}{2\sigma_1^2 s+1}\right]^i \left[\frac{1}{2\sigma_2^2 s+1}\right]^{h-i}$$

………(6.30)

The union bound for the word and bit probabilities of error are given in (6.1) and (6.2), respectively. In the case of pulsed noise jamming, given that i bits are jammed and ρ being the percentage of bits jammed, $P_2(h)$ is given as

$$P_2(h) = \sum_{i=0}^{h} \binom{h}{i} \rho^i (1-\rho)^{h-i} P_h(i)$$

………(6.31)

where $P_h(i)$ is the probability of selecting a code word a Hamming distance h from the correct code word given that i of h receptions are jammed. Hence, for a DPSK system with AWGN, pulsed noise jamming, no side information, and Rayleigh fading with no channel information, $P_h(i)$ is given by [Ref. 124]

$$P_h(i) = \int_0^\infty f_{V_1}(v_1|i)\left[1 - \int_0^{V_1} f_{V_2}(v_2|i)dv_2\right]dv_1$$

………(6.32)

178

where $f_{V_1}(v_1|i)$ and $f_{V_2}(v_2|i)$ are given by the inverse Laplace transforms of (6.29) and (6.30), respectively. Once (6.32) is solved numerically, it can then be substituted into (6.3) which is then used in (6.2) to obtain the probability of bit error.

4. **SCCC with Partial-Band Noise Jamming and No Side Information and with Slow Frequency-Hopped Spread Spectrum**

The simulation model for SCCC with DPSK and slow frequency-hopped spread spectrum (FH) is shown in Figure 6.3. Note that the additional interleaver is used to disperse burst errors.
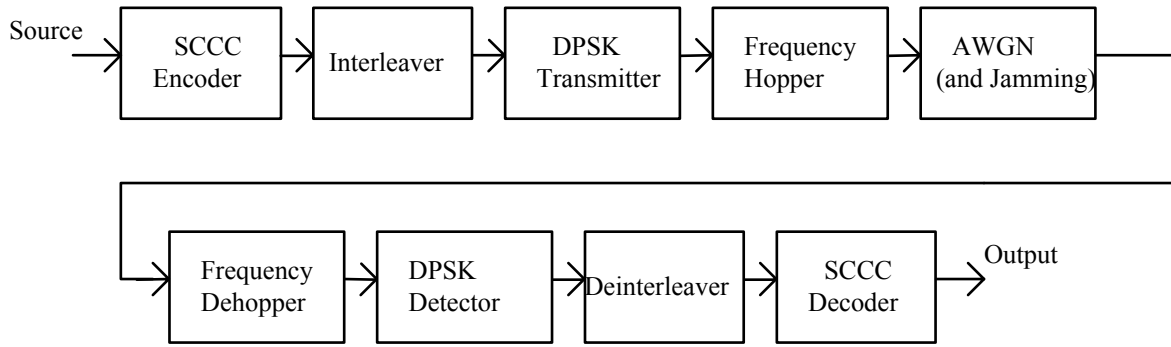
Figure 6.3. SCCC/DPSK simulation model with frequency-hopped spread spectrum.

Suppose that the SCCC system is attacked by a bandlimited noise-like signal that occupies a fraction of the frequency range. Let ρ be the fraction of the frequency range the jammer affects. It is also assumed that the power spectral density (PSD) of the jamming signal is $N_I/2$ within the null-to-null bandwidth of the SCCC signal when $\rho = 1$. There are two channel states when $\rho < 1$: jammed and unjammed. It is also assumed that the jammer stays on for the entire duration of a hop if it is jammed. Assume also that the overall average power transmitted by the jammer is the same whether the jammer is on or not, i.e., for smaller ρ the jamming power is higher. Thus the jammer's PSD is $N_I/2\rho$.

From Chapter II, the word probability of error (2.47) is bounded by

$$P_w \leq \sum_{w=w_m^o}^{NR_c^o} N^{-(d_f^o-1)/2} \frac{d_f^o d_f^o!}{p^{(d_f^o+1)/2}((d_f^o-3)/2)!} A_{w,d_f^o,1}^o A_{d_f^o,\frac{(d_f^o-3)d_{f,eff}^i}{2}+h_3,(d_f^o-1)/2}^i P_2(h)$$

$$\dots\dots(6.33)$$

and the equivalent bit probability of error (2.48) is bounded by

$$
P_b \leq \sum_{w=w_m^o}^{NR_c^o} N^{-(d_f^o+1)/2} \frac{d_f^o d_f^{d_f^o}!}{p^{(d_f^o-1)/2}((d_f^o-3)/2)!} \frac{w}{k} A_{w,d_f^o,1}^o A^i_{d_f^o, \frac{(d_f^o-3)d_{f,eff}^i}{2}+h_3,(d_f^o-1)/2} P_2(h)
$$

$$\ldots\ldots\ldots(6.34)$$

In the case of partial-band noise jamming, given that i bits are jammed with ρ being the percentage of frequency bins being jammed [Ref. 117],

$$
P_2(h) = \sum_{i=0}^{h} \binom{h}{i} \rho^i (1-\rho)^{h-i} P_h(i)
$$

$$\ldots\ldots\ldots(6.35)$$

where $P_h(i)$ is the probability of selecting a code word a Hamming distance h from the correct code word given that i of h receptions are jammed. For a system employing convolutional coding and soft decision Viterbi decoding, P_h is equivalent to a system with h-order diversity [Ref. 51]. It is assumed here that the effect of one bit jammed and an immediately succeeding bit not jammed, or vice versa, is negligible. For a square-law combining detector, the bit error probability for DPSK is equivalent to that of noncoherent binary frequency-shift keying (NCBFSK) with twice the SNR [Ref. 51]. The model of a NCBFSK system is shown in Figure 2.

For a BFSK system, $P_h(i)$ is given by [Ref. 110, 119, 120]

$$
P_h(i) = \int_0^\infty f_{V_1}(v_1|i) \left[1 - \int_0^{v_1} f_{V_2}(v_2|i) dv_2 \right] dv_1
$$

$$\ldots\ldots\ldots(6.36)$$

where V_1 and V_2 represents the decision variables for the branch containing the signal and the branch without the signal, respectively. V_{1k} and V_{2k} are random variables that model the output of the two branches of the BFSK detector. The probability density functions (pdfs) for the decision variables V_{1k} and V_{2k} are

$$
f_{V_{1k}}(v_{1k}) = \frac{1}{2\sigma_k^2} \exp\left[-\frac{(v_{1k}+2A_c^2)}{2\sigma_k^2} \right] I_o\left(\frac{A_c\sqrt{2v_{1k}}}{\sigma_k^2} \right)
$$

$$\ldots\ldots\ldots(6.37)$$

$$f_{V_{2k}}(v_{2k}) = \frac{1}{2\sigma_k^2} \exp\left(-\frac{v_{2k}}{2\sigma_k^2}\right)$$

$$\dots\dots\dots(6.38)$$

If we indicate the jammed bits and bits which are not jammed by the superscripts (1) and (2), respectively, the pdfs for the decision variables V_1 and V_2 are [Ref. 119, 120, 121]

$$f_{V_{1|i}}(v_1|i) = \left[f_{V_{1k}}^{(1)}(v_{1k})\right]^{\otimes i} \otimes \left[f_{1k}^{(2)}(v_{1k})\right]^{\otimes(d-i)}$$

$$\dots\dots\dots(6.39)$$

$$f_{V_{2|i}}(v_2|i) = \left[f_{V_{2k}}^{(1)}(v_{2k})\right]^{\otimes i} \otimes \left[f_{2k}^{(2)}(v_{2k})\right]^{\otimes(d-i)}$$

$$\dots\dots\dots(6.40)$$

where $\otimes$ indicates convolution. We designate the noise power σ_k^2 for jammed bits as σ_1^2 and for non-jammed bits as σ_2^2 where

$$\sigma_1^2 = \frac{N_o + \dfrac{N_I}{\rho c}}{2R_c T_b}$$

$$\dots\dots\dots(6.41)$$

$$\sigma_2^2 = \frac{N_o}{2R_c T_b}$$

$$\dots\dots\dots(6.42)$$

where R_c is the code rate, T_b is the duration of a bit, c is the number of chips per set and the factor of two is due to DPSK detection. Substituting the pdfs of V_{1k} and V_{2k} into (6.39) and (6.40) and taking the Laplace transforms, we obtain

$$F_{V_{1|i}}(s) = \left[\frac{1}{2\sigma_1^2 s + 1}\exp\left(\frac{-A_c^2}{\sigma_1^2}\frac{s}{s+\dfrac{1}{2\sigma_1^2}}\right)\right]^i \left[\frac{1}{2\sigma_2^2 s + 1}\exp\left(\frac{-A_c^2}{\sigma_2^2}\frac{s}{s+\dfrac{1}{2\sigma_2^2}}\right)\right]^{h-i}$$

$$\dots\dots\dots(6.43)$$

$$F_{V_{2|i}}(s) = \left[\frac{1}{2\sigma_1^2 s + 1}\right]^i \left[\frac{1}{2\sigma_2^2 s + 1}\right]^{h-i}$$

$$\dots\dots\dots(6.44)$$

181

No simple analytic solutions exist for the inverse Laplace transforms of the above expressions; therefore, the inverse Laplace transforms are determined numerically.

5. **SCCC with Partial-band Noise Jamming and Side Information and with Slow Frequency-hopped Spread Spectrum**

When perfect side information is available, i.e., we know which bits is jammed and which are not, we can disregard the jammed bits so that for $i < h$, the decision statistics consist of the summation of the signals of only the unjammed bits. Hence, the receiver with perfect side information has an equivalent diversity of $(h-i)$ when $i < h$, and $P_h(i)$ has the same probability of bit error for DPSK with $(h-i)$ fold diversity. The probability of error for binary DPSK with h-fold diversity is given in [Ref. 51]. Therefore, for $i < h$, we have

$$P_h(i) = \frac{1}{2^{2(h-i)-1}} \exp\left[-\frac{(h-i)R_c E_b}{N_o}\right] \sum_{n=0}^{h-i-1} C_n \left[\frac{(h-i)R_c E_b}{N_o}\right]^n$$

$$\ldots\ldots\ldots(6.45)$$

where

$$C_n = \frac{1}{n!} \sum_{m=0}^{h-i-1-n} \binom{2(h-i)-1}{m}$$

$$\ldots\ldots\ldots(6.46)$$

For $i = h$, all bits are used to compute the decision statistics, and $P_h(i = h)$ is the same as the probability of bit error of DPSK with h-fold diversity:

$$P_h(i = h) = \frac{1}{2^{2h-1}} \exp\left[-\frac{hR_c E_b}{N_o + N_I / \rho c}\right] \sum_{n=0}^{h-1} C_{nh} \left[\frac{hR_c E_b}{N_o + N_I / \rho c}\right]^n$$

$$\ldots\ldots\ldots(6.47)$$

where

$$C_{nh} = \frac{1}{n!} \sum_{m=0}^{h-1-n} \binom{2h-1}{m}$$

$$\ldots\ldots\ldots(6.48)$$

Therefore, $P_2(h)$ is given by

$$P_2(h) = \left\{ \sum_{i=0}^{h-1} \binom{h}{i} \rho^i (1-\rho)^{h-i} \frac{1}{2^{2(h-i)}} \exp\left[-\frac{(h-i)R_c E_b}{N_o} \right] \sum_{n=0}^{h-i-1} C_n \left[\frac{(h-i)R_c E_b}{N_o} \right]^n \right\} +$$

$$\frac{\rho^h}{2^{2h-1}} \exp\left[-\frac{hR_c E_b}{N_o + N_I / \rho c} \right] \sum_{n=0}^{h-1} C_{nh} \left[\frac{hR_c E_b}{N_o + N_I / \rho c} \right]^n$$

………(6.49)

where C_n and C_{nh} are given by (6.46) and (6.18), respectively. Substituting (6.49) into (6.33) and (6.34) with h from (2.43), we obtain

$$P_w \leq \sum_{w=w_m^o}^{NR_c^o} N^{-(d_f^o - 1)/2} \frac{d_f^o{}^{d_f^o} d_f^o!}{p^{(d_f^o+1)/2}((d_f^o-3)/2)!} A_{w,d_f^o,1}^o A_{d_f^o, \frac{(d_f^o-3)d_{f,eff}^i}{2}+h_3, (d_f^o-1)/2}^i$$

$$\left\{ \left[\sum_{i=0}^{\frac{(d_f^o-3)d_{f,eff}^i}{2}+h_3-1} \left(\frac{(d_f^o-3)d_{f,eff}^i}{2}+h_3 \right) \rho^i(1-\rho)^{\frac{(d_f^o-3)d_{f,eff}^i}{2}+h_3-i} \frac{1}{2^{2(\frac{(d_f^o-3)d_{f,eff}^i}{2}+h_3-i)-1}} \right. \right.$$

$$\left. \exp\left[-\frac{\left(\frac{(d_f^o-3)d_{f,eff}^i}{2}+h_3-i \right)R_c E_b}{N_o} \right] \sum_{n=0}^{\frac{(d_f^o-3)d_{f,eff}^i}{2}+h_3-i-1} C_n \left[\frac{\left(\frac{(d_f^o-3)d_{f,eff}^i}{2}+h_3-i \right)R_c E_b}{N_o} \right]^n \right]$$

$$\frac{\rho^{\frac{(d_f^o-3)d_{f,eff}^i}{2}+h_3}}{2^{2\left(\frac{(d_f^o-3)d_{f,eff}^i}{2}+h_3\right)-1}} \exp\left[-\frac{\left(\frac{(d_f^o-3)d_{f,eff}^i}{2}+h_3 \right)R_c E_b}{N_o + N_I / \rho c} \right] \sum_{n=0}^{\frac{(d_f^o-3)d_{f,eff}^i}{2}+h_3-1} C_{nh} \left[\frac{\left(\frac{(d_f^o-3)d_{f,eff}^i}{2}+h_3 \right)R_c E_b}{N_o + N_I / \rho c} \right]^n \right\}$$

……….(6.50)

and the equivalent bit probability of error (2.48) is

$$P_b \leq \sum_{w=w_m^o}^{NR_c^o} N^{-(d_f^o+1)/2} \frac{d_f^o d_f^{d_f^o}!}{p^{(d_f^o-1)/2}((d_f^o-3)/2)!} w_k A_{w,d_f^o,1}^o A_{d_f^o,\frac{(d_f^o-3)d_{f,eff}^i}{2}+h_3,(d_f^o-1)/2}^i$$

$$\left\{ \left[\sum_{i=0}^{\frac{(d_f^o-3)d_{f,eff}^i}{2}+h_3-1} \left(\frac{(d_f^o-3)d_{f,eff}^i}{2}+h_3 \atop i \right) \rho^i (1-\rho)^{\frac{(d_f^o-3)d_{f,eff}^i}{2}+h_3-i} \frac{1}{2^{2(\frac{(d_f^o-3)d_{f,eff}^i}{2}+h_3-i)-1}} \right. \right.$$

$$\exp\left[-\frac{\left(\frac{(d_f^o-3)d_{f,eff}^i}{2}+h_3-i\right)R_c E_b}{N_o} \right] \sum_{n=0}^{\frac{(d_f^o-3)d_{f,eff}^i}{2}+h_3-i-1} C_n \left[\frac{\left(\frac{(d_f^o-3)d_{f,eff}^i}{2}+h_3-i\right)R_c E_b}{N_o} \right]^n$$

$$\left. \frac{\rho^{\frac{(d_f^o-3)d_{f,eff}^i}{2}+h_3}}{2^{2\left(\frac{(d_f^o-3)d_{f,eff}^i}{2}+h_3\right)-1}} \exp\left[-\frac{\left(\frac{(d_f^o-3)d_{f,eff}^i}{2}+h_3\right)R_c E_b}{N_o+N_I/\rho c} \right] \sum_{n=0}^{\frac{(d_f^o-3)d_{f,eff}^i}{2}+h_3-1} C_{nh} \left[\frac{\left(\frac{(d_f^o-3)d_{f,eff}^i}{2}+h_3\right)R_c E_b}{N_o+N_I/\rho c} \right]^n \right] \right\}$$

……….(6.51)

B. THEORETICAL RESULTS

1. SCCC with Pulsed Noise Jamming and No Side Information

To study the effect of AWGN or SNR in a jamming environment, the theoretical bounds are plotted for three SNR values: 2 dB (low SNR), 10 dB (medium SNR), and 20 dB (high SNR where AWGN can be considered negligible). To analyze the effect of percentage of signal jammed (ρ), values of 0.001, 0.01, 0.1 and 1.0 are used. The theoretical bounds were found to be flat for $\rho = 0.001$ and $\rho = 0.01$ with a bit error ratio (BER) of between 10^{-5} and 10^{-4}, respectively, for low SNRs and low SJRs (< 10 dB) (Figures 6.4, 6.5 and 6.6 with 'NSI' labels). For $\rho = 0.1$ and $\rho = 1.0$, the typical 'waterfall' shape is obtained only for high SNR (Figure 6.5). As SNR is increased, the improvement in BER is best for $\rho = 1.0$ (compare Figures 6.5 and 6.6) for high signal-to-jamming noise ratio (SJR). This is because, although all the bits are jammed, the amount of jamming is small for high SNR and SJR. The SCCC decoder is effective for low power levels of barrage jamming.

For low SJR (2 dB), the theoretical worst case ρ is 1.0. As SJR increases, all the curves (for different ρ) converges to an asymptote of about 3 x 10^{-5} indicating that further increases in SJR will not result in lower BER. For SNR $\geq$ 10 dB, $\rho = 0.1$ becomes the

worst-case, followed by 0.01 and 0.001, respectively, for increasing SJR (Figure 6.5). As SJR increases, the SCCC decoder becomes more effective, especially for $\rho = 1.0$, since the jamming level has decreased. Jamming with smaller ρ is more effective for high SJR since the power is more concentrated and makes it more difficult for the SCCC decoder to correct. Note that all the curves in Figure 6.5 approach an asymptote for large SJR. For large SNR 20 dB, for 0 dB $\leq$ SJR $\leq$ 10 dB the worst-case ρ is 0.1, for 10 dB $\leq$ SJR $\leq$ 20 dB ρ_{wc} is 0.01, and for higher SJR, ρ_{wc} is 0.001 (Figure 6.6). We observe that for SNR = 20 dB where AWGN can be considered negligible, ρ_{wc} is inversely proportional to SJR. These results are similar to those obtained by Lee, French and Miller [Ref. 117] and Houston [Ref. 110] for DPSK with diversity under partial-band noise jamming interference.

2. SCCC with Pulsed Noise Jamming and Side Information

Analogous to the case with NSI, the theoretical results were plotted and found to be flat for $\rho = 0.001$ and 0.01 for SNR of 2 dB (Figure 6.4 with 'SI' labels). As SNR increases, the BER improves, although the bounds remain flat (Figure 6.5). With SI, similar results were also obtained for $\rho = 0.1$ for SNR $\leq$ 10 dB. However, unlike the case with NSI, the improvement in BER is greater as SNR increases. For SNR = 20 dB, these curves ($\rho = 0.001$, 0.01 and 0.1) assumed waterfall shapes for SJR > 15 dB (Figure 6.6). For $\rho = 1.0$, the BER continues to improve as SJR increases. For high SNR, the improvement in BER is best for $\rho = 1.0$ (Figure 6.6), although it is still the worst case for SJR < 10 dB. This is because, although all the bits are jammed, the amount of jamming is small for high SJR and the SCCC decoder is effective for low levels of barrage jamming. However, overall performance is much better for small ρ for SJR < 10 dB. As SJR increases, $\rho = 1.0$ becomes the best case.

In all cases except $\rho = 0.1$ and 1.0, SCCC/DPSK performs better with SI than without (Figures 6.4, 6.5, and 6.6). For low SNR, the difference in BER between SCCC with SI and SCCC without SI is small for $\rho = 0.001$ and 0.01. Their differences get larger as SNR increases. For $\rho = 0.1$ and SNR > 2 dB, it is possible for SCCC without SI to perform better than with SI for large SJR (Figures 6.4 and 6.5) by an order of

magnitude.   From a theoretical standpoint, this is possible because SNR becomes the limiting factor for SCCC with SI. For $\rho = 1.0$, SI is of little value since all the bits are jammed. Thus, both graphs (SI and NSI) are the same.

3.   SCCC with Pulsed Noise Jamming and No Side Information and Rayleigh Fading with No Channel Information

The theoretical results were plotted and found to be flat for $\rho = 0.001$ and $\rho = 0.01$ at bit error ratio (BER) of around 10^{-4} for low SNR (Figure 6.7 with 'fading' labels). For higher SNRs, the BER reduces to about 10^{-5} and 10^{-6} for $\rho = 0.01$ and $\rho = 0.001$, respectively for low SJR (< 10 dB) (Figures 6.8 and 6.9). When ρ is very small, the number of bits affected is small. The SCCC is able to correct most of these erroneous data, independent of SJR. The low BER is due to the interleaver gain. For higher SJRs, the bounds start to regain their "waterfall" shapes. From Figure 6.7, we see that for high SJRs, the bounds converge. This means that there is no noticeable difference in BER for different values of ρ for these SJRs and the BERs have reached an asymptotic limit.

For low SNR, the best case ρ is 0.001 and the worst-case ρ is 1.0 (Figure 6.7). For these SNRs, with all the bits jammed, it is possible that the jamming is too high for the SCCC decoder to correct, resulting in higher BER.   As SJR increases, the SCCC decoder becomes more effective since the jamming has decreased. For SNR = 10 dB, $\rho = 0.1$ becomes the worst case for SJR > 2.5 dB, followed by $\rho = 0.01$ and 0.001 for higher SJRs (Figure 6.8). Note that these graphs asymptotically approach 10^{-6} for very high SJRs. As SNR is increased to 20 dB, the crossover point for worst-case ρ occurs earlier, i.e., at SJR 1.5 dB for $\rho = 0.1$, 10 dB for $\rho = 0.01$ and 20 dB for $\rho = 0.001$ (Figure 6.9). Jamming for small ρ becomes more effective for high SJR since the power is more concentrated and makes it more difficult for the SCCC decoder to correct.

Comparing the BER for SCCC/DPSK with jamming with and without fading, the BER is worse off with fading for all SNRs (Figures 6.7, 6.8, and 6.9), with the fading graphs being more linear in shapes. For higher SNRs and $\rho = 0.001$ and 0.01, the bounds for both are close to each other indicating that fading does not affect their performance

much. In some cases, it appears that the performances for the fading case are better for very low ρ. This is due to the accuracy limitations of numerical methods.

4. SCCC with Partial-band Jamming and No Side Information and with Slow Frequency-hopped Spread Spectrum

With a processing gain of 64 for the FH and the assumption that a jammer occupies an integral number of hops, ρ cannot be less than 1/64. Thus, only the theoretical results for ρ = 0.1 and 1.0 are plotted. Moreover, with FH, high SNRs are usually not required; therefore, only SNRs of 2 and 10 dB are examined. Lower SJRs are used instead to examine the effects of the FH. With frequency-hopped spread spectrum, the disparity in BER for different ρ is negligible for low SNR (Figure 6.10). For higher SNR of 10 dB, ρ = 0.1 is the worst case (Figure 6.11). This is because for high ρ, due to the processing gain of the FH, the jamming is reduced to a level low enough for the SCCC decoder to correct the errors. For low ρ, the level of jamming is not low enough for the SCCC decoder to be as effective, resulting in more errors. Note that the two bounds approach 10^{-9} asymptotically for high SJRs.

As expected, SCCC with FH and achieved better results than SCCC with no FH in all cases (Figures 6.10 and 6.11). The use of frequency-hopped spread spectrum reduces the jamming noise level, thus achieving better results. For ρ = 0.1, the improvement due to FH increases as SJR increases while the reverse is true for ρ = 1.0. For low SJR, i.e., high jamming, FH reduces the noise to a low level resulting in better performance as SJR decreases. On the other hand, the jammer is more effective for ρ = 0.1 for higher SJRs. However, the jammer's effectiveness is reduced when FH is employed. Consequently, the BER improves for higher SJRs. Note that for low SJRs and ρ = 0.1, it appears that performance with FH is worse than without. This is probably due to numerical errors.

5. SCCC with Partial-band Jamming and Side Information and with Slow Frequency-hopped Spread Spectrum

For low SNR, the differences in BER between different values of ρ are small since FH reduces the jamming powers to similar levels (Figure 6.12 with 'SI' labels).

For higher SNR and $\rho = 1.0$, FH is able to reduce the jamming noise level enough for decoding to be more effective. Thus, $\rho = 0.1$ is the worst case for higher SJRs (Figure 6.13). Note that the performance for $\rho = 0.1$ is almost independent of SJR for the range of SJRs considered.

Within numerical error, for low SNR, the performance of FH SCCC/DPSK with SI is similar to that without SI (Figures 6.12). Since the SNR is small and the jamming noise is very low, SI is not vital. For higher SNRs, SI becomes more important since the relative noise contribution by the jammer is higher. For SNR = 10 dB, low SJR (< 2 dB) and $\rho = 0.1$, FH SCCC performs better with SI. For $\rho = 0.1$ and SNR 10 dB, it is possible for SCCC without SI to perform better than with SI for large SJR (Figure 6.13). From a theoretical standpoint, this is possible because SNR becomes the limiting factor for SCCC with SI. For barrage jamming, SI is of no value, thus both bounds (SI and NSI) are the same. Note that SI is more effective for small values of ρ and higher SNRs.

As expected, SCCC with SI and FH achieved better results than SCCC with SI and no FH in all cases (Figures 6.14 and 6.15). FH is able to reduce the jamming noise level, thus achieving better BER. The gain in performance is largest for $\rho = 1.0$. For $\rho = 0.1$, the gain due to FH is small.

C.   SUMMARY OF RESULTS

From the theoretical results, the following conclusions can be made:

1.   SCCC with frequency-hopped spread spectrum and with side information is the most effective in reducing the effects of jamming.

2.   Side information works best for high values of ρ when SNR is low and low values of ρ when SNR is high.

3.   When fading is present, barrage jamming is the most effective for lower SNRs and SJRs while smaller values of ρ are more effective at high SNRs and SJRs.

4.   Frequency-hopped spread spectrum works best for high values of ρ, i.e., barrage jamming and low overall SNR.
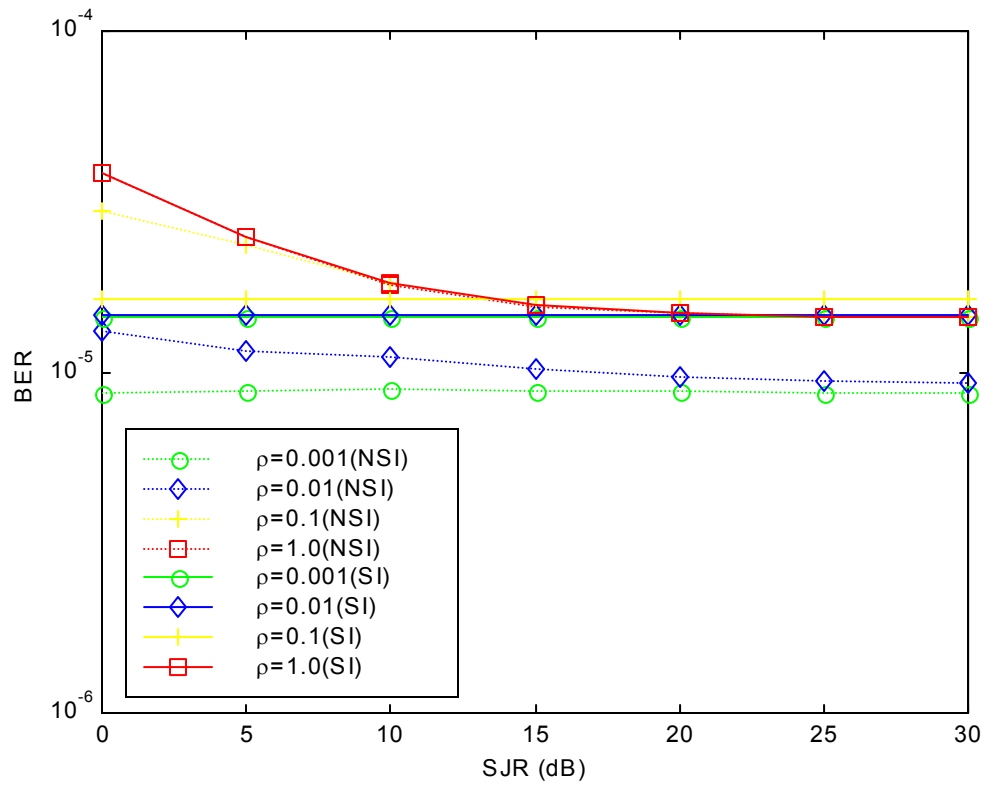
Figure 6.4.   Theoretical SCCC/DPSK with AWGN and pulsed noise jamming: effect of side information on BER for ρ = 0.001, 0.01, 0.1 and 1.0, SNR = 2 dB and SJR = 0 to 30 dB.
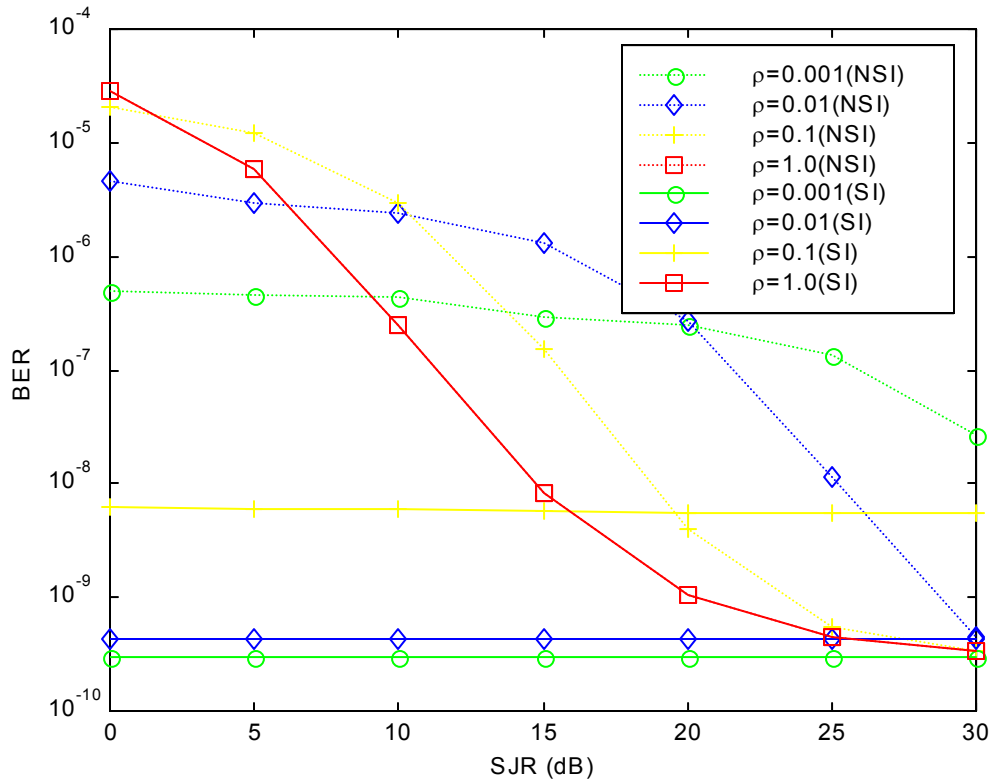
Figure 6.5.   Theoretical SCCC/DPSK with AWGN and pulsed noise jamming: effect of side information on BER for ρ = 0.001, 0.01, 0.1 and 1.0, SNR = 10 dB and SJR = 0 to 30 dB.
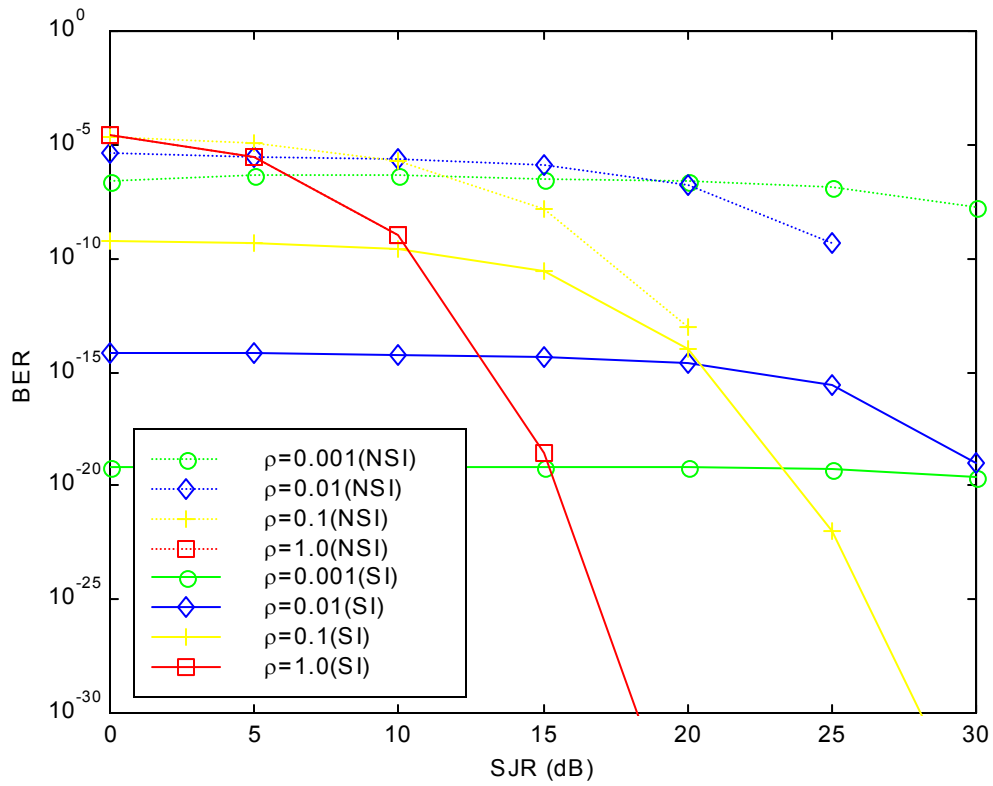
Figure 6.6.   Theoretical SCCC/DPSK with AWGN and pulsed noise jamming: effect of side information on BER for ρ = 0.001, 0.01, 0.1 and 1.0, SNR = 20 dB and SJR = 0 to 30 dB.
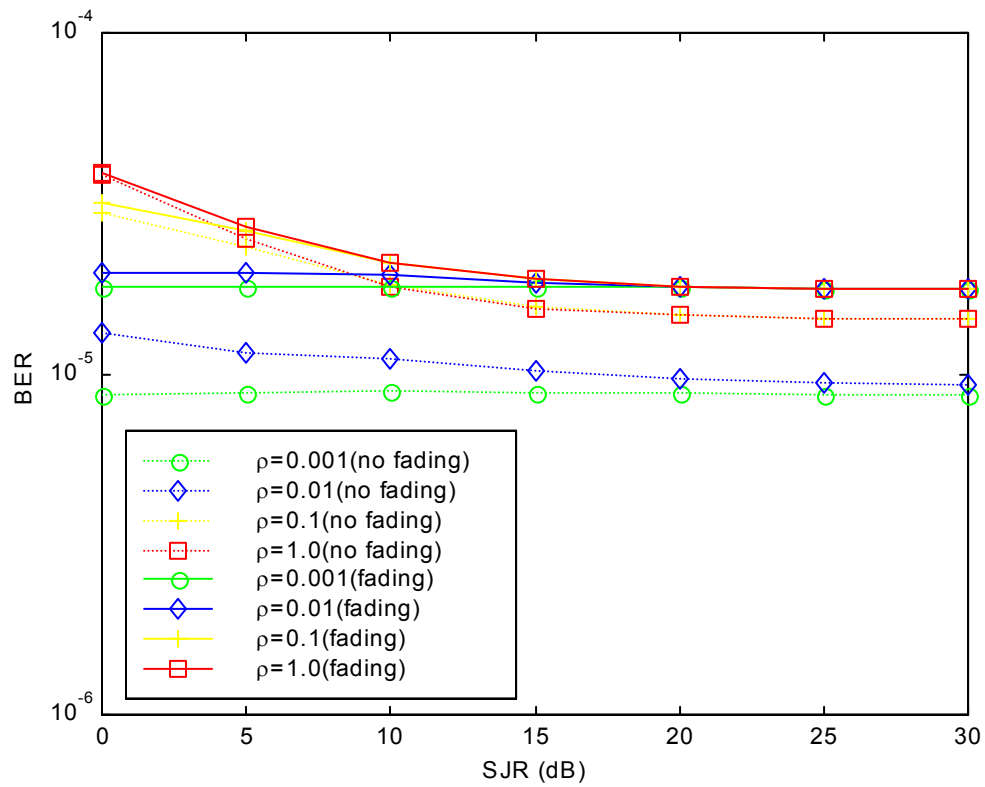
Figure 6.7. Theoretical SCCC/DPSK with AWGN and pulsed noise jamming with no side information: effect of Rayleigh fading with no channel information on BER for ρ = 0.001, 0.01, 0.1 and 1.0, SNR = 2 dB and SJR = 0 to 30 dB.
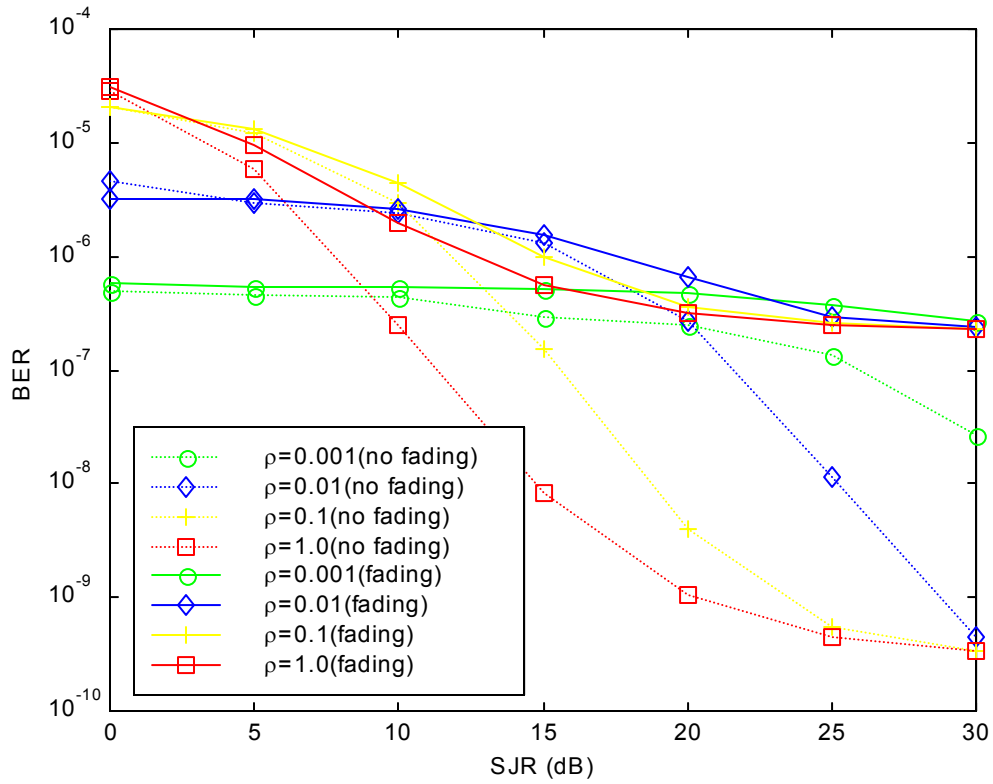
Figure 6.8. Theoretical SCCC/DPSK with AWGN and pulsed noise jamming with no side information: effect of Rayleigh fading with no channel information on BER for ρ = 0.001, 0.01, 0.1 and 1.0, SNR = 10 dB and SJR = 0 to 30 dB.
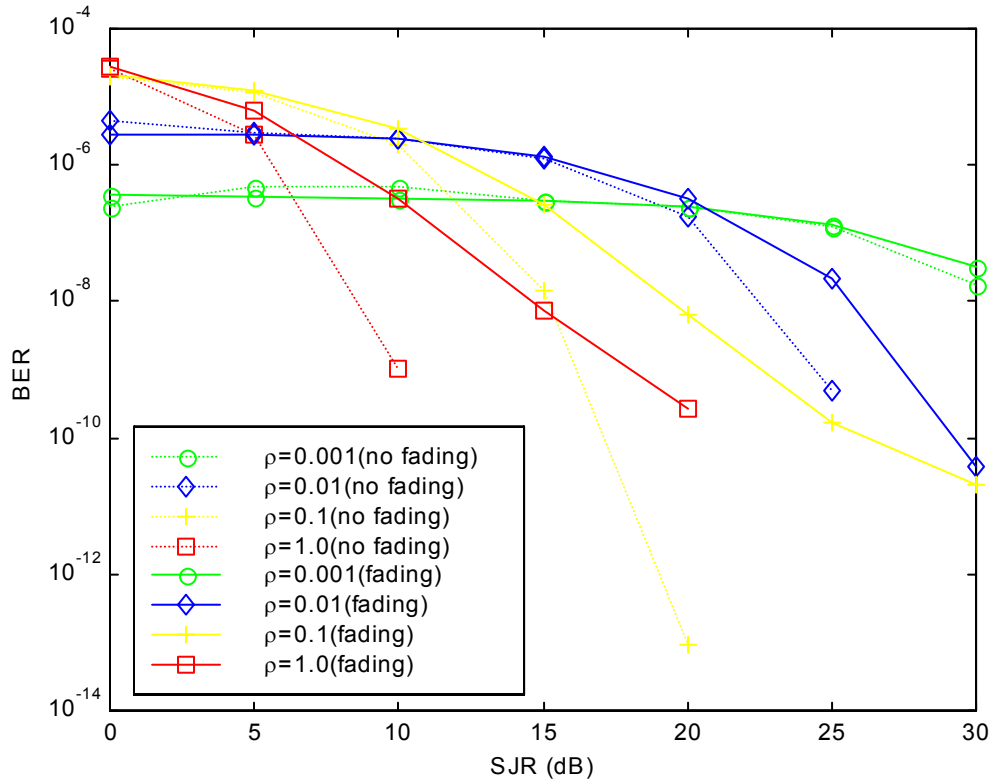
Figure 6.9.   Theoretical SCCC/DPSK with AWGN and pulsed noise jamming with no side information: effect of Rayleigh fading with no channel information on BER for ρ = 0.001, 0.01, 0.1 and 1.0, SNR = 20 dB and SJR = 0 to 30 dB.
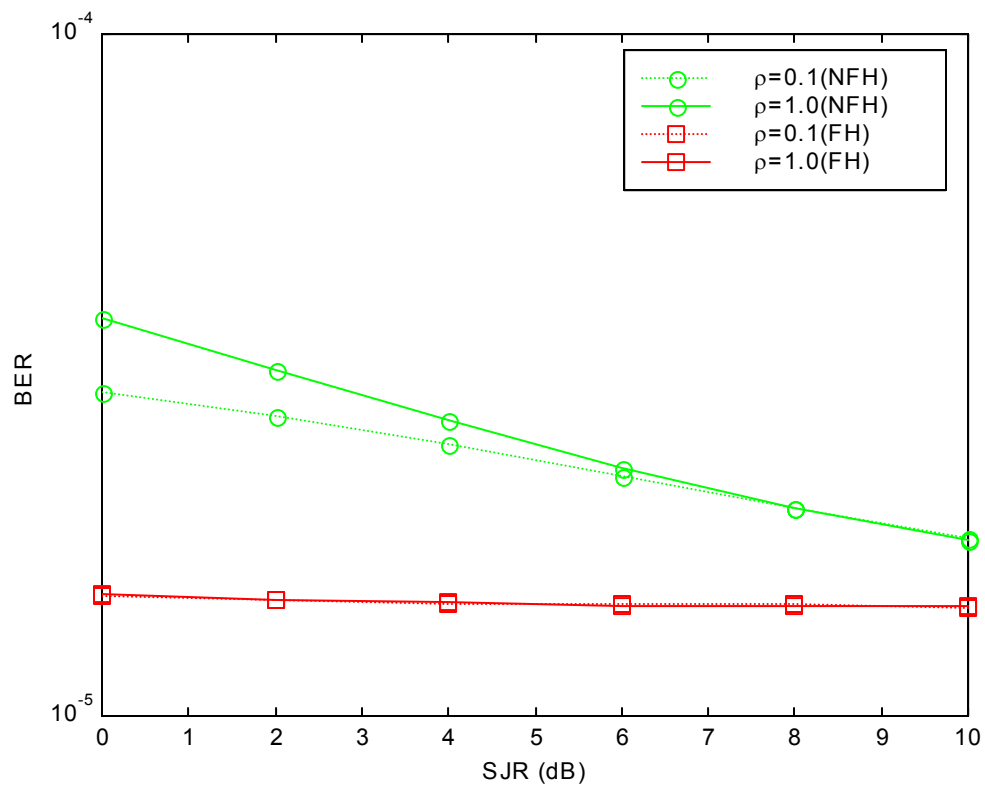
Figure 6.10.   Theoretical SCCC/DPSK with AWGN and noise jamming with no side information: effect of frequency-hopped spread spectrum on BER for ρ = 0.1 and 1.0, SNR = 2 dB and SJR = -10 to 10 dB.
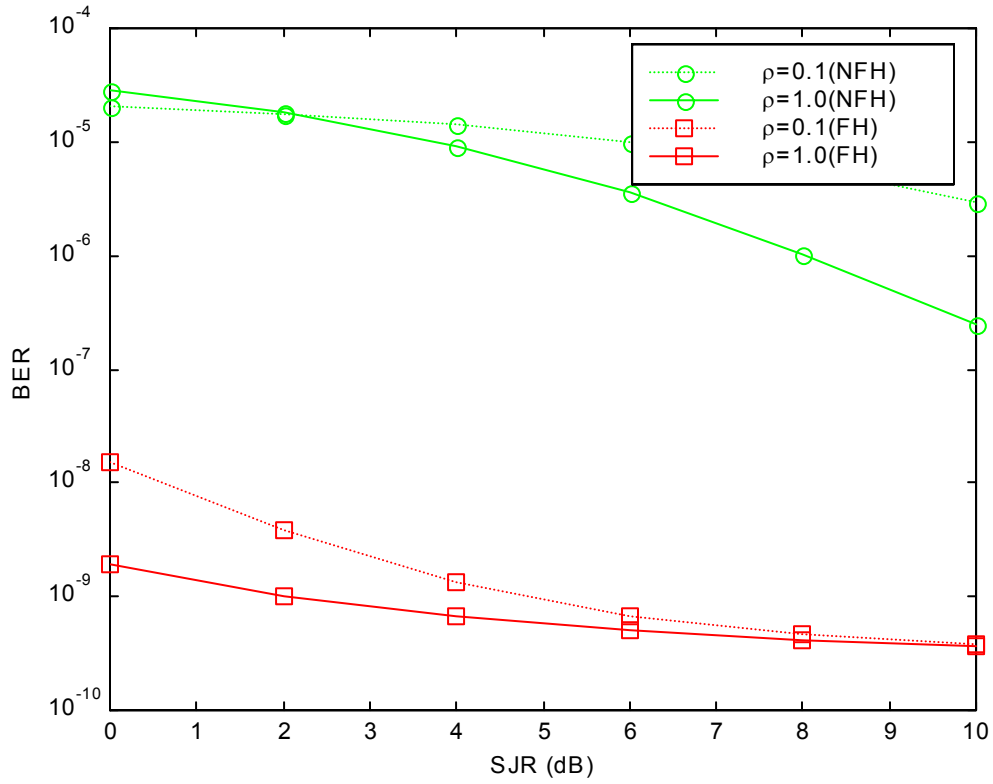
Figure 6.11. Theoretical SCCC/DPSK with AWGN and noise jamming with no side information: effect of frequency-hopped spread spectrum on BER for ρ = 0.1 and 1.0, SNR = 10 dB and SJR = -10 to 10 dB.
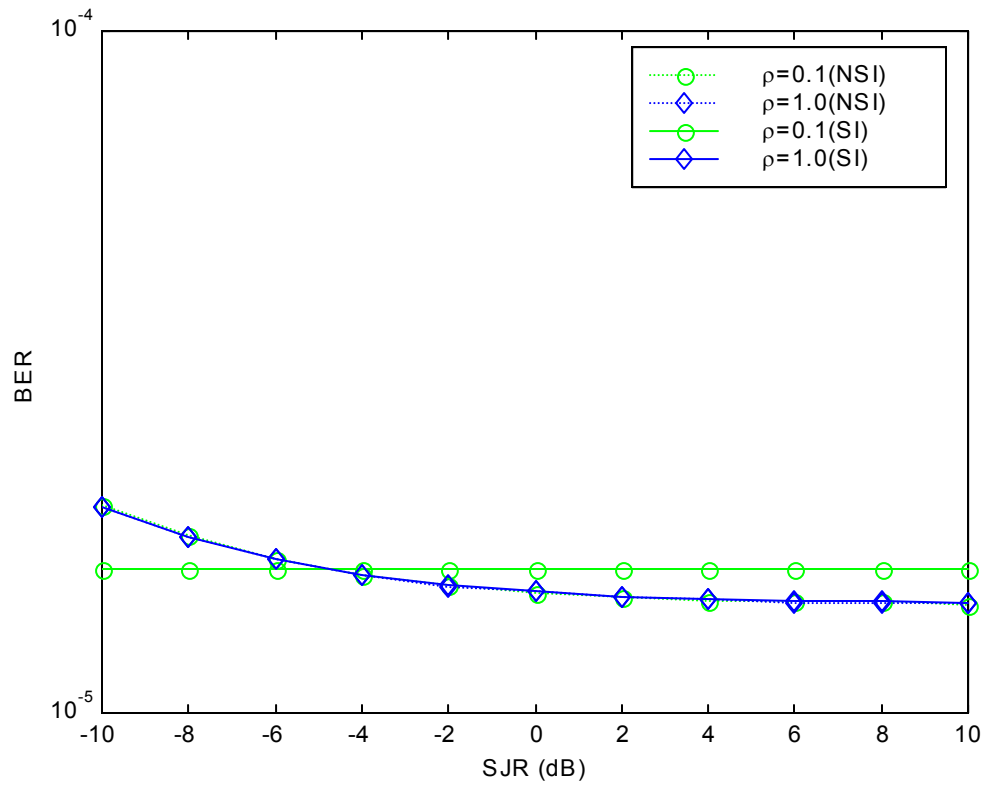
Figure 6.12.   Theoretical SCCC/DPSK with AWGN and partial-band noise jamming and frequency-hopped spread spectrum: effect of side information on BER for $\rho = 0.1$ and 1.0, SNR = 2 dB and SJR = -10 to 10 dB.
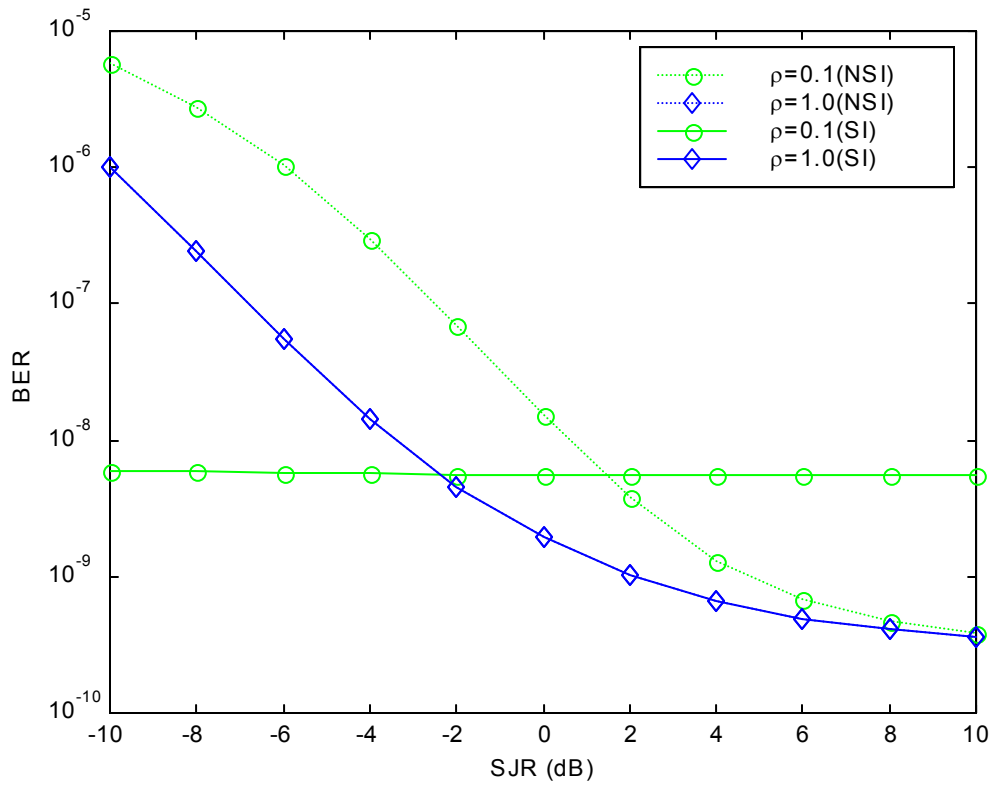
Figure 6.13. Theoretical SCCC/DPSK with AWGN and partial-band noise jamming and frequency-hopped spread spectrum: effect of side information on BER for $\rho = 0.1$ and 1.0, SNR = 10 dB and SJR = -10 to 10 dB.
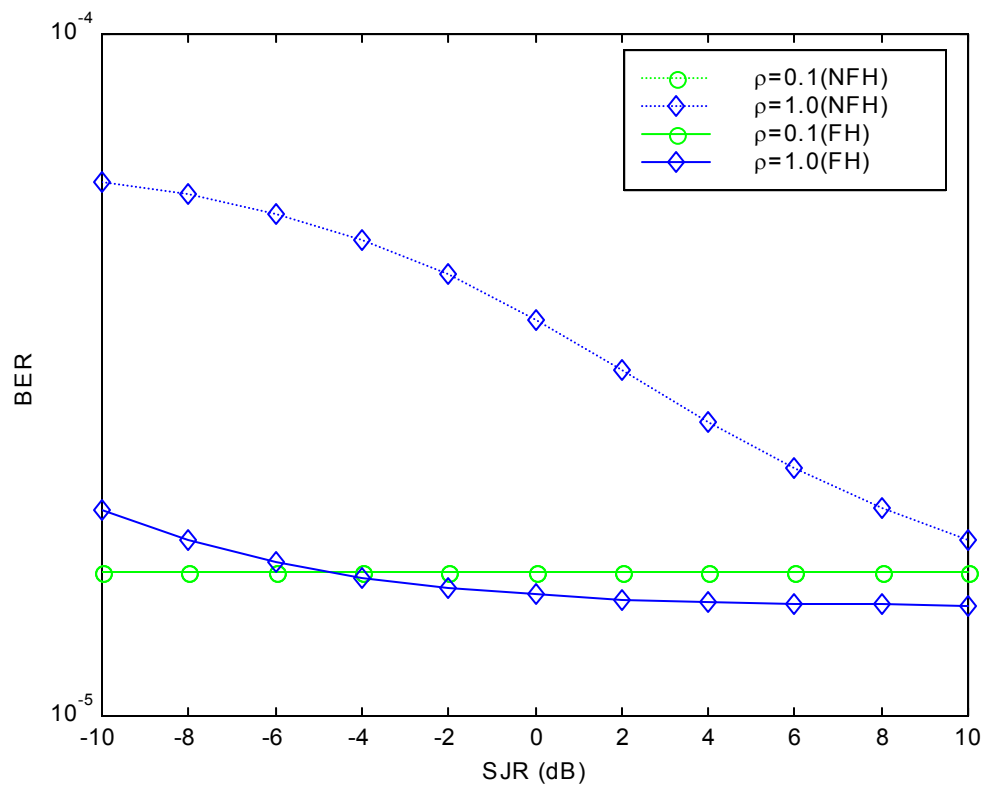
Figure 6.14.   Theoretical SCCC/DPSK with AWGN and noise jamming with side information: effect of frequency-hopped spread spectrum on BER for ρ = 0.1 and 1.0, SNR = 2 dB and SJR = -10 to 10 dB.
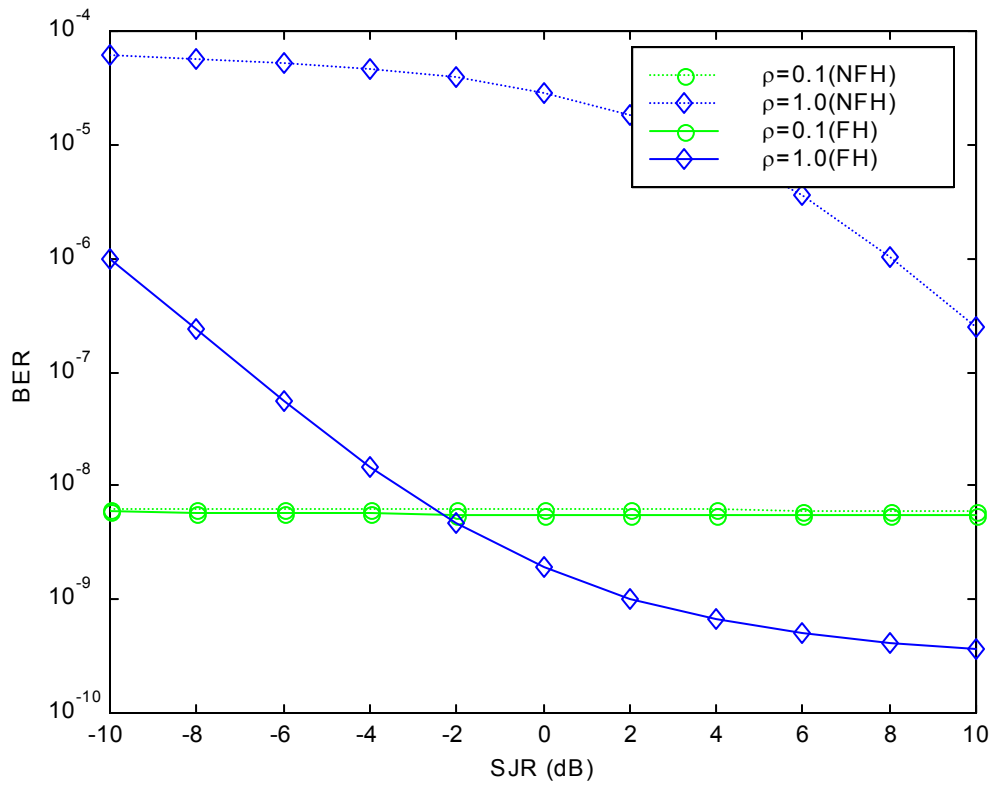
Figure 6.15. Theoretical SCCC/DPSK with AWGN and noise jamming with side information: effect of frequency-hopped spread spectrum on BER for $\rho = 0.1$ and 1.0, SNR = 10 dB and SJR = -10 to 10 dB.

VII. SIMULATION RESULTS OF SCCC WITH DPSK IN PULSED/PARTIAL-BAND NOISE JAMMING, RAYLEIGH FADING AND FREQUENCY-HOPPED SPREAD SPECTRUM

A. SIMULATION PARAMETERS

In this chapter, pulsed, partial-band noise jamming (with and without side information) was simulated for various conditions: AWGN, Rayleigh fading (without channel information), and frequency-hopped spread spectrum with a processing gain of 64. The pulsed/partial-band noise interference is assumed to be unaffected by the fading channel.

The Monte Carlo simulations were carried out with the following parameter values: a) ten iterations, b) signal-to-noise power ratio (SNR) from 0 to 20 dB in increments of 2 dB (in some cases increments of 0.2 dB), c) signal-to-jammer power ratio (SJR) from -10 to 10 dB in increments of 2 dB, d) percentage of signal jammed (ρ) of 0.1%, 1%, 10%, and 100%. In addition, based on the BER, the worst case ρ (ρ_{wc}) for each SJR was also determined,

The following types of graphs were plotted: a) BER vs. SJR for each value of SNR and with ρ as a parameter, b) BER vs. SJR for each value of SNR and for $\rho = 0.1$ to 1.0, and c) theoretical results of BER vs. SNR.

The following comparisons will be made: a) SCCC/DPSK with jamming and both with and without side information, b) SCCC/DPSK with jamming and both with and without Rayleigh fading, b) SCCC/DPSK with jamming and both with and without frequency-hopped spread spectrum. Theoretical results will also be compared with the simulation results.

B.   SCCC   WITH   PULSED   NOISE   JAMMING   AND   NO   SIDE INFORMATION

For the simulations in this section, the decoder has no side information (NSI), i.e., no information on which bits are jammed or knowledge of the SNR transmitted.

1.   Observations

The general performance of the SCCC with NSI is shown in Figure 7.1 for values of SJR from zero to ten dB and for SNR from zero to twenty dB. In the figure, in order to show the graphs for the different values of ρ, the SJR is offset by ρ in dB. Thus, for ρ = 0.001, 0.01, 0.1, 1.0, there are offsets of −30, -20, -10, 0 dB, respectively. In general, for a given SJR, BER improves as SNR increases. For zero SNR and up to 6 dB, BER is almost independent of SJR. As SNR increases, the effect of ρ is more pronounced. It is obvious that BER worsens as ρ increases. It will be shown later that the value of ρ_{wc} is dependent on SJR.

For ρ = 0.001, the effect of SJR is, over the range of SJR considered, negligible regardless of SNR (Figure 7.1). Since ρ is very small, the number of bits affected is small. The SCCC is able to correct most of the erroneous data bits. For SNR above 6.4 dB, all errors are corrected. This is about half a dB above the SNR where all erroneous data bits are correctly decoded for SCCC/DPSK with AWGN only. In other words, this level of pulsed noise jamming only degrades overall performance by about 0.5 dB. For ρ = 0.01, the BER decreases as SNR increases. For SNR > 6.8 dB, all errors are corrected. The effect for SJR < 0 dB on BER is also minimal. In this case, pulsed noise jamming degrades the overall performance by about 0.8 dB when compared with SCCC/DPSK with AWGN only. For ρ = 0.1, the BER is almost independent of SNR for SJR < 0 dB. For SNR > 20 dB and SJR > 2 dB, all errors are corrected. The improvement in BER is marginal for SNR > 16 dB. The worst case ρ is 1.0 for the range of SJR considered. For SNR $\leq$ 6 dB, the effect of SJR on BER is minimal. As SNR increases, the BER graphs take the usual 'waterfall' shapes for increasing SJR.

For SNR = 10 dB, ρ_{wc} = 1.0 for low SJR (< 6 dB), ρ_{wc} = 0.5 for 6 < SJR < 8 dB, and ρ_{wc} = 0.3 for 10 dB >SJR > 8 dB (Figure 7.2). It can be extrapolated that ρ_{wc}

decreases as SJR becomes larger. For higher SNR (20 dB), ρ_{wc} is between 0.4 and 0.5 for SJR > 4 dB (Figure 7.3).

For sufficiently high SNR ($\geq$ 12 dB) and ρ = 1.0, all errors are corrected except for SJR < 6 dB (Figure 7.1). Increasing SNR more than 16 dB for ρ = 1.0 has little effect on the BER.

2.   Comparison with Theoretical Values

For extremely low BERs, bounds are often calculated as it is often impractical to generate simulation results. From Figure 7.4, for SNR = 10 dB and SJR > 8 dB, ρ_{wc} is 0.1. The theoretical results appear to be an extension of the simulation results. Note that for these cases, AWGN is not ignored.

More often than not, the amount of jamming noise is much greater than AWGN so that AWGN can be ignored. In Figure 7.5, the simulation results and theoretical bounds for ρ = 0.1 and 1.0 and SNR = 20 dB are shown. We see that the simulation and theoretical results are compatible. The simulation results also show that for ρ = 1.0 and SJR > 6 dB, all errors were corrected. This is the same result obtained for SCCC/DPSK with no jamming and SNR > 6 dB.

C.   SCCC WITH PULSED NOISE JAMMING AND SIDE INFORMATION

In these simulations, the decoder is assumed to have knowledge of the jammed bits and their overall signal-to-total noise ratios (SI). The SI is used in the decoding algorithm.

1.   Observations

The general performance of the SCCC with SI is shown in Figure 7.6 for values of SJR greater than zero and for SNR from 0 to 20 dB in increments of 2 dB. In the figure, in order to show the graphs for the different values of ρ, the SJR is offset by ρ in dB. Thus, for ρ = 0.001, 0.01, 0.1, 1.0, there will be offsets of –30, -20, -10, 0 dB, respectively. In general, the BER improves as SNR increases. For SNR = 6 dB, the BER is almost independent of SJR and ρ. As SNR increases, the effect of ρ becomes more

pronounced. In general, $\rho_{wc} = 1.0$. It will be shown later that the value of ρ_{wc} is also dependent on SJR.

For $\rho = 0.001$, the effect of SJR on BER is negligible (Figure 7.6). Since ρ is very small, the number of bits that are affected is small and the SCCC is able to correct most of the erroneous data. For SNR above 6.4 dB, all errors with $\rho = 0.001$ are corrected. This is about half a dB above the SNR where all data bits are correctly decoded with only AWGN. This is also the same result obtained in the NSI case. Thus, SI does not improve the BER when ρ is very small. For $\rho = 0.01$, the BER performance improves as SNR increases. For SNR > 6.8 dB, all errors are corrected. The effect of SJR on BER is also minimal. In this case, pulsed noise jamming degrades the overall performance by about 0.8 dB compared with SCCC with AWGN only. This is similar to the case without SI. Thus, SI does not improve the BER when ρ is small. For $\rho = 0.1$, BER is almost independent of SJR for SJR < 0 dB. For SNR $\geq$ 20 dB and SJR $\geq$ 4 dB, all errors are corrected. The worst case ρ is 1.0 for the range of SJR considered (Figure 7.6). For low SNR (< 4 dB), the effect of SJR on BER is marginal. As SNR increases, the BER graphs take the usual 'waterfall' shapes for increasing SJR. The improvement in BER is marginal for SNR > 16 dB.

For SNR = 10 dB, $\rho_{wc} = 1.0$ for low SJR (< 6 dB), $\rho_{wc} = 0.5$ for 6 < SJR < 8 dB and $\rho_{wc} = 0.3$ for 10 dB > SJR > 8 dB (Figure 7.7). Clearly, ρ_{wc} gets smaller as SJR gets larger. For higher SNR (20 dB), ρ_{wc} is between 0.3 and 0.4 for SJR > 6 dB (Figure 7.8).

For sufficiently high SNR ($\geq$ 12 dB) and $\rho = 1.0$, all errors are corrected except for SJR < 6 dB (Figure 7.6). If SNR is large enough, the BER approaches asymptotically to that obtained with no jamming as expected.   Increasing SNR more than 16 dB for $\rho = 1.0$ has little effect on the BER.

2.   Comparison with Theoretical Values

From Figure 7.9, for SNR 10 dB and 10 dB > SJR > 8 dB, ρ_{wc} is 0.1 based on simulation results. The theoretical results show that ρ_{wc} is 1.0 from 10 < SJR < 16 dB and 0.1 for SJR > 16 dB. From the shapes of the curves, the theoretical bounds appear to be an extension of the simulation results.

In Figure 7.10, the simulation results and theoretical bounds for $\rho = 0.1$ and 1.0 and SNR = 20 dB are shown. We observe that ρ_{wc} is 1.0 for low SJR and ρ_{wc} is 0.1 for higher SJRs. For low SJRs at SNR = 20 dB, Kang and Stark [Ref. 96] also obtained ρ_{wc} = 1.0 for Turbo codes.

3. Comparison with SCCC with Pulsed Noise Jamming and No Side Information

Unlike SCCC/BPSK, the performance of the SCCC with SI is only slightly better than with NSI for SNR 10 dB (Figure 7.11). For higher SNR, the difference is negligible (Figure 7.12). Since DPSK demodulation is dependent on previous consecutive bits, side information may not be very useful.

D. SCCC WITH PULSED NOISE JAMMING AND NO SIDE INFORMATION AND RAYLEIGH FADING WITH NO CHANNEL INFORMATION

In this section, both jamming and Rayleigh fading are simulated. The decoder has no side information (NSI) on the jammed bits and no knowledge of fade amplitudes or channel information (NCI).

1. Observations

The general performance of SCCC with jamming and NSI and Rayleigh fading with NCI is shown in Figure 7.13 for values of SJR from zero to ten dB and for SNR from zero to twenty dB. In the figure, in order to show the graphs for the different values of ρ, the SJR is offset by ρ in dB. Thus, for $\rho = 0.001, 0.01, 0.1, 1.0$, there are offsets of $-30, -20, -10, 0$ dB, respectively. In general, for a given SJR, BER improves as SNR increases. For SNR of ≤ 6 dB, BER is almost independent of SJR. As SNR increases, the effect of ρ becomes more pronounced. It is obvious that BER worsens as ρ increases. It will be shown later that the value of ρ_{wc} is dependent on SJR.

From Figure 7.13, we observe that for $\rho = 0.001$, the effect of SJR is, over the range of SJR considered, negligible; i.e., it does not matter what the value of SJR is. Since ρ is very small, the number of bits affected is small. The SCCC is able to correct

most of the erroneous data bits. For SNR above 8.0 dB, all errors are corrected. This is the same SNR where all erroneous data bits are correctly decoded for Rayleigh fading and 1.5 dB above the case with jamming and no side information. In other words, fading degrades overall performance by about 1.5 dB in a jamming environment. Jamming with $\rho = 0.001$ appears not to degrade overall performance on a fading channel. For $\rho = 0.01$, the BER decreases as SNR increases. For SNR of greater than 8.4 dB, all errors are corrected (Figure 7.13). In this case, fading degrades performance by about 0.5 dB in a jamming environment. Jamming, on the other hand, degrades performance by 1.5 dB on a fading channel.   For $\rho = 0.1$ and 1.0, when SNR is $\geq$ 20 dB and SJR $\geq$ 8 dB, all errors are corrected. Note that for $\rho = 1.0$, the improvement in BER decreases for higher SNR. The worst case ρ varies between 0.2 and 0.5 (Figures 7.14 and 7.15) for different values of SNR.   For lower SJRs (< 8 dB), the worst BERs were obtained for larger values of ρ, but for higher SJRs, the smaller values of ρ yield the worst BERs.

2. Comparison with Theoretical Values

The simulation and theoretical results for SNRs of 10 dB and 20 dB, respectively, are shown in Figures 7.16 and 7.17. For low SJRs, the simulation results show that the worst case ρ is 1.0 while for higher SJRs, the theoretical results show $\rho_{wc} = 0.1$.   We observe, through the shapes of the graphs of the simulation, that the simulation results can generally be extended by the theoretical results, especially for high SNRs.

3. Comparison with SCCC with Pulsed Noise Jamming and No Side Information and with No Rayleigh Fading

With Rayleigh fading, the BERs have similar forms as without fading except that for a given SNR and SJR, BER is larger.

For SNR = 10 dB, all errors are corrected for $\rho = 0.001$ and 0.01 (Figure 7.18). The coding gain difference between the non-fading case and the fading case is 3 to 10 dB for $\rho = 0.1$ and less than 3 dB for $\rho = 1.0$. Note that for high SJR, $\rho_{wc} = 0.1$. This means that the decoder is having more difficulty in correcting the jammed bits due to the higher power in each jammed bit. For low SJR and $\rho = 1.0$, the performance difference is small. However, for larger SJRs or $\rho = 0.1$, the difference in performance widens. As the SNR

is increased further to 20 dB, the coding gain narrows to less than 4 dB for $\rho = 0.1$ and less than 2 dB for $\rho = 1.0$ (Figure 7.19).

E.   SCCC WITH PARTIAL-BAND NOISE JAMMING AND NO SIDE INFORMATION AND WITH SLOW FREQUENCY-HOPPED SPREAD SPECTRUM

In these simulations, the decoder has no side information (NSI) about the jammed bits, but the jamming noise power is reduced by frequency-hopped spread spectrum (FH) with a processing gain (PG) of 64.

1.   Observations

The general performance of the SCCC with NSI and with FH is shown in Figure 7.20 for values of SJR from zero to ten dB and for SNR from zero to twenty dB. In the figure, in order to show the graphs for the different values of ρ, the SJR is offset by ρ in dB. Thus, for $\rho = 0.001, 0.01, 0.1, 1.0$, there are offsets of $-30, -20, -10, 0$ dB, respectively. The effect of FH is tremendous, especially for larger ρ. As shown in Figure 7.20, for SNR < 8 dB, all the data bits are decoded correctly. We will therefore concentrate our simulations for SNR < 8 dB.

For $\rho = 0.001$, the effect of SJR is, over the range of SJR considered, negligible regardless of SNR; i.e., it does not matter what SJR is (Figure 7.20). Since ρ is very small, the number of bits affected is small. The SCCC is able to correct most of the erroneous data bits. For SNR above 6.4 dB, all errors are corrected. This is about half a dB above the SNR where all erroneous data bits are correctly decoded for AWGN only. In other words, this level of partial-band noise jamming only degrades overall performance by about 0.5 dB. This is the same result obtained earlier for SCCC with FH and no side information and for SCCC with no FH. Since the number of bits jammed is small, the reduced jamming power due to FH does not make much difference. For $\rho = 0.01$, BER decreases as SNR increases. For SNR of greater than 7.2 dB, all errors are corrected. In this case, partial-band noise jamming degrades the overall performance by about 1.2 dB when compared with AWGN. For $\rho = 0.1$, when SNR is ≥ 8 dB and SJR $\geq$

-4 dB, all the errors are corrected. For $\rho = 1.0$, when SNR is ≥ 8 dB and SJR ≥ -8 dB, all the errors are corrected. The worst case ρ varies between 0.1 and 0.5 (Figures 7.21 and 7.22) for different values of SNR.

2.   Comparison with Theoretical Values

The simulation and theoretical results for SNR = 7 dB are shown in Figure 7.23. Based on the shapes of the graphs, we note that they appear to converge to a BER of 10^{-6} for high SJR.

3.   Comparison with SCCC with Pulsed Noise Jamming and No Side Information and with No Frequency-hopped Spread Spectrum

SCCC with FH performs better especially for low SJRs, i.e., for high jamming noise power, since FH is able to reduce the noise. For SNR > 7 dB, SCCC with FH is able to correct all errors even for high jamming power (SJR > –4 dB). For $\rho = 1.0$, SCCC with FH has a coding gain of 18 dB at 10^{-2} over SCCC without FH (Figure 7.24).

F.   SCCC WITH PARTIAL-BAND NOISE JAMMING AND SIDE INFORMATION AND WITH SLOW FREQUENCY-HOPPED SPREAD SPECTRUM

In these simulations, the decoder has SI and FH incorporated in the SCCC.

1.   Observations

The general performance of SCCC with SI and FH is shown in Figure 7.25 for values of SJR from zero to ten dB and for SNR from zero to twenty dB. In the figure, in order to show the graphs for the different values of ρ, the SJR is offset by ρ in dB. Thus, for $\rho = 0.001, 0.01, 0.1, 1.0$, there are offsets of $-30, -20, -10, 0$ dB, respectively. The effect of FH is tremendous. As shown in Figure 7.25, for SNR < 8 dB, all data bits are decoded correctly. We will therefore concentrate our simulations for SNR < 8 dB. For $\rho = 0.001$, the effect of SJR is, over the range of SJR considered, negligible, i.e., it does not matter what the value of SJR is (Figure 7.25). Since ρ is very small, the number of bits affected is small. The SCCC is able to correct most of the erroneous data bits. For SNR above 6.4 dB, all errors are corrected. This is about half a dB above the SNR where

all erroneous data bits are correctly decoded for AWGN only. In other words, this level of partial-band noise jamming only degrades overall performance by about 0.5 dB. This is the same result obtained earlier for SCCC with FH and no side information. Since the number of bits jammed is small, SI does not make much difference to the SCCC. For $\rho =$ 0.01, BER decreases as SNR increases. For SNR greater than 7.2 dB, all errors are corrected. In this case, partial-band noise jamming degrades the overall performance by about 1.2 dB when compared with AWGN.   For $\rho = 0.1$, when SNR is $\geq$ 8 dB and SJR $\geq$ -4 dB, all the errors are corrected. For $\rho = 1.0$, when SNR is $\geq$ 8 dB and SJR $\geq$ -8 dB, all the errors are corrected. The worst case ρ varies between 0.1 and 0.5 (Figures 7.26 and 7.27) for different values of SNR.

2. Comparison with Theoretical Values

For SNR = 7 dB, the theoretical values can serve as an extension to the simulation results (Figure 7.28). Both theoretical and simulation results show $\rho = 0.1$ to be the worst case for SJR > -5 dB. For SNR = 8 dB, both theoretical and simulation results show $\rho =$ 0.1 to be the worst case for SJR > -8 dB (Figure 7.29).

3. Comparison with SCCC with Partial-band Noise Jamming and No Side Information and with Frequency-hopped Spread Spectrum

Performance of SCCC with SI is better than without SI in all cases. The gain is about 0.5 dB for both $\rho = 0.1$ and 1.0 for SNR = 7 dB (Figure 7.30).

4. Comparison with SCCC with Pulsed Noise Jamming and Side Information and with No Frequency-hopped Spread Spectrum

The performance of the SCCC with SI and FH is definitely better than the SCCC with SI and no FH. The improvement in BER performance is significant. The coding gain at 10^{-3} for SNR = 8 dB is about 18 dB for $\rho = 0.1$ and 1.0 (Figure 7.31).

G. CONCLUSIONS

The simulation results show that SCCC/DPSK is not as effective in a jamming environment as SCCC/BPSK. SCCC/DPSK requires at least a SNR of 6 dB to avoid the region of high BER. For SCCC/DPSK without FH, SI is not very useful; with FH, a 0.5

dB gain was observed with SI. Rayleigh fading is most detrimental to SCCC/DPSK with jamming for $0.1 < \rho < 1.0$. FH improves the performance of SCCC/DPSK remarkably.

Figure 7.1.　　Simulated SCCC/DPSK with AWGN and pulsed noise jamming with no side information: effect of SJR on BER for ρ = 0.001, 0.01, 0.1 and 1.0, SNR = 0 to 20 dB and SJR = 0 to 10 dB. Note that in order to show the graphs for the different values of ρ, the SJR is offset by ρ in dB. Thus, for ρ = 0.001, 0.01, 0.1 and 1.0, there are offsets of –30, -20, -10, 0 dB, respectively. The graphs start at 0 dB at the top with increments of 2 dB for each subsequent graph downwards. Note that when there is no graph for a particular SNR, it means that all errors were corrected for that SNR for the range of SJR considered.

Figure 7.2. Simulated SCCC/DPSK with AWGN and pulsed noise jamming with no side information: effect of ρ on BER for ρ = 0.1 to 1.0, SNR = 10 dB and SJR = 0 to 10 dB.
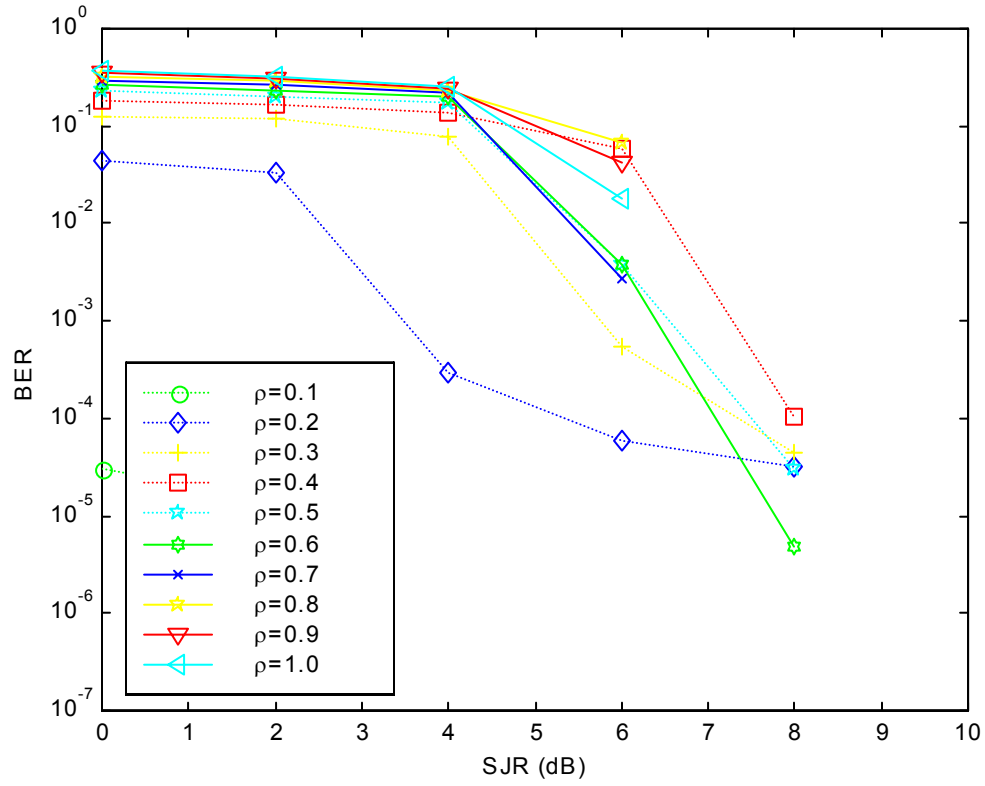
Figure 7.3.   Simulated SCCC/DPSK with AWGN and pulsed noise jamming with no side information: effect of ρ on BER for ρ = 0.1 to 1.0, SNR = 20 dB and SJR = 0 to 10 dB.
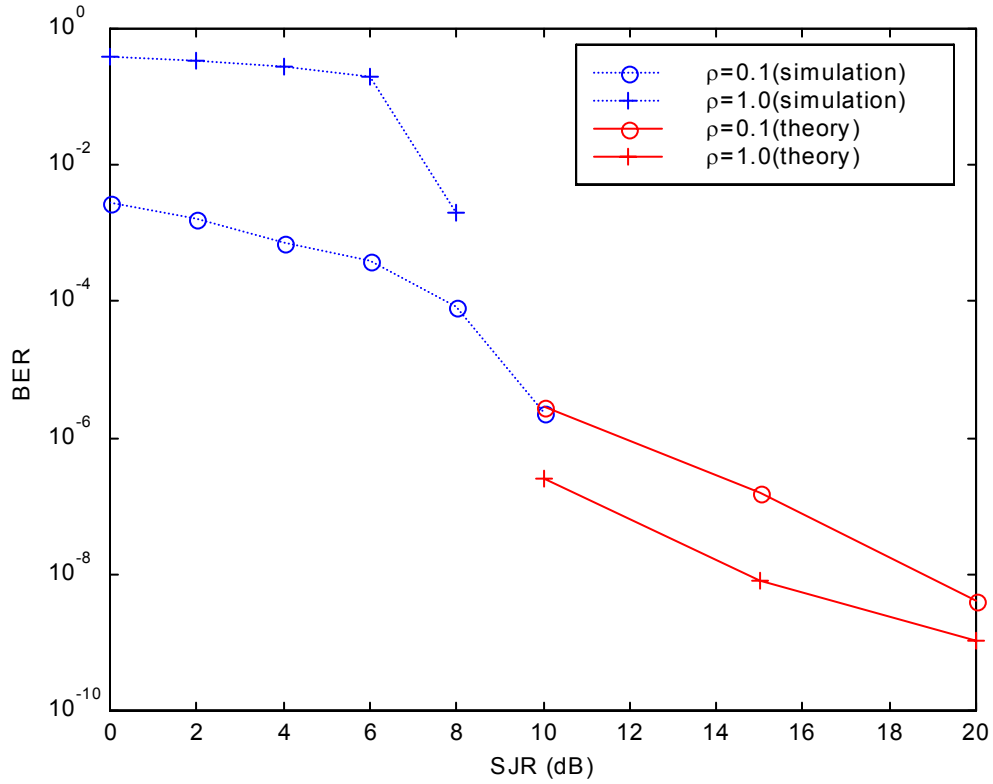
Figure 7.4.   Simulated and theoretical SCCC/DPSK with AWGN and pulsed noise jamming with no side information: effect of ρ on BER for ρ = 0.1 and 1.0, SNR = 10 dB and SJR = 0 to 20 dB.   Note that for ρ = 0.001 and 0.01, all errors were corrected for the range of SJR considered.

Figure 7.5. Simulated and theoretical SCCC/DPSK with AWGN and pulsed noise jamming with no side information: effect of ρ on BER for $\rho = 0.1$ and 1.0, SNR = 20 dB and SJR = 0 to 20 dB. Note that for $\rho = 0.001$ and 0.01, all errors were corrected for the range of SJR considered.
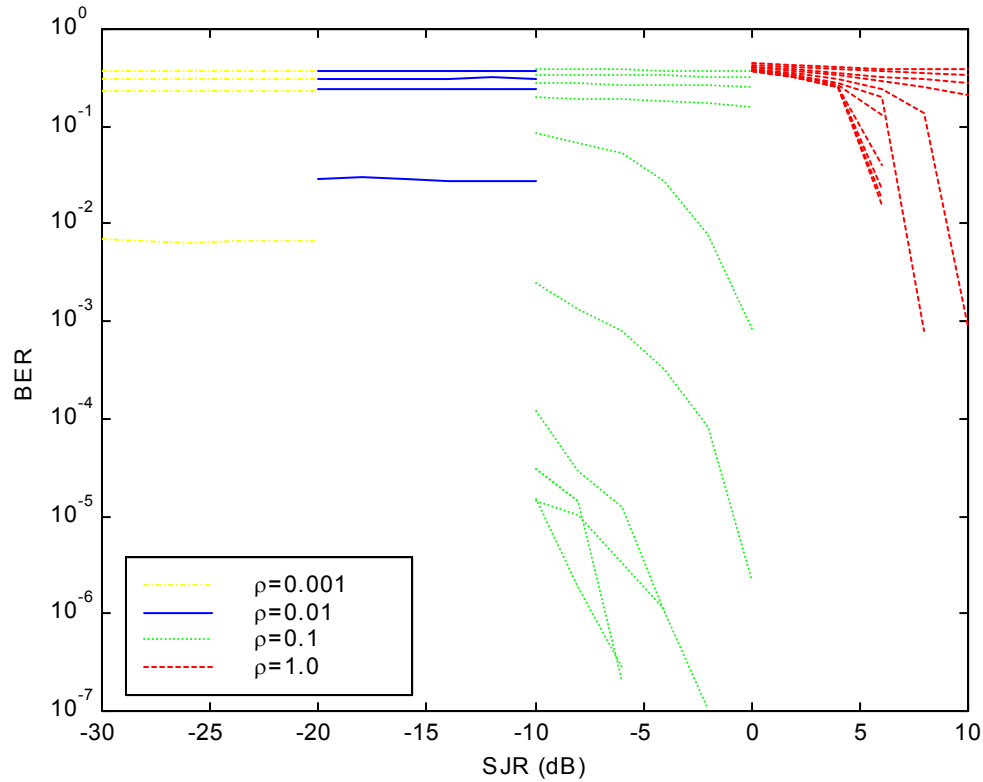
Figure 7.6. Simulated SCCC/DPSK with AWGN and pulsed noise jamming with side information: effect of ρ on BER for ρ = 0.001, 0.01, 0.1 and 1.0, SNR = 0 to 20 dB and SJR = 0 to 10 dB. Note that in order to show the graphs for the different values of ρ, the SJR is offset by ρ in dB. Thus, for ρ = 0.001, 0.01, 0.1 and 1.0, there are offsets of −30, -20, -10, 0 dB, respectively. The graphs start at 0 dB at the top with increments of 2 dB for each subsequent graph downwards. Note that when there is no graph for a particular SNR, it means that all errors were corrected for that SNR for the range of SJR considered.
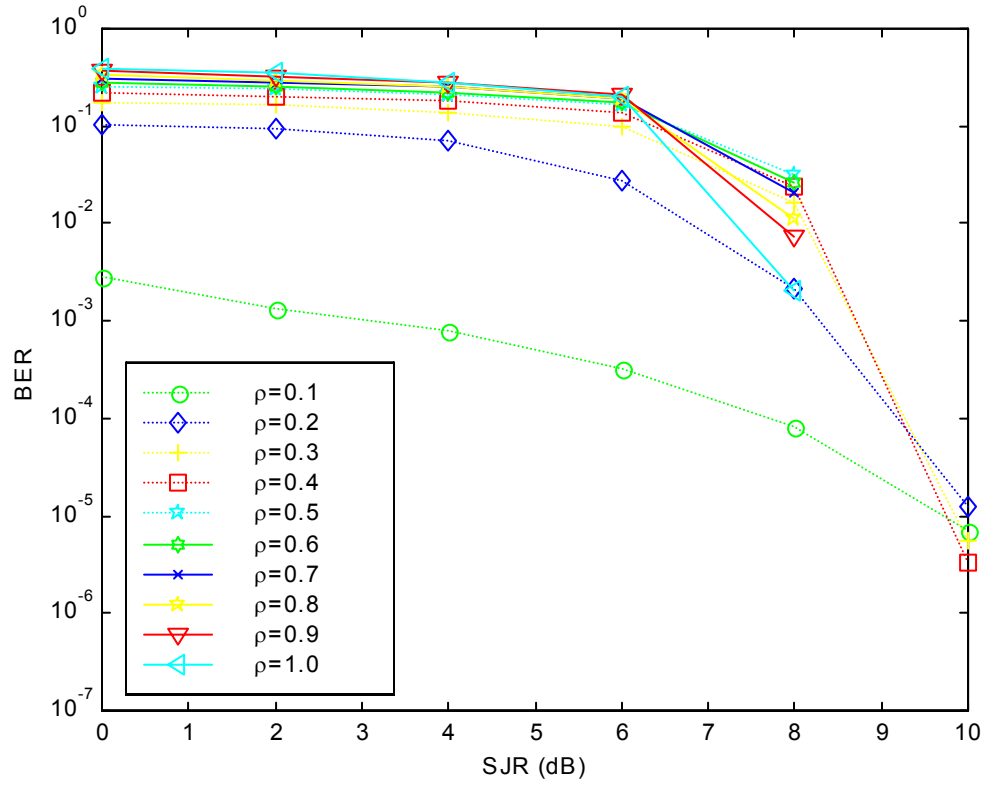
Figure 7.7.   Simulated SCCC/DPSK with AWGN and pulsed noise jamming with side information: effect of ρ on BER for ρ = 0.1 to 1.0, SNR = 10 dB and SJR = 0 to 10 dB.
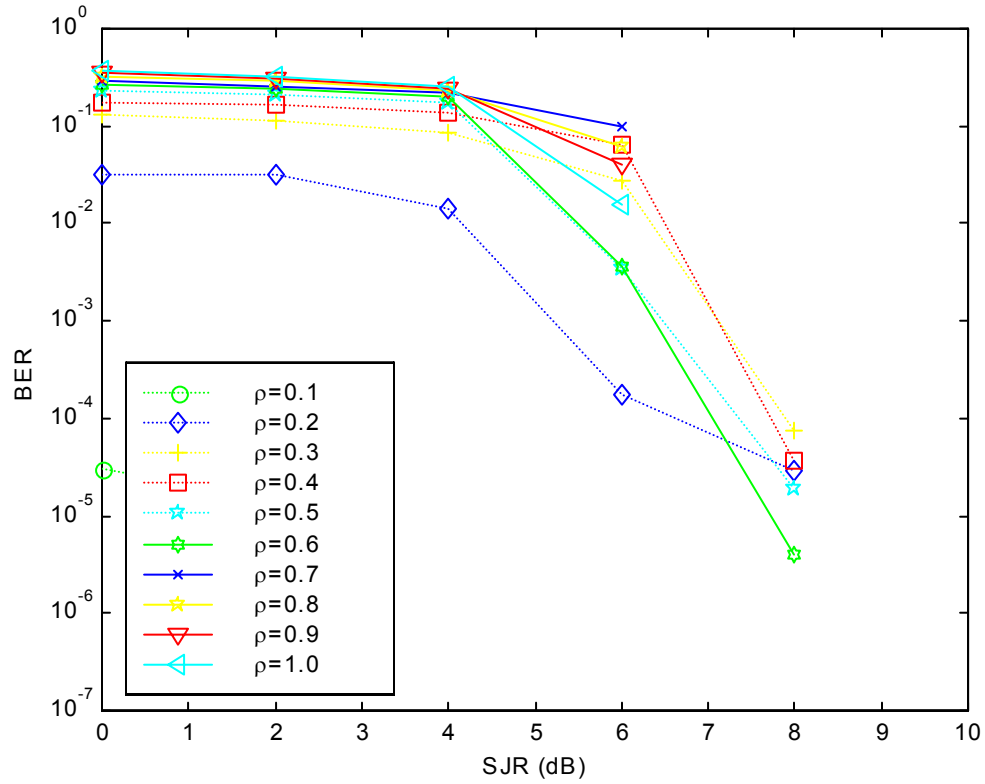
Figure 7.8.   Simulated SCCC/DPSK with AWGN and pulsed noise jamming with side information: effect of ρ on BER for ρ = 0.1 to 1.0, SNR = 20 dB and SJR = 0 to 10 dB.
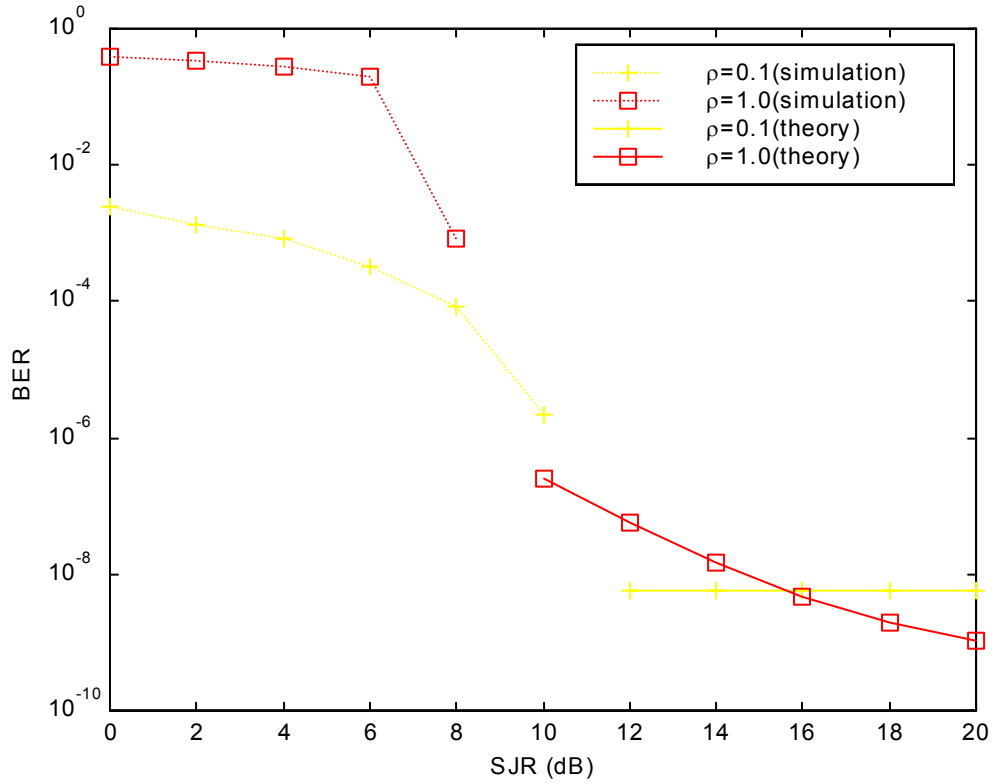
Figure 7.9. Simulated and theoretical SCCC/DPSK with AWGN and pulsed noise jamming with side information: effect of ρ on BER for $\rho = 0.1$ and 1.0, SNR = 10 dB and SJR = 0 to 20 dB. Note that for $\rho = 0.001$ and 0.01, all errors were corrected for the range of SJR considered.
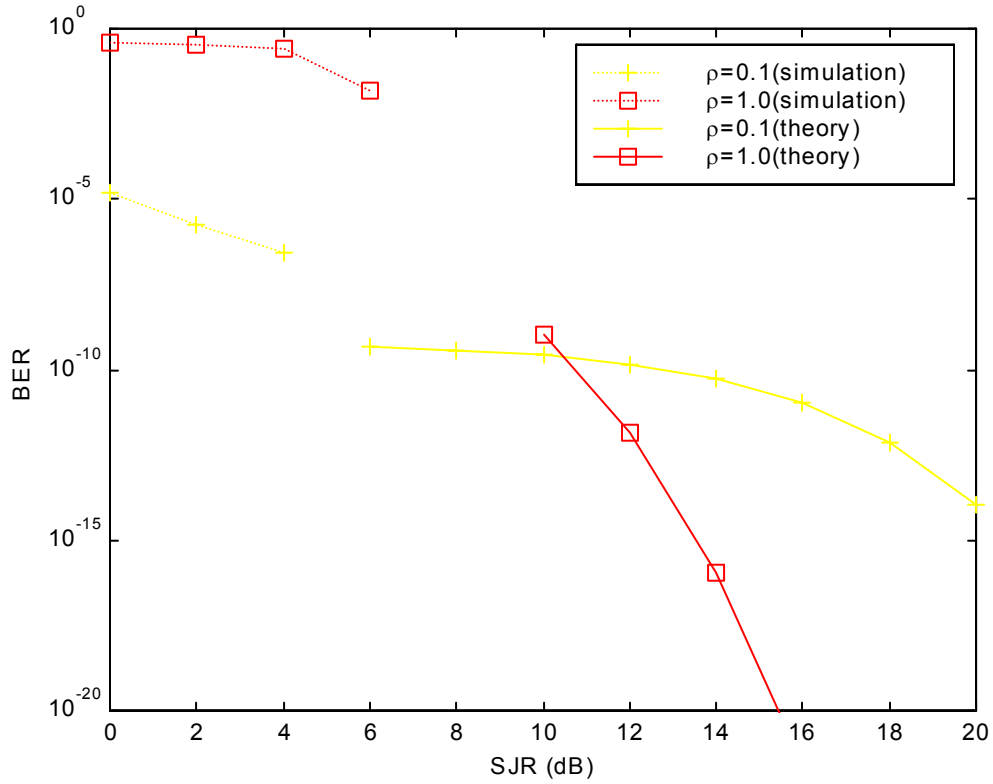
Figure 7.10. Simulated and theoretical SCCC/DPSK with AWGN and pulsed noise jamming with side information: effect of ρ on BER for ρ = 0.1 and 1.0, SNR = 20 dB and SJR = 0 to 20 dB. Note that for ρ = 0.001 and 0.01, all errors were corrected for the range of SJR considered.
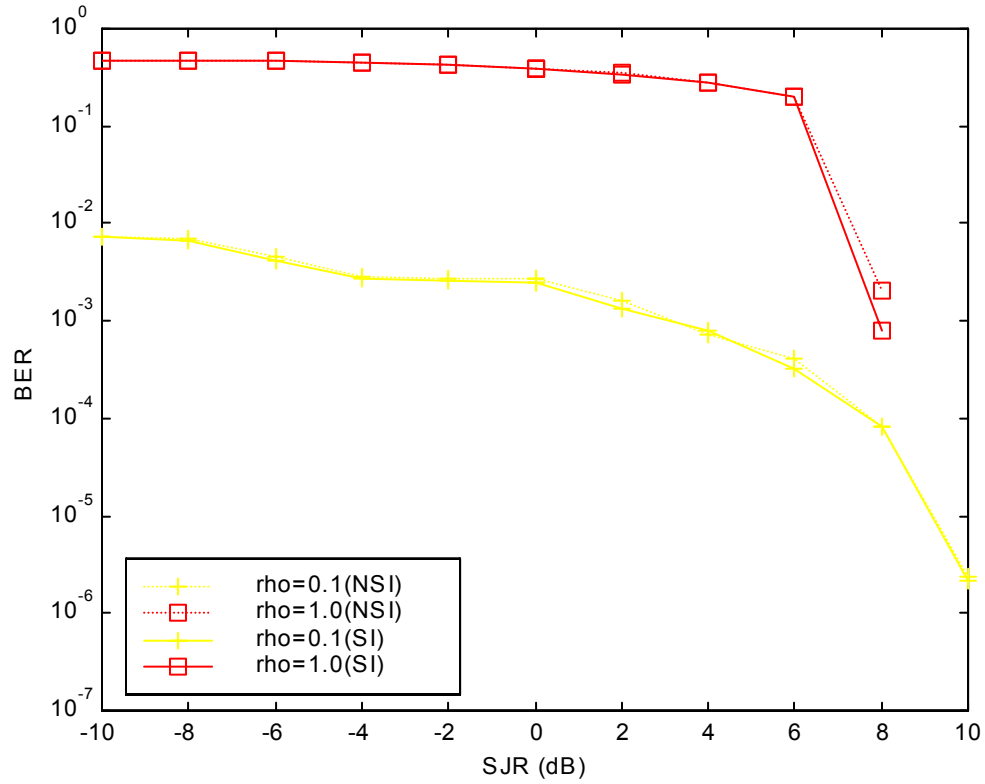
Figure 7.11. Simulated SCCC/DPSK with AWGN and pulsed noise jamming: effect of side information on BER for $\rho = 0.1$ and 1.0, SNR = 10 dB and SJR = -10 to 10 dB. Note that all errors were corrected for $\rho = 0.001$ and 0.01 for the range of SJR considered.
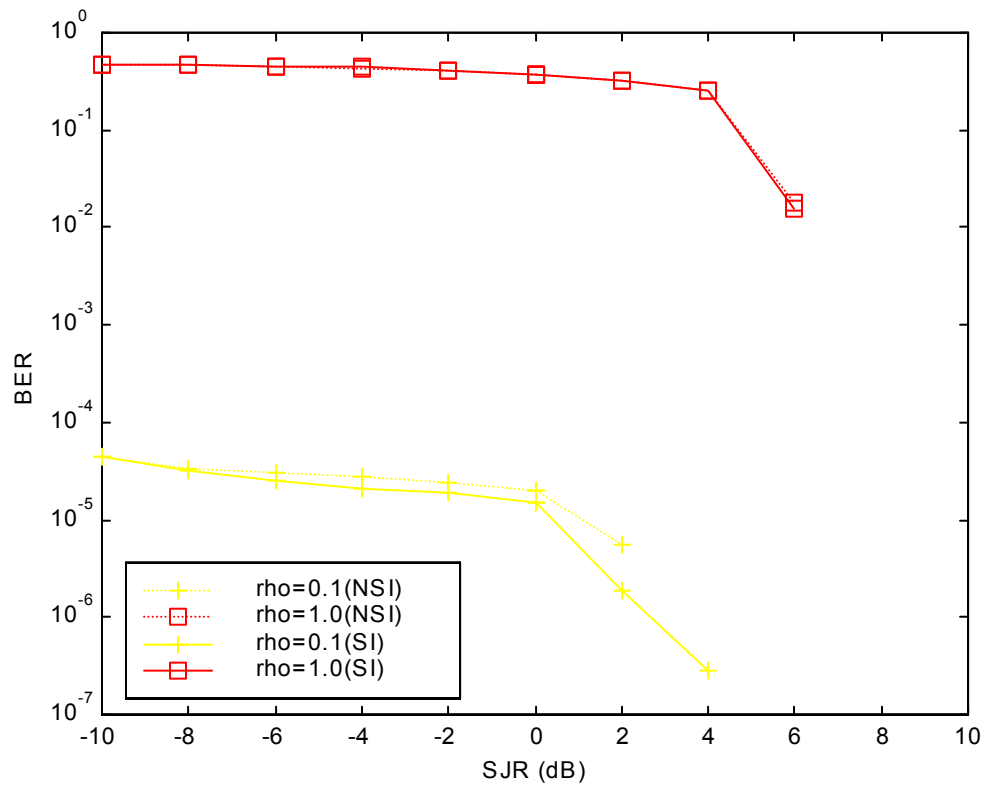
Figure 7.12.   Simulated SCCC/DPSK with AWGN and pulsed noise jamming: effect of side information on BER for ρ = 0.1 and 1.0, SNR = 20 dB and SJR = -10 to 10 dB. Note that all errors were corrected for ρ = 0.001 and 0.01 for the range of SJR considered.
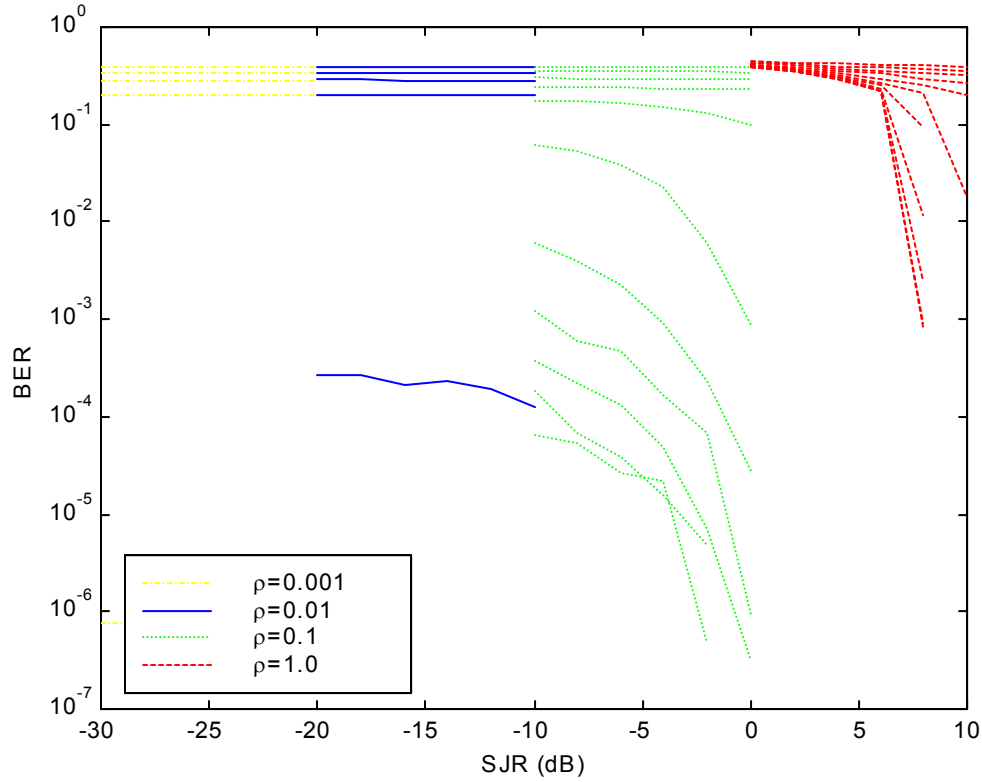
Figure 7.13. Simulated SCCC/DPSK with AWGN, pulsed noise jamming with no side information and Rayleigh fading with no channel information: effect of ρ on BER for ρ = 0.001, 0.01, 0.1 and 1.0, SNR = 0 to 20 dB and SJR = 0 to 10 dB. Note that in order to show the graphs for the different values of ρ, the SJR is offset by ρ in dB. Thus, for ρ = 0.001, 0.01, 0.1 and 1.0, there are offsets of –30, -20, -10, 0 dB, respectively. The graphs start at 0 dB at the top with increments of 2 dB for each subsequent graph downwards. Note that when there is no graph for a particular SNR, it means that all errors were corrected for that SNR for the range of SJR considered.

Figure 7.14. Simulated SCCC/DPSK with AWGN, pulsed noise jamming with no side information and Rayleigh fading with no channel information: effect of ρ on BER for ρ = 0.1 to 1.0, SNR = 10 dB and SJR = 0 to 10 dB.
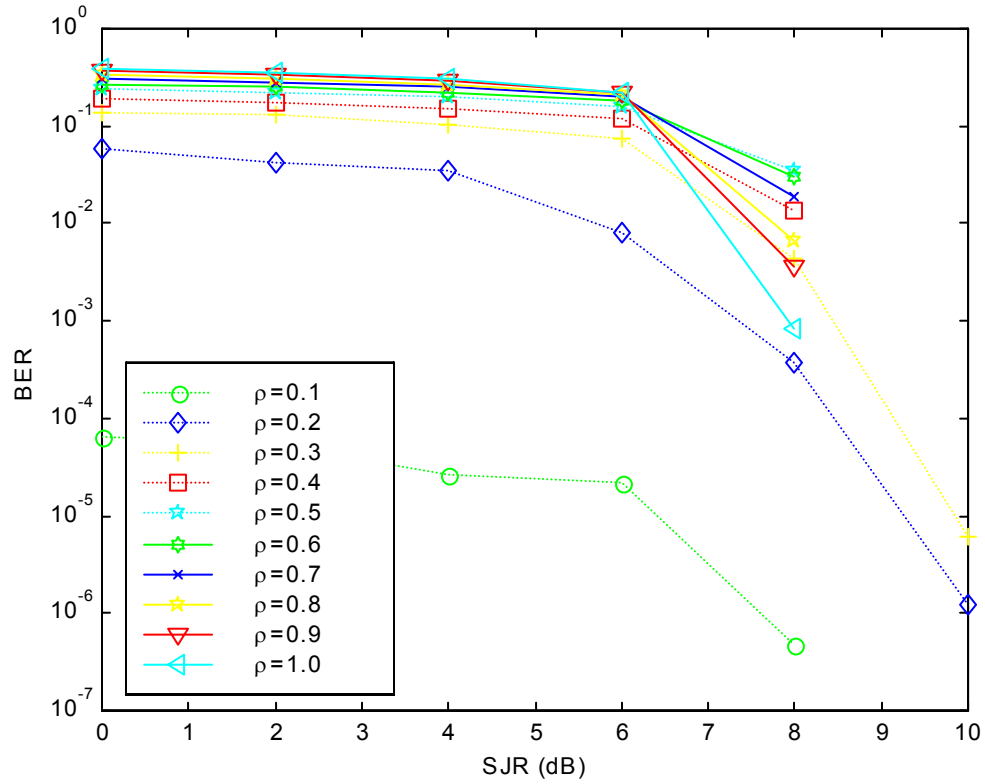
Figure 7.15. Simulated SCCC/DPSK with AWGN, pulsed noise jamming with no side information and Rayleigh fading with no channel information: effect of ρ on BER for ρ = 0.1 to 1.0, SNR = 20 dB and SJR = 0 to 10 dB.
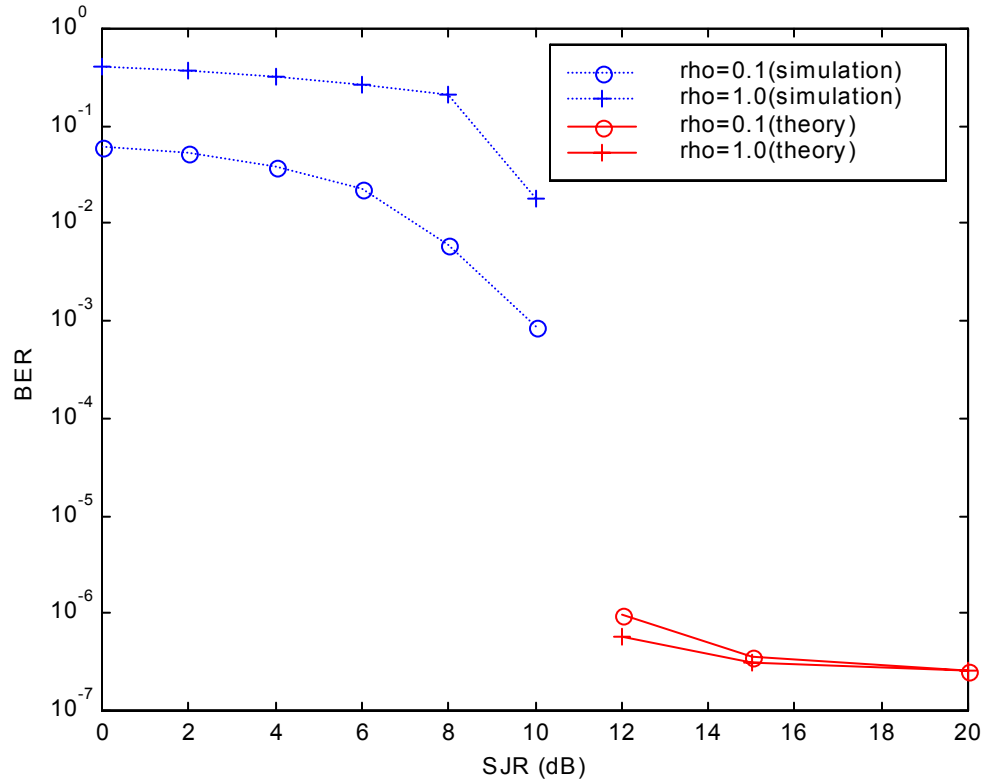
Figure 7.16. Simulated and theoretical SCCC/DPSK with AWGN, pulsed noise jamming with no side information and Rayleigh fading with no channel information: effect of ρ on BER for $\rho = 0.1$ and 1.0, SNR = 10 dB and SJR = 0 to 20 dB. Note that for $\rho = 0.001$ and 0.01, all errors were corrected for the range of SJR considered.
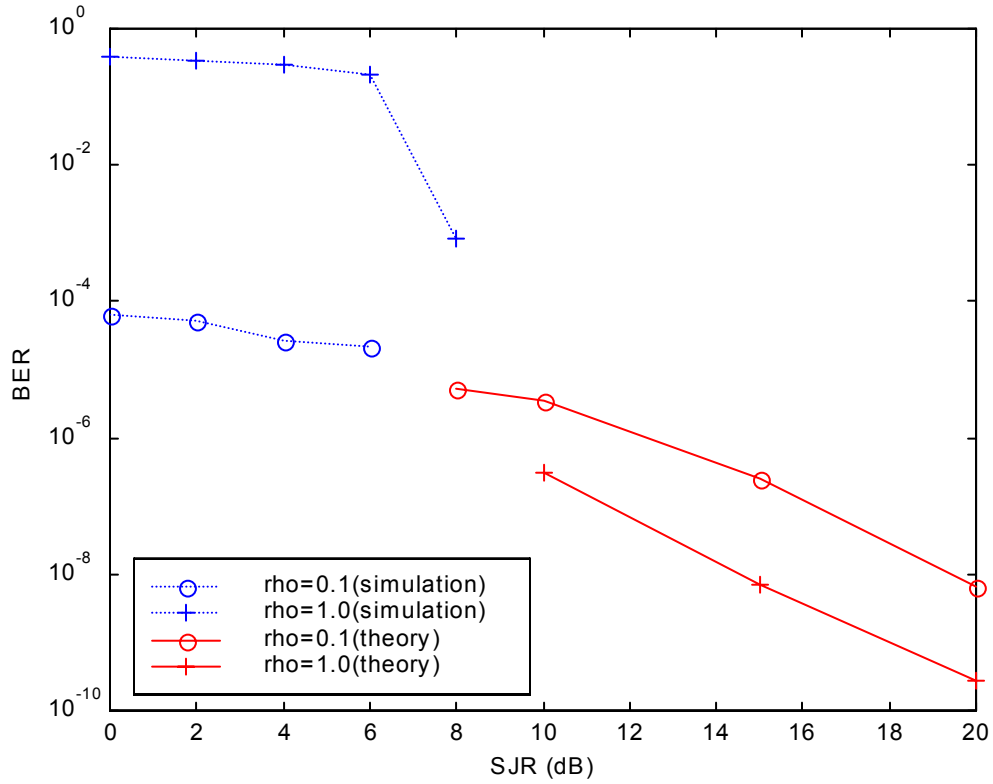
Figure 7.17. Simulated and theoretical SCCC/DPSK with AWGN, pulsed noise jamming with no side information and Rayleigh fading with no channel information: effect of ρ on BER for $\rho = 0.1$ and 1.0, SNR = 20 dB and SJR = 0 to 20 dB. Note that for $\rho = 0.001$ and 0.01, all errors were corrected for the range of SJR considered.
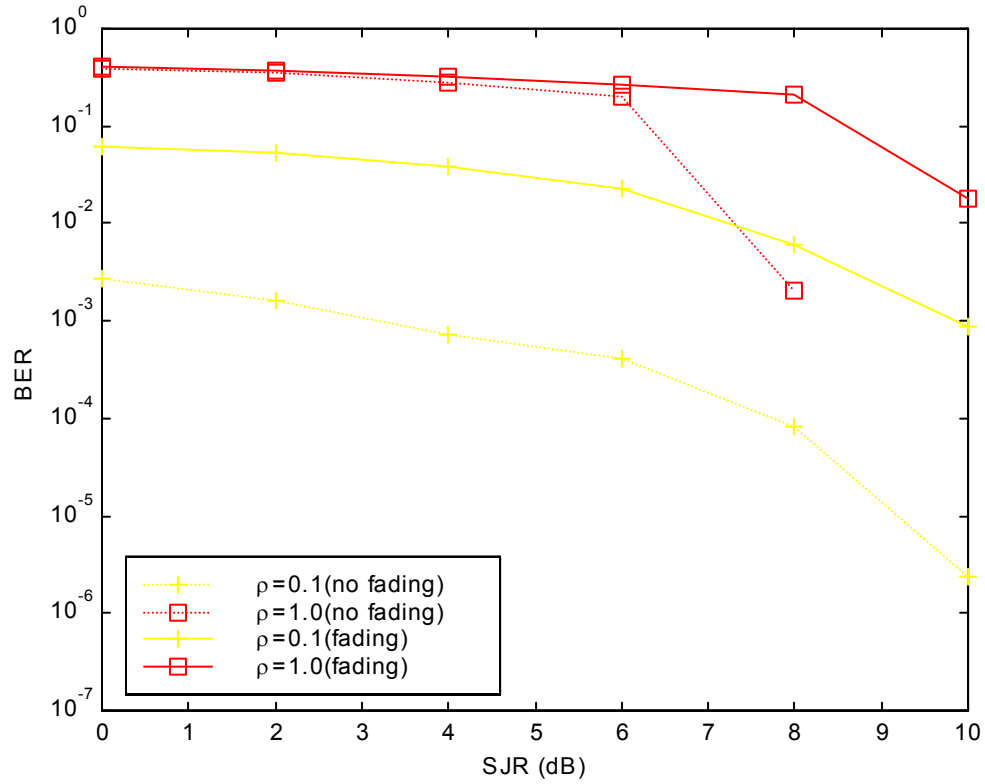
Figure 7.18.   Simulated SCCC/DPSK with pulsed noise jamming with no side information: effect of Rayleigh fading with no channel information on BER for $\rho = 0.1$ and 1.0, SNR = 10 dB and SJR = 0 to 10 dB. Note that for $\rho = 0.001$ and 0.01, all errors were corrected for the range of SJR considered.
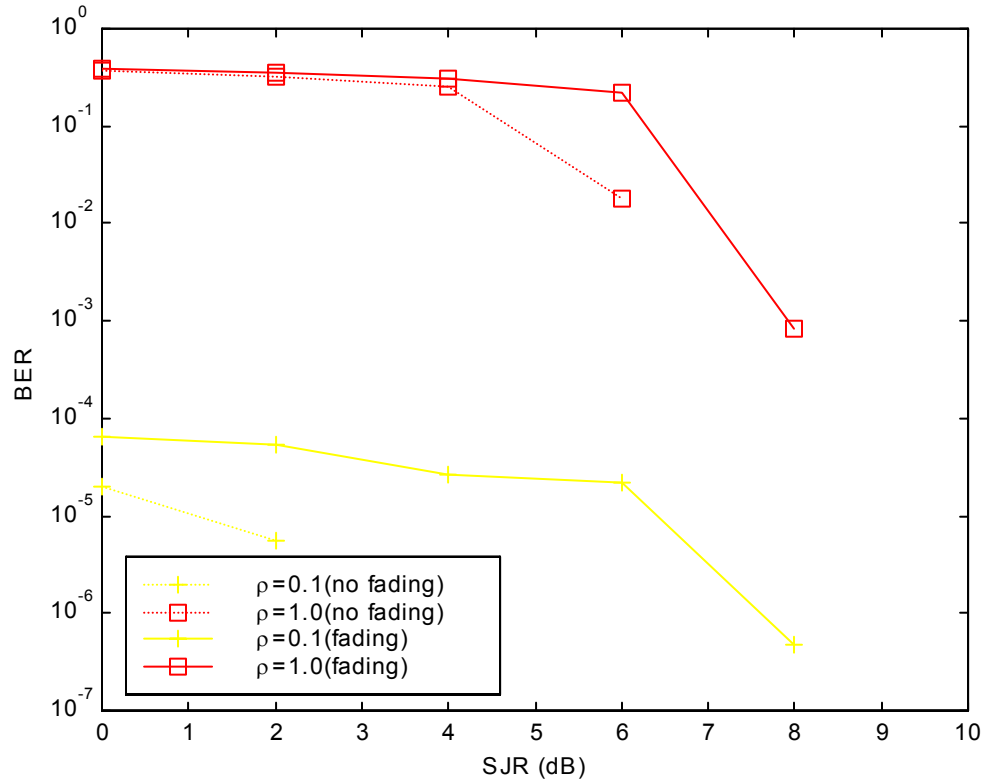
Figure 7.19. Simulated SCCC/DPSK with pulsed noise jamming with no side information: effect of Rayleigh fading with no channel information on BER for $\rho = 0.1$ and 1.0, SNR = 20 dB and SJR = 0 to 10 dB. Note that for $\rho = 0.001$ and 0.01, all errors were corrected for the range of SJR considered.
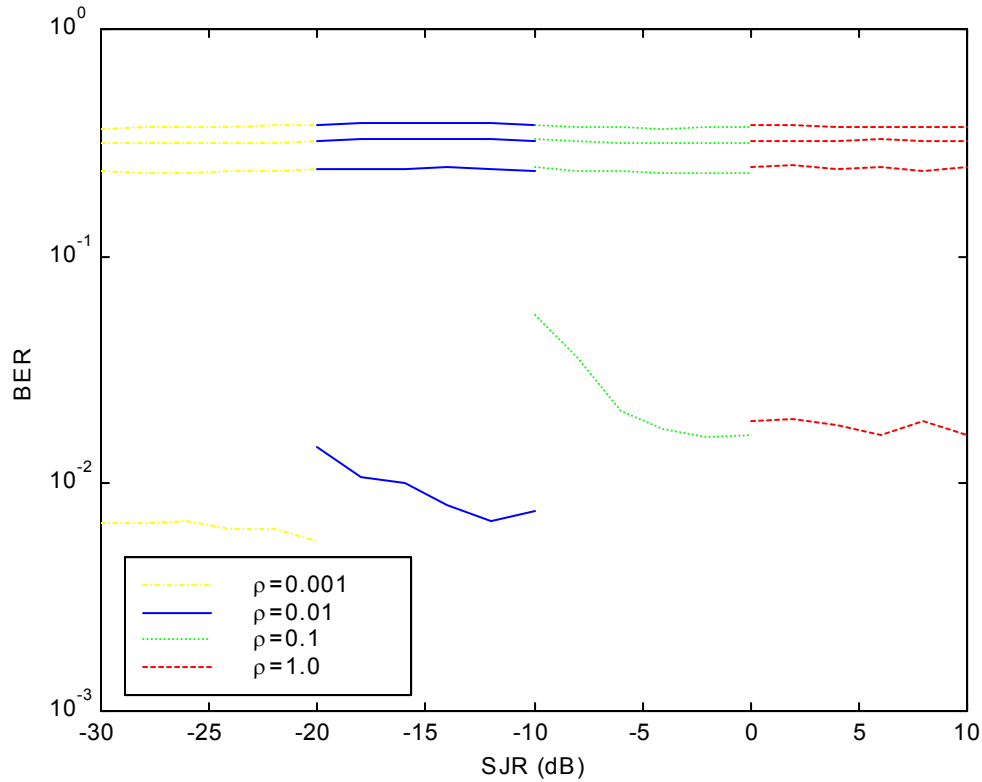
Figure 7.20.   Simulated SCCC/DPSK with AWGN, partial-band noise jamming with no side information and frequency-hopped spread spectrum: effect of ρ on BER for ρ = 0.001, 0.01, 0.1 and 1.0, SNR = 0 to 20 dB and SJR = 0 to 10 dB. Note that in order to show the graphs for the different values of ρ, the SJR is offset by ρ in dB. Thus, for ρ = 0.001, 0.01, 0.1 and 1.0, there are offsets of –30, -20, -10, 0 dB, respectively. The graphs start at 0 dB at the top with increments of 2 dB for each subsequent graph downwards. Note that when there is no graph for a particular SNR, it means that all errors were corrected for that SNR for the range of SJR considered.

Figure 7.21.   Simulated SCCC/DPSK with AWGN, partial-band noise jamming with no side information and frequency-hopped spread spectrum: effect of ρ on BER for ρ = 0.1 to 1.0, SNR = 7 dB and SJR = -10 to 10 dB.

Figure 7.22. Simulated SCCC/DPSK with AWGN, partial-band noise jamming with no side information and frequency-hopped spread spectrum: effect of ρ on BER for ρ = 0.1 to 1.0, SNR = 8 dB and SJR = -10 to 10 dB.

Figure 7.23. Simulated and theoretical SCCC/DPSK with AWGN, partial-band noise jamming with no side information and frequency-hopped spread spectrum: effect of ρ on BER for ρ = 0.01, 0.1 and 1.0, SNR = 7 dB and SJR = -10 to 10 dB. Note that for ρ = 0.001, all errors were corrected for the range of SJR considered.
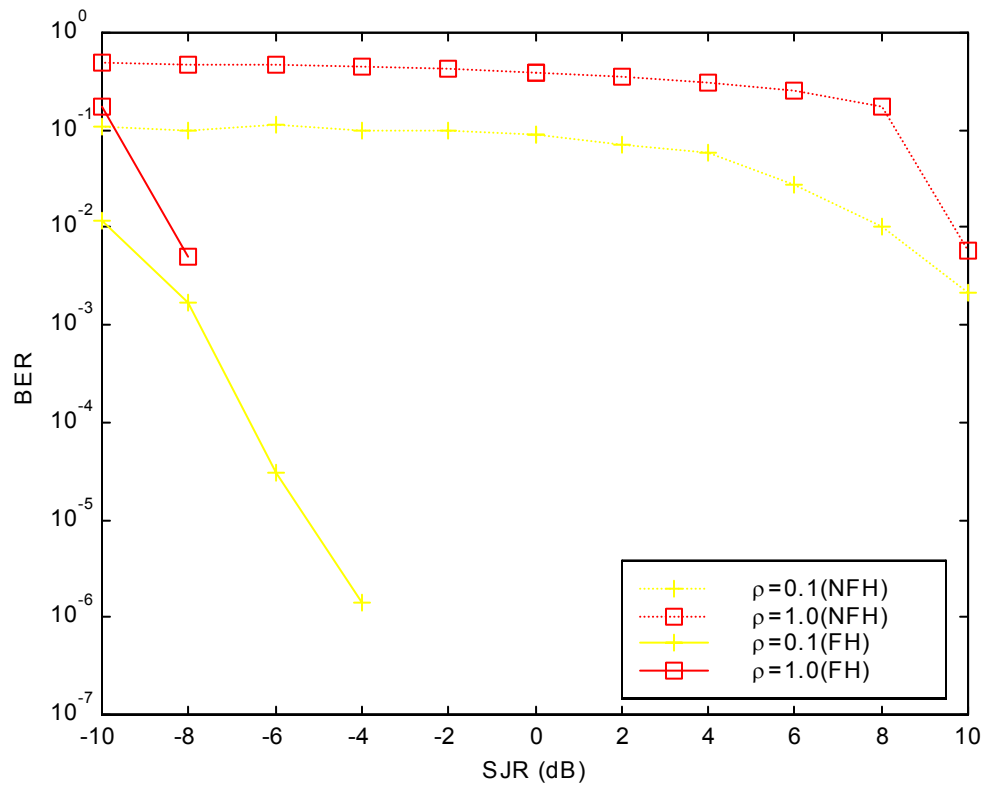
Figure 7.24.   Simulated SCCC/DPSK with AWGN and noise jamming with no side information: effect of frequency-hopped spread spectrum on BER for $\rho = 0.1$ and 1.0, SNR = 7 dB and SJR = -10 to 10 dB.   Note that for $\rho = 0.001$ and 0.01, all errors were corrected for the range of SJR considered.
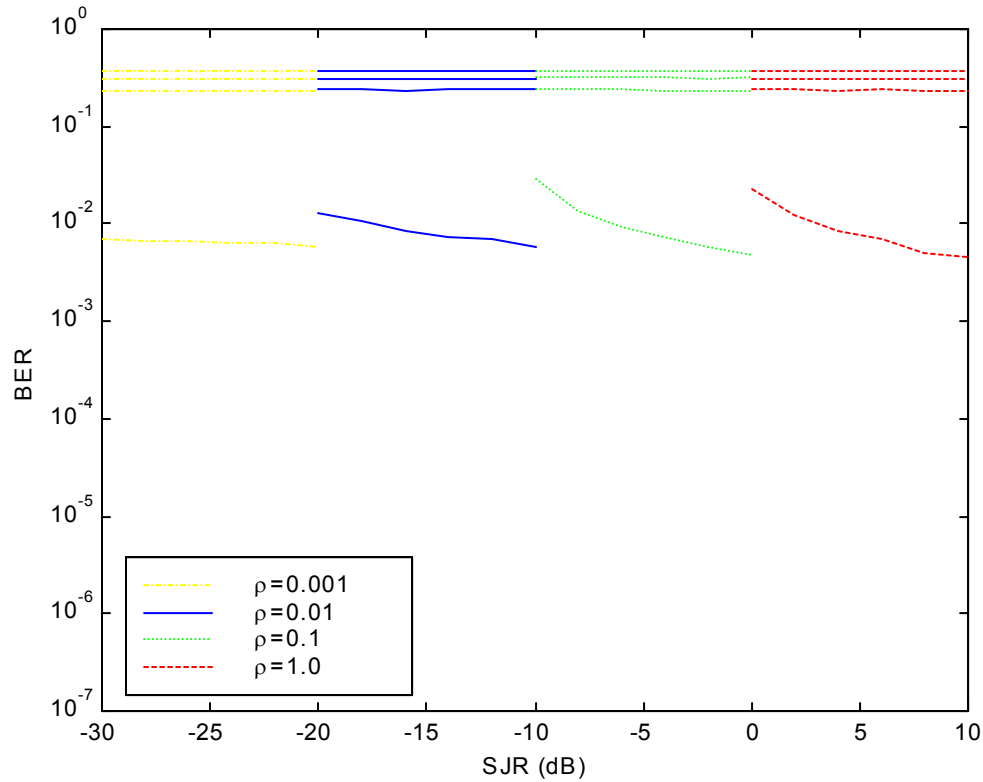
Figure 7.25. Simulated SCCC/DPSK with AWGN, partial-band jamming with side information and frequency-hopped spread spectrum: effect of SJR on BER for $\rho = 0.001$, 0.01, 0.1 and 1.0, SNR = 0 to 20 dB and SJR = 0 to 10 dB. Note that in order to show the graphs for the different values of ρ, the SJR is offset by ρ in dB. Thus, for $\rho = 0.001$, 0.01, 0.1 and 1.0, there are offsets of -30, -20, -10, 0 dB, respectively. The graphs start at 0 dB at the top with increments of 2 dB for each subsequent graph downwards. Note that when there is no graph for a particular SNR, it means that all errors were corrected for that SNR for the range of SJR considered.
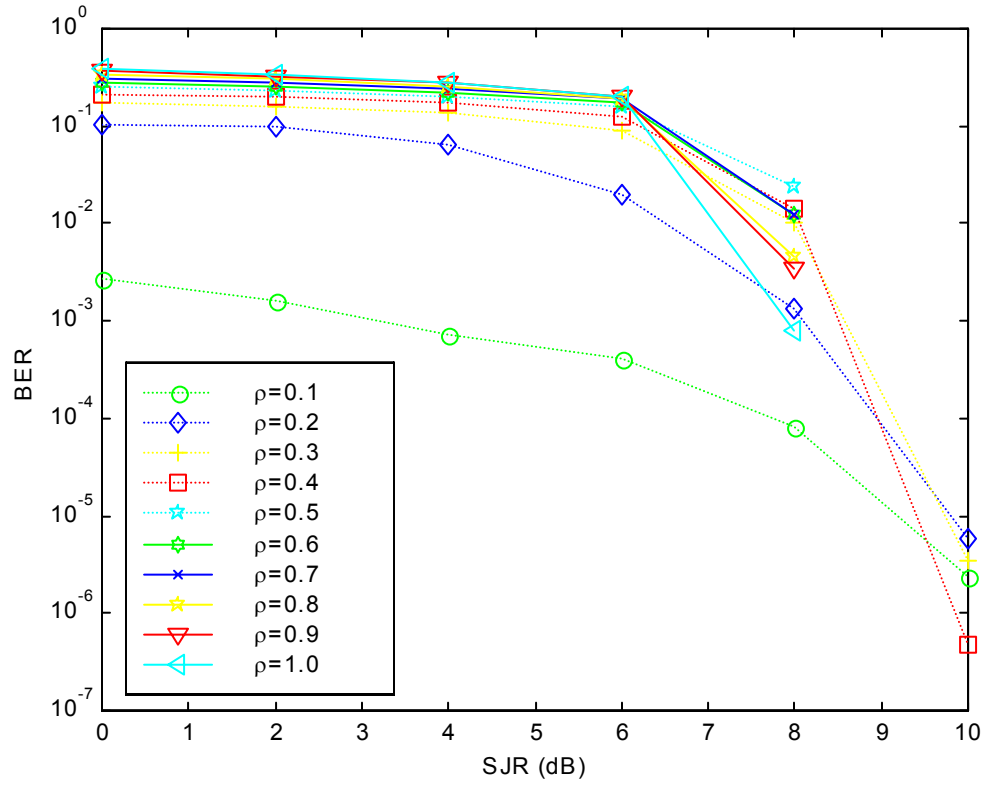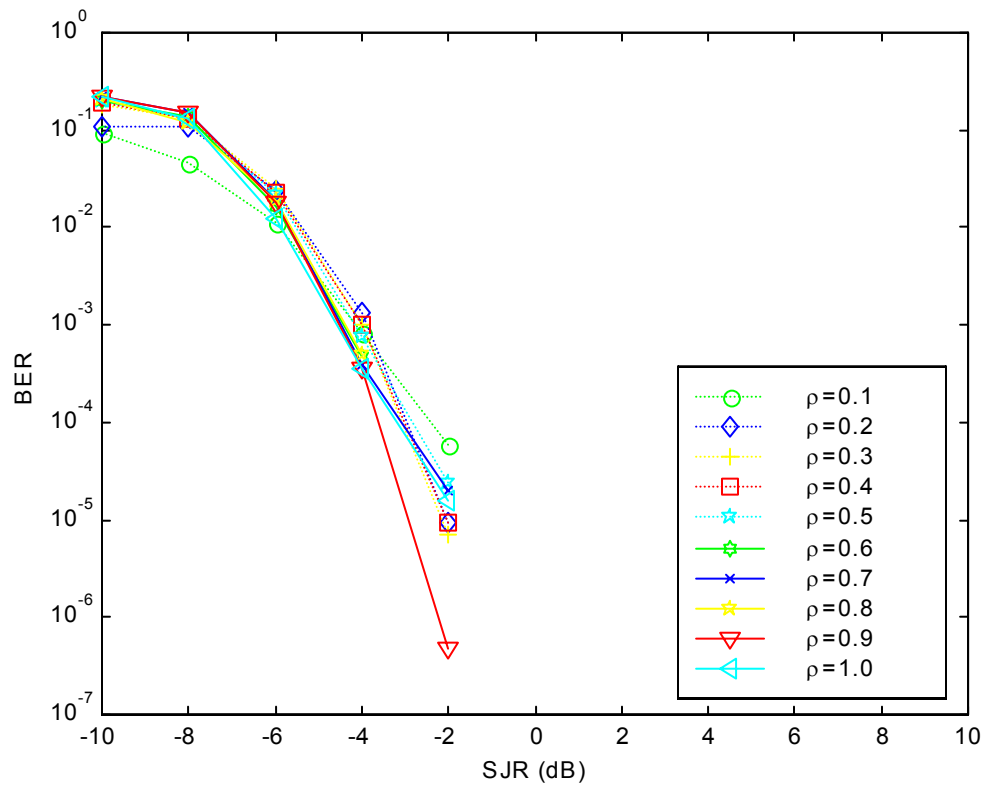
Figure 7.26.   Simulated SCCC/DPSK with AWGN, partial-band noise jamming with side information and frequency-hopped spread spectrum: effect of ρ on BER for $\rho = 0.1$ to 1.0, SNR = 7 dB and SJR = -10 to 10 dB.
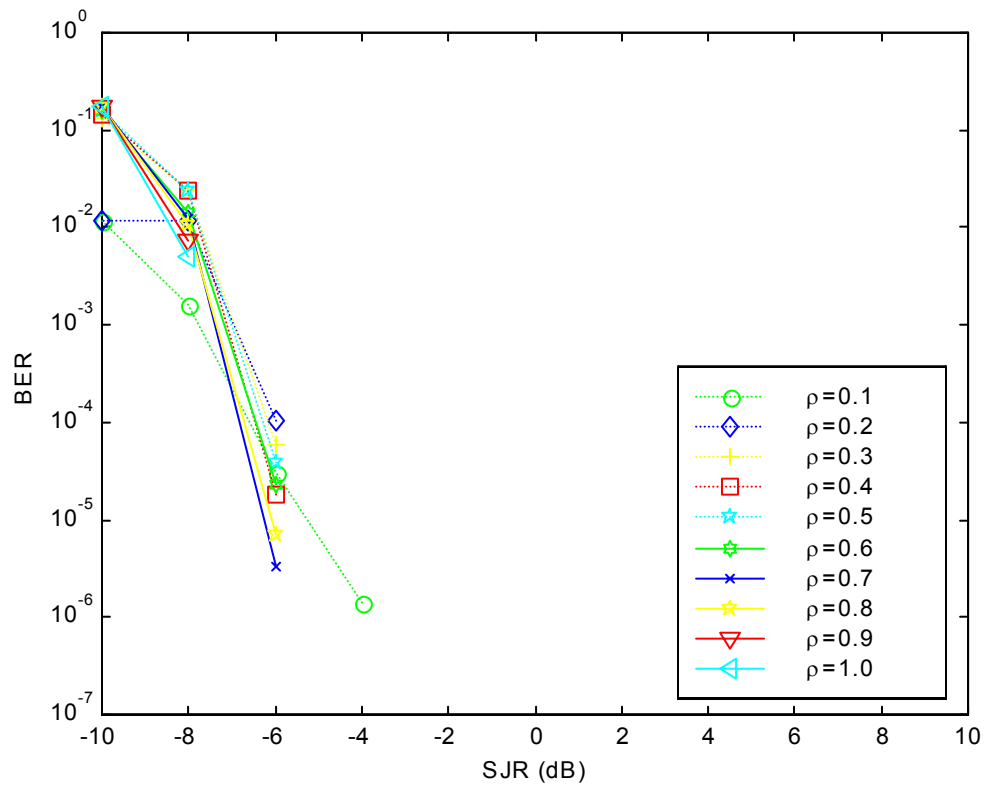
Figure 7.27.   Simulated SCCC/DPSK with AWGN, partial-band noise jamming with side information and frequency-hopped spread spectrum: effect of ρ on BER for $\rho = 0.1$ to 1.0, SNR = 8 dB and SJR = -10 to 10 dB.
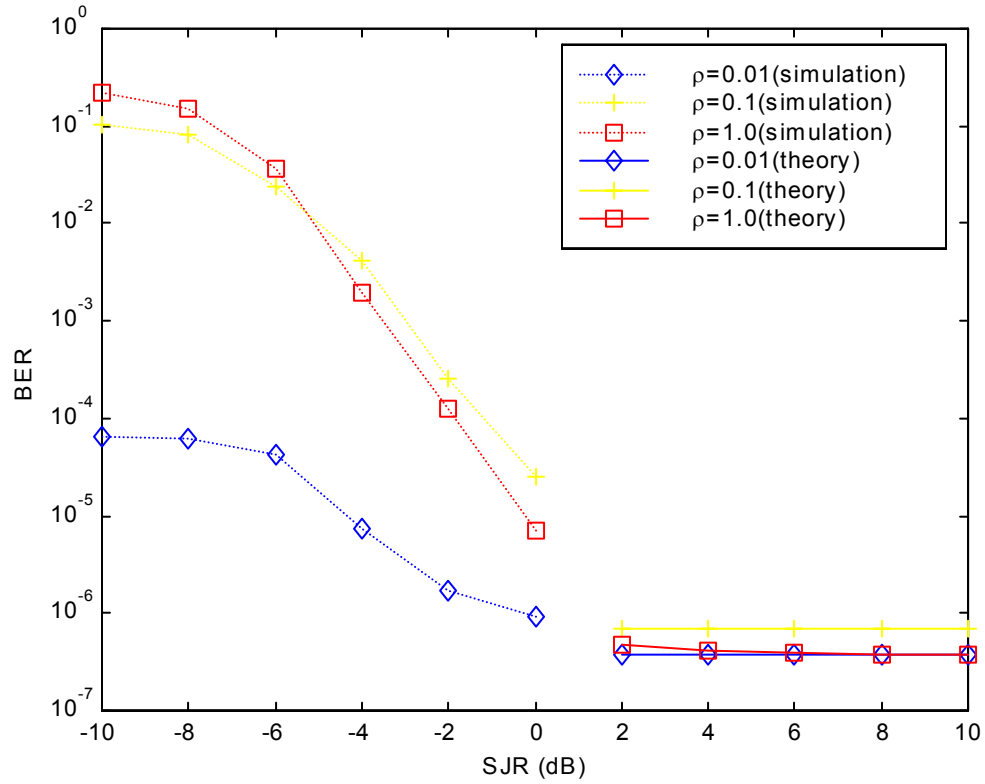
Figure 7.28.   Simulated and theoretical SCCC/DPSK with AWGN, partial-band noise jamming with side information and frequency-hopped spread spectrum: effect of ρ on BER for ρ = 0.01, 0.1 and 1.0, SNR = 7 dB and SJR = -10 to 10 dB.   Note that for ρ = 0.001, all errors were corrected for the range of SJR considered.
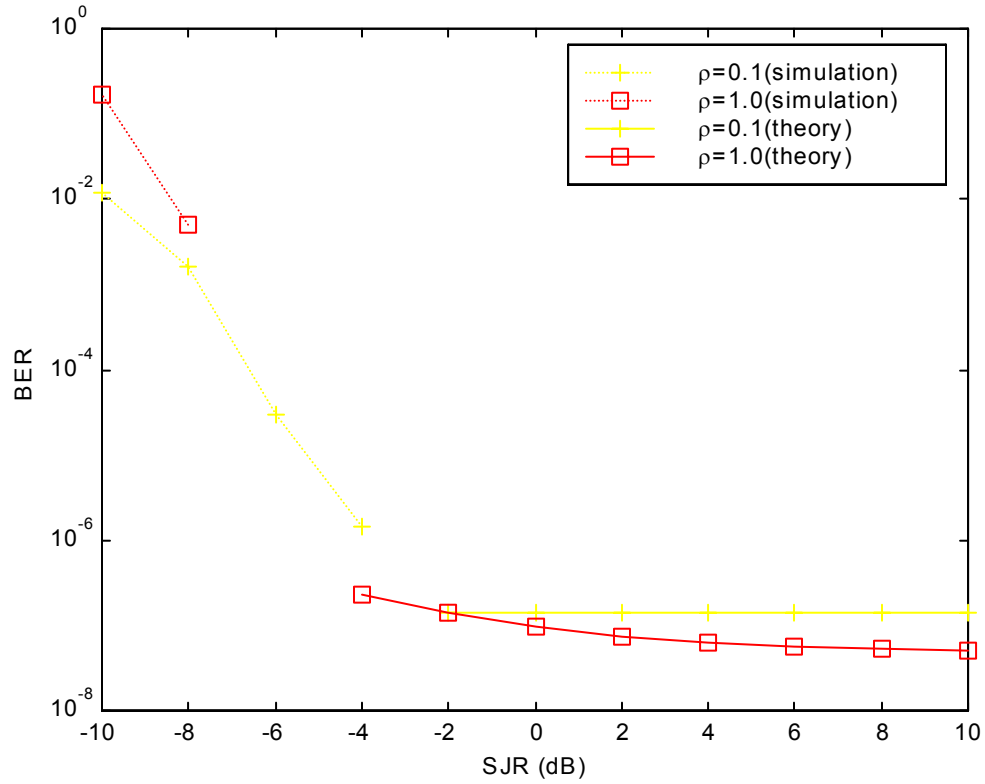
Figure 7.29.   Simulated and theoretical SCCC/DPSK with AWGN, partial-band noise jamming with side information and frequency-hopped spread spectrum: effect of ρ on BER for $\rho = 0.1$ and 1.0, SNR = 8 dB and SJR = -10 to 10 dB. Note that for $\rho = 0.001$ and 0.01, all errors were corrected for the range of SJR considered.
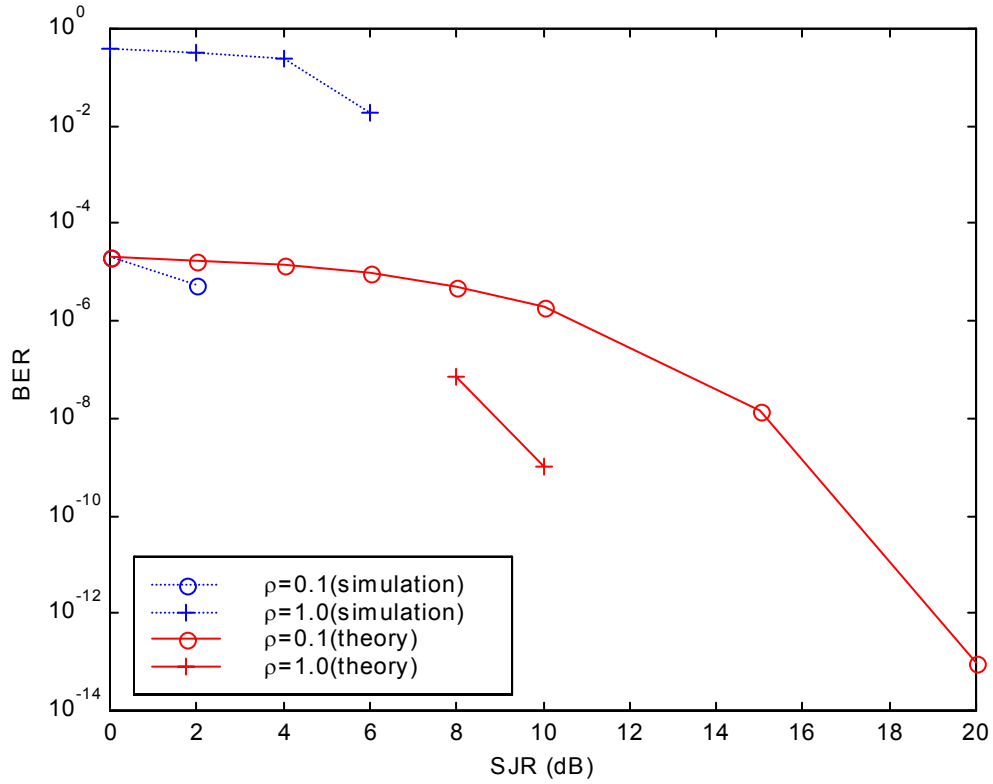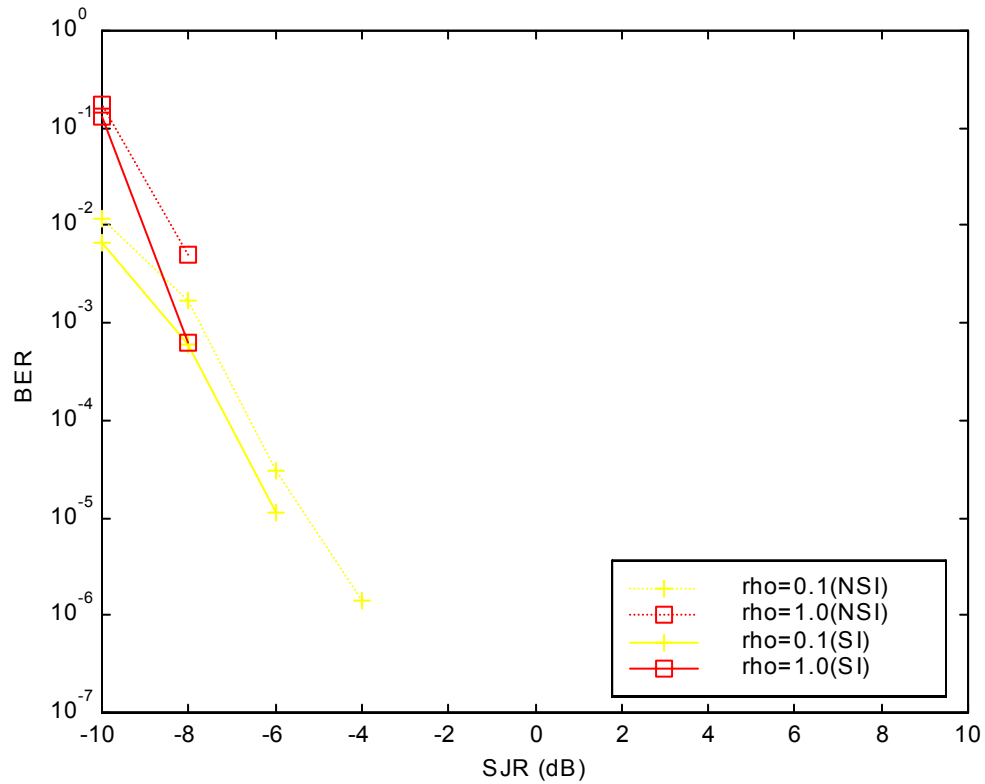
Figure 7.30.   Simulated SCCC/DPSK with AWGN, partial-band noise jamming with frequency-hopped spread spectrum: effect of side information on BER for $\rho = 0.1$ and 1.0, SNR = 7 dB and SJR = -10 to 10 dB. Note that $\rho = 0.001$ and 0.01, all errors were corrected for that SNR for the range of SJR considered.
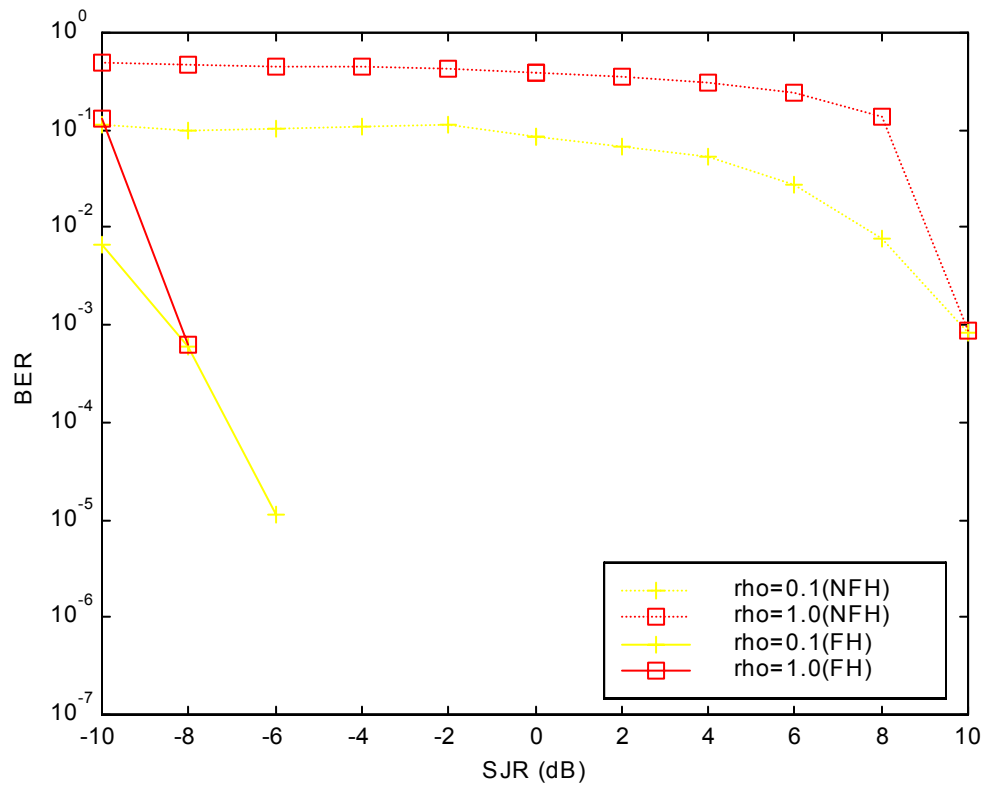
Figure 7.31.   Simulated SCCC/DPSK with AWGN and noise jamming with no side information: effect of frequency-hopped spread spectrum on BER for ρ = 0.1 and 1.0, SNR = 8 dB and SJR = -10 to 10 dB. Note that for ρ = 0.001 and 0.01, all errors were corrected for that SNR for the range of SJR considered.

THIS PAGE INTENTIONALLY LEFT BLANK

VIII. ANALYSIS OF RESULTS AND IMPLICATIONS FOR MILITARY USE

Based on the simulations results in Chapter V and VII, the following analyses are carried out from the perspective of the jammer (without side or channel information):

a.   SCCC/BPSK with pulsed noise jamming

b.   SCCC/BPSK with pulsed noise jamming and Rayleigh fading

c.   SCCC/BPSK with pulsed noise jamming and direct sequence spread spectrum

d.   SCCC/DPSK with pulsed noise jamming

e.   SCCC/DPSK with pulsed noise jamming and Rayleigh fading

f.   SCCC/DPSK with partial-band noise jamming and frequency-hopped spread spectrum.

A comparison of SCCC/BPSK and SCCC/DPSK will then be made. What the communications user can do when he is jammed will also be discussed.

A.   ANALYSIS FOR JAMMER

1.   SCCC/BPSK with Pulsed Noise Jamming

Since BER performance is dependent on SNR and SJR, one can categorize the performance of the SCCC into four regions. As shown in Table 8.1, these four regions depend on the ratio of the jamming noise power spectral density-to-AWGN.

	Low SJR (< 4 dB)	High SJR (≥ 4 dB)
Low SNR (< 1.5 dB)	Region I: Medium N_i/N_o	Region II: Very low N_i/N_o
High SNR (≥ 1.5 dB)	Region III: High N_i/N_o	Region IV: Medium N_i/N_o

Table 8.1.   Jamming regions for SCCC/BPSK.

In region I, there is low signal energy and a high level of jamming noise. BER is therefore high. It is easy for a jammer to degrade communications when SNR is low. For region II, although there is low signal energy, the level of jamming noise is very low. The SCCC is able to correct many of the errors in this case, resulting in low BER. High signal energy is accompanied by a very high level of jamming noise in Region III. In Region IV, high signal energy is combined with intermediate levels of noise. The best BER in a noise-jamming environment is obtained in Region IV. Although Regions I and IV have similar jamming noise to AWGN ratios, BER varies widely. High SNR is more important for SCCC decoding than noise ratios.

For the jammer, it is not effective to use very small ρ (< 0.001) to deny communications that are using SCCC. SCCC is effective in correcting errors. Although jamming power is high for low ρ, the SCCC is able to correct the affected bits since the numbers of bits affected are small. For $\rho = 0.01$, the attack may be more successful for high SJR. For high SJR, the jamming power is low, thus the attacker needs to concentrate the jamming power by reducing ρ. For low SJR, it is more effective to use higher values of ρ (greater than 0.1), with barrage jamming being the most effective. Figure 8.1 is a plot of BER vs. SNR for different values of SJR and barrage jamming. We observe that with SJR < 2 dB, the BER is driven to less than 10^{-3}.

For Region I, since the SJR is small, a moderately high jamming power with barrage jamming is effective for SJR less than 4 dB. In Region II, it is most effective to use barrage jamming. For Region III, a ρ between 0.6 and 1.0 inclusive is effective. The actual value of ρ depends on the SNR and SJR. Region IV is not very suitable for jamming since the high SJR negates the effects of jamming.

Thus, pulsed noise jamming is largely ineffective for sufficient SNR (> 10 dB) unless the jammer uses very high jamming power. For smaller SNR, the situation is more complicated. Pulse jamming with $\rho < 0.01$ is largely ineffective. Pulse jamming is effective for $1 \geq \rho \geq 0.1$ and for 8 dB > SNR > 0 dB. The most effective strategy for a jammer is to employ barrage jamming with SJR < 2 dB.

2.   SCCC/BPSK with Pulsed Noise Jamming and Rayleigh Fading

As in Table 8.1, one can categorize the performance of a SCCC with Rayleigh fading into four regions (Table 8.2) depending on SNR, SJR, and jamming noise power spectral density-to-AWGN ratio.

	Low SJR (< 6 dB)	High SJR (≥ 6 dB)
Low SNR (< 6 dB)	Region I: Medium N_i/N_o	Region II: Very low N_i/N_o
High SNR (≥ 6 dB)	Region III: High N_i/N_o	Region IV: Medium N_i/N_o

Table 8.2.   Jamming regions for SCCC/BPSK with Rayleigh fading.

As in the case with no Rayleigh fading, it is not effective to use very small ρ ($\leq$ 0.01) to deny communications signals that are using SCCC. The SCCC is effective in correcting errors. Although jamming power is high for low ρ, the SCCC is able to correct the affected bits since the numbers of bits affected are small. For SNR < 6 dB, it is best to use $\rho > 0.1$ with SJR < 6 dB (Figures 8.2 and 8.3). For higher values of SNR, $\rho = 0.4$ or 0.5 is the most effective (Figure 5.30).

For Region I, since the SJR is small, barrage jamming is effective for SJR less than 6 dB. In Region II, barrage jamming is also the most effective. For Region III, a ρ of around 0.5 is more effective than barrage jamming (Figure 5.30). Region IV is not very suitable for jamming since the high SJR negates the effects of jamming.

Pulse jamming is largely ineffective for sufficient SNR (> 12 dB) in Rayleigh fading except for very high jamming power (SJR < 2 dB). Fading makes it easier for the jammer since a lower jamming power is required to achieve the same effect as without fading and, in most cases, barrage jamming is more effective than pulsed noise jamming. Pulse jamming with $\rho < 0.01$ is largely ineffective. Pulse jamming is effective only for ρ = 0.4 or 0.5 and for 10 dB $> $ SNR > 6 dB and SJR < 6 dB. The most effective strategy for a jammer is to employ $\rho = 0.5$ with SJR < 6 dB.

3. SCCC/BPSK with Pulsed Noise Jamming and Direct Sequence Spread Spectrum

With direct sequence spread spectrum, one can categorize performance into the following four regions as shown in Table 8.3.

	Low SJR (< -4 dB)	High SJR ($\geq$ -4 dB)
Low SNR (< 1.5 dB)	Region I: Medium N_i/N_o	Region II: Very low N_i/N_o
High SNR (1.5$\leq$ SNR < 4 dB)	Region III: High N_i/N_o	Region IV: Medium N_i/N_o

Table 8.3.   Jamming regions for SCCC/BPSK with direct sequence spread spectrum.

There are differences between Table 8.3 and Table 8.1. In Table 8.3, since the DS is able to reduce the jamming noise to a small level, low SJR means less than –4 dB. Since for SNR > 4 dB, and –8 < SJR < 10 dB, all errors are corrected, the analysis for these conditions is not included in the table.

For the jammer, as in the case without DS, it is not effective to use very small ρ (0.001) to deny communications. The SCCC with DS is able to reduce the jamming effectiveness for very small ρ. The attacker will be most successful with $\rho = 0.01$ for SJR < –8 dB and SNR < 4 dB (Figure 8.4).

For Region I, since SJR is small, a moderately high jamming power with barrage jamming is effective for SJR < -4 dB. In Region II, the value of ρ is not critical since the BER performances for different values of ρ are similar. For Region III, $\rho = 0.01$ is effective for SNR < 4 dB and SJR < –8 dB. Region IV is not very suitable for jamming since the high SNR negates the effects of jamming.

Thus, pulsed noise jamming is ineffective for SCCC/BPSK with DS and sufficient SNR (> 4 dB), and the best jamming strategy is not to engage in pulsed noise jamming. For smaller SNR, the situation is more complicated. Pulse jamming with $\rho < 0.001$ is ineffective. Pulse jamming is only effective for $1 \geq \rho \geq 0.01$ and for SNR < 4 dB. For low SJRs, $\rho = 0.01$ is the most effective. The most effective strategy for a jammer is to operate with a SJR of < -8 dB and $\rho = 0.01$.

4. SCCC/DPSK with Pulsed Noise Jamming

For DPSK with jamming, the four regions are shown in Table 8.4.

	Low SJR (< 6 dB)	High SJR (≥ 6 dB)
Low SNR (< 8 dB)	Region I: Medium N_i/N_o	Region II: Very low N_i/N_o
High SNR (≥ 8 dB)	Region III: High N_i/N_o	Region IV: Medium N_i/N_o

Table 8.4.   Jamming regions for SCCC/DPSK.

For the jammer, it is not effective to use very small ρ (< 0.01) to deny communications signals that are using SCCC. The SCCC is effective in correcting errors. Although the jamming power is high for low ρ, the SCCC is able to correct the affected bits since the numbers of bits affected are small. For high SJR, the jamming power is low, thus the attacker needs to concentrate the jamming power by reducing ρ. For low SJR, it is more effective to use larger ρ (greater than 0.1), with barrage jamming being the most effective.

For Region I, since the SJR is small, barrage jamming is effective (Figure 8.5). In Region II, it is also most effective to use barrage jamming. For Region III, ρ of between 0.1 and 0.4 inclusive is effective (Figure 7.6). The optimum value of ρ depends on SNR and SJR. Region IV is not very suitable for jamming since the high SNR negates the effects of jamming. However, a value of ρ < 0.1 or lower may be effective for high SJRs based on theoretical results (Figure 6.6).

5. SCCC/DPSK with Pulsed Noise Jamming and Rayleigh Fading

For DPSK with jamming and Rayleigh fading, the four regions are shown in Table 8.5.

	Low SJR (< 6 dB)	High SJR (≥ 6 dB)
Low SNR (< 12 dB)	Region I: Medium N_i/N_o	Region II: Very low N_i/N_o
High SNR (≥ 12 dB)	Region III: High N_i/N_o	Region IV: Medium N_i/N_o

Table 8.5.   Jamming regions for SCCC/DPSK with Rayleigh fading.

Fading causes the SCCC's performance to worsen, especially for high SJRs and small ρ. For the jammer, it is not effective to use very small ρ (≤ 0.01) to deny communications that are using SCCCs. Although jamming power is high for low ρ, the SCCC is able to correct the affected bits since the numbers of bits affected are small. For moderate SJR, it is best to use barrage jamming. For higher SJR, $\rho = 0.2$ to 0.5 are effective (Figures 7.28 and 7.29).

For Region I, since the SJR is small, barrage jamming is effective (Figure 8.6). In Region II, it is also most effective to use barrage jamming. For Region III, ρ of between 0.2 and 0.5 inclusive is effective. The actual value of ρ depends on SNR and SJR. Region IV is not very suitable for jamming since the high SNR negates the effects of jamming. However, a value of $\rho < 0.1$ or lower may be effective for high SJRs based on theoretical results (Figure 6.15).

6. SCCC/DPSK with Partial-band Noise Jamming and Frequency-Hopped Spread Spectrum

As in Table 8.4, one can categorize the performance of the SCCC with FH into four regions (Table 8.6) depending on the jamming noise power spectral density-to-AWGN ratio.

	Low SJR (< -4 dB)	High SJR (≥ -4 dB)
Low SNR (< 7 dB)	Region I: Medium Ni/No	Region II: Very low Ni/No
High SNR ($7 \leq$ SNR < 8 dB)	Region III: High Ni/No	Region IV: Medium Ni/No

Table 8.6.　　Jamming regions for SCCC/DPSK with frequency-hopped spread spectrum.

There are differences between Table 8.6 and Table 8.4. In Table 8.6, since the FH is able to reduce the jamming noise to a small level, low SJR implies less than –4 dB. Since for SNR > 8 dB, and –4 < SJR < 10 dB, all errors are corrected, the analysis for these conditions is not included in the table.

As in the case without FH, it is not effective to use very small ρ (0.001) to deny communications. The SCCC with FH is able to reduce the jamming effectiveness for very small ρ. The attacker will be most successful with $\rho = 1.0$ for SJR < –8 dB and SNR < 10 dB (Figure 8.7).

For Region I, since SJR is small, a moderately high jamming power with barrage jamming is effective with SJR < -4 dB. In Region II, barrage jamming is also the most effective. For Region III, $\rho = 0.1$ to 0.5 are effective for SJR < –4 dB (Figures 7.39 and 7.40). Region IV is not suitable for jamming since the high SNR negates the effects of jamming.

Thus, partial-band noise jamming is ineffective for SCCC/DPSK with FH and sufficient SNR (> 8 dB), and the best jamming strategy may be not to engage in partial-band noise jamming. For smaller SNR, the situation is more complicated. Partial-band noise jamming with $\rho < 0.01$ is ineffective. Partial-band noise jamming is only effective for $1 \geq \rho \geq 0.1$ and for SNR < 8 dB. For low SJRs, $\rho = 0.1$ to 0.5 are most effective. The most effective strategy for a jammer is to operate with a SJR of < -8 dB and $\rho = 0.5$.

7. Comparison of SCCC/BPSK and SCCC/DPSK

The performance of SCCC/BPSK and SCCC/DPSK with jamming and no side information for SNR = 8 dB is compared in Figure 8.8. We observe that for $\rho = 1.0$, there is a gain of about 8 dB at 10^{-2} for BPSK and for $\rho = 0.1$ a gain of more than 10 dB at 10^{-3}. With side information, the gain is 6.5 dB for $\rho = 1.0$ at 10^{-1} and more than 10 dB for $\rho = 0.1$ at 10^{-3} (Figure 8.9). With jamming and no side information and Rayleigh fading with no channel information, the difference is 6 dB for $\rho = 1.0$ at 10^{-2} and 10 dB for $\rho = 0.1$ at 10^{-3} for SNR = 10 dB (Figure 8.10). DPSK is less affected by Rayleigh fading than BPSK.

B. ANALYSIS FOR COMMUNICATIONS USER

Without jamming, the communications user will require at least 1.4 dB to achieve a BER of 10^{-5} using SCCC/BPSK with AWGN present and 4.5 dB when there is

Rayleigh fading and no channel information. A comparison of uncoded BPSK (DPSK) and SCCC/BPSK (DPSK) with AWGN and Rayleigh fading to achieve a BER of 10^{-5} is found in Table 8.7. For a 16-state Turbo codes with interleaver length of 1024 in AWGN, Hall and Wilson [Ref. 124] found that SCCC/BPSK has a 4 dB advantage over SCCC/DPSK.

	BPSK	SCCC BPSK	DPSK	SCCC DPSK
AWGN	9.5	1.4	10.3	6.7
AWGN and Fading	44	4.5	47	8

Table 8.7.   SNR (dB) required for BER of 10^{-5}.

Thus, if it is feasible, the communications user should use SCCC/BPSK instead of SCCC/DPSK.

With jamming and SCCC/BPSK, for communications to be effective, a user should operate with SI, i.e., knowledge of overall SNR in Region IV of Tables 8.1, 8.2, and 8.3. SCCC with SI is more effective for larger ρ than for smaller ρ. For small ρ ($\leq$ 0.01), the differences between SI and NSI are minimal. The SCCC with SI is also more effective for low SNR than for high SNR. For SNR = 2 dB and ρ = 0.1, the coding gain can be as large as 3 dB at 10^{-2} (Figure 5.27). If direct sequence spread spectrum is not used, the user should transmit with as large an SNR as possible. However, based on the simulation results, the SNR need not exceed 10 dB since a greater SNR does not improve the BER performance significantly regardless of SJR. If the user is denied communications by barrage jamming, he should increase its SJR so that the SJR is greater than 2 dB (for SNR > 10 dB) as shown in Figure 5.21. With Rayleigh fading, the SJR should be greater than 6 dB as shown in Figure 5.32. If the pulsed noise jamming is not 100%, the user can vary SJR to achieve the BER required as shown by Figure 5.12 and Figure 5.29 (with fading). SCCC/BPSK in a pulsed noise jamming and fading environment with side and channel information performs better than without. For lower SNRs (4 dB or less), the difference in BER is large (Figure 5.47). For higher SNRs, e.g.

at 8 dB, difference in performance narrows down to less than 1 dB (Figure 5.48). With DS, the user should operate with SNR greater than 4 dB (Figure 5.66).

For SNR < 6 dB, SCCC/DPSK with jamming is not a viable option. Similarly, for SCCC/DPSK, the communications user should operate in Region IV of Tables 8.4, 8.5, and 8.6, if possible. If not, the next best alternative is Region II. Since the jammer is most likely to use barrage jamming, the user should increase SNR to more than 10 dB and ensure that SJR is greater than 8 dB (Figure 8.5). With fading, SJR should be more than 10 dB (Figure 8.6). With a gain of only 0.5 dB, SI is not very useful for SCCC/DPSK; therefore, it is not necessary to incorporate it into the receiver. With FH, the user should operate with a SNR greater than 10 dB (Figure 8.7).

Apart from improving upon the factors affecting performance mentioned in Chapter II, other longer-term methods of improving performance are:

a.   Double SCCC. A double SCCC with two interleavers consists of the cascade of an outer encoder, an interleaver permuting the outer codeword bits, a middle encoder, another interleaver permuting the middle codeword bits, and an inner encoder whose input words are the permuted middle codewords. It has been shown [Ref. 125] that the double SCCC offer superior performance when maximum likelihood decoded. There is no need for large interleavers to obtain low bit error probability, as in turbo codes and SCCC, and as a consequence, the scheme can be adopted when high performance is sought at not so low SNR with a small decoding latency.

b.   Hybrid Concatenation. A hybrid-concatenated code is a combination of parallel and serially concatenated codes. Divsalar and Pollara [Ref. 126] have shown that the hybrid scheme offers better performance at very low BER.

c.   Quantization. For convolutional codes, as far as soft input is concerned, an 8-level quantization has been known to achieve a performance near the optimum performance achievable with an unquantized demodulator output. Several papers [Ref. 127, 128, 129] have shown that increasing the number of bits for quantization can improve the BER performance of SCCC by about 0.3 dB.

d.   Multilevel Codes. The benefits of powerful binary codes, especially turbo codes, can be transferred to any digital transmission scheme via multilevel coding [Ref. 130] if the individual rates are chosen according to the random coding bound criterion for the individual levels. Rate design from information theory in multi-level coding schemes requires powerful codes over a wide and fine tunable range of code rates. These requirements can be satisfied by turbo codes via puncturing. Application of turbo codes to multilevel coding schemes offer digital communication close to capacity limit for a wide range of trade-off between power and bandwidth efficiency.

e.   Improved bounds. For very low BER, better methods for predicting the performance can be found in [Ref. 131, 132, 133, 134].

C.   CONCLUSIONS

From the preceding discussion, barrage jamming is the best option for the jammer unless the overall signal-to-noise ratio is very high. In this case, ρ less than 1.0 may be appropriate.   However, very small ρ (< 0.01) is ineffective. With soft decisions, the jammer has a possible strategy of transmitting very narrow, high-amplitude pulses [Ref. 26]. However, such a jammer is quite easy to detect, and those symbols that are jammed could be erased. This would force the jammer to have a higher duty cycle and, thus, smaller amplitude pulses.

For the user, the best defense is to increase SNR or improve the factors affecting the performance of the SCCC as mentioned in Chapter II and in the preceding section. Side information works best for high values of ρ and low SJR for SCCC/BPSK. Side information is not very useful for SCCC/DPSK. A knowledge of the number of iterations required will reduce delay. Graphs such as those in Figures 3.17, 3.19, 3.22, 3.24, 3.27 will help to determine the number of iterations required for lowest BER with minimum delays.
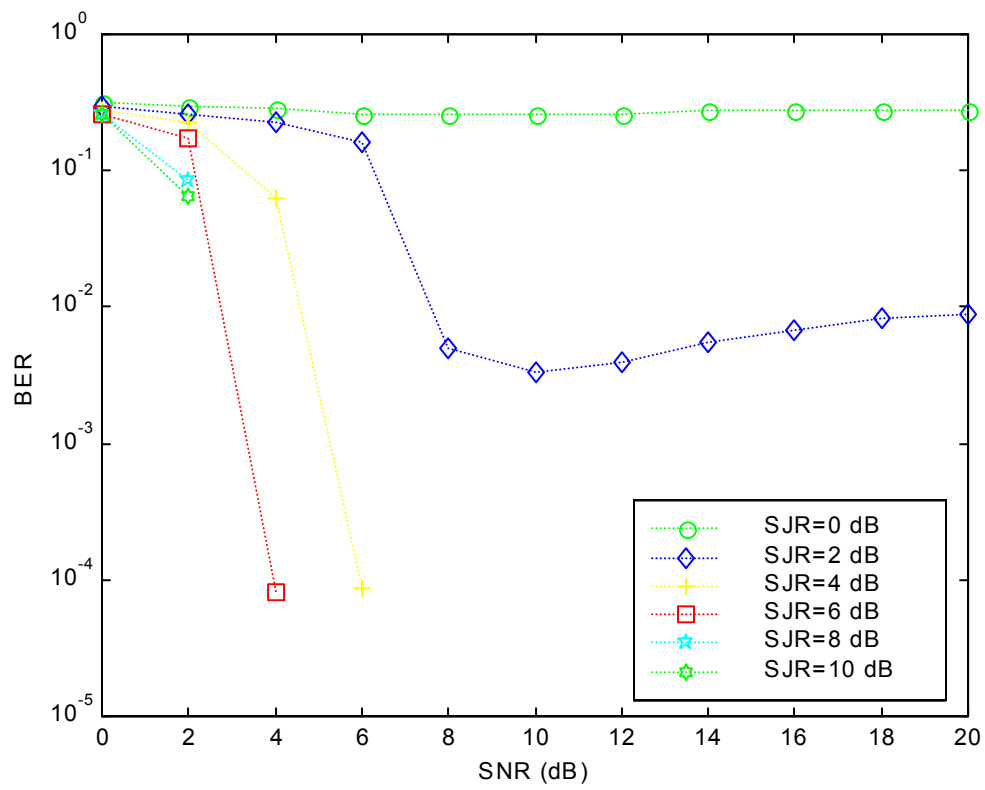
Figure 8.1.   Simulated SCCC/BPSK with AWGN and pulsed noise jamming with no side information: effect of SNR on BER for $\rho = 1.0$, SNR = 0 to 20 dB and SJR = 0 to 10 dB.
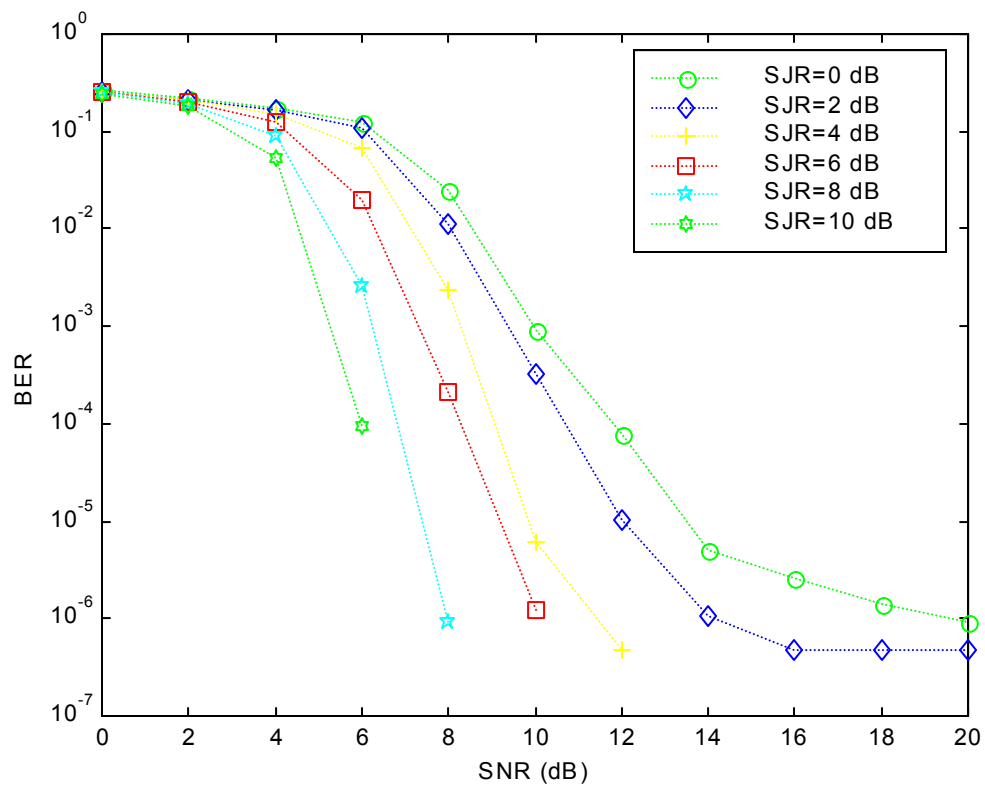
Figure 8.2.   Simulated SCCC/BPSK with AWGN, pulsed noise jamming with no side information and Rayleigh fading with no channel information: effect of SNR on BER for $\rho = 0.1$, SNR = 0 to 20 dB and SJR = 0 to 10 dB.
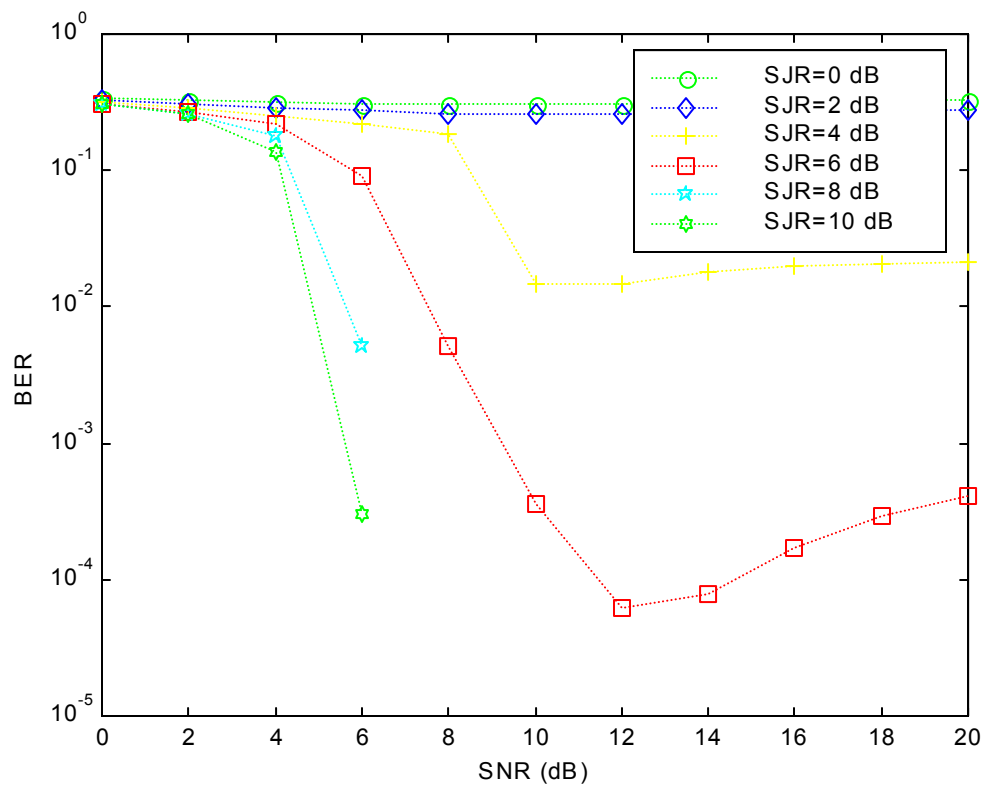
Figure 8.3.   Simulated SCCC/BPSK with AWGN, pulsed noise jamming with no side information and Rayleigh fading with no channel information: effect of SNR on BER for $\rho = 1.0$, SNR = 0 to 20 dB and SJR = 0 to 10 dB.
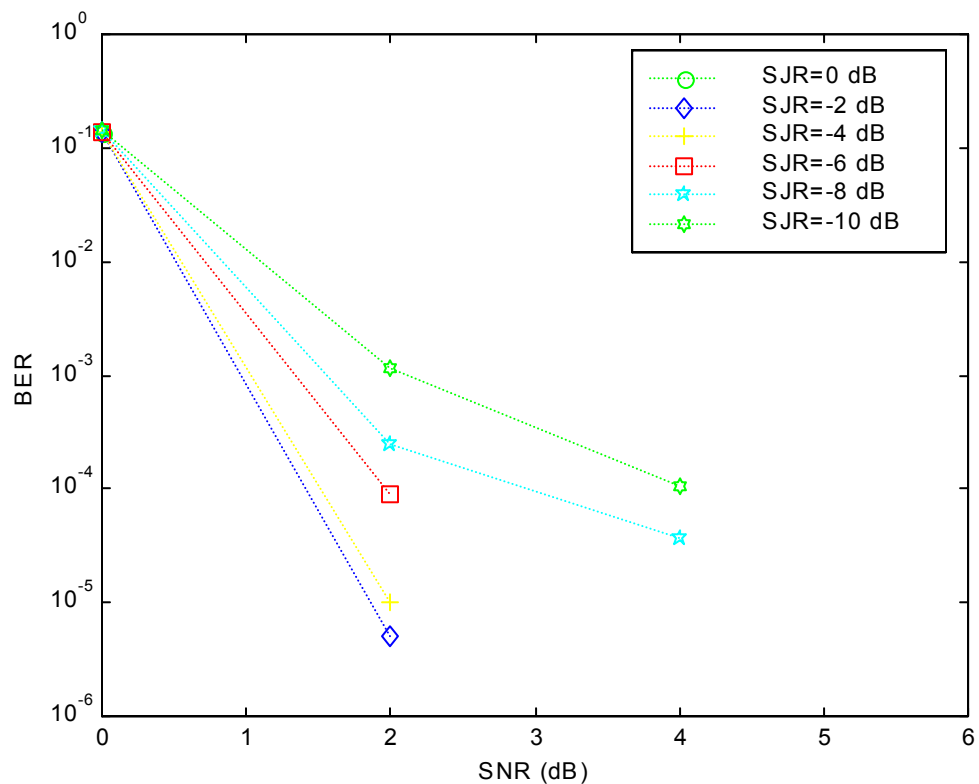
Figure 8.4.   Simulated SCCC/BPSK with AWGN, pulsed noise jamming with no side information and direct sequence spread spectrum: effect of SNR on BER for $\rho = 0.01$, SNR = 0 to 6 dB and SJR = -10 to 0 dB. Note that for SNR > 4 dB, all errors were corrected for the range of SJR considered.
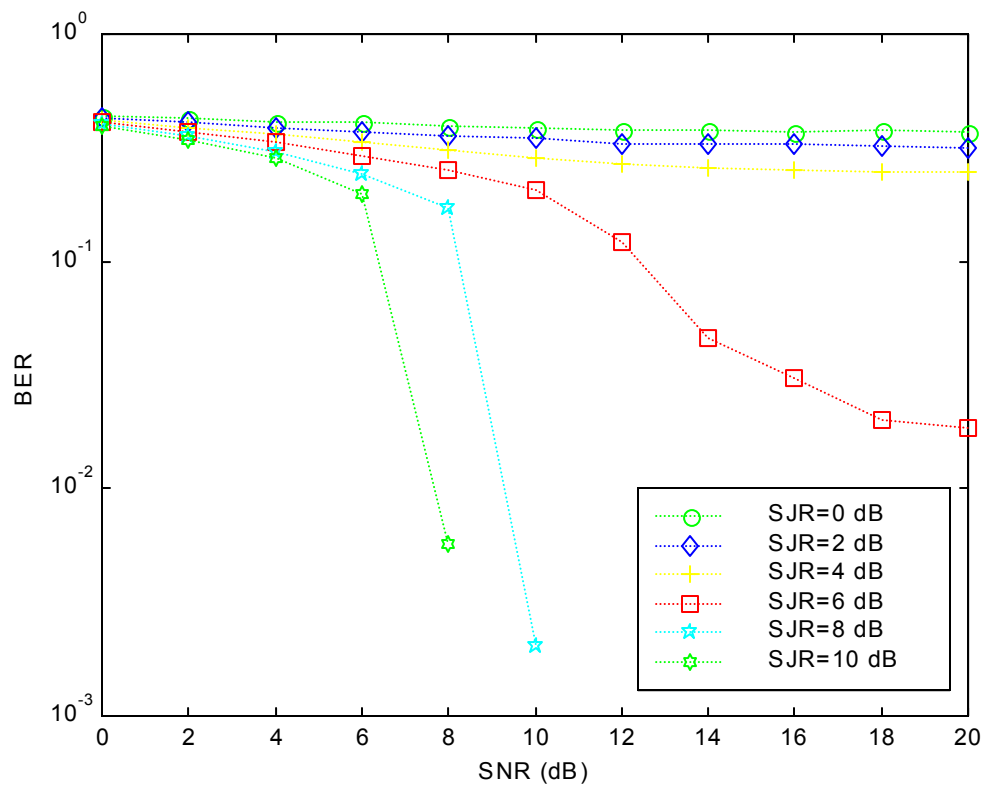
Figure 8.5. Simulated SCCC/DPSK with AWGN and partial-band noise jamming with no side information: effect of SNR on BER for $\rho = 1.0$, SNR = 0 to 20 dB and SJR = 0 to 10 dB.
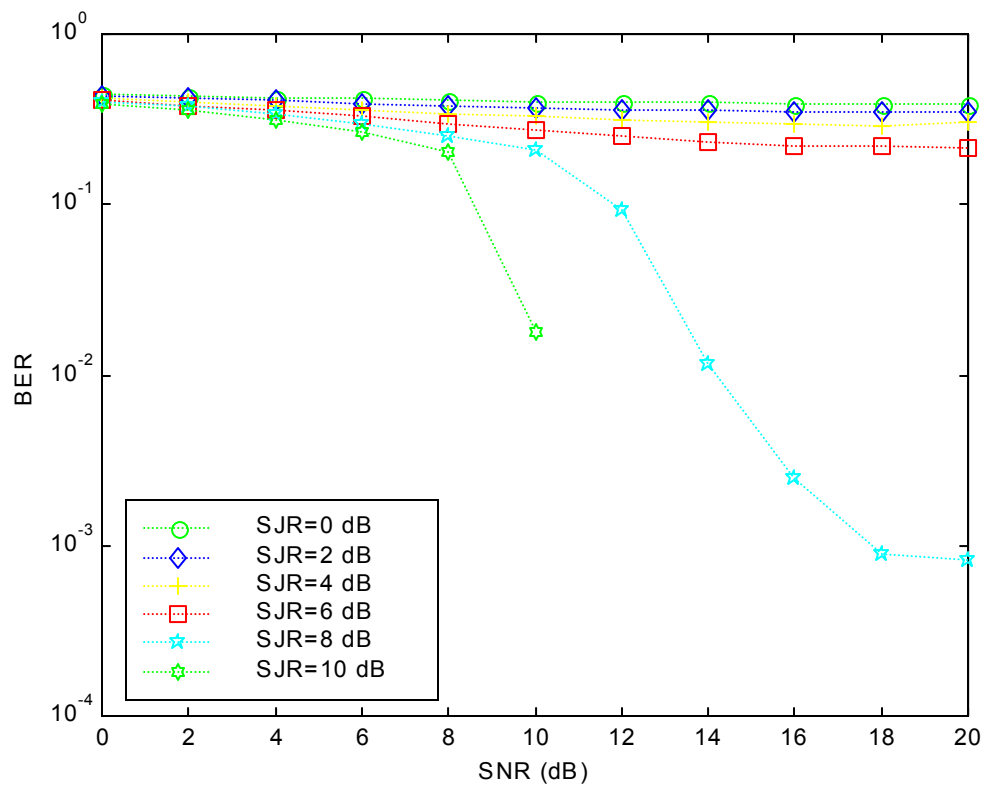
Figure 8.6.   Simulated SCCC/DPSK with AWGN, partial-band noise jamming with no side information and Rayleigh fading with no channel information: effect of SNR on BER for $\rho = 1.0$, SNR = 0 to 20 dB and SJR = 0 to 10 dB.
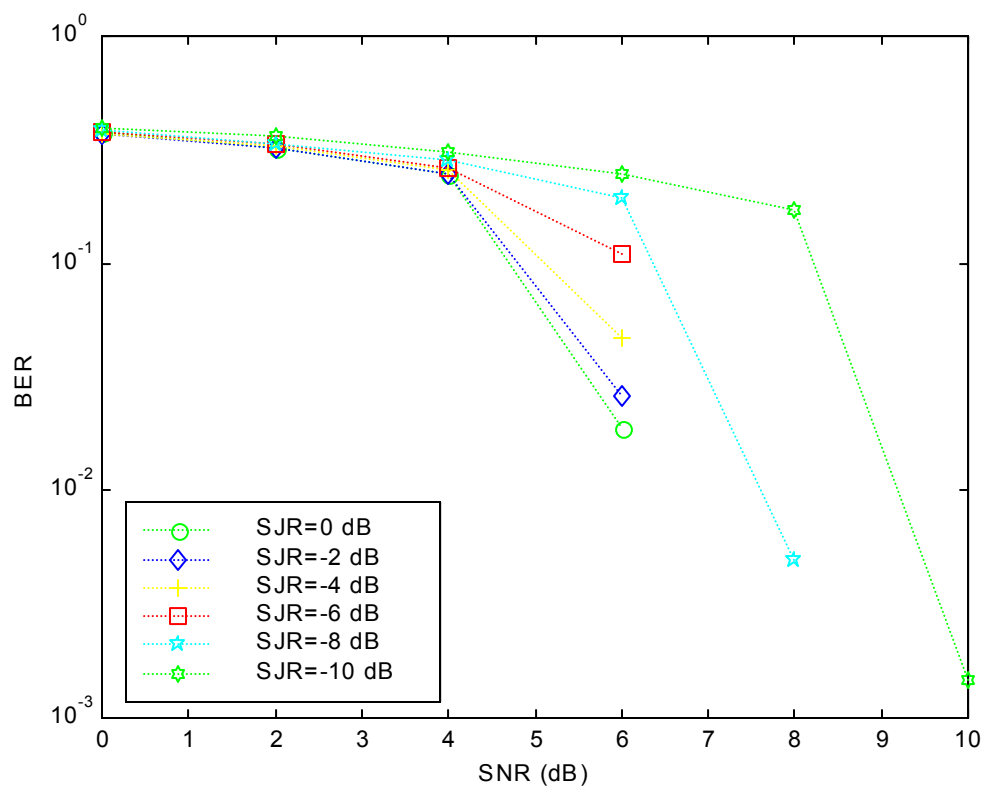
Figure 8.7. Simulated SCCC/DPSK with AWGN, partial-band jamming with no side information and frequency hopped spread spectrum: effect of SNR on BER for $\rho = 0.01$, SNR = 0 to 10 dB and SJR = -10 to 0 dB. Note that for SNR > 10 dB, all errors were corrected for the range of SJR considered.
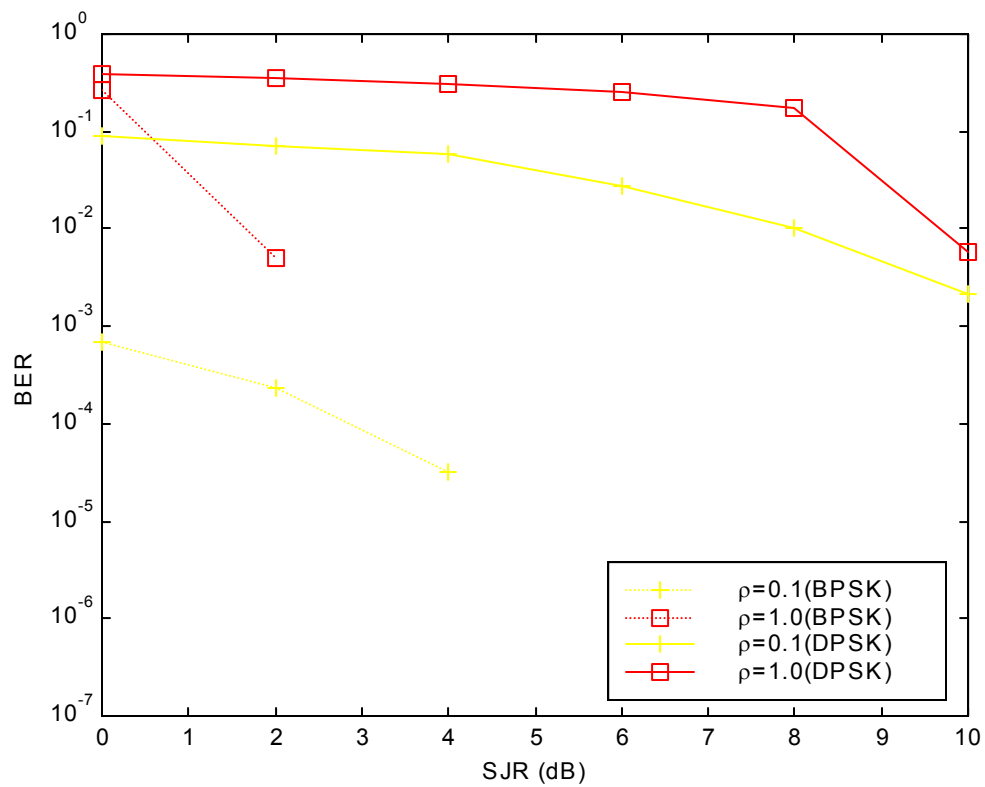
Figure 8.8.   Simulated SCCC with AWGN and pulsed noise jamming with no side information: effect of BPSK and DPSK modulation on BER for $\rho = 0.1$ and 1.0, SNR = 8 dB and SJR = 0 to 10 dB.
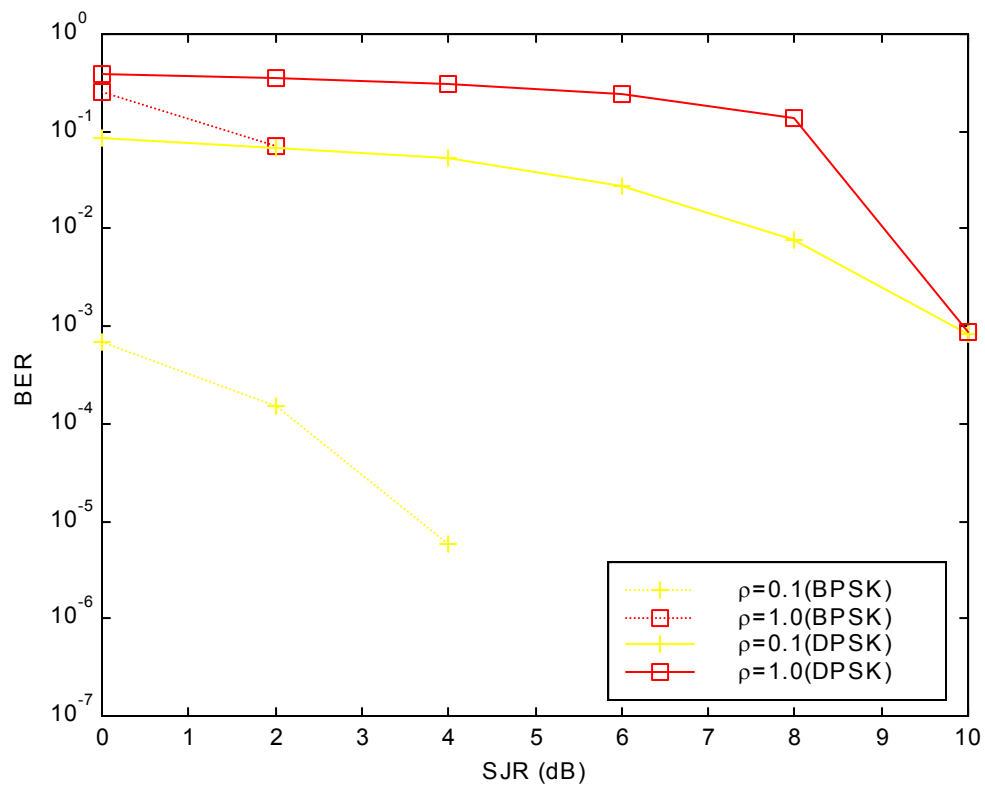
Figure 8.9.   Simulated SCCC with AWGN and pulsed noise jamming and side information: effect of BPSK and DPSK modulation on BER for ρ = 0.1 and 1.0, SNR = 8 dB and SJR = 0 to 10 dB.
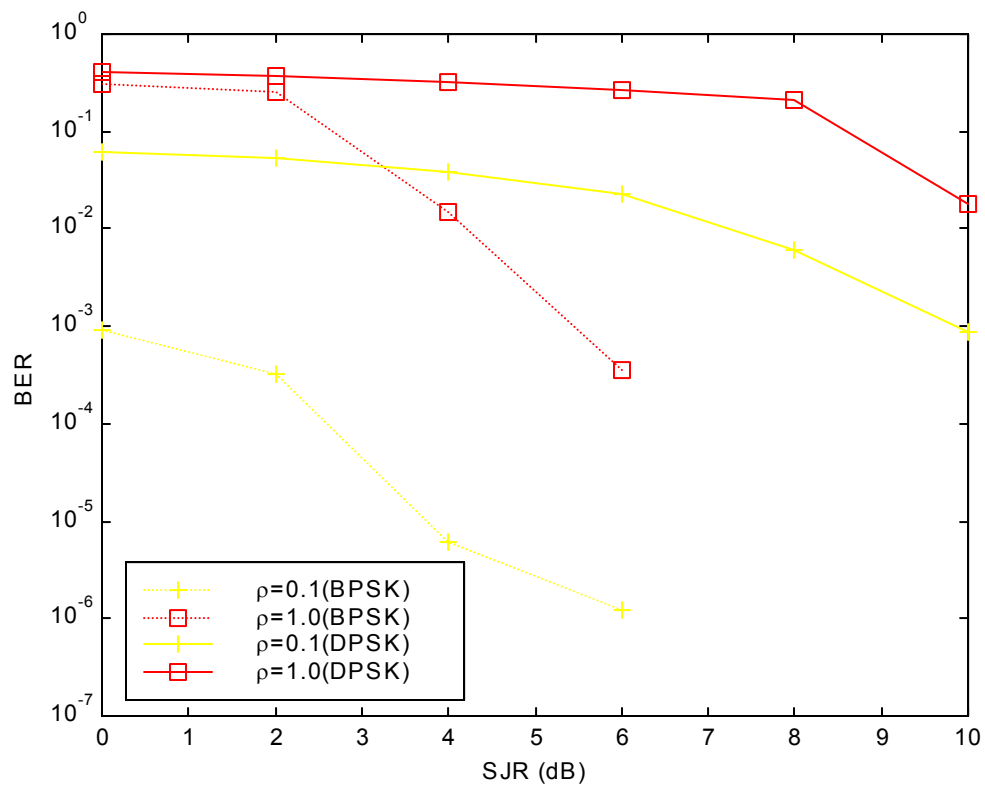
Figure 8.10. Simulated SCCC with AWGN, pulsed noise jamming with no side information and Rayleigh fading with no channel information: effect of BPSK and DPSK modulation on BER for $\rho = 0.1$ and 1.0, SNR = 10 dB and SJR = 0 to 10 dB.

IX.   CONCLUSIONS

A.   SUMMARY OF WORK

In this dissertation, the BER of serially concatenated convolutional codes (SCCC) with AWGN, noise jamming, Rayleigh fading, and spread spectrum are considered. For low signal-to-noise ratios, analytic solutions based on union bounds are found inaccurate. Thus, simulation results are used to obtain the BER. For higher signal-to-noise ratios, an average upper bound is developed. The bound serves to illustrate the achievable performance of SCCC. To the knowledge of the author, the theoretical bounds and simulations involving interference and Rayleigh fading for SCCC obtained in this dissertation have not been published before.

In Chapter II, the theoretical bounds of SCCC in AWGN and Rayleigh fading are obtained and analyzed. Chapter III describes the simulation model, design considerations as well as transmitter, channel, and receiver design. The theoretical BER results, based on this model, are obtained and compared with the simulation results for AWGN with and without Rayleigh fading. The BER of SCCC with binary phase shift keying (SCCC/BPSK) with no Rayleigh fading is compared with both Rayleigh fading without channel side information and Rayleigh fading with channel side information. For both simulated and theoretical results, SCCC/BPSK with Rayleigh fading and without channel side information performs the poorest and the SCCC/BPSK with no fading performs the best. However, all the results show a vast improvement in BER over the uncoded case when Rayleigh fading is present. Without channel information, SCCC/BPSK with Rayleigh fading requires about 2.5 dB more to obtain the same BER as SCCC/BPSK with no fading for large BER (10^{-2}). For small BER (10^{-8}), SCCC/BPSK with Rayleigh fading requires 7 dB more than SCCC/BPSK with no fading. Channel information offers one to two dB gain for SCCC/BPSK with Rayleigh fading.

Similarly, for both simulated and theoretical results, SCCC with differential phase shift keying (SCCC/DPSK) with Rayleigh fading without channel side information performs poorer than SCCC/DPSK with no fading. All results also show a vast

improvement in BER over the uncoded case in Rayleigh fading. SCCC/DPSK with no fading requires about 1.5 dB less than SCCC/DPSK with Rayleigh fading and without channel information for large BER. For small BER, SCCC/DPSK with no fading requires 4.5 dB less than SCCC/DPSK with Rayleigh fading. Without channel information, simulation results show that SCCC/BPSK has a coding gain advantage of 5 dB more than SCCC/DPSK for large BER.

The theoretical bounds for SCCC/BPSK with AWGN, pulse-noise jamming (with and without side information), Rayleigh fading (with and without channel information), and with and without direct sequence spread spectrum are obtained in Chapter IV. From the theoretical results, we found that SCCC/BPSK with direct sequence spread spectrum, side information, and channel information is the most effective in reducing the effects of jamming and fading. We also discover that side information works best for large values of ρ when SNR is low and small values of ρ when SNR is high. When fading is present, barrage jamming is most effective for lower SNRs and SJRs while smaller values of ρ are more effective for higher SNRs and SJRs.

In Chapter V, the simulation results for SCCC/BPSK are obtained and compared with their theoretical bounds. These results are also compared with the best rate 1/3 convolutional codes with four states and uncoded BPSK. The simulation results show that SCCC is effective in a jamming environment. SCCC with direct sequence spread spectrum and jamming side information makes it even more effective. The theoretical bounds were found not to be accurate for SNR (or SJR) below 2 or 3 dB, as expected. Rayleigh fading is most detrimental to SCCC/BPSK with jamming at small ρ and low SNR. Comparing the SCCC results with the best rate 1/3 convolutional code, we observe that for SJR < 0 dB, SCCC with no direct sequence spread spectrum does not perform as well as the convolutional code. However, with direct sequence spread spectrum, SCCC outperforms the convolutional code.

The theoretical bounds for SCCC/DPSK with AWGN, partial-band noise jamming (with and without side information), Rayleigh fading (without channel information), and with and without frequency-hopped spread spectrum are obtained in

Chapter VI. Similar to SCCC/BPSK, the theoretical results show that SCCC/DPSK with frequency-hopped spread spectrum and with side information is the most effective in reducing the effects of jamming. Moreover, side information works best for high values of ρ when SNR is low and low values of ρ when SNR is high. When fading is present, barrage jamming is the most effective for lower SNRs and SJRs, while smaller values of ρ are more effective at high SNRs and SJRs. Frequency-hopped spread spectrum works best for high values of ρ, i.e., barrage jamming and low overall SNR.

The simulation results show that SCCC/DPSK is not as effective in a jamming environment as SCCC/BPSK. SCCC/DPSK requires at least a SNR of 6 dB to avoid the region of high BER. For SCCC/DPSK without frequency-hopped spread spectrum, side information is less useful since DPSK modulation is dependent on previous consecutive bits; with frequency-hopped spread spectrum, a 0.5 dB gain is observed with side information. Without frequency-hopped spread spectrum, Rayleigh fading is most detrimental to SCCC/DPSK with jamming for $0.1 < \rho < 1.0$. Frequency-hopped spread spectrum improves the performance of SCCC/DPSK remarkably.

In Chapter VIII, we found that for each channel condition, four jamming regions can be identified. Based on these regions, the appropriate jamming policy or defensive measures can be devised. The performance of SCCC/BPSK and SCCC/DPSK for the different channel conditions is also compared in Chapter VIII. For barrage jamming, SCCC/BPSK has an advantage of about eight to ten dB for large BER. With jamming and Rayleigh fading with no channel information, the difference is 6 dB for barrage jamming for large BER. DPSK is less affected by Rayleigh fading than BPSK.

Barrage jamming appears to be the best option for the jammer unless the overall signal-to-noise ratio is very high. In this case, ρ less than 1.0 may be appropriate. However, very small values of ρ (< 0.01) are ineffective. Moreover, for such a jammer, it is quite easy to detect and erase jammed symbols. This forces the jammer to have a higher duty cycle and thus, smaller amplitude pulses.

For the user, the best defense is to increase SNR or improve the factors affecting the performance of the SCCC as mentioned in Chapter II and Chapter VIII. With the

same interleaver length, SCCC generally suffers longer delays than Turbo codes. However, knowing the minimum number of iterations necessary for the required BER can reduce these delays.

B. SUGGESTIONS FOR FUTURE WORK

SCCC decoding requires knowledge of the SNR of the received signal. In an ordinary AWGN channel, performance is optimized when the estimated SNR (side information) matches the actual channel SNR. One assumption that was made in this work is that precise estimates of the noise variance and fading amplitudes are available to the decoding algorithm. In some scenarios, e.g. fading, it is impossible to realistically utilize perfectly matched side information for decoding. In practical systems, the channel must be estimated at the receiver. Because of the low signal-to-noise ratios typical of SCCCs or Turbo code systems, it is difficult to obtain perfect estimates of the fading amplitudes. Thus, the performance of SCCC operating in fading environments will be degraded when the channel is estimated at the receiver. Several suggestions have been made to estimate the SNR for Turbo codes. Wang [Ref. 86] suggested using biased side information for Turbo codes while Valenti and Woener [Ref. 57] suggested using a Kalman filter. These suggestions can be incorporated into the SCCC.

Another assumption made in this dissertation is that the fades are fully interleaved, and thus, the fading amplitudes are statistically independent realizations of a Rayleigh random variable. In order for this assumption to be valid, a channel interleaver is required and must have a depth greater than the ratio t_c / T_s where t_c is the channel coherence time and T_s is the symbol duration. There are many instances when this requirement is not met, such as when communication is between a fixed base station and a slowly moving mobile. When the fading is very slow, the interleaver does not satisfactorily separate the fades and performance suffers. The effect of time-correlated Rayleigh fading channel on Turbo codes was examined by Hall and Wilson [Ref. 52]. However, Hall and Wilson did not include the effect of jamming on a Rayleigh fading

266

channel.   Future studies on time-correlated Rayleigh fading for SCCC/BPSK and SCCC/DPSK with interference are recommended.

While there are many studies that investigate the performance of Turbo codes over flat Rayleigh fading channels, we are not aware of similar studies concerning Rician fading in the presence of jamming. Rician fading arises when there is a direct component along with the diffuse energy, a situation that occurs where there is line-of-sight path in addition to non-line-of-sight. This type of fading is typically observed in micro-cellular urban and suburban land-mobile [Ref. 135], pico-cellular indoor [Ref. 136], and factory [Ref. 137] environments. It also applies to the dominant line-of-sight path of satellite [Ref. 138, 139] and ship-to-ship [Ref. 140] radio links.

THIS PAGE INTENTIONALLY LEFT BLANK

LIST OF REFERENCES

1.   D. J. Costello, J. Hagenauer, H. Imai and S. B. Wicker, "Applications of error-control coding," IEEE Transactions on Information Theory, Vol. 44, No. 6, October 1998.

2.   S. Benedetto, D. Divsalar, J. Hagenauer and L. Milstein, "Concatenated coding techniques and iterative decoding: Sailing towards channel capacity," IEEE Journal on Selected Areas in Communications, Vol. 16, No. 2, February 1998.

3.   P. Elias, "Error-free coding," IEEE Transactions on Information Theory, Vol. IT-4, pp. 29-37, September 1954.

4.   S. Hirasawa et al., "Modified product codes," IEEE Transactions on Information Theory, Vol. IT-30, pp. 299-306, March 1984.

5.   G. D. Forney, Jr., *Concatenated Codes*, Cambridge, MA: M.I.T. Press, 1966.

6.   G. Battail, C. Berrou, and A. Clavieux, "Pseudo-random recursive convolutional coding for near-capacity performance," Proceedings of IEEE Global Telecommunications Conference, Vol. 4, pp. 23-27, 1993.

7.   C. Berrou and A. Glavieux, "Turbo-codes: General principles and applications," Proceedings of 6th International Tirrenia Workshop on Digital Communications, Tirrenia, Italy, September 1993.

8.   C. Berrou, A Glavieux and P. Thitimajshima, "Near Shannon limit error-correcting coding and decoding: Turbo codes," Proceedings of IEEE International Conference on Communications, Vol. 2, pp. 1064-1070, May 1993.

9.   J. Lodge, "Separable MAP filters for the decoding of product and concatenated codes," Proceedings of IEEE International Conference on Communications, Vol. 3, pp. 1740-1745, May 1993.

10.   L. Bahl, J. Cocke, F. Jelinek and J. Raviv, "Optimal decoding of linear codes for minimizing symbol error rate," IEEE Transactions on Information Theory," vol. IT-20, pp. 284-287, March 1974,

11.   J. Lodge, R. Yound, P. Hoeher, and J. Hagenauer, "Separable MAP 'filters' for the decoding of product and concatenated codes," Proceedings of IEEE International Conference on Communications, pp. 1740-1745, May 1993.

12.   S. Benedetto, and G. Montorsi, "Unveiling turbo codes: Some results on parallel concatenated coding schemes," IEEE Transactions on Information Theory, Vol. 42, pp. 409-428, March 1996.

13.   S. Benedetto, and G. Montorsi, "Design of parallel concatenated convolutional codes," IEEE Transactions on Communications, Vol. 44, pp. 591-600, May 1996.

14.   D. Divsalar and F. Pollara, "On the design of turbo codes," JPL TDA Progress Report, Vol. 42-123, November 15, 1995.

15.   S. Benedetto, D. Divsalar, G. Montorsi and F. Pollara, "Serial concatenation of interleaved codes: Performance analysis, design and iterative decoding," JPL TDA Progress Report, Vol. 42-126, August 15, 1996.

16.   D. J. C. MacKay and R. M. Neal, "Near Shannon limit performance of low density parity check codes," IEEE Electronic Letters, Vol. 32, pp.1645-1646, August 1966.

17.   J. Hagenauer, F. Burkert, and H. Nicki, "The race to Shannon's limit: Discipline high-rate codes," Proceedings of International Symposium on Turbo Codes and Related Topics, pp. 239-242, September 1997.

18.   J. Hagenauer, E. Offer, and L. Papke, "Iterative decoding of binary block and convolutional codes," IEEE Transactions on Information Theory, Vol. 42, pp. 429-445, March 1996.

19.   J. Hagenauer and P. Hoeher, "Concatenated Viterbi decoding," Proceedings of 4th Joint Swedish-Soviet International Workshop on Information Theory, pp. 29-33, August 1989.

20.   S. Benedetto, D. Divsalar, G. Montorsi, F. Pollara, "Serial concatenation of interleaved codes: Performance analysis, design and iterative decoding," IEEE Transactions on Information Theory, Vol. 44, pp. 909-926, May 1998.

21.   S. Benedetto, L. Gaggero, R. Garello and G. Montorsi, "On the design of binary serially concatenated convolutional codes," Proceedings of Communication Theory Mini-Conference, pp. 32 –36, 1999.

22.   S. Benedetto and G. Montorsi, "Iterative decoding of serially concatenated convolutional codes," IEEE Electronic Letters, Vol. 32, No. 13, pp. 1186-1188, 1996.

23.   S. Benedetto, D. Divsalar, G. Montorsi and F. Pollara, "Iterative decoding of serially concatenated codes with interleavers and comparison with Turbo codes," Proceedings of IEEE Global Telecommunications Conference, Vol. 2, pp. 654-658, 1999.

24.   S. Benedetto and G. Montorsi, "Design of parallel concatenated convolutional codes," IEEE Transactions on Communications, Vol. 44, pp. 5, 1996.

25.   B. K. Levitt and J. K. Omura, "Coding tradeoffs for improved performance of FH/MFSK systems in partial band noise," in Proceedings of National Telecommunication Conference, pp. D9.1.1-D9.1.5, December 1981

26.   J. K. Omura and B. K. Levitt, "Coded error probability evaluation for anti-jam communication systems," IEEE Transactions on Communications, Vol. COM-30, pp. 896-903, May 1982.

27.   H. H. Ma and M. A. Poole, "Error-correcting codes against the worst case partial band jammer," IEEE Transactions on Communications, Vol. COM-32, pp. 124-133, February 1984.

28.   A. J. Viterbi and I. M. Jacobs, "Advances in coding and modulation for non-coherent channels affected by fading partial band, and multiple access interference," Advances in Communication Systems, Vol. 4, pp. 279-308, 1975.

29.   J. S. Lee, R. H. French and L. E. Miller, "Error-correcting codes and non-linear diversity combining against worst case partial-band noise jamming of frequency-hopping MFSK systems," IEEE Transactions on Communications, Vol. 36, No. 4, April 1988.

30.   W. E. Stark, "Coding for frequency-hopped spread spectrum communication with partial band interference – Part II: Coded performance," IEEE Transactions on Communications, Vol. COM-33, No. 10, pp. 1045-1057, October 1985.

31.   C. Liang and W. E. Stark, "Turbo codes in DS-SS with adaptive nonlinear suppression of impulsive interference," Proceedings of IEEE Military Communications Conference, Vol. 1, pp. 408 –412, 1999.

32.   B. R. Vojcic and R. L. Pickholtz, "Performance of direct sequence spread spectrum in a fading dispersive channel with jamming," IEEE Journal on Selected Areas in Communications, Vol. 7, pp. 561-568, May 1989.

33.   B. R. Vojcic and R. L. Pickholtz, "Performance of coded direct sequence spread spectrum in a fading dispersive channel with pulsed jamming," IEEE Journal on Selected Areas in Communications, Vol. 8, pp. 934-942, June 1990.

34 .   W. E. Stark, "Coding for frequency-hopped spread spectrum communication with partial band interference – Part II: Coded performance," IEEE Transactions on Communications, Vol. COM-33, No. 10, pp. 1045-1057, October 1985.

35.   B. Sklar, *Digital Communications Fundamentals and Applications*, pp. 166, Prentice Hall, New Jersey, 1988.

36.   R. L. Peterson, R. E. Ziemer and D. E. Borth, *Introduction to Spread Spectrum Communications*, Prentice Hall, New Jersey, 1995.

37.   R. H. Deng and D. J. Costello, "High rate concatenated coding systems using bandwidth efficient trellis inner codes," IEEE Transactions on Communications, Vol. 37, pp. 420-427, May 1989.

38.   J. Hagenauer and P. Hoeher, "A Viterbi algorithm with soft-decision outputs and its applications," Proceedings of IEEE Global Telecommunications Conference, pp 1680-1686, 1989.

39.   H. Yang, S. Yoon and C. Kang, " Iterative decoding of serially concatenated convolutional codes applying the SOVA," Proceedings of 48th IEEE Vehicular Technology Conference, Vol. 1, pp. 353-357, 1998.

40.   J. Hagenauer, "Source-controlled channel decoding, " IEEE Transactions Communications Theory, Vol. 43, No. 9, pp. 2449-2457, September 1995.

41.   C. Berrou, P. Adde, E. Angui and S. Faudeil, "A low complexity soft-output Viterbi decoder architecture," Proceedings of IEEE International Conference on Communications, pp. 737-740, November 1993.

42.   S. Benedetto and G. Montorsi, "Serial concatenation of interleaved codes: performance analysis, design and iterative decoding," TDA Progress Report 42-126, pp. 1-26, August 15, 1996.

43.   S. Benedetto and G. Montorsi, "A soft-input soft-output maximum a posteriori (MAP) module to decode parallel and serial concatenated codes," TDA Progress Report 42-127, pp. 1-20, November 15, 1996.

44.   A. Ghrayeb and W. Ryan, "Performance of high rate turbo codes employing the soft-output Viterbi algorithm (SOVA)," Proceedings of 33rd Asilomar Conference, Vol. 2, pp. 1665-1669, 1999.

45.   S. Benedetto, D. Divsalar, G. Montorsi and F. Pollara, "A soft-input soft-output APP module for iterative decoding of concatenated codes," IEEE Communications Letter, Vol. 1, No. 1, pp. 22-24, January 1977.

46 .   R. J. McEliece, "On the BCJR trellis for linear block codes," IEEE Transactions on Information Theory, Vol. 42, pp. 1072-1091, July 1996.

47.   P. Robertson, E. Villebrun and P. Hoeher, "A comparison of optimal and suboptimal MAP decoding algorithms operating in the log domain," Proceedings of IEEE International Conference on Communications, Vol. 2, pp. 1009-1013, 1995.

48.   S. Benedetto, D. Divsalar, G. Montorsi and F. Pollara, "Soft-input soft-output building blocks for the construction and distributed iterative decoding of code networks, European Transactions on Telecommunications, April 1998.

49 .   D. Divsalar and F. Pollara, "Turbo codes for PCS applications," Proceedings of IEEE International Conference on Communications, Vol. 1, pp. 54-59, 1995.

50.   S. Benedetto, E. Biglieri, and V. Castellani, *Digital Transmission Theory*, Prentice Hall, Eaglewood Cliffs, New Jersey, 1987.

51.   J. G. Proakis, *Digital Communications*, McGraw Hill, Inc, New York, pp. 489, 1995.

52.   E. K. Hall and S. G. Wilson, "Design and analysis of turbo codes on Rayleigh fading channels," IEEE Journal on Selected Areas in Communications, Vol. 16, No. 2, February 1998.

53.   C. C. Wang, "Improving faded Turbo code performance using biased channel side information," Proceedings of IEEE Military Communications Conference, Vol. 1, pp. 543-546, 1999.

54.   R. Kennedy, *Fading Dispersive Communication Channels*, Wiley-Interscience, 1969.

55.   J. Hagenauer, "Viterbi decoding of convolutional codes for fading and burst-channels," Proceedings of International Zurich Seminar, 1980.

56.   C. L. Wang, J. M. Hsu and T. Y. Chang, "Performance of Turbo codes in Rayleigh fading channels with adaptive channel estimation," IEEE International Conference on Communications, Vol. 3, pp. 1665-1669, 2000.

57.   M. C. Valenti and B. D. Woerner, "Performance of Turbo codes in interleaved flat fading channels with estimated state information," Proceedings of 48th IEEE Vehicle Technology conference, Vol. 1, pp. 66-70, 1998.

58.   J. K. Cavers, "An analysis of pilot symbol assisted modulation for Rayleigh fading channels," IEEE Transactions on Vehicle Technology, Vol. 40, pp. 686-693, Nov 1991.

59.   M. C. Valenti and B. D. Woerner, "Refined channel estimation for coherent detection of Turbo codes over flat fading channels," Electronic Letters, Vol. 34, pp. 1648-1649, August 1998.

273

60.   J. W. Modestino and S. Y. Mui, "Convolutional code performance in the Rician fading channel," IEEE Transactions on Communication Technology, Vol. COM-24, pp. 592-606, 1976.

61.   F. Babich, G. Montorsi and F. Vatta, "Transfer function bounds on Turbo codes performance in the Rician fading channel," IEEE International Conference on Communications, Vol. 1, pp. 108-112, 1999.

62.   S. A. Al-Semari and M. Abulbashar, "Exact calculation of the union bound for the performance of turbo codes over fading channels," Proceedings of IEEE Wireless Communications and Networking Conference, Vol. 1, pp. 457-460, 1999.

63.   O. C. Yue, "Useful bounds on the performance of a spread-spectrum mobile communication system in various fading environments," IEEE Transactions on Communications, Vol. COM-28, No. 10, pp. 1819-1823, October, 1980.

64.   W. C. Lindsey, "Error probabilities for Rician fading multichannel reception of binary and N-ary signals," IEEE Transactions on Information Theory, Vol. IT-10, pp. 339-250, October 1964.

65.   A. S. Barbulescu and S. S. Pietrobon, "Interleaver design for Turbo codes," IEEE Electronics Letters, Vol. 30, No. 25, pp. 2107-2108, December 1994.

66.   K. Koora and H. Betzinger, "Interleaver design for Turbo codes with selected inputs," IEEE Electronics Letters, Vol. 34, No. 7, pp. 651, April 1998.

67.   B. He and M. Z. Wang, "Interleaver design for Turbo codes," Proceedings of IEEE International Conference on Information, Communications and Signal Processing, Vol. 1, pp. 453-455, September 1997.

68.   J. Hokfelt, O. Edfors and T. Maseng, "Interleaver design for Turbo codes based on the performance of iterative decoding," Proceedings of IEEE International Conference on Communications, Vol. 1, pp. 93-97, 1999.

69.   M. Namokel, " Error performance bounds of turbo-codes employing non-uniform interleavers," Proceedings of IEEE International Conference on Personal Wireless Communication, pp. 404-408, 1999.

70.   F. Daneshgaran and M. Mondin, "Design of interleavers for Turbo codes: Iterative interleaver growth algorithms of polynomial complexity," IEEE Transactions on Information Theory, Vol. 45, No. 6, pp. 1845-1859, September 1999.

71.   A. K. Khandani, "Design of Turbo code interleaver using the Hungarian method," IEEE Electronic Letters, Vol. 34, No. 1, pp. 63-65, January 1998.

72. J. Yuan, B. Vucetic and W. Feng, "Combined Turbo codes and interleaver design," IEEE Transactions on Communications, Vol. 47, No. 4, pp. 484-487, April 1999.

73. C. Heegard and S. Wicker, *Turbo Coding*, pp. 47-53, Kluwer Academic Publishers, Massachusetts, 1999.

74. R. Achiba and M. Mortazavi, "Turbo code performance and design trade-offs," Proceedings of IEEE Military Communications Conference, Vol. 1, pp. 174-180, 2000.

75. G. Battail, "A conceptual framework for understanding Turbo codes," IEEE Journal on Selected Areas in Communications, Vol. 16, No. 2, pp. 245-254, February 1998.

76. S. Benedetto and G. Montorsi, "Performance of continuous and blockwise decoded turbo codes," IEEE Communications Letters, Vol. 1, No. 3, May 1997.

77. E. K. Hall and S. G. Wilson, "Stream oriented Turbo codes," Proceedings of 48th IEEE Vehicular Technology Conference, Vol. 1, pp. 71-75, 1998.

78. N. Chayat, "Turbo codes for incoherent M-ary orthogonal signaling," Proceedings of Nineteenth Convention of Electrical and Electronics Engineers in Israel, pp. 471-474, 1996.

79 J. Hagenauer, "Rate-compatible punctured convolutional codes (RCPC codes) and their applications," IEEE Transactions on Communications, Vol. 36, No. 4, pp. 389-400, April 1988.

80. O. F. Acikel and W. E. Ryan, "Punctured high rate SCCCs for BPSK/QPSK channels," Proceedings of IEEE International Conference on Communications, Vol. 1, pp. 434-439, 2000.

81. E. K. Hall, "Performance and design of Turbo codes on Rayleigh fading channels," Master's thesis, University of Virginia, Charlottsville, 1996.

82. I. Sason and S. Shamai, "Improved performance bounds on the ML decoding error probability of parallel and serial concatenated Turbo codes via their ensemble distance spectrum," IEEE Transactions on Information Theory, Vol. 46, No.1, pp. 24-47, January 2000.

83. C. Wang, "On the performance of Turbo codes," Proceedings of IEEE Military Communications Conference, Vol. 3, pp. 987-992, 1998.

84. A. J. Viterbi, "Convolutional codes and their performance in communications systems," IEEE Transactions on Communication Technology, Vol. COM-19, Oct 1971.

85.   J. Gass, "Performance of a frequency-hopped system with Turbo trellis-coded modulation in partial band interference," Proceedings of IEEE Military Communications Conference, Vol. 2, pp. 866-870, 2000.

86.   C. Wang, "On the optimization of channel side information for Turbo decoding," Proceedings of IEEE Aerospace Conference, Vol. 1, pp. 311-315, 2000.

87.   G. Poltyrev, "Bounds on the decoding error probability of binary linear codes via their spectra," IEEE Transactions on Information Theory, Vol. 40, pp. 1284-1292, July 1994.

88.   A. J. Viterbi and J. K. Omura, *Principles of Digital Communication and Coding*, McGraw-Hill, New York, 1979.

89.   T. M. Duman and M. Salehi, "New performance bounds for Turbo codes," Proceedings of IEEE Global Telecommunications Conference, Vol. 2, pp. 634-638, 1997.

90.   P. Frenger, "Turbo decoding on Rayleigh fading channels with noisy channel estimates," Proceedings of 49th IEEE Vehicular Technology Conference, Vol. 2, p 884-888, 1999.

91.   P. Frenger, "Turbo decoding for wireless systems with imperfect channel estimates," IEEE Transactions on Communications, Vol. 48, No. 9, pp. 1437-1440, September 2000.

92.   A. J. Viterbi, "Spread spectrum communications – Myths and realities," IEEE Communication Society Magazine, Vol. 17, pp. 11-18, May 1979.

93.   J. K. Omura and B. K. Levitt, "Coded error probability evaluation for anti-jam communication systems," IEEE Transactions on Communications, Vol. COM-30, No 5, May 1982.

94.   J.K. Juntti, P.A. Leppanen, "Performance of a convolutionally coded hard-decision DS receiver in pulsed noise interference," Proceedings of IEEE Military Communications Conference, Vol. 1, pp. 267-272, 1991.

95.   M. A. Jordan, "Turbo code performance in partial-band jamming," Proceedings of IEEE Military Communications Conference, Vol. 3, pp. 982-986, 1998.

96.   J. H. Kang and W. E. Stark, "Turbo codes for coherent FH-SS with partial band interference," Proceedings of IEEE Military Communication Conference, Vol. 1, pp. 5-9, 1997.

97.   J. S. Lee, R. H. French and L. E. Miller, "Error-correcting codes and nonlinear diversity combining against worst case partial-band noise jamming of frequency-hopping

MFSK systems," IEEE Transactions on Communications, Vol. 36, No. 4, pp. 471-478, April 1988.

98.   R. C. Clark, H. Iwasaki and M. Kragh, "Performance of a fast frequency-hopped noncoherent MFSK receiver with non-ideal adaptive gain control," IEEE Transactions on Communications, Vol. 46, No. 1, pp. 104-114, January 1998.

99.   S. Benedetto and E. Biglieri, *Principles of digital transmission with wireless applications*, pp. 716, Kluwer Academic, New York, 1999.

100.   D. Divsalar, S. Dolinar, and F. Pollara, "Transfer function bounds on the performance of Turbo codes," Telecommunication and Data Acquisition Progress Report 43-122, Jet Propulsion Laboratory, August 1995.

101.   T. A. Summers, and S. G. Wilson, "SNR mismatch and online estimation in turbo decoding," IEEE Transactions on Communications, Vol. 46, No. 4, pp. 421-423, April 1998.

102.   J. G. Dunham and K. H. Tzou, "Performance bounds for convolutional codes with digital Viterbi decoders in Gaussian noise," IEEE Transactions on Communications, Vol. COM-31, No. 10, pp. 1124-1132, October, 1983.

103.   A. Worm, P. Hoeher and N. Wehn, "Turbo decoding without SNR estimation," IEEE Communications Letters, Vol. 4, Issue 6, pp. 193-195, June 2000.

104.   M. A. Jordan and R. A. Nichols, "The effects of channel characteristics on turbo code performance," Proceedings of IEEE Military Communications Conference, pp. 17-21, October 1996.

105.   P. A. Bello and B. P. Nelin, "The influence of fading spectrum on the binary error probabilities of incoherent and differentially coherent matched filter receivers," IRE Transactions, CS-10, pp. 160-168, 1962.

106.   M. K. Simon, J. K. Omura, R. A. Scholtz, and B. K. Levitt, *Spread spectrum communications, Vol. 1, 2, 3*, Computer Science Press, Rockville, Maryland, 1985.

107.   W. C. Lindsey, S. H. An and R. M. Vacek, "Performance of M-ary FH-DPSK systems in the presence of jamming," Proceedings of IEEE Military Communications Conference, pp. 34.2.1-34.2.5, 1988.

108.   Y. T. Su, "Decoding metrics for slow frequency-hopped DPSK systems," IEE Proceedings-I, Vol. 39, No. 5, October 1992.

109.   S. W. Houston, "Modulation techniques for communication – Part I: Tone and noise jamming performance of spread spectrum M-ary FSK and 2, 4-ary DPSK

waveforms," Proceedings of IEEE National Aerospace Electronics Conference, pp. 51-58, June 1975.

110.　G. R. Cooper and R. W. Nettleton, "A spread spectrum technique for high-capacity mobile communications,' IEEE Transactions on Vehicular Technology, VT-27, pp. 264-275, 1978.

111.　M. Matsumoto and G. R. Cooper, "Performance of a non-linear FH-DPSK spread-spectrum receiver with multiple narrow band interfering signals," IEEE Transactions on Communications, COM-30, pp. 937-942, 1982.

112.　Y. T. Su, "Anti-jam performance of a FH/DPSK system (I)," LinCom Corporation, TM-8520-25, 1987.

113.　J. S. Lee and L. E. Miller, "Error probability analysis of differential phase-shift-keyed/frequency hopping spread–spectrum communications in the partial-band noise jamming environments," IEEE Transactions on Communications, COM-30, pp. 943-952, 1982.

114.　R. A. Yost, "On the symbiotic nature of key anti-jamming and anti-scintillation functions fro MFSK and DPSK channels," IEEE Journal on Selected Areas in Communications, Vol. 8, pp. 887-894, 1990.

115.　J. H. Kang and W. E. Stark, "Performance of Turbo-coded FH-SS with partial-band interference and Rayleigh fading," Proceedings of IEEE Military Communications Conference, Vol. 3, pp. 977-981, 1998.

116.　J. S. Lee, R. H. French and L. E. Miller, "Probability of error analyses of a BFSK frequency-hopping system with diversity under partial-band noise jamming interference – Part I: Performance of square-law linear combining soft decision receiver," IEEE Transactions on Communications, Vol. COM-32, No. 6, June 1986.

117 .　T. W. Tedesso and R. C. Robertson, "Performance analysis of a SFH/ NCBFSK communications system with rate ½ convolutional coding in the presence of partial-band noise jamming," Proceedings of IEEE Military Communications Conference, Vol. 2, pp. 484-488, 1998.

118.　R. C. Robertson, K. Y. Lee, "Performance of slow frequency-hopped MFSK receivers with linear and self normalization combining in a Ricean fading channel with partial-band interference," IEEE Journal on Selected Areas in Communications, Vol. 10, No 4, pp. 731-741, May 1992.

119.　R. C. Robertson and T. T. Ha, "Error probabilities of slow frequency-hopped MFSK with noise normalization combining in a fading channel with partial-band

interference," IEEE Transactions on Communications, Vol. 40, No. 2, pp. 404-412, February 1992.

120.   R. C. Robertson, I. Hidetoshi, and K. Melody, "Performance of a slow frequency-hopped non-coherent MFSK receiver with non-ideal adaptive gain control," IEEE Transactions on Communications, Vol. 46, No. 1, pp. 104-114, January 1998.

121.   R. S. Simon, M. T. Stroot and G. H. Weiss, "Numerical inversion of Laplace transforms with applications to percentage labeled mitoses experiments," Comput. Biomed. Res., Vol. 5, pp. 596-607, 1972.

122.   W. H. Press, S. A. Teukolsky , W. T. Vetterling and B. P. Flannery, *Numerical Recipes in Fortran*, Cambridge University Press, New York, 1992.

123.   M. D. Theodoss and R. C. Robertson, "Performance of the FFH/BFSK self-normalized receiver with convolutional coding and soft decision decoding over Rician fading channel with partial-band noise interference," Proceedings of IEEE Military Communications Conference, Vol. 2, pp. 436-441, 1996.

124.   E. Hall and S. G. Wilson, "Turbo codes for noncoherent channels," IEEE Globecom 1997 - 6th Communication Theory Mini-conference, Phoenix, AZ, USA.

125.   S. Benedetto, D. Divsalar, G. Montorsi, F. Pollara, "Analysis, design, and iterative decoding of double serial concatenated codes with interleavers," IEEE Journal on Selected Areas in Communications, Vol. 16, pp. 231-244, February 1998.

126.   D. Divsalar and F. Pollara, "Hybrid concatenated codes and iterative decoding," Proceedings of IEEE International Symposium on Information Theory, pp. 10, 1997.

127.   G. Jeong and D. Hsia, "Optimal quantization for soft decision turbo decoder," Proceedings of 50th IEEE Vehicular Technology Conference, Vol. 3, pp. 1620-1624, 1999.

128.   Y. Wu and B. D. Woerner, "The influence of quantization and fixed point arithmetic upon the BER performance of Turbo codes," Proceedings of 49th IEEE Vehicular Technology Conference, Vol. 2, pp. 1683-1687, 1999.

129.   H. Michel, A. Worm and N. Wehn, "Influence of quantization on the bit error performance of Turbo decoders," Proceedings of 51st IEEE Vehicular Technology Conference, Vol. 1, pp. 581-585, 2000.

130.   U. Wachsmann, R. F. H. Fischer, and J. B. Huber, "Multilevel codes: theoretical concepts and practical design rules," IEEE Transactions on Information Theory, Vol. 45 Issue 5, pp. 1361 −1391, July 1999.

131.   N. Kahale and R. Urbanke, "On the minimum distance of parallel and serially concatenated codes," Proceedings of IEEE International Symposium on Information Theory, pp. 31, 1998.

132.   I. Sason and S. Shamai, "Improved upper bounds on the performance of parallel and serial concatenated turbo codes via their ensemble distance spectrum," Proceedings of IEEE International Symposium on Information Theory, pp. 30, 1998.

133.   A. M. Viterbi and A.J.Viterbi, "Improved union bound on linear codes for the input-binary AWGN channel, with applications to Turbo codes" Proceedings of IEEE International Symposium on Information Theory, pp. 29, 1998.

134.   T. M. Duman and M. Salehi, "New performance bounds for Turbo codes," IEEE Transactions on Communications, Vol. 46, Issue 6, pp. 717-723, June 1998.

135.   K. A. Stewart, G. P. Labedz and K. Sohrabi, "Wideband channel measurement at 900 MHz", Proceedings of IEEE Vehicular Technology Conference, pp. 236-240, July 1995.

136.   R. J. C. Bultitude, S. A. Mahmoud, and W. A. Sullivan, "A comparison of indoor radio propagation characteristics at 910 MHz and 1.75 GHz," IEEE Journal on Selected Areas in Communications, Vol. 7, pp. 20-30, January 1989.

137.   T. S. Rappaport and C. D. McGillem, "UHF fading in factories," IEEE Journal on Selected Areas in Communications, Vol. 7, pp. 40-48, January 1989.

138.   G. H. Munro, "Scintillation of radio signals from satellites," J. Geophys. Res., Vol. 68, April 1963.

139.   H. Suzuki, "A statistical model for urban multi-path propagation," IEEE Transactions on Communications, Vol. COM-25, pp. 673-680, July 1977.

140.   T. L. Staley, R. C. North, W. H. Ku, and J. R. Zeidler, "Performance of coherent MPSK on frequency selective slowly fading channels," Proceedings of IEEE Vehicular Technology Conference, pp. 784-788, April, 1996.

INITIAL DISTRIBUTION LIST

1.   Defense Technical Information Center
        Fort Belvoir, Virginia

2.   Dudley Knox Library
        Naval Postgraduate School
        Monterey, California

3.   Chairman
        Department of Electrical and Computer Engineering
        Naval Postgraduate School
        Monterey, California
        jknorr@nps.navy.mil

4.   Prof. Clark Robertson
        Department of Electrical and Computer Engineering
        Naval Postgraduate School
        Monterey, California
        crobertson@nps.navy.mil

5.   Prof. Tri Ha
        Department of Electrical and Computer Engineering
        Naval Postgraduate School
        Monterey, California
        ha@nps.navy.mil

6.   Prof. Murali Tummala
        Department of Electrical and Computer Engineering
        Naval Postgraduate School
        Monterey, California
        mtummala@nps.navy.mil

7.   Prof. Ramakrishna Janaswamy
        Department of Electrical and Computer Engineering
        Naval Postgraduate School
        Monterey, California
        janaswam@nps.navy.mil

8. Prof. Bert Lundy
Department of Electrical and Computer Engineering
Naval Postgraduate School
Monterey, California
blundy@nps.navy.mil

9. Director, DSTA
Ministry of Defense
Singapore
chng_lay_peng@dsta.gov.sg

10. MAJ Eng Seng Chia
Ministry of Defense
Singapore
chia_aaron@hotmail.com